UNIVERSITÀ
DEGLI STUDI
FIRENZE

DOTTORATO DI RICERCA IN
Area del Farmaco e Trattamenti Innovativi, Curriculum Scienze Farmaceutiche
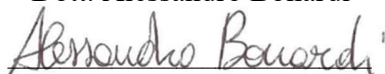
CICLO XXXIII

COORDINATORE Prof. Carla Ghelardini

In silico strategies for the rational design, synthesis, and biological evaluation of ligands targeting macromolecules of pharmaceutical interest
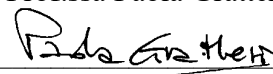
Settore Scientifico Disciplinare CHIM/08

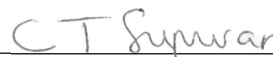**Dottorando**
Dott. Alessandro Bonardi

Tutore Scientifico
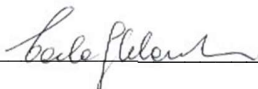Prof.ssa Paola Gratteri

Tutore Teorico
Prof. Claudiu T.Supuran

Coordinatore
Prof.ssa Carla Ghelardini

Anni 2017-2020

Abstract

Carbonic anhydrases (CAs, EC 4.2.1.1) are a superfamily of ubiquitous metalloenzymes, widely expressed in all kingdoms of life and encoded by eight evolutionarily unrelated gene families: α-, β-, γ-, δ-, ζ-, η-, θ- and ι-CAs. The CAs catalyze the reversible hydration of carbon dioxide into bicarbonate and proton that is physiologically crucial for all living beings because involved in respiration, pH and CO_2 homeostasis, transport of CO_2/HCO_3^- and a multitude of biosynthetic reactions. In *Homo sapiens*, fifteen α-class CA isoforms were identified, which are implicated in a *plethora* of physiological processes such as electrolytes secretion in many tissues/organs, metabolic reactions (*e.g.* gluconeogenesis, lipogenesis, ureagenesis), bone resorption, calcification, and carcinogenesis. Thus, an abnormal expression/activity of specific human CAs results in a multitude of human pathological processes that can be targeted with a pharmacological intervention based on CA modulation. Moreover, numerous α-, β-, γ- and η-CAs were identified in many bacteria, protozoa, and fungi that act as human pathogens. In this context, CAs were shown to be crucial for the virulence, growth or acclimatization of the parasites in the hosts. Their inhibition produces growth impairment and defects in the pathogen, being a promising strategy for chemotherapy.

The research activity included in this Ph.D. thesis fits in the context of the spreading interest of the scientific community on CAs as drug targets for the treatment of a multitude of disorders. Thus, a set of projects involving drug-design, synthesis, biological evaluation and *in silico* investigation of the ligand-target interactions of new CA inhibitors (CAIs) were the focus of the three-year Ph.D. cycle.

In the first reported project, the concept of *tail-* (and *dual tail*) *approach* was extended up to the *three tail approach*. This study aimed to increase the selectivity of the benzenesulfonamide scaffold against certain CA isoforms over others, through the introduction of three pendants called "*tails*" with different lipophilic/hydrophilic nature. Hence, it was possible both to target simultaneously the most variable residues of the inner/outer rim of the hydrophobic and hydrophilic half of the active site and to interact with the peculiar accessory subpockets which differentiate the various isoforms. The synthesized

three-tailed inhibitors (TTIs) resulted to be more selective against the glaucoma-associated CA isoforms (hCA II, IV and XII) with respect to the mono-tailed precursors. A massive *in silico* study of the TTIs-targets interactions was carried out to extend the X-ray crystallography results and the IOP-lowering ability of the three most promising derivatives was evaluated.

The second project adopted the *multi-targets approach* for the treatment of multifactorial diseases, such as inflammation and tumors. Inhibitors of target CA isoforms, to repristinate the correct synovial fluid pH value (against IV, IX and XII), were endowed with an H_2S releasing ability, to exploit the gasotransmitter relieving effect in inflammation, developing innovative H_2S releaser-CAI hybrids. The stopped-flow kinetic assay pointed out selective inhibition profiles against CAs IX and XII for most synthesized compounds over the off-target CAs I and II. Four compounds were submitted to the Paw pressure and Incapacitance tests to evaluate their ability as anti-inflammatory agents.

In the third project, an *in silico* study was conducted to optimize the CA IV inhibitory properties of a set of benzenesulfonamide derivatives, that produced potent but unselective CA IV inhibition. A peculiar hydrophilic cleft of the CA IV active site (pocket A) was the target for the drug optimization process. The introduction of a pendant with an H-bond acceptor/donor group in a position suitable for the interaction with pocket A was predicted to improve the binding to the target CA and not to off-target isoforms. As a result, the newly reported set of derivatives showed enhanced CA inhibition up to a subnanomolar range.

The research of new CAI chemotypes is an important strategy to selectively inhibit specific isoforms over others. In the fourth and fifth projects, the joint use of docking studies, MM-GBSA and molecular dynamic (MD) simulations allowed to evaluate the binding mode of derivatives with CAI scaffolds other than sulfonamides such as hydantoin, saccharin and acesulfame. A zinc binder inhibition mechanism was computed for the hydantoins, which are able to exist in a deprotonated form at the physiological pH. A mechanism based on the anchorage to zinc-bound water molecule was instead proposed and assessed for tertiary sulfonamides, saccharin- and acesulfame derivatives.

The sixth project was here reported as representative for a series of *in silico* investigations carried out to figure out the SAR of several sets of benzenesulfonamide CAIs.

The design of N-nitrosulfonamide silver salts was reported to combine the compounds selective inhibition of certain pathogens CAs (over human isozymes) and the antiseptic properties of silver. Indeed, a subset of such compounds showed effective and selective inhibition of the CAs from *Trypanosoma cruzi* (TcCA) and *Leishmania donovani chagasi* (LdcCA) compared to hCAs I and II as well as effective chemotherapic action *in vitro* against several protozoan strains and forms.

Another project consisted of the *in silico* characterization of the binding mode of benzoxaborole derivatives within the α-, β-, and γ-CA active site of the bacterial *Vibrio cholerae* (VchCA). Primarily the targets homology models were built to proceed therefore with docking studies, MM-GBSA and MD calculations with the boron-based ligands. The computational analysis, for the first time carried out on a γ-class CA, showed that benzoxaborole derivatives adopt both a tetrahedral and trigonal bipyramidal zinc coordination in complex with VchCA (α-CA), a tetrahedral geometry within VchCAβ and two alternative penta-coordinated geometries around the zinc ion in VchCAγ active site.

GABA$_A$ receptors (GABA$_A$Rs) are another crucial target for the treatment of several human diseases, such as anxiety disorders, insomnia, epilepsy, restlessness, and aggressive behaviors. Many clinically important drugs were discovered to target GABA$_A$Rs, interacting at different allosteric binding sites such as benzodiazepine and benzodiazepine site ligands, barbiturates, intravenous and volatile anesthetics, anticonvulsants, ethanol and neuroactive steroids, and performing their pharmacological effects. Nowadays, several natural products such as flavonoids, menthol, magnolol, honokiol, coronaridines and others, were found to modulate GABA$_A$Rs. All of these compounds exhibit diverse pharmacology mediated by known and unknown binding sites and their potential for clinical application is currently being explored. In this scenario, the identification of the binding site and the investigation of the binding mode of coronaridine congeners, such as (+)-catharanthine, is an actual challenge. The joint use of electrophysiological, radioligand displacement and *in silico* studies promoted the identification of the (+)-catharanthine binding site at the β(+)α(-), concluding that this ligand acts according to a loreclezole-like mechanism.

Finally, during my stage in the organic chemistry laboratory of Prof. Vittorio Pace (University of Vienna) I was involved in a study on the reductive lithiation arene-catalyzed of imines as a new method for the synthesis of amino alcohols.

TABLE OF CONTENTS

List of Abbreviations and Acronyms

α-CA	α-Carbonic anhydrase		**HPLC**	High Performance Liquid Chromatography
β-CA	β-Carbonic Anhydrase		**HRMS**	High-Resolution Mass Spectrometry
γ-CA	γ-Carbonic Anhydrase		**ia**	intra-articular
β-ADRs	β-Adrenergic Receptors		**IC$_{50}$**	Half Maximal Inhibitory Concentration
3-APA	3-Aminopropylphosphonic acid		**IND**	Indisulam
3-APMPA	3-Aminopropyl(methyl) phosphinic acid		**IOP**	Intraocular Pressure
3-APPA	3-Aminopropylphosponous acid		**JIA**	Juvenile Idiopathic Arthritis
(+)-CAMP	(+)-*cis*-2-aminomethylcyclopropane carboxylic acid		**K$_A$**	Activation Constant
AAZ	Acetazolamide		**K$_I$**	Inhibition Constant
ACE	Acesulfame K		**LdcCA**	*Leishmania chagasi* Carbonic Anhydrase
AG	Anchoring Group		**MgCA**	*Malassezia globosa* Carbonic Anhydrase
Ag-NPs	Silver nanoparticles		**MD**	Molecular Dynamics
BRZ	Brinzolamide		**MS**	Mass Spectrometry
BZA	Benzolamide		**MZA**	Methazolamide
CA	Carbonic Anhydrase		**NHS**	*N*-hydroxysuccinamide
CACA	*cis*-4-Aminocrotonic acid		**NSAID**	Nonsteroidal Anti-Inflammatory Drug
CAI	Carbonic Anhydrase Inhibitor		**NTDs**	Neglected tropical diseases
CAAs	Carbonic Anhydrase Activators		**NO**	Nitric Oxide
Can2	*Cryptococcus neoformans* Carbonic Anhydrase		**PBS**	Phosphate Buffer Solution
CARPs	CA-Related Proteins		**PDB**	Protein Data Bank
CFA	Complete Freund's Adjuvant		**PyBOP**	Benzotriazole-tris-pyrrolidino-phosphonium PF$_6^-$
CLX	Celecoxib		**K$_i$**	Inhibition Constant
CNS	Central Nervous System		**RA**	Rheumatoid Arthritis
Cryo-EM	Cryo-Elettron Microscopy		**RMSD**	Root-mean-square Deviation
DCM	Dichloromethane		**RNS**	Reactive Nitrogen Species
DIPEA	N,N-Diisopropylethylamine		**ROS**	Reactive Oxygen Species
DMCM	Methyl-6,7-dimethoxy-4-ethyl-β carboline-3-carboxylate		**SA**	Sulfanilamide
DMF	Dimetilformammide		**SAC**	Saccharin
DMAP	4-Dimethylaminopyridine		**SAR**	Structure-Activity Relationship
DRZ	Dorzolamide		**SG**	Sticky Group
DTCs	Dithiocarbamates		***SI***	*Selectivity Index*
DTT	Dithiolthionic		**SLP**	Sulpiride
EDC	1-Ethyl-3-(3-dimethylaminopropyl)carbodiimide		**SLT**	Sulthiame
EZA	Ethoxzolamide		**TcCA**	*Trypanosoma cruzi* Carbonic Anhydrase
GABA	γ-Aminobutyric acid		**TFA**	Trifluoroacetic Acid
GABA$_A$Rs	GABA$_A$ receptors		**TPM**	Topiramate
GABA$_B$Rs	GABA$_B$ receptors		**TPMPA**	(1,2,5,6-tetrahydropyridine-4-yl)-methyl-phosphinic acid
GABA$_c$Rs	GABA$_c$ receptors		**TTIs**	Three-tailed inhibitors
hCA	Human Carbonic Anhydrase		**VchCA**	*Vibrio cholerae* Carbonic Anhydrase
HBA	Hydrogen bond acceptor		**VLX**	Valdecoxib
HBD	Hydrogen bond donor		**VFT domain**	Venus flytrap domain
HCT	Hydrochlorothiazide		**ZBG**	Zinc Binding Group
HD domain	Heptahelica membrane domain		**ZNS**	Zonisamide

Part I
Introduction

Chapter 1. Carbonic anhydrases: classification, biochemistry, and structure

Carbonic anhydrases (CAs, EC 4.2.1.1) are a superfamily of phylogenetically ubiquitous metalloenzymes, present in eukaryotes and prokaryotes.[1-12] The ubiquity of CAs is owed to the catalysis of a simple physiologically crucial reaction for living beings,[1] that is the reversible hydration of carbon dioxide to bicarbonate and proton (Equation 1).

$$CO_2 + H_2O \leftrightarrows HCO_3^- + H^+ \qquad\qquad (Eq.1)$$

Normally, this reaction occurs slowly at the pH values typically marking most tissues and organisms (turnover number - k_{cat} - of 10^{-1} s^{-1}). Thus CAs are evolved to catalyze the carbon dioxide hydration to handle the great loads of CO_2 produced by most organisms, making the reaction substrates easily available for physiologic processes and tuning acid-base equilibria.[1-3] As a result, CAs are present in organisms of all life kingdoms (Animalia, Plantae, Fungi, Protista, Bacteria, and Archaea), becoming, during the evolutionary process, among the fastest enzymes known that effectively speed up the rate of the overall reaction up to 10^6 s^{-1}.[13]

In many organisms, CAs are involved in the crucial physiological processes of respiration, pH and CO_2 homeostasis, transport of CO_2/HCO_3^- and a variety of biosynthetic reactions.[1-4] Additionally, in mammals, CAs promotes the secretion of electrolytes in many tissues/organs, metabolic reactions such as gluconeogenesis, lipogenesis, ureagenesis, calcification, bone resorption, and tumorigenicity.[14-23] In algae, cyanobacteria and plants, these enzymes are implicated in photosynthesis,[6-9] whereas in diatoms CAs play a pivotal role in CO_2 fixation and SiO_2 cycle.[11] In pathogen microorganisms, such as bacteria, fungi, and protozoa, CAs were shown to be crucial for the virulence, growth, or acclimatization of the parasites in the hosts.[12]

1.1 Classification of carbonic anhydrases

The CAs are classified in eight evolutionarily unrelated families (α-, β-, γ-, δ-, ζ-, η-, θ-, and ι-CAs) that are characterized by different structural features and phylogenetic distribution (Table 1).[1-12]

The α-CAs are present in vertebrates, protozoa, algae, corals, bacteria, and green plants.[1,12] The β-CAs have been identified in bacteria, fungi, archaea, algae, and chloroplasts of both mono- and dicotyledons.[12,24,25] The γ-CAs are encoded in archaea, bacteria, and plants.[9] The δ-CAs were found in marine phytoplankton, such as haptophytes, dinoflagellates, diatoms, and chlorophyte prasinophytes,[8] whereas ζ-CAs seem to be present only in marine diatoms.[4] A unique η-CA has been identified to date in the protozoa *Plasmodium falciparum*.[7] The θ-CAs were detected in the marine diatom *Phaeodactylum tricornutum*.[11] The first ι-CA was identified in the marine diatom *Thalassiosira pseudonana*,[5] and more recently it was also found in bacteria.[26]

Table 1. Structural features and phylogenetic distribution of the eight evolutionarily unrelated families: α-, β-, γ-, δ-, ζ-, η-, θ- and ι-CAs.

Family	Metal atom	Coordinated residues	Quaternary structure	Organisms
α	Zn^{2+}	His, His, His	Monomer, dimer	Vertebrates, bacteria, protozoa, fungi, green plants, algae, and corals
β	Zn^{2+}	His, Cys, Cys	Dimer, tetramer, octamer	Bacteria, protozoa, fungi, archaea, algae, and chloroplasts of mono- and dicotyledons.
γ	Zn^{2+}, Fe^{2+}, Co^{2+}	His, His, His	Trimer	Archaea, bacteria, and plants
δ	Zn^{2+}, Cd^{2+}, Co^{2+}	His, His, His	Not available	Marine phytoplankton
ζ	Cd^{2+}, Zn^{2+}	His, Cys, Cys	Trimer	Marine diatoms
η	Zn^{2+}	His, His, Gln	Not available	Plasmodium spp.
θ	Zn^{2+}	His, Cys, Cys	Dimer	Marine diatoms
ι	Mn^{2+}	His, His, Glu	Not available	Marine diatoms, and bacteria

A wider collection of kinetic and X-ray crystallographic data enabled a detailed comprehension of the structure-function relationship in the CAs superfamily.[2,13] These metalloenzymes are catalytically effective when a metal ion is bound within the active site cavity. The catalytic system commonly includes a metal(II) ion in a tetrahedral geometry, three coordinated amino acid residues, and a water molecule/hydroxide ion completing the coordination sphere around the metal atom. Zn(II) is the metal ion spread in all CA genetic families, but it can be exchanged with Cd(II) in ζ-CAs,[4] and Fe(II) is presumably present in γ-CAs in anaerobic conditions.[8] A Co(II) ion can replace the zinc ion in several α-CAs not giving a significant loss of the catalytic efficiency,[8] while an Mn(II) appears to be the constitutive ion of the ι-CA.[5,26]

1.2 Catalytic mechanism of carbonic anhydrases

In all CA classes, the catalytic mechanism occurs in two steps (Eq. 2 and 3).

$$E\text{-}M^{2+}\text{–}OH^- + CO_2 \rightleftarrows E\text{-}M^{2+}\text{–}HCO_3^- + H_2O \rightleftarrows E\text{-}M^{2+}\text{–}H_2O + HCO_3^- \qquad \text{(Eq.2)}$$
$$E\text{-}M^{2+}\text{–}H_2O + B \rightleftarrows E\text{-}M^{2+}\text{–}OH^- + BH^+ \qquad \text{(Eq. 3)}$$
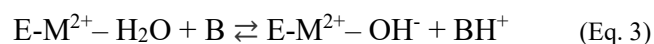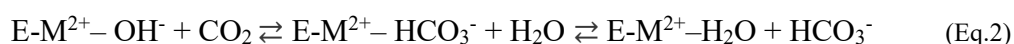
The catalytically active species of the enzyme is the metal hydroxide ones (E-M^{2+}-OH^-). In the first step of the reaction, at neutral pH this species acts as a strong nucleophile against the CO_2 molecule bound in a hydrophobic pocket nearby, with consequent formation of HCO_3^-. Therefore, the bicarbonate ion is displaced by a second water molecule and released outwards (Eq. 2). When a water molecule is bound to the zinc ion (E-M^{2+}-H_2O), the enzyme is in its acidic, catalytically inactive form. In the second and rate-determining step, the catalytically active metal hydroxide species is regenerated by a proton transfer reaction from the metal-bound water to an exogenous proton acceptor or an active site residue (B).[1-3] The overall catalytic mechanism is shown in Figure 1A. In the catalytically very active isozymes, (such as the human isoforms II, IV, VI, VII, IX, XII, XIII, and XIV), the proton transfer process is assisted by a histidine residue placed at the entrance of the active site (H64 known as "proton shuttle residue"), or by a cluster of histidines (Figure 1B), which protrudes from the rim of

the active site to the surface of the enzyme, thus assuring efficient proton-transfer pathways.[2] The absence of His64 in other CAs markedly decreases their catalytic efficiency.
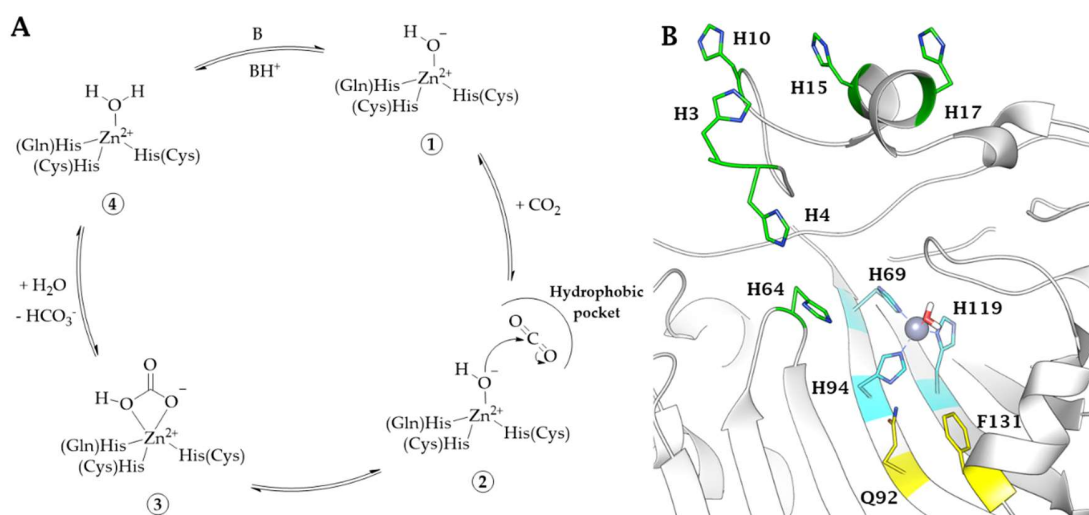
Figure 1. (A) Schematic representation of the CA catalytic mechanism; (B) His64, known as "proton shuttle residue" and cluster of His residues which ensure an efficient proton-transfer pathway (shown in hCA II, PDB 3KKX).

A catalytic turn-over reaching k_{cat}/K_M values over 10^8 M^{-1} x s^{-1} in some α- and ζ-CAs places CAs among the most efficient natural catalysts.[27] This efficient catalysis is also due to a peculiar architecture common among all CA families that differentiates the active site in two very different environments: one made of hydrophobic residues and the other lined by hydrophilic amino acids.[13,27] Indeed, the hydrophobic part could have the role of entrapping the CO_2 molecule while the hydrophilic one could represent the escape outwards of the polar species produced by the CO_2 hydration reaction.[2] The latter process was demonstrated at least for the protons, aided in their moving towards outside of the cavity by a network of water molecules and histidine residues.[3]

1.3 Characteristics of the major families of carbonic anhydrases
1.3.1 α-Carbonic anhydrases

α-CAs are spread in vertebrates, protozoa, algae, corals, bacteria, and green plants. A wealth of studies allowed to identify sixteen different isozymes in mammals, and several other

isozymes in non-mammalian vertebrates.[1,2] Undeniably, the most important α-CAs subset is represented by the fifteen isoforms identified to date in *Homo sapiens* (Table2).[1-3,16]

Table 2. Organ/Tissue Distribution, Subcellular Localization, CO_2 Hydrase Activity, and Diseases in which each isoform is involved.

hCA	Organ/tissue distribution	Subcellular localization	k_{cat}/K_M $(M^{-1}s^{-1})$	Diseases in which the isoform is involved
CA I	Erythrocytes, gastrointestinal tract, eye, CNS (motoneurons)	Cytosol	5.0×10^7	Retinal/cerebral edema, neurodegenerative diseases
CA II	Erythrocytes, eye, gastrointestinal tract, bone osteoclasts, kidney, lung, testis, brain (choroid plexus, oligodendrocytes, astrocytes, and axons myelin sheath)	Cytosol	1.5×10^8	Glaucoma, edema, epilepsy, altitude sickness, cancer, neurodegenerative diseases
CA III	Skeletal muscle, adipocytes	Cytosol	2.5×10^5	Oxidative stress
CA IV	Kidney, lung, pancreas, colon, heart muscle, eye, brain (brain capillaries, BBB, thalamus, and hippocampus)	Membrane-bound	5.1×10^7	Glaucoma, retinitis pigmentosa, stroke, neurodegenerative disease
CA VA	Liver, CNS (astrocytes and neurons)	Mitochondria	2.9×10^7	Obesity, diabetic cerebrovascular and neurodegenerative disease
CA VB	Heart and skeletal muscle, pancreas, kidney, spinal cord, gastrointestinal tract, CNS (astrocytes and neurons)	Mitochondria	9.8×10^7	Obesity, neurodegenerative disease
CA VI	Salivary and mammary glands	Secreted	4.9×10^7	Cariogenesis
CA VII	CNS (pH regulation)	Cytosol	8.3×10^7	Epilepsy, neuropathic pain, neurodegenerative disease
CA IX	Tumors, gastrointestinal mucosa	Transmembrane	5.4×10^7	Cancer
CA XII	Renal, intestinal, reproductive epithelia, eye, tumors	Transmembrane	3.5×10^7	Cancer, glaucoma
CA XIII	Kidney, brain, lung, gut, reproductive tract	Cytosol	1.1×10^7	Sterility
CA XIV	Kidney, brain, liver, skeletal muscle	Transmembrane	3.9×10^7	Epilepsy, retinopathies

These isoenzymes differ by molecular features, oligomeric arrangement, cellular localization, distribution in organs and tissues, expression levels, kinetic properties and response to different classes of inhibitors.[1-3] Twelve are catalytically active isoforms (I, II, III, IV, VA, VB, VI, VII, IX, XII, XIII, XIV), whereas the remaining three (VIII, X, XI),

called CA-related proteins (CARPs), have no catalytic activity as they lack the zinc ion in the active site and one or more histidine residues usually belonging to its coordination sphere.[1-3] Human CAs can be grouped into four different subsets depending on their subcellular localization (Figure 2). CA I, II, III, VII, VIII, X, XI, XIIII are cytosolic proteins, CA VA and VB are present in the mitochondrial matrix, CA VI is a secreted enzyme, CA IV is a glycosylphosphatidylinositol (GPI)-anchored protein, and CA IX, XII and XIV are trans-membrane isoforms.[29] These enzymes are widely distributed in many tissues and organs where they are involved in a wealth of essential physiological processes. Thus, their dysregulated expression and/or abnormal activity can result in severe pathological conditions (Table 2).
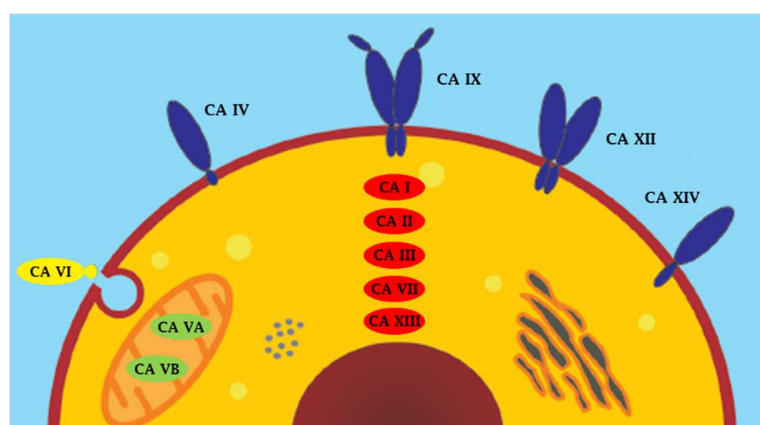
Figure 2. Schematic illustration of domain composition and subcellular localization of catalytically active human α-CAs.

PDB[28] database contains the 3D structures of all catalytically active human isoforms, except CA VA and VB. These enzymes hold common structural features independently on their subcellular localization. Indeed, in agreement with the high sequence identity among hCA isoforms, structural studies have demonstrated that all these enzymes share the same fold characterized by a central ten-stranded β-sheet, surrounded by α- and 3_{10}- helices and additional β-strands (Figure 3A). The active site is located in a large conical cavity, about 15 Å deep, at the base of which the zinc ion is accommodated, coordinated by three conserved histidine residues (H94, H96, and H119) and the solvent molecule/hydroxide ion. The Zn^{2+}-

bound water molecule/hydroxide ion is involved in a network of hydrogen bonds that enhance its nucleophilicity (Figure 3B).
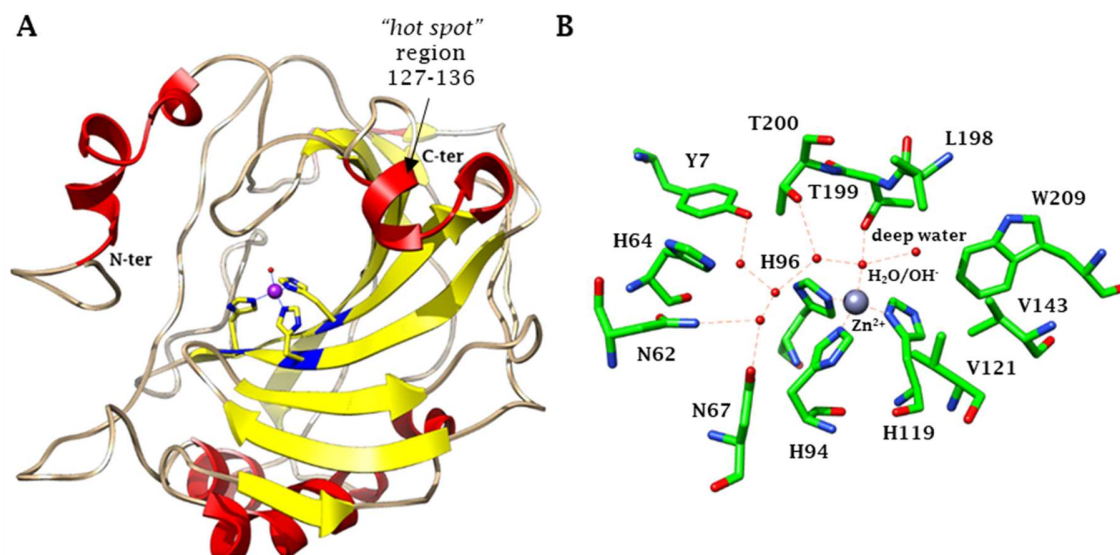
Figure 3. (A) Ribbon diagram of hCA II structure (PDB code 1CA2), which has been chosen as representative CA isoform. The active site Zn^{2+} coordination is also shown. Helix and β-strand regions are colored in red and yellow, respectively. (B) View of CA II active site. The Zn^{2+} is tetrahedrally coordinated by the three catalytic histidines and a water molecule/hydroxide ion, which is engaged in a well-defined network of hydrogen bonds. Water molecules are indicated as red spheres.

In particular, it establishes a hydrogen bond with the hydroxyl moiety of the conserved T199 residue and with two water molecules, located on two opposite sides: the first one also called the "deep water", is located in a hydrophobic cavity delimited by conserved residues V121, V143, L198, and W209, while the second one is in a hydrophilic environment toward the entrance of the active site (Figures 3B and 4A). These two peculiar active site environments are supposed to be responsible for the rapid catalytic cycle of CO_2 to bicarbonate; in fact, the hydrophobic region is necessary to take the CO_2 substrate and orient the carbon atom for the nucleophilic attack by the zinc-bound hydroxide (Figure 4B), while the hydrophilic region creates a well-ordered hydrogen-bonded solvent network, which is necessary to allow the proton transfer reaction from the zinc-bound water molecule to the bulk solvent (Figure 4C).[13,27]
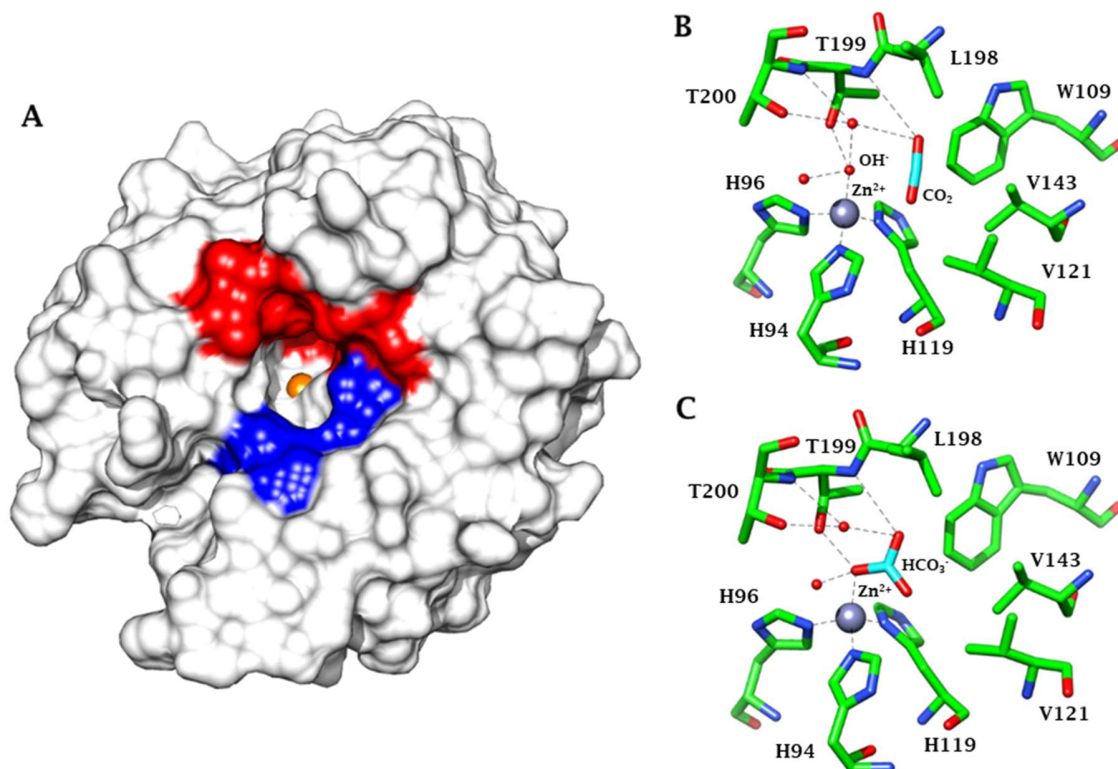
Figure 4. (A) Solvent accessible surface of CA II. Residues delimiting the hydrophobic half of the active site cleft are shown in red (I91, F131, V121, V135, L141, V143, L198, P202, L204, V207 and W209), while residues delimiting the hydrophilic one is shown in blue (N62, H64, N67 and Q92). The active site of CA II showing: (B) the position of CO_2 molecule (PDB code 2VVA), and (C) the binding of the bicarbonate ion (PDB code 2VVB). Zn^{2+} coordination and polar interactions are also reported.

A detailed comparison between all hCA isoforms reveals that the main sequence and structural differences between these enzymes are observed in the region 127-136 (Figure 3A), which thus has to be considered a ''hot spot'' in the structure-based drug design of selective hCA inhibitors.[27] The 12 catalytically active isoforms show also important differences in the quaternary structure; indeed, whereas CAs I-IV, VA, VB, VII, XIII, and XIV are monomers, CAs VI, IX, and XII are dimers. Interestingly, the dimeric interface is different in each one of these hCA dimers.
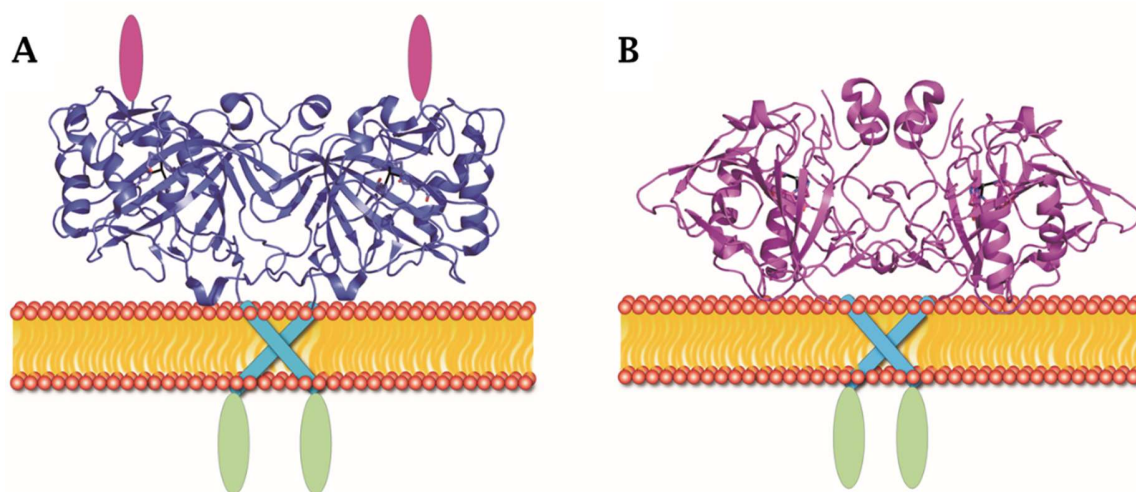
Figure 5. Proposed models of full-length CA IX (A)[29] and CA XII (B)[30] on the cell membrane. Both CA IX and CA XII contain an extracellular CA domain, a transmembrane region (cyan), and an intracellular tail (green). Additionally, CA IX contains a proteoglycan-like (PG) domain (magenta) at the N-terminus.

Differently, the bacterial α-CAs, such as those identified in *Sulfurihydrogenibium yellowstonense*, *Sulfurihydrogenibium azorense,* and *Neisseriagonorrhoeae*, are dimers formed by two identical active monomers.[12]

Additionally, α-CAs possess a certain catalytic versatility that enables the fulfillment of several other hydrolytic processes presumably involving non-physiological substrates. These promiscuous reactions include the hydration of cyanate to carbamic acid (Equation 4), or of cyanamide to urea (Equation 5), the aldehyde hydration to gem-diols (Equation 6), the hydrolysis of carboxylic, sulfonic, and phosphate esters (Equations 7-9).[2]

$$HOCN + H_2O \rightleftarrows H_2NCOOH \tag{Eq.4}$$

$$H_2NCN + H_2O \rightleftarrows CO(NH_2)_2 \tag{Eq.5}$$

$$RCHO + H_2O \rightleftarrows RCH(OH)_2 \tag{Eq.6}$$

$$RCOOR' + H_2O \rightleftarrows RCOOH + R'OH \tag{Eq.7}$$

$$H_2PO_4Ar + H_2O \rightleftarrows H_3PO_4 + ArOH \tag{Eq.8}$$

$$RSO_3R' + H_2O \rightleftarrows RSO_3H + R'OH \tag{Eq.9}$$

1.3.2 β-Carbonic anhydrases
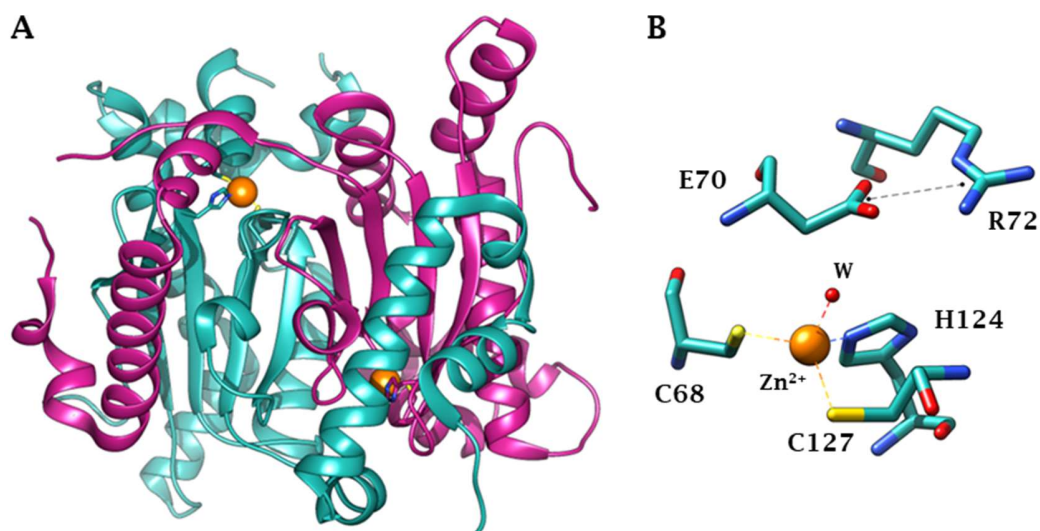
Figure 6. (A) Overall structure of a representative β-CA from fungi *Cryptococcus Neoformans* (Can2) dimer. One monomer is colored magenta, while the other one is colored sea green. The Zn^{2+} ions are shown as orange spheres. (B) The active site of Can2. Coordination of the active-site Zn(II) by C68, H124, C127, and a water molecule is shown by colored dashed lines, and the D70-R72 salt bridge is colored black.

The β-class CAs are broadly distributed and identified in plants, yeast, bacteria, archaea, fungi, and invertebrates.[10] Conversely from α-class isozymes, β-CAs are oligomers formed by two or more identical subunits, generally dimers, tetramers, and octamers (Figure 6A).[31] The active site exists at the dimer interface and contains hydrophobic and hydrophilic areas similar to hCAs. The residues of the catalytic triad are highly conserved among β-CA isoforms: the Zn(II) ion is coordinated by two cysteine residues, a residue of His and the carboxyl group of a residue of Asp or, alternatively, a water molecule/hydroxide ion (Figure 6B and Figure 7).

At a pH of 7.5 or lower, the β-CA active site, formed by residues belonging to two different subunits, is "closed" (type II enzyme), since the carboxyl group of the aspartic acid of the conserved dyad arginine-aspartate coordinates the zinc ion, thus completing the coordination sphere (Figure 7A). At pH values higher than 8.3, the aspartate and arginine of this dyad form a salt bridge leading the enzyme in its "open" active form (type I enzyme).[10,13,21] A molecule of water/hydroxide ion completes the tetrahedral geometry coordination pattern around the

metal ion (Figure 7B). The catalytic mechanism of β-CAs with the active site in the "open" form is rather similar to α-class enzymes.
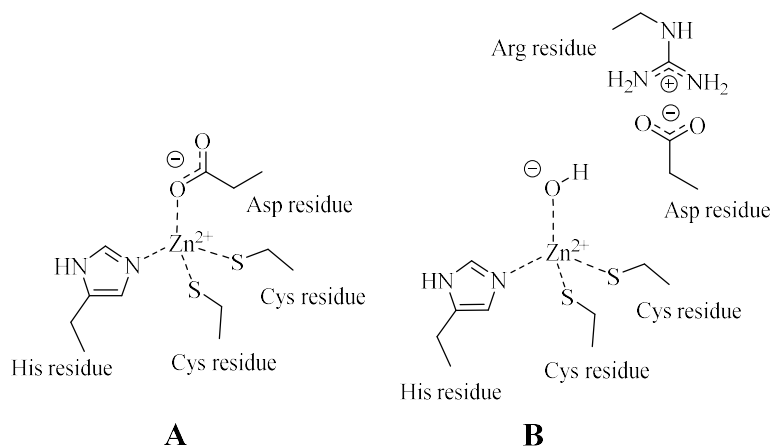
Figure 7. Inactive (A) and active (B) forms of β-CAs active sites.

1.3.3 γ-Carbonic anhydrases

Up to now, γ-class CAs have been identified in archaea, bacteria, and plants.[9] Cam, the carbonic anhydrase from the methanearcheon *Methanosarcina thermophila*, is the prototype of the γ-class.[32] The crystal structure of Cam showed that one monomer consists of seven complete turns of a left-handed parallel β-helix topped by a short α-helix, followed by a second C-terminal α-helix which is positioned antiparallel to the axis of the β-helix (Figure 8A).[32] Each face of the beta-helix is comprised of parallel beta-strands, containing two or three residues each, and is connected to the subsequent face by a 120° turn, so that the cross-section of the β-helix resembles an equilateral triangle. Each turn of the β-helix contains two type II β-turns positioned between strands 1 and 2 and between strands 2 and 3 and is completed by a loop, connecting strand 3 with strand 1 of the next turn. The interior of the helix is dominated by hydrophobic interactions between aliphatic side chains of residues originating from equivalent positions in adjacent turns of the helix. The active enzyme is a homotrimer resulting from the packing of three left-handed β-helices with the axis all parallel (Figure 8B and 8C). Three residues, R59, D61, and D76, are important amino acids for *trimer* formation. R59 forms a salt bridge with D61 of the same monomer and D76 of another

monomer. These three residues are almost entirely conserved in all γ-CAs sharing homology with Cam.

The active site is localized at the interfaces between two subunits. In the active site a Zn(II) ion is coordinated by H81 and H122, which extend from equivalent positions of the adjacent turn of one monomer, and by H117 located in a neighboring monomer (Figure 8C). Two water molecules complete the zinc coordination sphere forming a distorted trigonal bipyramidal geometry. The two water molecules are within hydrogen bond distance of the side chain of Q75 and E62.[13,32]
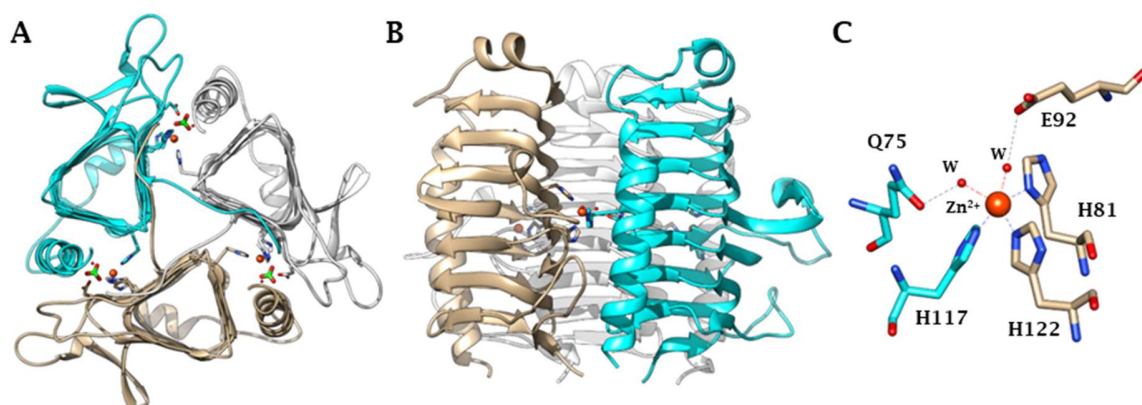
Figure 8. Ribbon representation of the Cam trimer. (A) Top view of the enzyme / HCO_3^- complex (PDB 1QRL). (B) Side view (PDB 1QRG). The overall fold is a left-handed β-helix, consisting of three untwisted, parallel β-sheets connected by left-handed crossovers. (C) Metal coordination within the active site which consists of a distorted trigonal bipyramidal geometry. Residues belonging to different subunits are depicted using different colors.

1.4 Carbonic anhydrases as drug targets

1.4.1 Human carbonic anhydrases

Human CAs have been the first isoforms to have been studied as drug-targets from both the inhibition and activation standpoints.[1] Human CA inhibitors (CAIs) have written a long pharmacological history in many fields due to the involvement of CAs in a variety of important physio/pathological processes such as respiration, pH regulation, calcification, gluconeogenesis, lipogenesis, or tumorigenesis.[15-24] In contrast, CA activators have been

much less studied to date.[13,33] Nonetheless, as a subset of CAs is abundant in the brain and was shown to be activatable by drug-like compounds, the possibility to design agents that enhance cognition has been recently emerging, with potential therapeutic applications in aging and neurodegenerative diseases as well as tissue engineering.[1-4,13]

CAIs of the sulfonamide/sulfamate type have been long used as diuretics, systemic anti-convulsants, topically acting anti-glaucoma agents, or for the treatment of altitude sickness.[1,15-24,34] More recently CAIs have shown promising results as anti-obesity, anti-inflammatory, anti-neuropathic pain, and anti-tumor agents/diagnostic tools.[13-24]

CAIs of the first-generation show an isoform promiscuous inhibitory activity, which leads to serious side effects for all pathologies in which they are used.[3] Hence, in the last decades, some innovative strategies were adopted to produce isoform-selective sulfonamide-like derivatives as well as new classes of isoform-specific CAIs were produced which showed alternative mechanisms of action. Understanding the factors governing selective inhibition of the single isoforms is clearly of pivotal importance and represents the breakthrough step to yield potential drugs that avoid the serious side effects due to promiscuous inhibition in the treatment of all pathologies in which CAIs will be employed.[3] In fact, the great potential of hCAs as drug targets resides in the wide multitude of diseases that can be targeted by selectively modulating the different isoforms.[34-58]

CA I is abundantly expressed in red blood cells and colon, but is still considered an "orphan target" as it remains an "obscure object" for medicinal chemists.[13,35] However, several pieces of evidence have demonstrated that CA I is involved in some types of anemia and chronic acidosis, diabetic macular edema, and proliferative diabetic retinopathy.[13,27]

The deregulation of the activity of the most physiologically relevant CA II has important pathological consequences in one or more tissues, such as glaucoma, edema, epilepsy, and is also involved in other pathologies such as acute mountain sickness[22] and, apparently, atherosclerosis[21] and osteoporosis.[27] CA II is also a target for imaging in various pathological conditions, in organs where the enzyme is present, such as the brain and cerebrospinal fluid of the gastrointestinal tract.[13]

Inhibition of CA III has not been determined to be advantageous for treating several diseases.[13] On the contrary, several natural and non-natural amino acid and

aromatic/heterocyclic activators of CA III have been discovered, which might increase the defense mechanism against reactive oxygen species (ROS) in hepatocytes especially in the case of hepatotumorogenesis or infection by hepatitis B or C virus or might be beneficial therapeutics aimed to treat obesity.[27,37] However, because CA III has recently been proposed to be associated with acute myeloid leukemia and the progression of liver carcinoma, CA III specific inhibitors may have potential against tumor proliferation and invasiveness in myeloid and liver tissue.[50]

CA IV was proven to be a promising drug target in the treatment of glaucoma, inflammation, retinitis pigmentosa, some types of brain cancers, and stroke.[35-38]

The involvement of CA VA and VB in *de novo* lipogenesis and the clear indications that the antiepileptic drugs topiramate and zonisamide (also potent inhibitors of the mitochondrial CAs) elicit significant weight loss in obese patients suffering from epilepsy, led pharmaceutical companies to show interest in hCA V enzymes as novel drug targets for the treatment of obesity.[40] Activators of CA V (probably CA VB) might have clinical potential in diabetes, due to the implication of CA V in glucose-mediated insulin secretion from pancreatic β-cells.[27] CA VA has been also recently proposed as a specific target for the prevention of diabetic cerebrovascular pathology.[13]

It could be speculated that the caries-inducing effect of CA VI is a result of enzymatic activity, and thus the inhibition of CA VI could reduce carcinogenesis. A CA inhibitor might be added to oral hygiene products, such as toothpaste, mouthwash, tooth varnish, and chewing gum, to reduce the risk for the formation of enamel caries lesions.[43,44]

CA VII might represent a safe drug-target in the treatment of febrile seizures or eventually other epileptiform diseases as it is involved in these pathologies and is almost uniquely expressed in the central nervous system (CNS).[27,45] As the treatment with acetazolamide in combination with midazolam synergistically reduces neuropathic allodynia after spinal nerve damage,[47] CA VII together with CA II may represent a new drug target for managing neuropathic pain. Considering the importance of pH and ion homeostasis in reproductive organs to ensure normal fertilization, the use of CA XIII inhibitors could be used for the development of anti-contraceptive agents.[55]

Data are available on the involvement of CA XIV in some retinopathies and epileptogenesis, which make CA XIV inhibitors useful agents for the management of such diseases.[57]
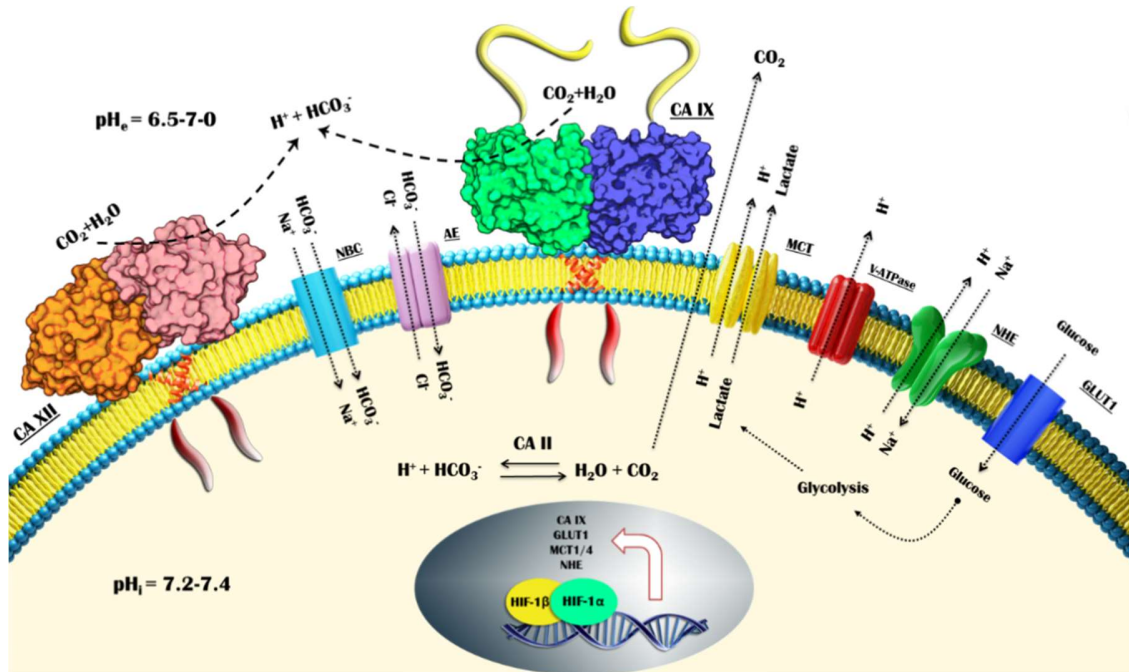
Figure 9. pH modulation machinery in hypoxic tumor cells. HIF-1 upregulates the expression of glucose transporters (GLUT1), glycolytic enzymes and proteins involved in pH regulation: monocarboxylate transporter (MCT), V-type H^+ATP (V-ATPase), Na^+/H^+ exchanger (NHE), bicarbonate co-transport (NBC), anion exchanger (AE), carbonic anhydrase IX (CA IX) and XII (CA XII).

The tumor (and inflammation) associated CA IX and XII were consistently validated as drug-targets and markers of disease progression in many solid tumors.[23,48,49] Overexpression of tumor-associated CAs is part of tumor cells adaptive responses to hypoxic conditions.[48] In fact, the inadequate delivery of oxygen to tumor cells (hypoxia) does induce a shift to glycolytic metabolism. The high glycolytic rate of tumor cells leads to increased production of acid metabolites, including lactate, carbon dioxide, and protons that creates an intracellular acidosis (pH_i) incompatible with the basic cellular functions. To survive and reduce intracellular acidification, cells activate complex molecular mechanisms involving ion exchangers, pumps, transporters, and carbonic anhydrases, which maintain a slightly alkaline pH_i acidifying the extracellular environment (pH_e) (Figure 9).[23]

CA IX was even more studied in this context being almost uniquely overexpressed in hypoxic tumors by the major pathway of HIF-1 transcription factor and serving as a prognostic/predictive factor for hypoxic, aggressive, and malignant tumors.[29,49] Nonetheless, both CA IX and XII were shown to be involved in chemoresistance, tumor cell migration, invasion, and maintenance of cancer cell stemness.[13,23]

Besides, CA IX and XII were lately identified to be overexpressed in inflamed tissues, being likely implicated in the acidification marking these tissues.[39] Furthermore, CA XII is also a validated target for the treatment of glaucoma.[34]

The 3D structures are available for all human isoforms except CA VA and VB and are of significant importance for structure-based drug design campaigns for yielding disease-targeting CA selective modulators.[59-68]

1.4.2 Carbonic anhydrases from pathogens

CAs are also emerging as innovative targets for the development of anti-infective agents with novel mechanisms of action to overcome cross-resistance shown against various existing anti-microbial drugs. A *plethora* of α-, β-, γ-CAs were cloned and characterized in many bacterial, fungal and protozoan pathogens and were shown to be promising anti-infective targets, though to date no CAI as anti-microbial agent is available for clinical use. CAs are essential in the pathogens life cycle and their inhibition can lead to growth impairment and defects.[15,69] One of the best-studied bacterial α-CA is the one from the gastric pathogen provoking ulcer and gastric cancer, *Helicobacter pylori*.[70-72] In fact, the genome of *H. pylori* encodes two CAs with different subcellular localization: a periplasmic α-class CA (hpαCA) and a cytoplasmic β-class CA (hpβCA).[70-72] These two enzymes were shown to be catalytically efficient, exhibiting an almost identical activity as the human isoform hCA I in the CO_2 hydration reaction, and are highly inhibited by many clinically used sulfonamides/sulfamates.[72] Since the efficacy of *H. pylori* eradication therapies currently employed has been decreasing due to drug resistance and side effects of the commonly used drugs, the dual inhibition of α- and/or β-CAs of *H. pylori* could be applied as an alternative

therapy against the infection or for the prevention of gastroduodenal diseases provoked by this widespread pathogen.[71,72]

Vibrio cholerae is a Gram-negative bacterium, the causative agent of cholera, that colonizes the upper small intestine where sodium bicarbonate, an inducer of virulence gene expression, is present at a high concentration. *V. cholera* utilizes the CA system to accumulate bicarbonate into its cells, thus suggesting a pivotal role of these metalloenzymes in the microbial virulence.[73] *V. cholera* encodes CAs of three distinct classes, which are called VchCA (α-CA), VchCAβ and VchCAγ. These enzymes are efficient catalysts for CO_2 hydration.[73,74]

CAs are also abundantly spread in fungi and yeasts.[21,75-80] *Saccharomyces cerevisiae*,[79] *Candida albicans*[75,76,] and *Candida glabrata*[76,77] have only one β-CA, whereas multiple copies of β-CA- and α-CA-encoding genes were reported in other fungi.[78] A recent work demonstrated that these CAs play an important role in the CO_2-sensing of the fungal pathogens and the regulation of sexual development.[77] Finally, another yeast, which has been investigated in detail for the presence of CAs is *Malassezia globosa*, which induced the production of dandruff.[80] As the above-mentioned fungi/yeasts, it contains only one β-CA, denominated MgCA. Few protozoan parasites have been investigated for the presence and druggability of CAs. The malaria-provoking *Plasmodium falciparum* encodes the unique example of η-CA identified to date.[7,78-83] An α-CA has also been cloned and characterized in the unicellular protozoan *Trypanosoma cruzi*, the causative agent of Chagas disease.[74-85] The enzyme (TcCA) has a very high catalytic activity for the CO_2 hydration reaction, being similar kinetically to the human isoform hCA II.

In addition, another β-CA from the unicellular parasitic protozoan *Leishmania donovani chagasi* (LdcCA), which causes visceral leishmaniasis was identified, cloned and characterized.[86]

1.4.3 Main categories of carbonic anhydrase inhibitors

The mechanisms through which CAs are inhibited or activated have been studied for decades and are well-understood processes. However, new discoveries in the field continuously

emerge.[3,87-127] Four inhibition mechanisms have been kinetically and structurally validated, while a significant subset of CA inhibitors lacks mechanistic characterization yet. A superimposition of compounds binding to the representative CA II by four distinct inhibition mechanisms is depicted in Figure 10 and classification is reported below:
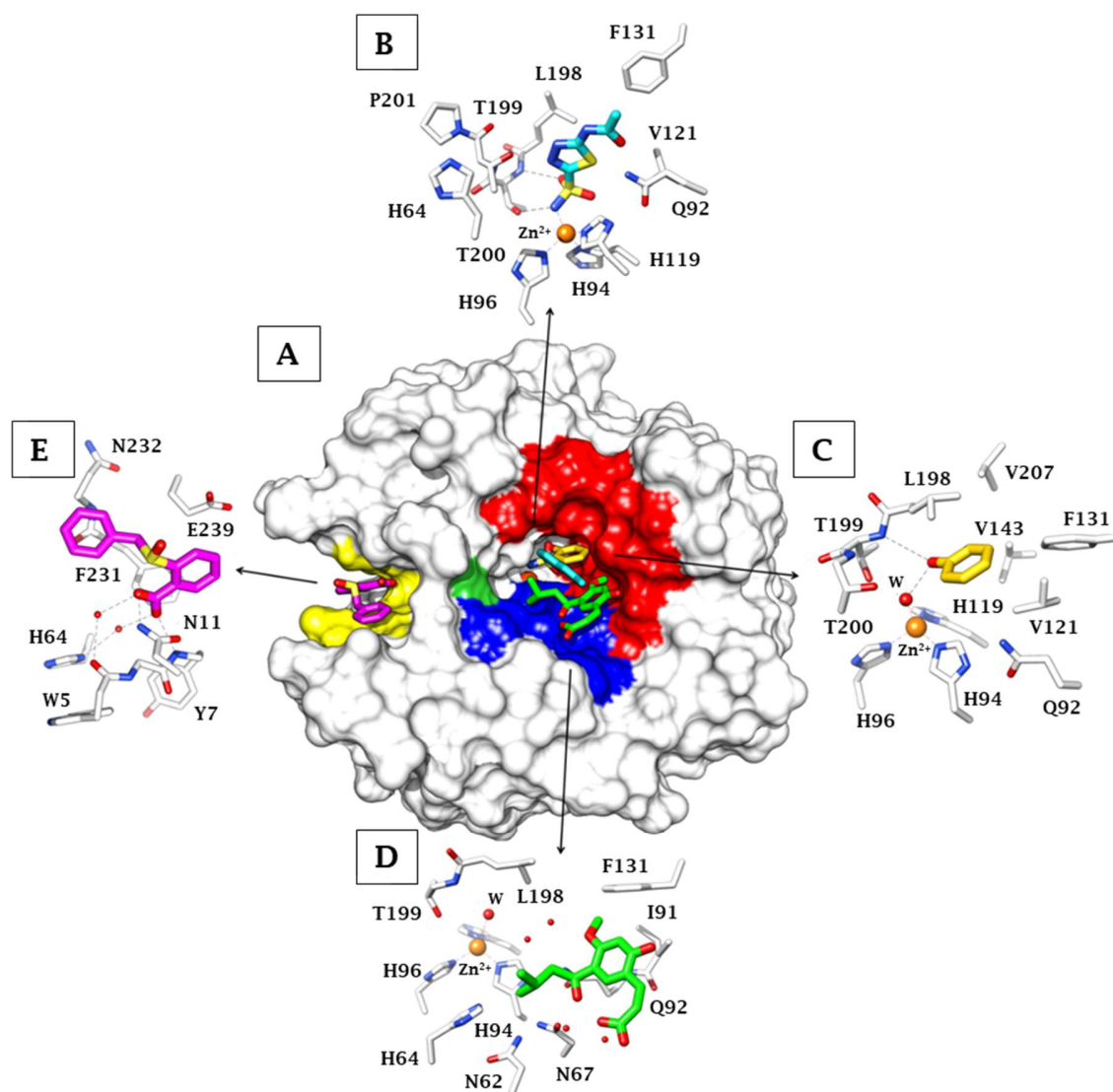
Figure 10. (A) hCA II active site with three superimposed inhibitors: acetazolamide (blue); phenol (yellow), hydrolyzed natural product coumarin (green). The hydrophobic half of the active site is colored in red, the hydrophilic one in blue. His64, the proton shuttle residue is in green (surface representation) (PDB files codes: 3HS4, 3F8E, 4QY3). The hydrophobic adjacent pocket where inhibitors bind outside the active site is shown in yellow with a benzoic acid derivative represented in magenta. The detailed interactions for the binding of the

four inhibitors, with their different inhibition mechanisms, are shown in (B) for acetazolamide, (C) for phenol, (D) for the 2-hydroxy-cinnamic acid derivative, and (E) for the benzoic acid derivative.

a) the zinc-binders, among which inorganic anions, sulfonamides, and their bioisosteres (sulfamides, sulfonates, sulfamates), monothiocarbamates, dithiocarbamates, xanthates, thioxanthenes, hydroxamates, carboxylates, phosphates, selenols, benzoxaboroles (Figure 10B).[91-111]

b) compounds that anchor to the zinc-bound water molecule/hydroxide ion, such as phenols, thiophenols, polyphenols, carboxylates, polyamines, 2-thioxocoumarins, sulfocoumarins (Figure 10C).[112-119]

c) compounds that occlude the entrance of the active site, namely coumarins and their bioisosteres (Figure 10D).[120-127]

d) compounds binding out of the active site (to date this inhibition mechanism has been shown uniquely for 2-(benzylsulfonyl)-benzoic acid – Figure 10E).[128]

Compounds such as secondary/tertiary sulfonamides, N-substituted saccharin, imatinib, and nilotinib inhibit specific CA by an unknown mechanism of action.[129,130]

Among these categories, compounds belonging to a, b and c classes are described more in-depth.

1.4.3.1 Zinc binders
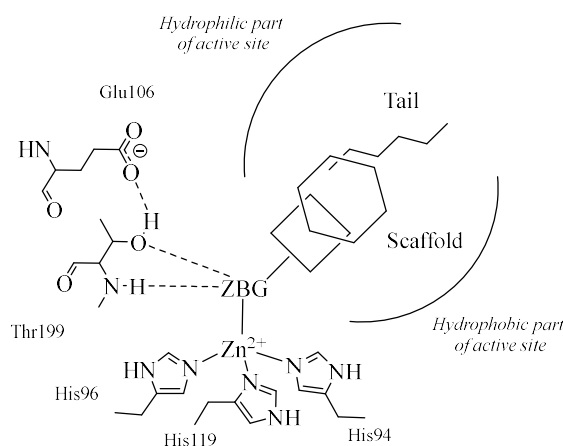
Figure 11. Schematic illustration of the key interactions between a zinc-binder and a representative human CA active site.

Compounds containing a zinc-binding group (ZBG) directly coordinate the metal ion with a tetrahedral or trigonal bipyramidal geometry, displacing the zinc-bound nucleophile (water molecule or hydroxide ion; Figure 11).[1-3,81] In addition, the ZBG interacts with various residues (i.e. such as with T199, a conserved residue in all α-CAs) nearby the metal ion, mainly by hydrogen bonds, whereas the scaffold of the inhibitor participates in several other interactions with the hydrophilic and/or hydrophobic areas of the active site. The sulfonamide group (R-SO$_2$NH$_2$) is the most important and widely used zinc-binding function for designing CAIs,[87-91] with at least 20 such compounds in clinical use for decades or clinical development in the last period (Figure 12).[87-93]
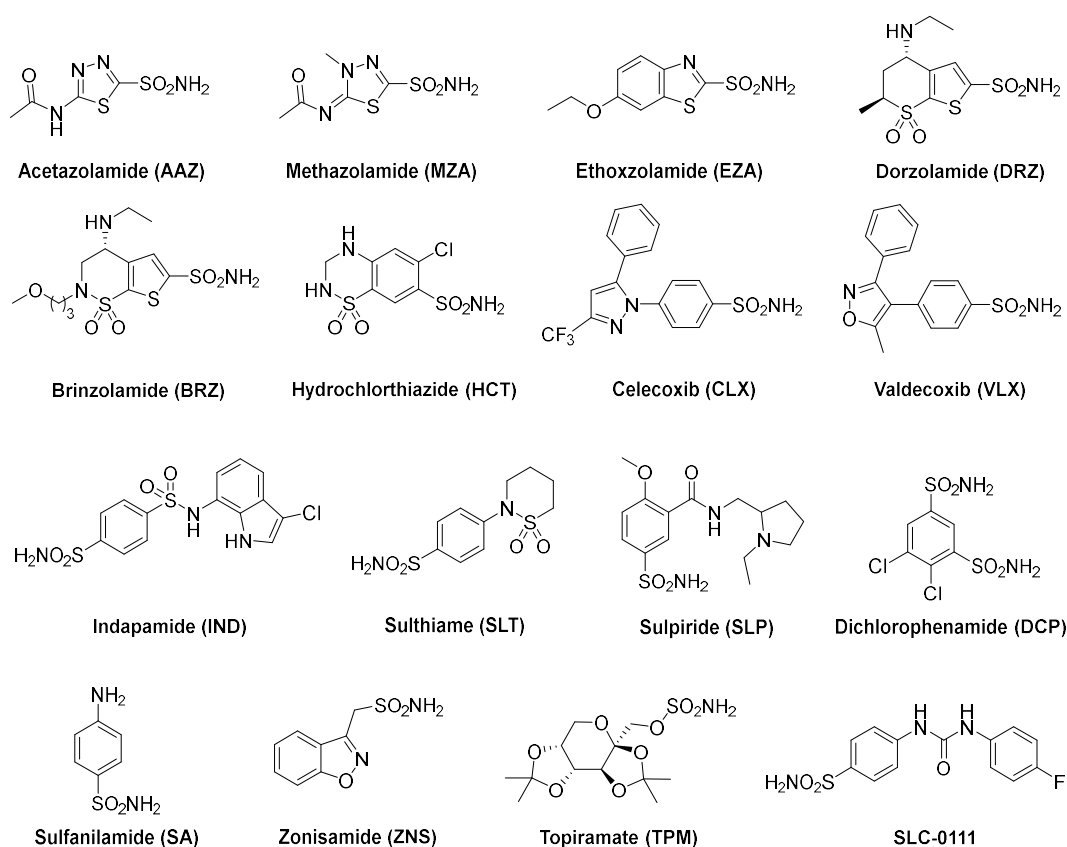
Figure 12. Examples of clinically used or studied sulfonamides.

A wealth of X-ray crystallographic evidence showed the binding mode of the zinc-binder-type CAIs, to which sulfonamides and their bioisosteres sulfamates and sulfamides belong.

21

The latter binds in the deprotonated form to the Zn(II) ion from the enzyme active site, replacing the zinc-bound water molecule and retaining the tetrahedral coordination geometry (Figure 13).[1,2,90,91,93]

Figure 13. Schematic illustration of the key interactions between a primary sulfonamide and the hCA II active site as determined by X-ray crystallography.

It is commonly accepted that the sulfonamide group is the ideal ZBG for the CAs as it combines a negative charge of the deprotonated nitrogen with the positively charged zinc ion and, on the other hand, the presence of one proton on the coordinated nitrogen atom satisfies the hydrogen bond acceptor character of T199 OG1 atom.[1-3]

The first- and second-generation sulfonamide CAIs and their sulfamate/sulfamide analogs act as non-selective and rather efficient inhibitors of all CA isoforms. The consequence of this inhibition profile is the multitude of undesired side effects due to inhibition of isoforms not involved in the targeted pathology. This was and it is in fact the main drawback of the first- and second-generation CAIs, although they are still in clinical use.[1-3] As most differences among hCAs active site occur at the entrance of the cavity, compounds that would interact with that part may lead to isoform-selective inhibitors. Thus, the idea to attach "tails" to the scaffolds of the sulfonamide inhibitors emerged in 1999,[91-93] and indeed led to a certain degree of isoform selectivity already with the initial derivatives for which it has been proposed. Originally conceived for the design of water-soluble, antiglaucoma sulfonamides,[96-98] the tail approach was subsequently extended for the design of a multitude

of CAIs possessing a variety of desired physicochemical properties, among which membrane impermeability,[98] enhanced liposolubility,[97] and more importantly, isoform-selective inhibitory profiles.[3] In fact, nowadays it is the most used synthetic approach for designing CAIs belonging to a variety of classes. The main outcome to date of the application of the tail approach is an ureidobenzenesulfonamide **SLC-0111** (Figure 12), selective inhibitor of CAs IX and XII over CAs I and II, which successfully completed Phase I clinical trials for the treatment of advanced, metastatic hypoxic tumors over-expressing hCA IX, and is currently in Phase Ib/II clinical trials in a multi-center, open-label study of oral in combination with gemcitabine (administered *i.v.*) in subjects affected by metastatic pancreatic ductal adenocarcinoma.[99,100]

Beyond sulfonamides, in the last period, a multitude of new ZBG for CAs have been identified, among which carboxylates,[105,106] hydroxamates,[107,108] phosphonates.[109] Lately crucial advances have been made in this field with mono- and dithiocarbammates,[101-103] xanthates,[103] thioxanthates,[103] boroles,[110] phosphonamidates,[109] and selenols[111] identified as novel zinc-binders. X-ray crystallographic evidence was achieved for dithiocarbamates (Figure 14A) and their derivatives,[101] hydroxamates,[107] some carboxylates,[105] one phosphonate,[109] and some boroles (Figure 14B).[110] It should be stressed that a certain versatility was observed in the binding mode of some such ZBGs, with hydroxamates and boroles coordinating the metal ion in monodentate or bidentate manners.[91]
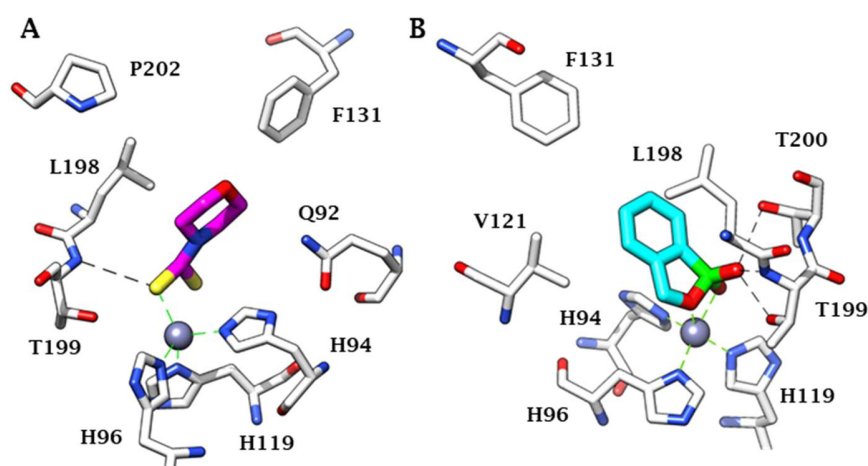

Figure 14. Active site view of the hCA II adduct with (A) a DTC (PDB 3P5A) and (B) benzoxaborole (PDB 5JQT).

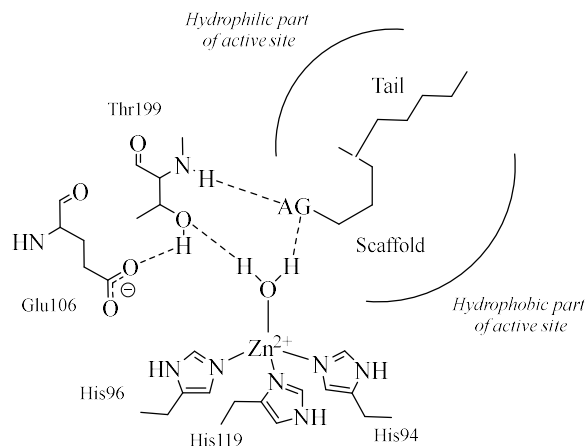## 1.4.3.2 Anchorage to the metal-bound water/hydroxide ion

Figure 15. Compounds that anchor to the Zn(II)-coordinated water molecule/hydroxide ion. The anchoring group (**AG**) is of the phenol, amino, carboxylic acid, ester (COOR), sulfonate type.

Phenols, polyamines (*e.g.* spermine and spermidine), some carboxylates, sulfocoumarins (after having been hydrolyzed by the sulfatase activity of α-CAs to the corresponding hydroxyphenyl-ω-ethenylsulfonic acid), and thioxocoumarins have been chronologically shown to anchor to the zinc-bound water molecule/hydroxide ion by means of X-ray crystallography (Figure 15).[112-119,131] The anchoring is granted by an H-bond between the zinc-ligand and a precise anchoring group (AG) in the inhibitor of the OH, NH_2, COOH, $COOCH_3$, and SO_3H type. As in the case of zinc-binders, the ligand/target adduct is stabilized by further interactions the inhibitor scaffold establishes with amino acid residues from the active site.

The phenol is anchored to the Zn-bound hydroxide ion i.e. the preponderant species at the pH of experimental conditions, by a hydrogen bond between the donor zinc bound hydroxide ion (E-M^{2+}– OH^-) and the ligand OH.[112] In addition, a second hydrogen bond involves the gate-keeping residue Thr199, whose backbone NH group participates in a second hydrogen bond with the phenol (Figure 16A).
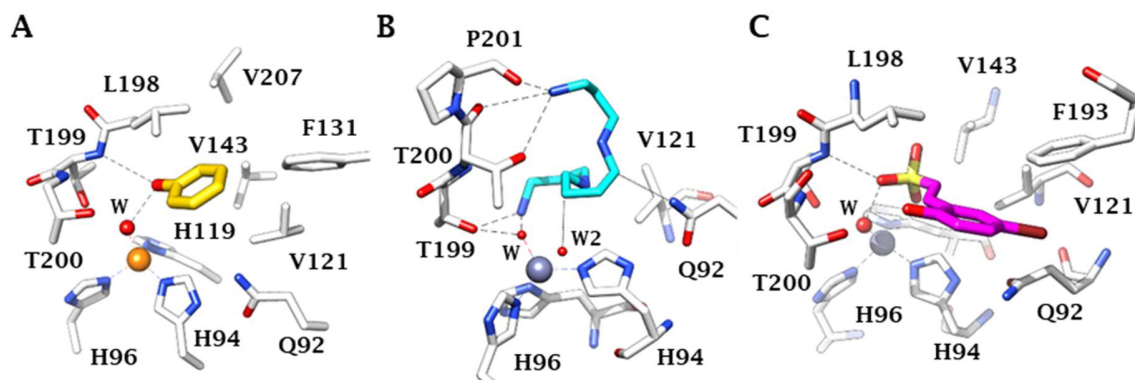
Figure 16. Active site view of the hCA II adduct with (A) phenol, (B) spermine (PDB 3KWA), and (C) hydroxyphenyl-ω-ethenylsulfonic acid deriving from sulfocoumarin hydrolysis (PDB 4BCW).

Spermine binds in a rather similar manner as phenol, although with a slightly different network of hydrogen bonding (Figure 16A).[114] Thus, one of the primary amine moieties of the inhibitor, probably as ammonium salt, anchors by means of a hydrogen bond to the zinc-coordinated water molecule/hydroxide ion, and also makes a second hydrogen bond with the side chain OH group of Thr199. The other terminal primary amine of spermine participates in hydrogen bonding with Thr200 and Pro201 (Figure 16B). The sulfonic acid from the hydrolyzed sulfocoumarin derivative was found to anchor to the Zn-bound hydroxide ion, thus making this CA inhibition mechanism much more general than initially considered when phenols were discovered as inhibitors (Figure 16C).[118]

1.4.3.3 Occlusion of the active site entrance
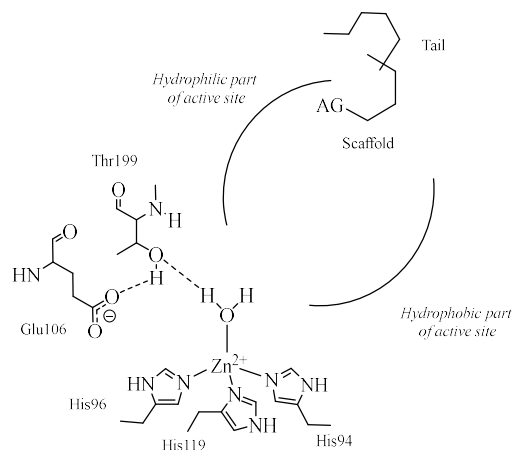
Figure 17. Schematic representation of compounds occluding the entrance to the active site. **AG** represents an anchoring group, of the phenol, carboxylic acid, or amide-type for sticking at the entrance of the active site cavity whereas the tail, when present, interacts with residues at the outer edge of the cleft.

The third main CA inhibition mechanism consists of the active site entrance occlusion (Figure 17). These inhibitors bind further away from the metal ion compared to the zinc binders in compounds anchoring to the zinc coordinated water molecule.[3,81] The occlusion of the entrance of the binding site cavity as inhibition mechanism, has been proposed for the first time for coumarins,[120] but thereafter other compounds such as the antiepileptic drug lacosamide,[121] 5- and 6-membered lactones and thiolactones or quinolinones[123-125] were observed to possess significant CA inhibitory properties probably sharing a common mechanism of action (Figure 18).

Figure 18. Proposed inhibition mechanism of CAs by coumarins/thiocoumarins, leading to *cis-* or *trans*-2-hydroxy/mercapto-cinnamic acids. A) Hydrolysis of the lactone ring. B) Movement of the hydrolysis product (as *cis* stereoisomer) towards the entrance of the active site cavity. C. *Cis-trans* isomerization of the hydrolysis product.[121]

X-ray crystallography studies primarily carried out on the coumarin derivatives isolated from the Australian plant *Leionema ellipticum* showed that coumarins (as the sul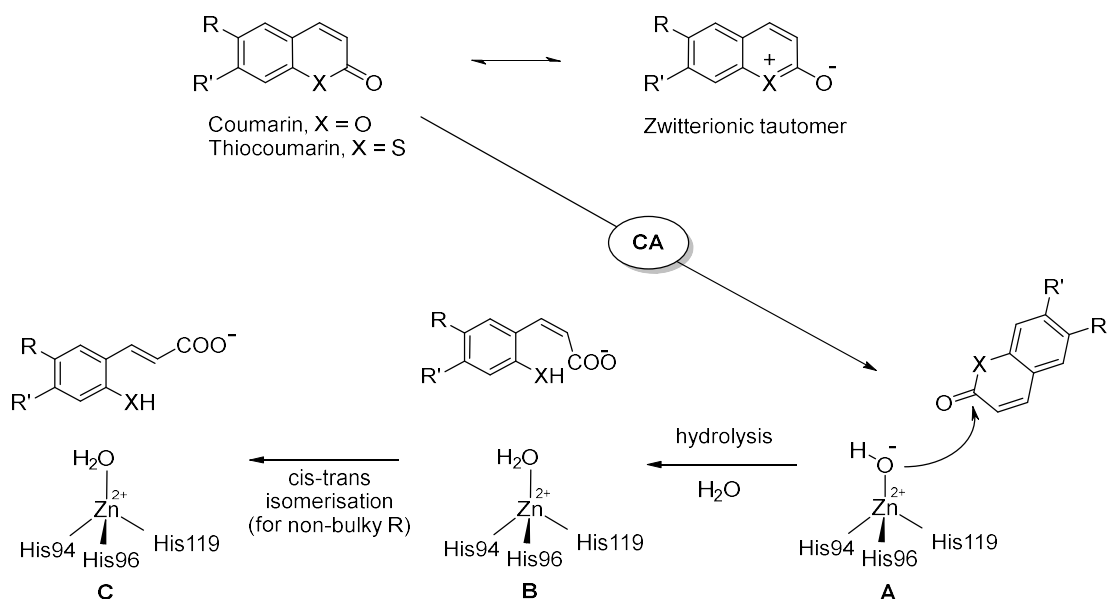focoumarins) acts as prodrug - at least- in human CAs and are hydrolyzed to the active species 2-hydroxycinnamic acids by the CA esterase activity (Figure 18).[120] In fact, unexpectedly the electron density data for the hCA II adduct with coumarins revealed that the actual inhibitory species is the coumarin hydrolyzed form that, depending on how bulky the moieties attached on the scaffold are, might bind as *cis* isomers (Figure 19A) or as *trans*-isomers (Figure 19B). Indeed, for the not bulky substitution pattern on the coumarin scaffold, the trans isomer was observed in the CA active site, whereas for bulkier such groups the isomerization did not occur.

The most notable aspect of this inhibition mechanism is the fact that the inhibitors bind in an active site region where more significant differences in the amino acid compositions among hCAs occur.[1-3] This produces important consequences in the inhibition profiles exhibited by such a class of derivatives which showed a unique isoform-selective action. In fact, wide series of diversely substituted coumarin/thiocoumarin derivatives were investigated which

reported significantly selective inhibition against isoforms such as CA IX, XII, XIII, and XIV over the ubiquitous CA I and II.[120-127]
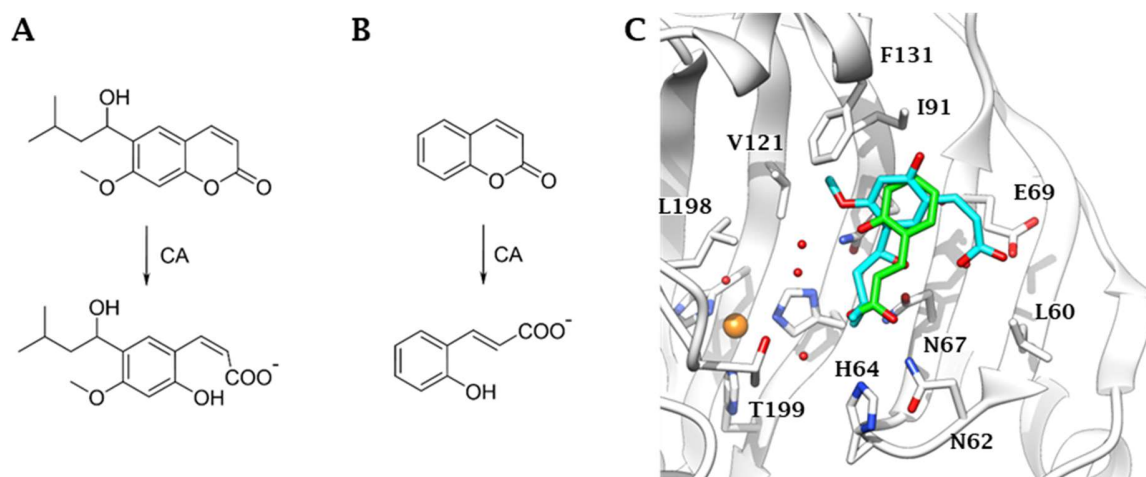
Figure 19. CA-mediated hydrolysis of (A) the coumarin extracted from *Leionema ellipticum* and (B) coumarin. (C) Active site view of the superimposed hCA II adducts with of the coumarins hydrolysis products shown in panel A (blue, PDB 3F8E) and B (green PDB 5BNL).

1.4.4 Carbonic anhydrase activators

CA activation with biogenic amines, such as histamine, amino acids, and peptides was reported in the early 40s, but it was validated only in the late 90s.[1] Using methods such as stopped-flow kinetic assays, spectroscopy, and X-ray crystallography, the CA activators (CAAs) were shown to take part in the catalytic cycle, as shown in equation 10 below.[132-134]

$$EZn^{2+}-OH_2 + A \rightleftharpoons [EZn^{2+}-OH_2 - A] \rightleftharpoons [EZn^{2+}-HO^- - AH^+] \rightleftharpoons EZn^{2+}-HO^- + AH^+ \text{ (Eq. 10)}$$
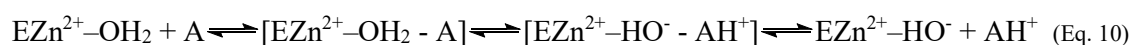
The CAA binds within the enzyme active site with the formation of the enzyme – activator complex. The activator participates in the rate-determining step of the catalytic cycle, which is the proton shuttling between the zinc coordinated water and the reaction medium. In many CA isoforms, His64 placed in the middle of the CA active site plays this role through its imidazole moiety with a pK_a in the range of 6-7.[33] In the enzyme-activator complexes, this proton transfer reaction is achieved more efficiently both by His64 and the activator

molecule. The activator does not influence K_M (the affinity for the substrate) but affects the k_{cat} of the enzyme-catalyzed reaction, thus leading to the efficient formation of the nucleophilic species of the enzyme (EZn^{2+}–OH^-).[13,33]

To date, several X-ray crystal structures of CAAs bound to several hCA isoforms have been reported (Figure 20).[132-137] The histamine–hCA II adduct crystallography was the first published such study,[132] and successively activators of the amines and amino acid type, such as L- and D-His, L- and D-Phe, D-Trp and L-adrenaline were studied by this technique.[3,13,132-137] All these activators except D-Trp bind in the same region of the CA active site, which has been denominated the activator binding site A (Figure 20).[33]

In this position, at the entrance of the active site and not far away from His64, the activator participates in favorable interactions with several amino acid residues and water molecules, supplementing the proton shuttling effects of His64.

It is supervising the activators and the coumarins binding sites are in fact superimposable, as shown in Figure 20.
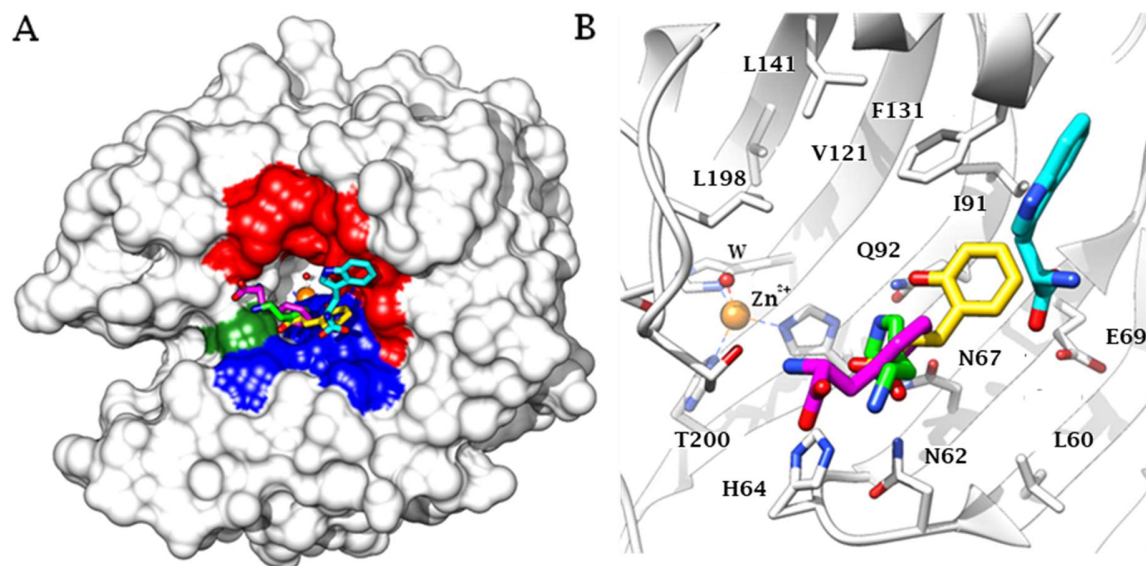
Figure 20. hCA II complexed with CAAs and the hydrolyzed coumarin (2-hydroxycinnamic acid). Histamine is shown in green (PDB 1AVN) D-Phe in magenta (PDB 2EZ7) and D-Trp in cyan (PDB 3EFI). 2-Hydroxycinnamic acid (in yellow, PDB 5BNL) is also superimposed to the hCA II – activator adducts. a) Complete view of the enzyme-ligands superimposed adducts. b) Active site view of the three activators and the hydrolyzed coumarin in a slightly different orientation, compared to panel A.

A series of drug design studies are also available for CAAs, mainly using histamine and histidine as lead molecules.[3,33] Some of these compounds showed an increased affinity for many CA isoforms (compared to histamine), but the level of isoform selectivity achieved up to now is very poor.[3]

The present Ph.D. thesis mainly focused on CA isoforms belonging to α-, β-, and γ- classes and concerns ligands that act as zinc-binders and anchor to the zinc-bound water molecule/hydroxide ion.

Chapter 2. GABA receptors: classification and pharmacological complexity

GABA is the principal mediator of inhibitory synaptic transmission in the mammalian brain and it exerts its effects via two different types of GABA receptors (GABARs). While fast ionotropic GABA$_A$ receptors (GABA$_A$Rs) belong to the family of ligand-gated ion channels, metabotropic GABA$_B$ receptors (GABA$_B$Rs) are coupled to G-proteins. Activation of GABARs induces membrane hyperpolarization, reduces the frequency of the generation of action potentials, and results in inhibition. Mainly local-circuit interneurons that constitute 15-20% of all cortical neurons predominantly use GABA as the neurotransmitter.[138-140]

GABA exerts most of its effects by stimulating GABA$_A$Rs, which can be:

- incorporated into the postsynaptic membrane where they mediate transient and fast synaptic inhibition occurring in milliseconds,

- situated in extrasynaptic locations where they respond to environmental GABA concentrations and mediate a long-term inhibition,

- located at a presynaptic level to regulate the neurotransmitter release in synapses.

In fast synaptic inhibition, GABA is released from the presynaptic membrane terminals and rapidly diffuses across the synaptic cleft, achieving its binding sites at postsynaptic GABA$_A$Rs. Subsequently, these receptors undergo a rapid conformational change that produces the opening of the channel, allowing the flow of chloride ions along their chemical gradient through the postsynaptic membrane. This ensures the propagation of neurotransmission and represents the basis of neural communication.[141,142]

Several drugs act on distinct binding sites on the GABA$_A$Rs and modulate GABA action, such as the selective agonist muscimol, the principal psychoactive constituent of the mushroom *Amanita muscaria*, the partial agonist gaboxadol, the competitive antagonists bicuculline and picrotoxin, that selectively prevent inhibitory action of the neurotransmitter, and a wide variety of clinically important drugs, including anticonvulsants (e.g., loreclezole), anxiolytics (benzodiazepines such as diazepam), general anesthetics (e.g., isoflurane, enflurane, (+)-etomidate and propofol), barbiturates (e.g., phenobarbital), neuroactive

stereoids (e.g., allopregnanolone), and ethanol, that are allosteric modulators of these receptors (Figure 21).[142,143]

ORTHOSTERIC LIGANDS

GABA
(neurotransmitter)

Muscimol
(agonist)

Gabaxadol
(partial agonist)

Bicuculline
(antagonist)

Picrotoxin
(antagonist)

ALLOSTERIC LIGANDS

Diazepam
(agonist)

Zolpidem
(agonist)

DMCM
(inverse agonist)

Flumazenil
(antagonist)

Ethanol

Loreclezole

Isoflurane

Enflurane

Phenobarbital

Propofol

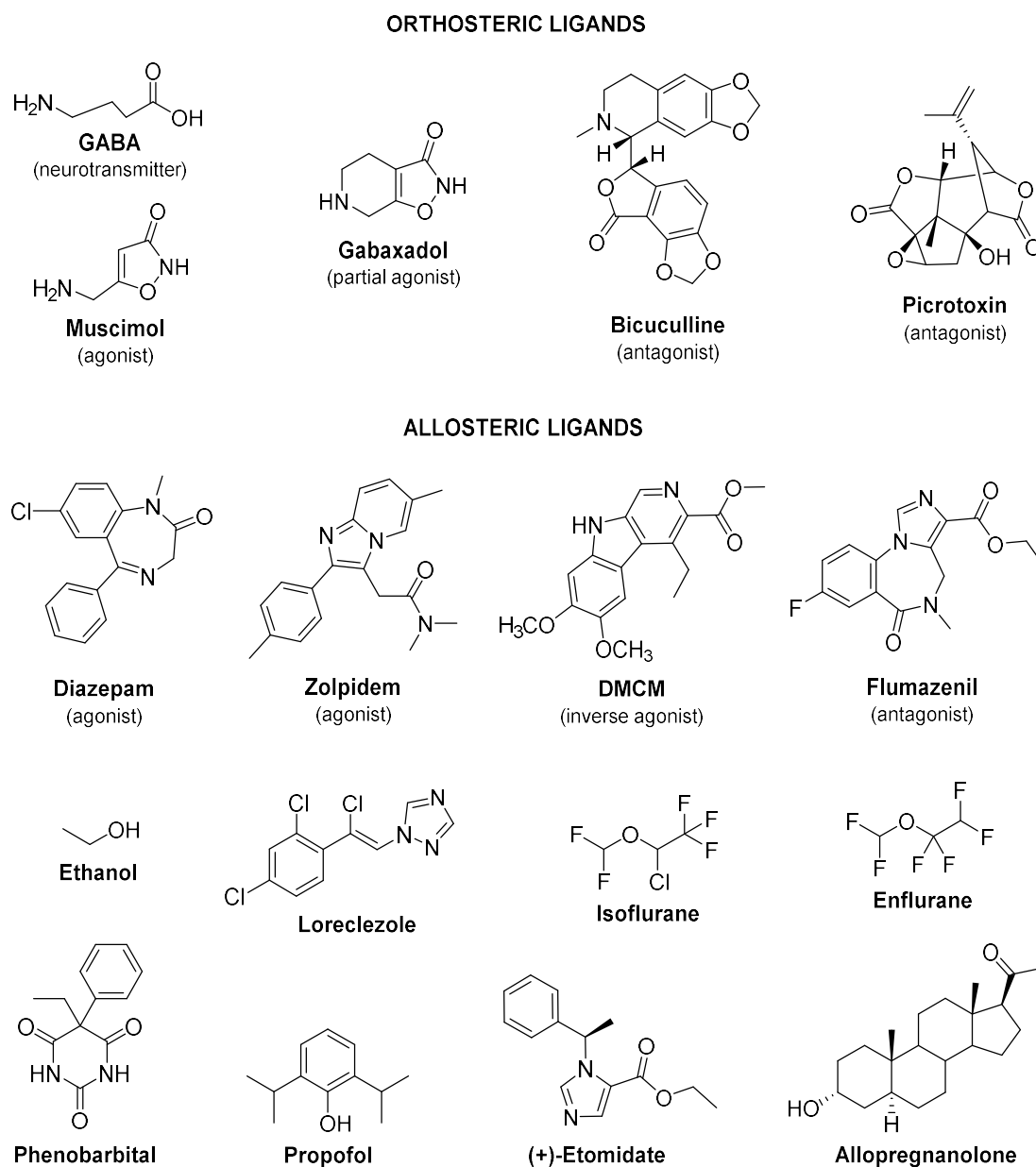**(+)-Etomidate**

Allopregnanolone

Figure 21. Chemical structures of orthosteric and allosteric ligands of GABA$_A$Rs.

The different binding and activity of all these drugs, together with the structural diversity of GABA$_A$Rs, shape the complex nature of GABA$_A$Rs pharmacology, although simultaneously

offer a great opportunity for the design of novel and more selective compounds for improved therapeutic applications.[144] Unfortunately, there are severe problems related to the long-term use of drugs acting at GABA$_A$Rs, that include loss of efficacy, and development of tolerance and dependence, widely limiting the time window of their desirable therapeutic benefits.[141,145-148]

As previously mentioned, GABA also achieves inhibitory effects by acting at G-protein-coupled metabotropic GABA$_B$ receptors (GABA$_B$Rs). The slow, longer-lasting inhibition of GABA$_B$Rs is mediated by indirect gating of either potassium or calcium channels by second messengers. The characteristic GABA analogs, that act as GABA$_B$Rs agonists, are baclofen and 3-aminopropylphosphinic acid (3-APPA), while saclofen, phaclofen and 2-hydroxysaclofen act as antagonists of GABA$_B$Rs (Figure 22).[149]
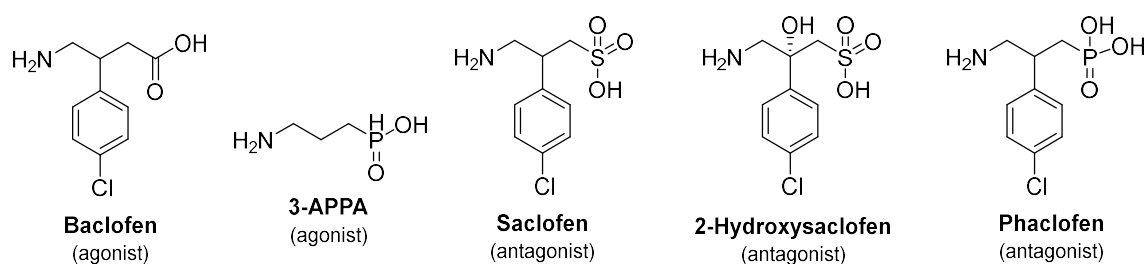
Figure 22. Chemical structures of agonists and antagonists of GABA$_B$Rs.

Moreover, old nomenclature also included GABA$_C$ receptors (GABA$_C$Rs), predominantly expressed in the retina. However, the International Union of Basic and Clinical Pharmacology has recommended that GABA$_C$Rs should be assumed as one of the many isoforms of GABA$_A$Rs, namely are GABA$_A$-ρ receptors.[142]

2.1 GABA$_A$ receptors

GABA$_A$ receptors are ubiquitously expressed and are the major receptors of inhibitory neurotransmission across the central nervous system (CNS) that play a major role in virtually all brain physiological functions. They are homo- or heteropentameric ligand-gated proteins that form a specific transmembrane channel for chloride ions (Figure 23). These receptors

are members of the Cys-loop ligand-gated ion channel superfamily due to the presence of a disulfide-bridged loop in the extracellular domain, which includes nicotinic acetylcholine (nACh), 5-hydroxytryptamine type 3 (5HT$_3$) and glycine receptors, sharing structural and functional homology with the members of this family.[150,151]
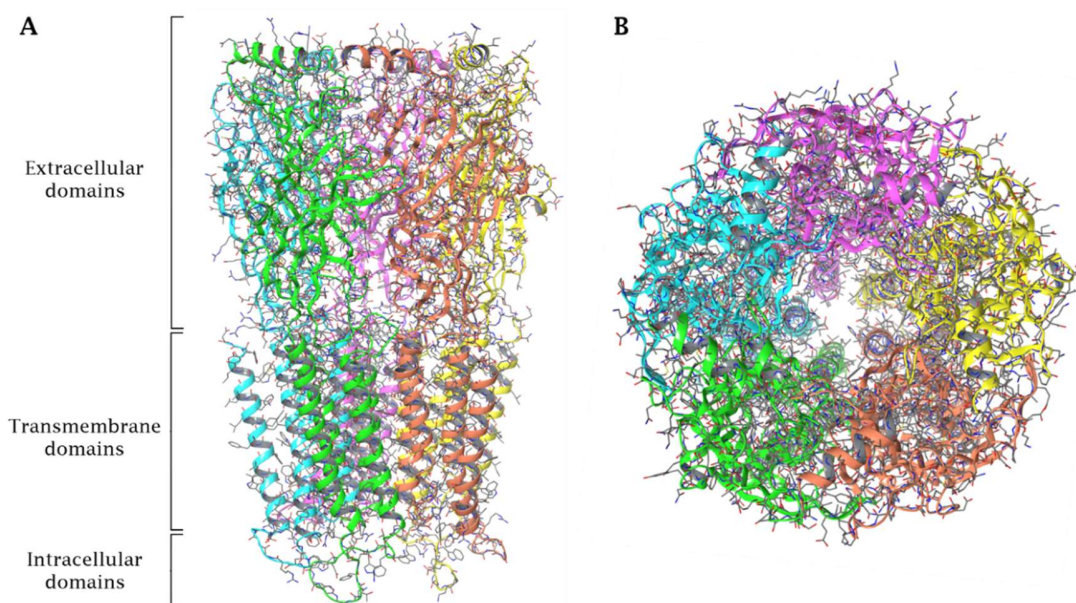
Figure 23. (A) Longitudinal and (B) extracellular view of the pentameric ligand-gated chlorine channel GABA$_A$R.

GABA$_A$ receptors are assembled by several subunits that are encoded from a pool of 19 different genes, identified by molecular cloning techniques. These are six α (α$_{1-6}$), three β (β$_{1-3}$), three γ (γ$_{1-3}$), δ, ε, θ, π, and three ρ (ρ$_{1-3}$).[143,151-153] Some subunits are broadly expressed throughout the CNS, while others exhibit a more restricted expression.[154,155] For example, the most abundant α$_1$ subunit is expressed almost ubiquitously in the brain, α$_5$ is highly expressed in the hippocampus, α$_6$ subunit is expressed only in granule cells of the cerebellum, while ρ-subunits, the major molecular components of the formerly called GABA$_A$-ρ receptors, are expressed mainly in the retina.[156-159] Moreover, the β$_2$ and β$_3$ subunits expression is strongly related with that of α$_1$ and α$_2$, respectively, whereas among the γ subunits the γ$_2$ isoform is the most widely distributed.[154] Each GABA$_A$ receptor subtype, composed of different subunits, represents distinct receptor populations with unique

functional and pharmacological properties, that are differentially regulated at the transcriptional, post-transcriptional, and translational levels.[160]

During the development of CNS, the receptor subtypes are expressed in a specific spatio-temporal pattern. In the adult brain, the most prevalent combination of $\alpha_1\beta_2\gamma_2$ subunits is broadly distributed in different brain areas, while the expression of some other subtypes of GABA$_A$Rs is restricted to specific regions.[161]

Mature subunits have approximately 450 amino acid residues in length and share a common topological organization that consists of a large extracellular N-terminal domain, containing the already mentioned Cys loop, followed by four transmembrane domains (TM1-TM4), and a short extracellular C-terminal domain (Figure 23).

TM2 domains of all five subunits line the pore of the ion channel, while their intracellular loops between TM3 and TM4 domains are phosphorylatable by several proteins, that play an important role in the regulation of GABA$_A$Rs function. In particular, they can modulate a broad spectrum of GABA$_A$Rs activities, such as trafficking enhancement, surface stabilization, receptor internalization, anchoring of receptors in the cytoskeleton, and regulation of GABA$_A$Rs modification.[142,162]

The majority of GABA$_A$Rs is composed of two α, two β, and a single γ, δ or ϵ subunits.[163,164] As previously mentioned, the isoform $\alpha_1\beta_2\gamma_2$ is considered the most prevalent subtype of adult GABA$_A$Rs, with clockwise arrangement $\alpha_1\beta_2\gamma_2\alpha_1\beta_2$.[165] It is estimated that approximately 60% of all GABA$_A$ receptors have the subunit composition $\alpha_1\beta_2\gamma_2$, about 15–20% are $\alpha_2\beta_3\gamma_2$, 10–15% have the $\alpha_3\beta_n\gamma_2$ combination, approximately 5% are $\alpha_4\beta_n\gamma$ or $\alpha_4\beta_n\delta$, less than 5% have the $\alpha_5\beta_2\gamma_2$ composition and, less than 5% are $\alpha_6\beta_{2/3}\gamma_2$ type receptors.[141] Furthermore, GABA$_A$Rs can contain two different α subunits. Thus, $\alpha_1\alpha_6\beta_x\gamma_2$ and $\alpha_1\alpha_6\beta_x\delta$ receptors have been found in the cerebellum.[166]

The composition and arrangement of GABA$_A$Rs subunits induce the synaptic response to GABA, as well as electrophysiological, functional, and pharmacological properties of GABA$_A$Rs, including potency and efficacy of different drugs to exert their effects.[143,167,168] In fact, the various types of drugs that act on GABA$_A$Rs have binding sites in different regions of the receptor at the interface of specific subunits. Studies on the human embryonic kidney (HEK) 293 cells, expressing different subtypes of GABA$_A$Rs, demonstrated that not

all drugs are active on all receptor subtypes and their pharmacological properties are different in receptors with the same subunit composition but of different types (e.g., $\alpha_1\beta_1\gamma_2$ vs $\alpha_1\beta_2\gamma_2$).[169]

Some subunits, such as δ subunits, are located only at the extrasynaptic level, where GABA$_A$Rs are activated by low environmental concentrations of the neurotransmitter present in the extracellular fluid, mediating a so-called "tonic" inhibition that is relatively non-desensitizing. Instead, isoforms containing γ subunits are mainly expressed in synapses and modulate the rapidly desensitizing "phasic" GABAergic neurotransmission. After GABA release from presynaptic vesicles, synaptic GABA$_A$Rs are transiently activated, while extrasynaptic ones are generally activated continuously, controlling neuronal excitability and the strength of synaptic transmission.[170-174]

The tonic and phasic conductions exerted by GABA are the basis of several physiological and behavioral processes.[141] Receptors containing subunits δ regulate numerous behavioral functions, such as anxiety, nociception, memory, and can modulate neurogenesis. Because the δ subunit-containing receptors are highly sensitive to sedative-hypnotic drugs, sleep stimulants, general anesthetics, alcohol, and neuroactive steroids, they are considered as potential therapeutic targets for the treatment of insomnia, mood disorders, memory deficit, pain, and post-stroke recovery.[172,174]

To date, a limited number of mutations in GABA$_A$Rs subunit genes have been found to be specific for different diseases. For example, point mutations in the α_1 and γ_2 subunits are found in patients with genetic epilepsies, while single nucleotide polymorphisms (SNPs) in the gene encoding the α_2 subunit are involved in alcohol dependence and illicit drug dependence. The gene encoding the β_1 subunit also has been linked to alcohol dependence and bipolar disorder, whereas the genes encoding the α_1, α_6, β_2, and π subunits have been linked to schizophrenia.[141]

2.1.1 GABA$_A$-ρ receptors

Initially distinguished as GABA$_C$ receptors, GABA$_A$-ρ receptors are considered as a subtype of GABA$_A$ receptors because of their structural homology but they differ in biochemical,

pharmacological, and physiological properties.[175-177] They are mainly expressed in the retina, where they play a unique functional role in retinal signal processing, but they are also expressed throughout the brain and periphery.[178,179] GABA$_A$-ρ receptors are involved in numerous processes throughout the central nervous system, including vision, olfactory senses, sleep, cognitive functions and memory, hormonal secretion, and pain perception, with promising potential for the treatment of myopia, sleep disorders, memory and learning enhancement, and fear and anxiety-related disorders.[179,180]

There are three isoforms of ρ subunits (ρ_1-ρ_3) in mammals, while only two are expressed in human (ρ_1 and ρ_2), that are assembled to form homo- o heteropentameric GABA$_A$-ρ receptor pentamers.[177-181]

GABA$_A$-ρ receptors are not sensitive to bicuculline and baclofen, which are selective ligands of GABA$_A$Rs and GABA$_B$Rs, respectively[179-182] but they are more sensitive to GABA than GABA$_A$Rs. GABA$_A$-ρ receptors are activated by three GABA molecules and they have a smaller chloride conductance,[179] longer channel opening time, and desensitize less readily in the presence of the neurotransmitter concerning GABA$_A$Rs.[175] The activity of GABAA-ρ receptors is not modulated by benzodiazepines and barbiturates but high concentrations of neuroactive steroids may control GABA-induced current at GABA$_A$-ρ_1 receptors, in both positive and negative manner.[175,183]

The identification of selective agonists, CACA and (+)-CAMP,[175] and antagonist of GABA$_A$-ρ receptors, TPMPA, 3-APMPA, and 3-APA, both the evidence that GABA$_A$-ρ receptors are much less sensitive to GABA$_A$Rs antagonist gabazine, pointed out that agonist/antagonist binding pockets of GABA$_A$ and GABA$_A$-ρ receptors are different (Figure 24).[177,184,185]
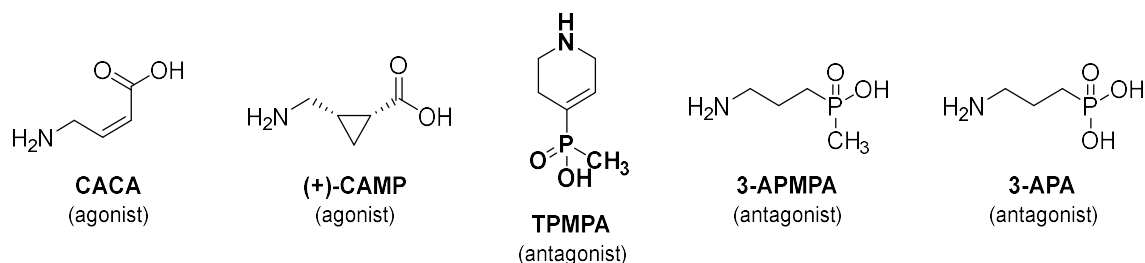

Figure 24. Chemical structures of agonists and antagonists of GABA$_A$-ρ receptors.

Compound imidazole-4-acetic acid exhibits a ρ subunit-dependent pharmacological profile: at ρ_1 and ρ_3 receptors it acts as a potent antagonist, while at ρ_2 receptors as a potent partial agonist.[179]

2.2 GABA$_B$ receptors

Metabotropic GABA$_B$ receptors are G-protein coupled receptors with seven transmembrane domains that mediate slow and prolonged inhibitory neurotransmission in the brain.[186] They are widely expressed and distributed in the CNS with presynaptic and postsynaptic localization, but they are present in a reduced number compared to the GABA$_A$Rs.[187] GABA$_B$Rs differ from GABA$_A$Rs by their structural and functional properties but also exhibit numerous pharmacological effects, including central muscle relaxation, epileptogenesis, antinociception, suppression of drug craving, cognitive impairment, and hormones release inhibition.[149,186]

The stimulation of presynaptic GABA$_B$Rs decreases the conductance of calcium ions via voltage-gated calcium channels. Consequently, activation of presynaptic GABA$_B$ autoreceptors induces inhibition of GABA release, while presynaptic GABA$_B$ heteroreceptors suppress the release of other neurotransmitters and bioactive peptides.[188] Presynaptic GABA$_B$Rs facilitate or suppress neuronal excitability thus playing important role in tuning various synapses, depending on whether the synaptic terminal releases an inhibitory or excitatory neurotransmitter.[149,189,190] On the other hand, postsynaptic GABA$_B$Rs are coupled via G-proteins to modulate potassium channels and determine slow inhibitory postsynaptic currents. These receptors stimulate the efflux of potassium ions that hyperpolarizes the neuronal membrane, shunting excitatory currents. Furthermore, the observed association of GABA$_B$Rs with glutamatergic synapses suggests their important role in the modulation of glutamatergic neurotransmission.[189,191,192]

Recently, a Cryo-Electron Microscopy (Cryo-EM) solved structure of 3-AMPA in complex with GABA$_B$R was released (PDB 6UO9; Figure 25).[193]
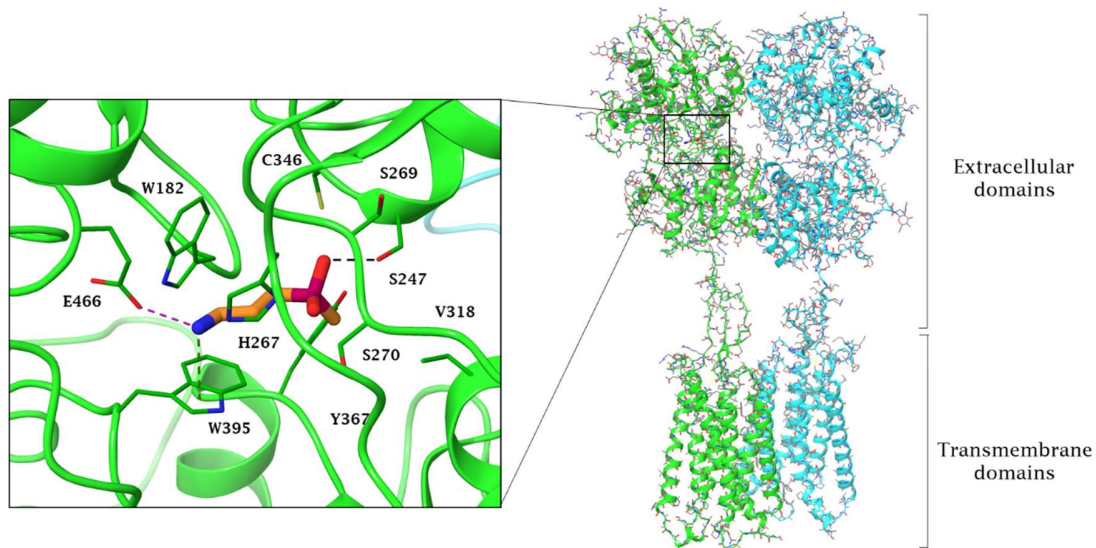
Figure 25.[193] Cryo-EM solved structure of GABA$_B$R in complex with the agonist 3-AMPA (PDB 6UO9). Ligand, GABA$_{B1}$ and GABA$_{B2}$ subunits are colored in orange, green and cyan, respectively. In detail, an H-bond (black dashed line) occurs between the P-O$^-$ group of the ligand and the hydroxyl moiety of S247 side chain, while the NH$_3^+$ group of the agonist engages a salt bridge (magenta dashed line) and a π-cation interaction (green dashed line) with the E466 COO$^-$ and W395 indolic ring, respectively.

In particular, GABA$_B$Rs are heterodimers consisting of two subunits GABA$_{B1}$ and GABA$_{B2}$ that formed functional GABA$_B$Rs (Figure 25).[194] Neither of these two subunits can work alone, in fact, GABA$_{B1}$ is involved in ligand recognition through its extracellular N-terminal domain and binds GABA,[195] while GABA$_{B2}$ is responsible for G-protein coupling.[196] There are two physiologically significant isoforms of the GABA$_{B1}$ subunit, called GABA$_{B1a}$ and GABA$_{B1b}$, which differ for the N-terminal region. The expression of these two subunits is regulated at the transcription level. They are transcribed by the same gene after the activation of alternative promoters.[197] Consequently, there are two main GABA$_B$Rs subtypes, assembled by GABA$_{B2}$ with GABA$_{B1a}$ and GABA$_{B1b}$ subunits, respectively.[189] GABA$_{B1}$ and GABA$_{B2}$ subunits are structurally homologous and both possess two main domains: a heptahelical membrane domain that is responsible for recognition and activation of G-proteins (HD domain), and a large extracellular "Venus flytrap" domain (VFT domain) involved in ligand binding. GABA and other agonists bind exclusively at the VFT domain of the GABA$_{B1}$ subunit, but the VFT domain of the GABA$_{B2}$ subunit is necessary for the activation of the whole receptor and to increase the agonist affinity on GABA$_{B1}$. On the other

hand, HD of GABA$_{B1}$ improves the coupling efficacy of GABA$_{B2}$ HD domain with the G-protein. A trans-activation mechanism, due to the binding of GABA at the VFT domain of the GABA$_{B1}$ subunit, promotes a conformational variation of the GABA$_B$Rs that led to the coupling activation between the HD domain of GABA$_{B2}$ with G-protein, by HD domain of GABA$_{B1}$.[198-200] GABA$_B$ receptors are not modulated by benzodiazepines, barbiturates, or steroids, and are not sensitive to bicuculline.[175,182] Characteristic agonists of GABA$_B$ receptors are baclofen, and 3-APPA, while saclofen, phaclofen and 2-hydroxysaclofen act as antagonists of GABA$_B$ receptors.[149] Baclofen, commercially available since 1972, is used to treat spasticity and skeletal muscle rigidity in patients with spinal cord injury, multiple sclerosis, amyotrophic lateral sclerosis, and cerebral palsy. However, although GABA$_B$ agonists showed promising therapeutic effects in a whole range of other indications, they exhibit numerous side effects, including sedation, tolerance, and muscle relaxation.[186,201]

2.3 GABA$_A$ receptors as drug targets

Many clinically important drugs target GABA$_A$ receptors, interacting at different allosteric binding sites such as benzodiazepine (e.g., diazepam) and benzodiazepine site ligands (e.g., flumazenil and zolpidem), barbiturates, intravenous and volatile anesthetics (e.g., (+)-etomidate and isoflurane, respectively), anticonvulsants (e.g., loreclezole), ethanol and neuroactive steroids, and performing their pharmacological effects (Figure 26).[143,154,202]
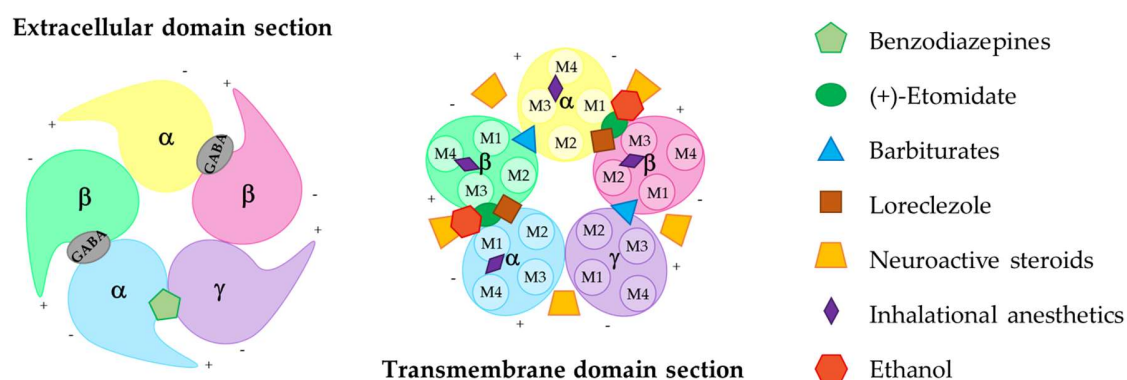

Figure 26. Schematic localization of orthosteric and allosteric binding sites in the extracellular/transmembrane domain of αβγ-type GABA$_A$R.

These drugs modulate the effects of GABA and affect GABAergic transmission, exerting a wide spectrum of pharmacological effects and inducing numerous conformational states of GABA$_A$Rs.

Several approaches have been applied in last years to more precisely identify various binding sites on the GABA$_A$Rs complex, as this knowledge is a prerequisite for the design of subtype-specific, selective drugs of clinical relevance.

While the drugs that act at the benzodiazepine binding sites can only modulate GABA$_A$Rs, barbiturates, neuroactive steroids, and anesthetics are able to directly activate GABA$_A$Rs in the absence of GABA at higher concentrations.[164,203-207] Binding sites for all of these drugs are allosterically coupled. Therefore, a drug that fits or binds to any of these multiple binding pockets induces conformational changes of the receptor complex and modulates GABA-elicited response.[208,209] For some of these multiple binding sites ligands have been identified, whereas, for other sites, ligands are unknown. Similarly, the sites of action of a large number of compounds that allosterically modulate GABA$_A$Rs are still not identified.[210]

The activation of GABA$_A$Rs leads to anxiolysis, ataxia, myorelaxation, sedation, hypnosis, anesthesia, and anterograde amnesia, while a decrease in GABA$_A$Rs activity leads to increased vigilance, memory enhancement, anxiety, and convulsions.[143,211] GABA$_A$Rs are therefore widely used in the treatment of anxiety disorders, insomnia, epilepsy, restlessness, and aggressive behavior.[154,212] A recent overview of the role of GABA$_A$Rs subtypes in cognitive and emotional behavior has shown the importance of some of these receptors in cognitive dysfunction in Down syndrome, anxiety disorders, depression, schizophrenia, and autism.[213] To date, an inverse partial agonist acting on GABA$_A$Rs containing α_5 subunits is in a clinical study in individuals with Down's syndrome. Substances that selectively reduce the function of GABA$_A$Rs containing α_5 are considered as potential cognition enhancers for Alzheimer's syndrome and other dementias, in line with genetic studies involving GABA$_A$Rs in learning performance.[214] Anxiety disorders, non-sedating anxiolytics probably are based on the modulation of GABA$_A$Rs containing α_2 and α_3 subunits. In addition, abnormalities in GABAergic neurotransmission seem to be a valid hypothesis for depression that opens new possibilities for the development of innovative antidepressant drugs. It has also been pointed out that cognitive symptoms in schizophrenia are attributed to a cortical GABAergic deficit,

and that a dysfunctional GABAergic inhibition contributes to the pathophysiology of autistic spectrum disorders.[213]

Furthermore, the properties of GABA$_A$Rs specific to interneurons may differ significantly from those found on projecting neurons, offering the possibility of developing interneuron-specific drugs that is of great therapeutic interest as more and more neurological and psychiatric disorders are linked to malfunction or deficits of interneurons.[140] Cells of glial origin also express GABA$_A$R subunit isoforms and form functional ion channels that are modulated by classical GABA$_A$R drugs, including diazepam and anesthetics etomidate and propofol.[215]

2.3.1 GABA binding site

A common feature of Cys-loop receptors is that the neurotransmitter binding pocket also called "orthosteric site", is located in the extracellular domain at the interface between two adjacent subunits (Figure 27). Each subunit contributes three/four noncontiguous regions that form the binding site. By convention, the principal (+) face of the neurotransmitter binding site is made up of three loops (A, B, and C) and the complementary (-) face has three β-strands and/or one loop (D, E, F, and/or G; Figure 27A).[216] For GABA$_A$Rs, the β and α subunits bear the principal and complementary components of the GABA binding site, respectively. In the most prevalent αβγ subtype, there are two GABA binding sites per receptor at the β(+)α(-) interfaces (Figure 26). Channel opening occurs with GABA occupying just one site, but the probability increases greatly when both sites are engaged.[217-219] These identical sites contribute asymmetrically to receptor activation, attributable to the different proteic surroundings, determining different conformational variations of the receptor depending on their flanking subunits (one site is located between γ and β, the other between α and γ; Figure 26).[217]

Recently, the Cryo-EM solved structure of GABA in complex with α$_1$β$_2$γ$_2$ GABA$_A$R was released (PDB 6D6U),[220] unveiling the binding mode of the neurotransmitter in these GABA$_A$-type receptors. In detail, GABA engages two H-bonds with α$_1$Arg66 and an H-

bonds with β_2Thr202 with its COO$^-$ function, and a π-cation interaction between the NH$_3^+$ moiety and β_2Tyr205 (Figure 27B).
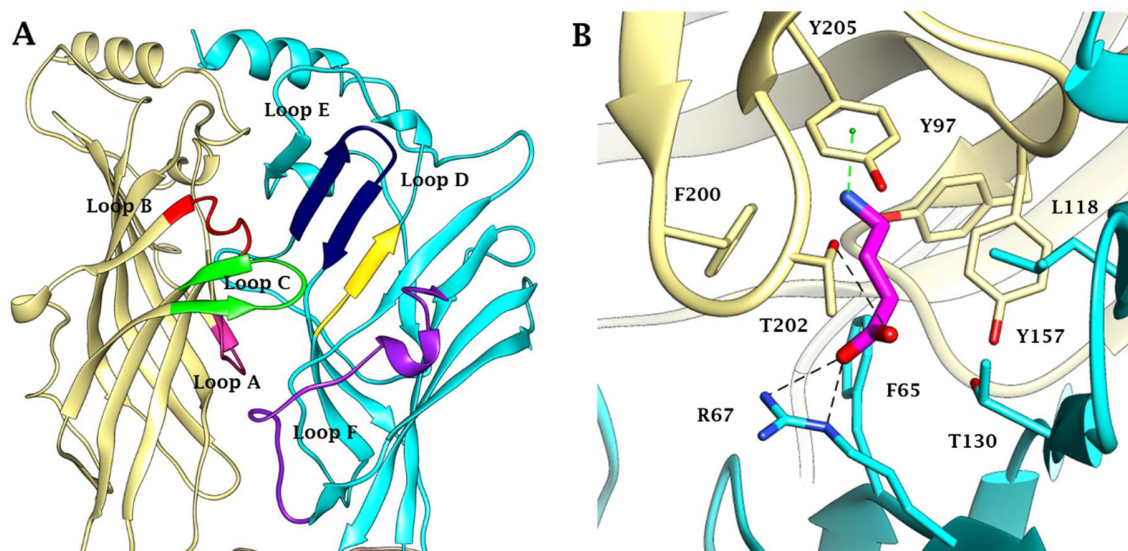

Figure 27.[220] (A) Architecture of the orthosteric binding site and (B) Cryo-EM solved structure of GABA in complex with $\alpha_1\beta_2\gamma_2$ GABA$_A$R (PDB 6D6U). β-subunit and α-subunit are colored in khaki and cyan, respectively. H-bonds (black) and π-cation (green) interactions are depicted as dashed lines.

Other structural analogs of GABA, such as the agonist muscimol, partial agonist gaboxadol, and competitive antagonists bicuculline can interact in the orthosteric binding sites to elicit distinct functional responses (Figure 21). The classification of ligands as agonists or partial agonists is not absolute and is relative to the function of GABA, which is dependent on receptor subtype. For instance, GABA is known to act as a full agonist on $\alpha\beta\gamma$ receptors while is a partial agonist at $\alpha\beta\delta$ receptors, exhibiting higher affinity and lower intrinsic efficacy.[221,222] Such functional difference has resulted in the agonist muscimol and partial agonist gaboxadol at $\alpha\beta\gamma$ receptors to exhibit super-agonism (higher maximal efficacy than GABA) at $\alpha\beta\delta$ receptors.[223,224]

A strong consensus that GABA can only bind to the $\beta(+)\alpha(-)$ interfaces has formed since the elucidation of the GABA binding sites. Nonetheless, *in vitro* studies demonstrating that the neurotransmitter is able to activate functional receptors lacking the α subunit, such as homomeric β, and binary $\beta\gamma$ and $\beta\delta$ receptors.[225,226] The ability of GABA to activate also

these receptors without the canonical GABA binding sites raised the question of whether additional agonist binding sites exist. A logical explanation would be the structural requirement for GABA binding sites is more flexible than they are generally perceived, *i.e.*, homologous interfacial subunit sites exist. Homologous orthosteric binding sites exist in alternative subunit interfaces for two reasons:

- the integrity of the aromatic box formed at the conventional β(+)α(-) interface lined by βY97, βY157, βF200, βY205, and αF64 residues, a common feature among the Cys-loop receptors which is essential in agonist recognition, is maintained at the β(+)β(-), β(+)γ(-), and β(+)δ(-) interfaces, as the aromatic side chain of the complementary face is conserved at homologous positions in the β, γ, and δ subunits (α1F64; β2Y61; γ2F77; δF74); [227,228]

- other α subunit residues implicated in GABA binding/function such as L127, T129, and R131 are also mostly conserved at the corresponding positions in the β, γ, and δ subunits.[216] Therefore, the overall architecture of the agonist binding site may be maintained across most β(+)X(-) subunit interfaces. However, differences in other critical binding residues may alter the GABA binding affinity of these interfaces. For instance, the replacement of $α_1$R66, responsible to form a salt bridge with GABA within the β(+)α(-) cavity,[227] the apolar alanine residue in the $γ_2$ subunit (γ2A79), could explain the lower GABA potency reported at βγ receptors.[229] The physiological relevance of these alternative GABA binding interfaces is to date an open question.

2.3.2 Benzodiazepines binding site

At the extracellular interface α(+)γ(-) (Figure 26), there is the "high-affinity" allosteric site of benzodiazepines. Benzodiazepines do not directly activate GABA$_A$Rs, because they need the concomitant presence of the neurotransmitter, but are able to modulate the receptor function. This binding site is the target of:

- benzodiazepines (e.g., diazepam; Figure 21), which are agonists that potentiate GABA$_A$Rs, producing sedation, anxiolysis, anticonvulsant, myorelaxant, and amnesia effects useful for the treatment of insomnia, anxiety disorders, epilepsy, muscle spasms, and for invasive medical procedures;

- inverse agonists (e.g., DMCM; Figure 21) that inhibit GABA$_A$Rs, exerting anxiogenic, convulsant, and memory-enhancing effects;

- antagonists (e.g., flumazenil; Figure 21) that block the actions of other benzodiazepines and can be clinically used as an antidote against benzodiazepine toxicity;

- ligands that are structurally unrelated to the benzodiazepines and can also access the high-affinity benzodiazepine site (e.g., zolpidem; Figure 21) to elicit similar responses.

To delineate the pharmacology of benzodiazepines the representative ligand of diazepam has been used. It is now clear that diazepam, at low concentrations, indiscriminately modulates $\alpha_1\beta\gamma_2$, $\alpha_2\beta\gamma_2$, $\alpha_3\beta\gamma_2$, and $\alpha_5\beta\gamma_2$ GABA$_A$Rs, and is insensitive at $\alpha_4\beta\gamma_2$ and $\alpha_6\beta\gamma_2$ GABA$_A$Rs. A conserved histidine residue found in the α_1, α_2, α_3, and α_5 subunits ($\alpha_{1/2}$H101, α_3H126, and α_5H105) confers high-affinity diazepam sensitivity, whereas the homologous arginine in the α_4 and α_6 subunits (α_4R99 and α_6R100) renders these receptors diazepam insensitive.[230-232] Genetic studies have exploited this functional switch to engineer point-mutated mice bearing diazepam-insensitive α_1, α_2, α_3, and/or α_5 subunits. Behavioral analysis of single point-mutated (only one type of diazepam-insensitive α subunit) and triple point-mutated (only one type of diazepam-sensitive α subunit) mice in response to diazepam has helped define the functional role(s) of individual α subunits.[233,234] These studies strongly suggested that $\alpha_1\beta\gamma_2$ GABA$_A$Rs primarily mediate sedation, $\alpha_2\beta\gamma_2$ anxiolysis, $\alpha_{2/3}\beta\gamma_2$ myorelaxant effect, and $\alpha_5\beta\gamma_2$ amnesia.

Basing on this evidences, there is an emergent interest in the development of subtype-selective benzodiazepine site agonists with improved therapeutic profiles.[141] In particular, α_2-selective modulators with anxiolytic effects devoid of sedating property are highly sought after.[141]

Many benzodiazepines also display additional "low-affinity" components at GABA$_A$Rs, due to their activities in a different poorly characterized binding site and that does not require the γ subunit. The classical benzodiazepine diazepam, for instance, modulates $\alpha_1\beta_2\gamma_2$ GABAARs via two distinct mechanisms manifested as a biphasic potentiation with nanomolar and micromolar potencies.[236] The nanomolar component is mediated by the high-affinity benzodiazepine site and can be selectively blocked by the antagonist flumazenil, while the micromolar component is flumazenil insensitive and is affected by mutations in the TMD

where anesthetics usually bind. The physiological function of the low-affinity component is unclear but has been postulated to underlie diazepam's anesthetic property.[236]

2.3.3 Anesthetics binding site

The transmembrane region of GABA$_A$Rs harbors the binding sites of many clinically and structurally different used drugs, including volatile anesthetics (e.g., enflurane, isoflurane), general anesthetics (e.g., etomidate, propofol), anticonvulsants (e.g., loreclezole, barbiturates), and sedative-hypnotics (Figure 21). These chemicals exhibit an activity dose-dependent on GABA$_A$Rs, enhancing the GABA effect at clinical concentrations, directly activating receptors at high micromolar concentrations, and in some cases, acting as open-channel blockers at even higher concentrations.[237,238] Experimental evidence has indicated that these sites are not unique to the prototype drugs from which they are generally named, so it is more appropriate to describe them based on their location.

2.3.3.1 β(+)α(-) interfaces: etomidate binding sites

The first anesthetic binding site, commonly referred to as the etomidate binding site, has been identified, thanks to two key approaches, that are:
- the photolabeling studies, that used photoreactive analogs of etomidate ([³H]-azietomidate and [³H]TDBzl-etomidate) which covalently label binding residues upon UV irradiation, jointly identifying the βM286 and αM236 residues located in the M3 and M1 domain, respectively.[239] Etomidate is able to inhibit the photolabeling of these residues in a concentration-dependent manner, further supporting etomidate's interaction with both residues;
- the cysteine-substitution mutagenesis studies, that have also demonstrated that these methionine residues are important determinants of etomidate binding and function.[240]
This evidences located the etomidate binding site at the β(+)α(-) interfaces in the TMD just below the orthosteric binding sites (Figure 26). Also βM286 and αM236 residues, other

amino acids are detected to be implicated in the etomidate binding, such as βF289 (M3), βV290 (M3), αL232 (M1), αT237 (M1), and αI239 (M1).[239,240]

Moreover, it was demonstrated *in vitro* that the ability of etomidate to modulate and activate the GABA$_A$Rs is uniquely dependent upon the β subunit type (β$_{1-3}$).[241] In fact, the mutation of residues β$_{2/3}$N265 (M2) with methionine or the presence of β$_1$S265 (M2) strongly suppressed the GABA-modulatory and GABA-mimetic effects of etomidate, confirming that β$_2$- or β$_3$-, but not β$_1$-type receptors, are highly sensitive to etomidate.[241]

2.3.3.2 α(+)β(-) and γ(+)β(-) interfaces: barbiturates binding sites

Using a R-[^{3}H]mTFD-MPAB, a photoreactive barbiturate analog, another class of anesthetic binding sites has recently been identified in α$_1$β$_3$γ$_2$ GABA$_A$Rs.[242] These binding pockets, targeted by barbiturates, are located at the α(+)β(-) and γ(+)β(-) interfaces, in homologous positions to the etomidate binding sites (Figure 26). The photolabeled binding residues by R-[^{3}H]mTFD-MPAB include αA291 (M3; equivalent to βM286), αY294 (M3), and γS301 (M3; equivalent to βM286) found on the principal faces of the respective subunits, whereas the βM227 (M1; equivalent to αL232) is found on the complementary face.

2.3.3.3 β(+)β(-) interface

Studies on α$_1$β$_3$ GABA$_A$Rs have also demonstrated that the photoreactive etomidate analogs, which preferentially label β(+) residues, and R-[^{3}H]mTFD-MPAB, which preferentially label β(-) residues, also contact residues found on the opposite faces.[239,243] [^{3}H]Azietomidate and [^{3}H]TDBzl-etomidate have been shown to photolabel βM227 on the complementary side (labeled by R-[^{3}H]mTFD-MPAB), whereas R-[^{3}H]mTFD-MPAB also photolabeled βM286 and βF289 located on the principal face (labeled by photoreactive etomidate analogs). These results suggest that a homologous cavity at the β(+)β(-) interface, which is absent in the αβγ subtypes is also accessible to these anesthetics. Moreover, the existence of the transmembrane β(+)β(-) anesthetic binding site is also corroborated by evidence obtained

from photoaffinity labeling, structural modeling, and functional studies focusing on propofol actions at β_3 homomeric GABA$_A$Rs.[149,244,245]

2.3.3.4 The promiscuity of anesthetics binding

While [^{3}H]azietomidate and [^{3}H]TDBzl-etomidate are highly selective for the $\beta(+)\alpha(-)$ interfaces, and R-[^{3}H]mTFD-MPAB prefers the $\alpha(+)\beta(-)$ and $\gamma(+)\beta(-)$ interfaces, the different classes of binding pockets are not exclusive to etomidate or barbiturates. In fact, structurally dissimilar anesthetics able to compete with these photoreactive analogs, preventing residue photolabeling.[242] Moreover, evidence from mutagenesis studies are in concordance with these findings, where the mutation βM286W attenuates the etomidate, volatile anesthetics, propofol, and methaqualone activity at GABA$_A$Rs.[246-248] In addition, the substituted cysteine accessibility method (SCAM) has also revealed that propofol protects the modification of α_1M236C and β_2M286C mutants by sulphydryl-reactive reagent, indicating that propofol also contacts these residues.[246-248] General anesthetics such as etomidate and propofol, initially believed to bind only to the $\beta(+)$-$\alpha(-)$ interfaces are able to activate the α-lacking $\beta\gamma$ receptors.[249,250] Thus, it appears that a structurally diverse set of chemicals including, but most likely not limited to the ligands investigated to date are able to access different numbers and classes of interfacial anesthetic binding sites to exert their clinical effects. This heterogeneity is best exemplified by the convulsant S-mTFD-MPAB which selectively binds to the $\gamma(+)\beta(-)$ interface to inhibit GABA$_A$Rs,[251] and the general anesthetic propofol that binds nonselectively to the $\beta(+)\alpha(-)$, $\alpha(+)\beta(-)$, $\gamma(+)\beta(-)$, and $\beta(+)\beta(-)$interfaces to potentiate GABA$_A$Rs.[242,243]

The issue seems to be more complex because of the presence of possible additional binding sites in the $\alpha(+)\gamma(-)$ interface transmembrane region, intrasubunit helical bundles, and intracellular loop.[210] However, due to limitations associated with available experimental techniques, and the lack of crystal structures of anesthetic-bound GABA$_A$Rs, their existence remains to be confirmed.

2.3.4 Neurosteroids binding site

In addition to GABA, neurosteroids are the most important endogenous ligands of GABA$_A$ receptors. Endogenous steroids such as allopregnanolone (Figure 21) and their synthetic analogs have neuroactive effects such as anxiolysis, analgesia, hypnotic sedation, anticonvulsant, and anesthesia mediated via GABA$_A$Rs.[252] At low nanomolar concentrations these ligands potently enhance GABA$_A$R function, while they are able to directly activate the receptor at submicromolar to- micromolar concentrations. Mutational,[253] kinetic,[254] photoaffinity labeling,[255] and transgenic mice behavioral studies[256,257] demonstrated that the action mechanisms of neurosteroids are different from those of benzodiazepines and anesthetics. To date, the precise locations of the neurosteroid binding sites remain to be confirmed, but several residues in the TMDs have been demonstrated to influence distinct actions of neurosteroids. For instance, residues such as αS240 (M1), αQ241 (M1), αN407 (M4), and αY410 (M4) are implicated in neurosteroid potentiation, whereas αT236 (M1) and βY284 (M3) mediate neurosteroid activation (Figure 26).[254,258,259]

Moreover, neurosteroids such as pregnenolone sulfate that block GABA$_A$Rs also exist, but their physiological actions are not well defined. Evidence from binding and mutational studies suggest that inhibitory neurosteroids do not share the same sites with neurosteroids that augment GABA$_A$R function.[254] The α$_1$V256 (M2) residue which is located further down the channel pore is found to be implicated, but this putative inhibitory neurosteroid binding cavity is controversial and awaits additional clarification.[260,261]

Generally, neurosteroids appear to interact in a complex manner with at least three distinct transmembrane sites to potentiate, activate, and inhibit GABA$_A$Rs.

2.3.5 Natural product modulate GABA$_A$ receptors

GABA$_A$Rs are the molecular target for a large variety of natural products. The most important examples included the potent psychoactive agonist of GABA$_A$Rs muscimol (*Amanita muscaria*), the antagonist bicuculline (from *Dicentra cucullaria*), and the pore-blocking convulsant picrotoxin (*Menispermaceae* family). Over the course of history, herbal

medicines are widely used to alleviate symptoms such as anxiety and insomnia, but recently the pharmacologically active constituents of these herbs became of great therapeutical interest. To date, among these natural products has been identified GABA$_A$R ligands such as the flavonoids (e.g., flavone, quercetin), that are able to interact with both the "high-" and "low-affinity" binding sites,[262,263] valerenic acids, that binds at β(+)α(-) interfaces binding pockets in the TMD,[264] menthol, magnolol, honokiol, and others (Figure 28).[265-267] All of these compounds exhibit diverse pharmacology mediated by known and unknown binding sites. The potential for the clinical application of several of these compounds is currently being explored. [262-267]

Moreover, the research group of Professor Arias of the Oklahoma State University discovered for the first time that also coronaridine congeners are able to potentiate GABA$_A$Rs, but to date is not identified the binding site of these compounds (Figure 28).[268]
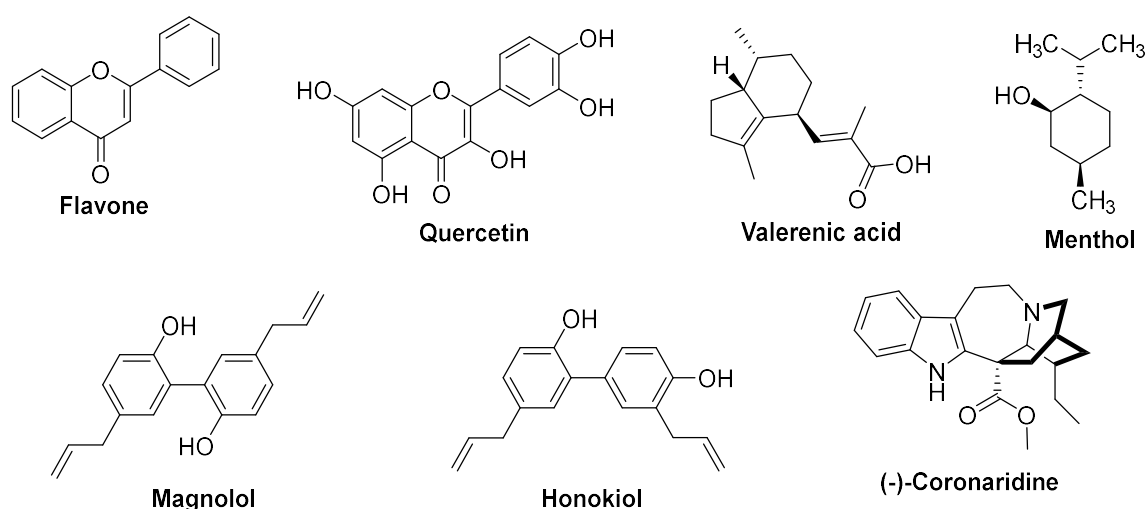

Figure 28. Structure of some natural ligands at GABA$_A$Rs.

Part II
Chemistry,
enzymatic kinetic assays,
and *in silico* studies

Chapter 3. Application of strategies for improving efficacy and selectivity of hCAs inhibitors: tail approach, multi-target strategy, and in silico investigations.

This chapter illustrates the Ph.D. projects having hCAs as targets. Design, synthetic and/or *in silico* strategies were adopted to enhance the sulfonamide CAI efficacy and selectivity of action for developing molecules to treat specific pathologies.

Zinc-binders are surely the most common and potent CAI. Sulfonamides, and their bioisosteres, which are the prototype of this class, are widely used in therapy since 1950 (Figure 12, Chapter 1) for the treatment of many diseases.[1] The significant lack of selectivity against the several hCA isoforms (Table 3) is the main drawback of sulfonamides, preventing their use as first-line drugs because of their secondary or side effects.[1]

Table3. Inhibition data of the clinically used sulfonamides and their bioisosteres (Figure 12, Chapter 1).

	K_I (nM)											
	hCA I	hCA II	hCA III	hCA IV	hCA VA	hCA VB	hCA VI	hCA VII	hCA IX	hCA XII	mCA XIII	hCA XIV
AAZ	250	12	$2x10^5$	74	63	54	11	2.5	25	5.7	17	41
MZA	50	14	$7x10^5$	6200	65	62	10	2.1	27	3.4	19	43
EZA	25	8	$1x10^6$	93	25	19	43	0.8	34	22	50	2.5
DCP	1200	38	$6.3x10^5$	15000	630	21	79	26	50	50	23	345
DRZ	50000	9	$7.7x10^5$	8500	42	33	10	3.5	52	3.5	18	27
BRZ	45000	3	$1.1x10^5$	3950	50	30	0.9	2.8	37	3.0	10	24
ZNS	56	35	$2.2x10^6$	8590	20	6033	89	117	5.1	11000	430	5250
TPM	250	10	$7.8x10^5$	4900	63	30	45	0.9	58	3.8	47	1460
SLP	12000	40	10600	$6.5x10^5$	174	18	0.8	3630	46	3.9	295	110
VLX	54000	43	78000	1340	912	88	572	3900	27	13	425	107
CLX	50000	21	74000	880	794	93	94	2170	16	18	98	689
IND	31	15	10400	65	79	23	47	122	24	3.4	11	106
SLT	374	9	$6.3x10^5$	95	81	91	134	6	43	56	1450	1540
HTC	328	290	$7.9x10^5$	427	4225	603	3655	5010	367	355	3885	4105

a. Mean from 3 different assays, by a stopped-flow technique (errors were in the range of ± 5e10% of the reported values); h = human; m = murine.

To overcome this issue some strategies were developed such as those of the "*ring approach*" and the "*tail approach*". The former consists in exploring various aromatic/heterocyclic scaffolds on which the sulfonamide zinc-binding group (ZBG) is attached, whereas the

second one is focused on appending one or more *"tails"* to a scaffold, usually an aromatic or heterocyclic ring system, already incorporating a ZBG of the sulfonamide, sulfamate or sulfamide type, to achieve and interact with the residues of the middle/outer rim of the actives site, which are the most variable among the hCA isoforms.[95] Examples of the *"ring approach"* are the clinically used drugs sulfanilamide (SA), acetazolamide (AAZ), ethoxzolamide (EZA), or dichlorphenamide (DCP), whereas sulthiame (SLT), celecoxib (CLX), and **SLC-0111** (Figure 12, Chapter 1) are an example of the "tail approach" applied to sulfanilamide (SA).[95]

In particular, the *"tail approach"*, proposed in 1999,[91-93] gave many and positive results in enhancing the water solubility,[96-98] the membrane (im)permeation,[97,98] and the isoform-selective inhibitory profiles (i.e. SLC-0111).[3]

Instead, in the context of pharmacologic strategies against multi-factorial diseases, the choice of multi-potent agents is spreading worldwide overwhelming the co-administration of multiple drugs.[269-272] In fact, pharmacokinetic and metabolic issues deriving from multiple drug intake are reduced by the administration of a single multi-target agent, which provides an improved pharmacokinetic, better patient compliance, reduced drug-drug interactions as well as a synergistic effect in the treatment of the pathology.[269] Thus, a further strategy, the *"molecular hybridization approach"* has been emerging which consists of putting together scaffolds affecting distinct targets that are involved in the progression of the same illness. The achievement of balanced hybrids that equally affect the two systems is desirable to trigger a synergic effect at the biological level.[271]

A valuable aid for exploring the ligand-target interaction mode is the knowledge of the 3D structural features of targets. Nowadays, the coordinates of most CA isoforms are available which, together with *in silico* tools such as docking techniques, MM-GBSA, and molecular dynamics simulations, are widely applied for designing new CAIs and/or rationalize the inhibitory profile measured *in vitro*.

3.1 Sulfonamide inhibitors of human carbonic anhydrases designed through a three-tails approach: improving ligand/isoform matching and selectivity of action (Series A)

As simple as effective, the so-called *"tail approach"* made its appearance in the field of CA inhibition in 1999 and led to the development of a large number of studies and compounds that expanded the database of CA isoform-selective inhibitors by appending a wide spectrum of chemical functionalities, named *"tails"*, to the main zinc-binding scaffold.[95,96,99,274-276] The original aim was to increase the water solubility[96] and subsequently membrane (im)permeability of aromatic sulfonamide derivatives.[273] Afterwards, the design was shifted toward the modulation of the interactions between the ligand and the middle and outer rim of the hCAs active sites, which contain the most variable polypeptide regions among the various isoforms, in order to increase isoform specificity. Simple tailed CAIs are composed of the following elements: 1) a zinc-binding function, 2) a main scaffold that can include a linker, and 3) the tail (Figure 29A).

An extension of this approach was proposed in 2015 by Tanpure et al.,[277] with the simultaneous inclusion of two tails of diverse nature onto aromatic sulfonamide scaffolds, at a nitrogen atom branching point, allowing distinct binding to the hydrophobic and hydrophilic sections of the hCAs active site (Figure 29B). However, a limited number of compounds was reported (three) and an *in vitro* assay was performed solely on hCA II, which makes this pioneering study rather unfulfilled. More recently, Fares et al. used a similar approach proposing a diverse type of dual tails to benzenesulfonamide CAIs.[278]

The detailed knowledge of the active site composition and architecture of hCAs (mostly available by X-ray crystallographic studies, except for CAs VA and VB) derived from many previous studies[279-281] led to the conclusion that the simple hydrophobic/hydrophilic division of the isoforms binding pocket may no longer be sufficient. In fact, some CA isozymes do not exhibit such a precise distinction as originally noticed in hCA I, II and IX,[13] and bulk of accessory subpockets exist which differentiate the various CA isoforms. Here, the inclusion of a third tail is proposed as an approach to improve the matching and fitting of the target-ligand interaction within the different hCAs active sites (Figure 29C).
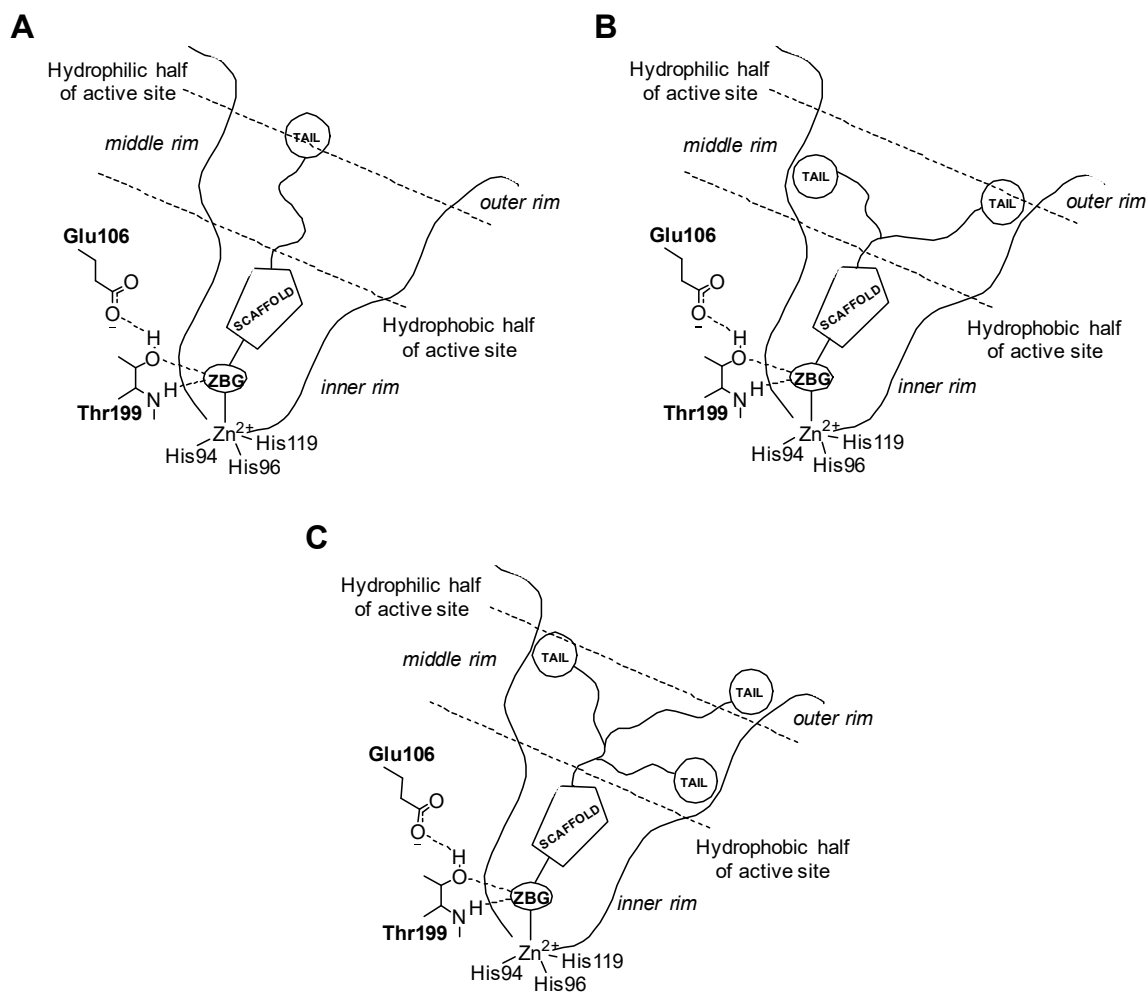
Figure 29. Schematic representation of the (A) "tail", (B) "two-tails" and (C) "three-tails" approach for the design of zinc-binding CAIs.

As a first proof-of-concept of this improved approach, a diverse array of tail combinations were investigated with the aim of identifying suitable isoform-imprints. Described here, is the screening of hCA isozymes I, II, IV, and XII against thirty-two benzenesulfonamide derivatives incorporating three tails. A comprehensive structural study was also undertaken by X-ray crystallography with hCA II and *in silico* with isozymes hCA IV and XII, to assess the ligand-/target interaction modes. A selection of the three-tailed inhibitors most active against hCAs implicated in glaucoma was assessed *in vivo* in a rabbit model of the diseases and compared to classical clinically used CAIs.

Currently, the tail approach has been a focus of CAIs research area with most design studies adopting the *p*-substituted benzenesulfonamide scaffold as the main foothold to include a variety of chemical frameworks.[3] In fact, avoiding heteroaromatic sulfonamide scaffolds markedly eases the synthetic procedures, moving the focus on the inclusion of pendants on the inhibitor structure.[277] Likewise, to converge efforts and attention on studying the three-tailing effects on CA inhibition, a *p*-substituted benzenesulfonamide was here adopted as a CAI scaffold.

It should be stressed that it is not possible to easily include three chemically diverse tails on a single branching atom (e.g. a nitrogen atom, as proposed by Tanpure et al. in the two-tails approach),[277] unless obtaining an ammonium salt or a chiral center. As a result, among several identified alternatives to branch a spacer attached to the main scaffold into three tails, the general structure **TTI** (Figure 30) was selected to combine easy and versatile chemistry with the possibility to extend it to many diverse chemical groups, which is relevant for producing a range of tail combinations. As a result, **TTI** was designed in the following manner: 1) a benzenesulfonamide scaffold (blue) which assures the interaction with the zinc ion and the bottom of the active site; 2) an ethylenic spacer (red) which has the function to allow sufficient space between the main scaffold and the tails; 3) a first ramification point (N atom, in black) from which the first tail T_1 (green) branches off; 4) an amide-based spacer (red); 5) a second intersection point (N atom, in black) by which T_2 and T_3 (green) branches off. Having the benzenesulfonamide bound to the Zn(II) at the bottom of the active site, the linkers in red (Figure 30) were chosen in such a way as to explore a vast chemical space at the medium and outer rims of the binding clefts.
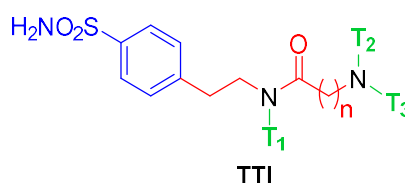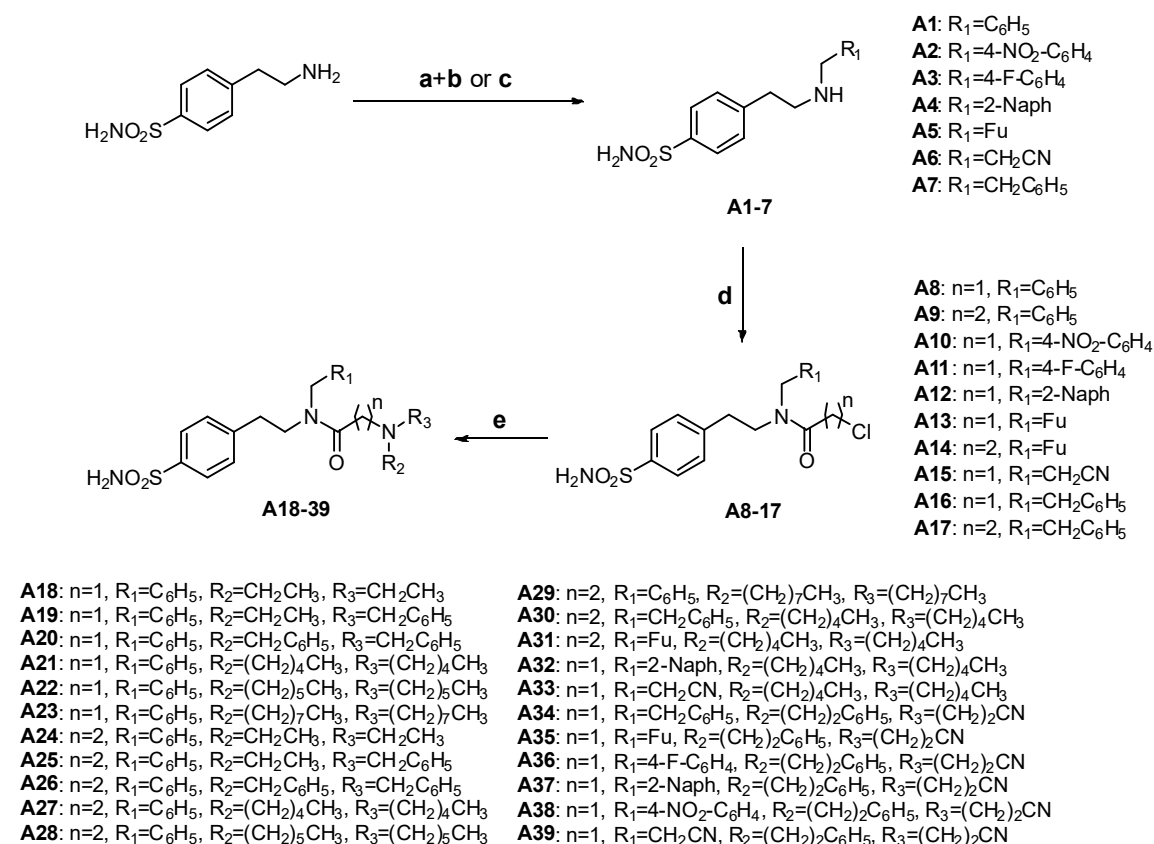

**Figure 30.** General structure of the designed three-tailed inhibitors (**TTIs**).

The synthetic strategies adopted to yield the **TTI** derivatives are reported in *Schemes 1-3*. T_1 was introduced on the 4-(2-aminoethyl)benzenesulfonamide by reductive amination in the

presence of an aromatic aldehyde and sodium borohydride or, alternatively, by nucleophilic substitution with the appropriate halides to furnish secondary amines **A1-5** and **A6**, **A7**, respectively. The latter were reacted with chloroacetyl chloride or chloropropionyl chloride to provide amides **A8-17**. T_2 and T_3 were finally included through a nucleophilic substitution with commercially available or synthesized secondary amines in anhydrous ACN and TEA as a base to produce **TTIs A18-39** (*Scheme 1*).


A1: $R_1=C_6H_5$
A2: $R_1=4\text{-}NO_2\text{-}C_6H_4$
A3: $R_1=4\text{-}F\text{-}C_6H_4$
A4: $R_1=2\text{-Naph}$
A5: $R_1=Fu$
A6: $R_1=CH_2CN$
A7: $R_1=CH_2C_6H_5$

A8: n=1, $R_1=C_6H_5$
A9: n=2, $R_1=C_6H_5$
A10: n=1, $R_1=4\text{-}NO_2\text{-}C_6H_4$
A11: n=1, $R_1=4\text{-}F\text{-}C_6H_4$
A12: n=1, $R_1=2\text{-Naph}$
A13: n=1, $R_1=Fu$
A14: n=2, $R_1=Fu$
A15: n=1, $R_1=CH_2CN$
A16: n=1, $R_1=CH_2C_6H_5$
A17: n=2, $R_1=CH_2C_6H_5$

A18: n=1, $R_1=C_6H_5$, $R_2=CH_2CH_3$, $R_3=CH_2CH_3$
A19: n=1, $R_1=C_6H_5$, $R_2=CH_2CH_3$, $R_3=CH_2C_6H_5$
A20: n=1, $R_1=C_6H_5$, $R_2=CH_2C_6H_5$, $R_3=CH_2C_6H_5$
A21: n=1, $R_1=C_6H_5$, $R_2=(CH_2)_4CH_3$, $R_3=(CH_2)_4CH_3$
A22: n=1, $R_1=C_6H_5$, $R_2=(CH_2)_5CH_3$, $R_3=(CH_2)_5CH_3$
A23: n=1, $R_1=C_6H_5$, $R_2=(CH_2)_7CH_3$, $R_3=(CH_2)_7CH_3$
A24: n=2, $R_1=C_6H_5$, $R_2=CH_2CH_3$, $R_3=CH_2CH_3$
A25: n=2, $R_1=C_6H_5$, $R_2=CH_2CH_3$, $R_3=CH_2C_6H_5$
A26: n=2, $R_1=C_6H_5$, $R_2=CH_2C_6H_5$, $R_3=CH_2C_6H_5$
A27: n=2, $R_1=C_6H_5$, $R_2=(CH_2)_4CH_3$, $R_3=(CH_2)_4CH_3$
A28: n=2, $R_1=C_6H_5$, $R_2=(CH_2)_5CH_3$, $R_3=(CH_2)_5CH_3$

A29: n=2, $R_1=C_6H_5$, $R_2=(CH_2)_7CH_3$, $R_3=(CH_2)_7CH_3$
A30: n=2, $R_1=CH_2C_6H_5$, $R_2=(CH_2)_4CH_3$, $R_3=(CH_2)_4CH_3$
A31: n=2, $R_1=Fu$, $R_2=(CH_2)_4CH_3$, $R_3=(CH_2)_4CH_3$
A32: n=1, $R_1=2\text{-Naph}$, $R_2=(CH_2)_4CH_3$, $R_3=(CH_2)_4CH_3$
A33: n=1, $R_1=CH_2CN$, $R_2=(CH_2)_4CH_3$, $R_3=(CH_2)_4CH_3$
A34: n=1, $R_1=CH_2C_6H_5$, $R_2=(CH_2)_2C_6H_5$, $R_3=(CH_2)_2CN$
A35: n=1, $R_1=Fu$, $R_2=(CH_2)_2C_6H_5$, $R_3=(CH_2)_2CN$
A36: n=1, $R_1=4\text{-}F\text{-}C_6H_4$, $R_2=(CH_2)_2C_6H_5$, $R_3=(CH_2)_2CN$
A37: n=1, $R_1=2\text{-Naph}$, $R_2=(CH_2)_2C_6H_5$, $R_3=(CH_2)_2CN$
A38: n=1, $R_1=4\text{-}NO_2\text{-}C_6H_4$, $R_2=(CH_2)_2C_6H_5$, $R_3=(CH_2)_2CN$
A39: n=1, $R_1=CH_2CN$, $R_2=(CH_2)_2C_6H_5$, $R_3=(CH_2)_2CN$

Scheme 1. Reagents and conditions: a) R_1CHO, anhydrous MeOH, reflux, 4h; b) $NaBH_4$, anhydrous MeOH, reflux, 0.5-2h; c) R_1-X, dry DMF; d) $ClCO(CH_2)_nCl$, acetone, r.t, 1h; e) R_2R_3NH, TEA, anhydrous ACN, reflux, 4-24h.

The nitrile derivatives **A33-37** were further converted to the corresponding amines **A40-44** through a Ni/Raney catalyzed hydrogenation or hydrolyzed in $NaOH_{(aq)}$ into the corresponding carboxylic acids **A45-49** (*Scheme 2*).
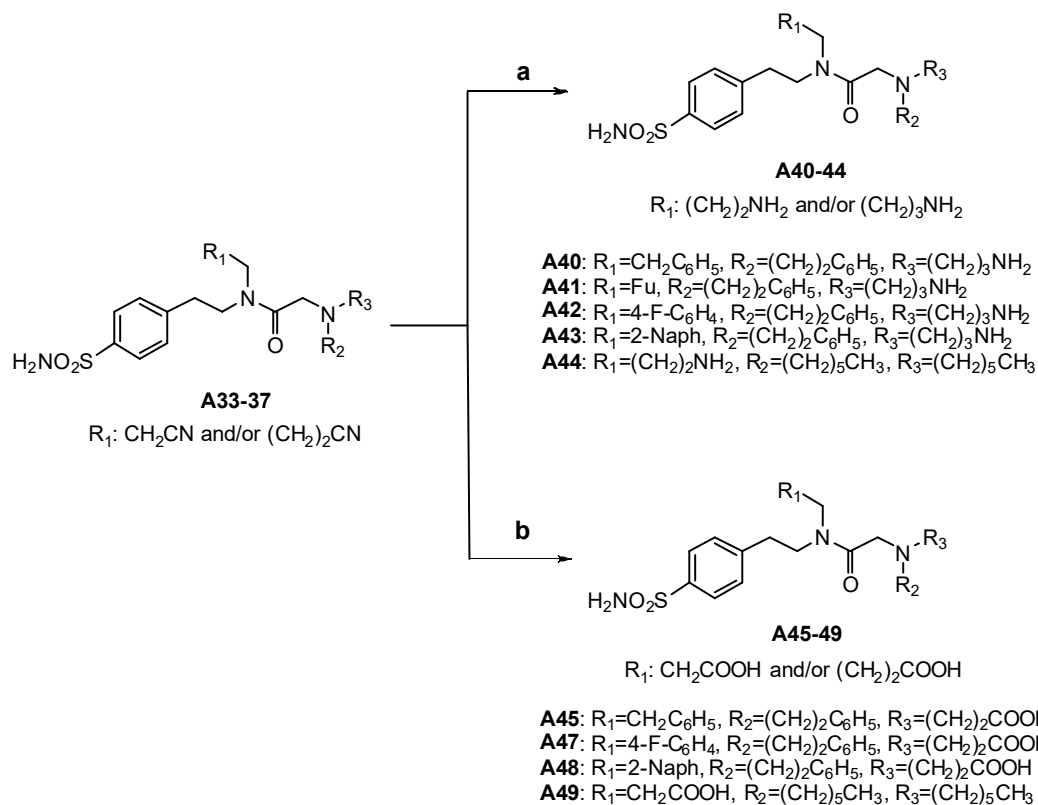
Scheme 2. Reagents and conditions: a) H_2, Ni/Raney, NaOH, EtOH, r.t., o.n.; b) NaOH, EtOH, reflux, o.n.

Additionally, the markedly hydrophobic oleylamide derivative **A50** was yielded by coupling the carboxylic acid **A46** with oleylamine in presence of EDC and DMAP in anhydrous DMF (*Scheme 3*).
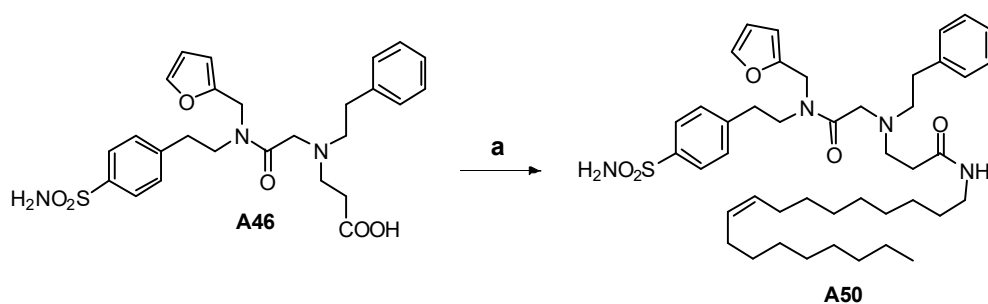
Scheme 3. Reagents and conditions: a) oleylamine, EDC·HCl, DMAP, anhydrous DMF, r.t, o.n.

All derivatives were purified by silica gel chromatography eluting with MeOH/DCM gradients and fully characterized by ^{1}H-NMR, ^{13}C-NMR, and HRMS.

In a first screening, mono-tailed (**A1-7**) and three-tailed (**A18-50**) compounds were analyzed by a stopped-flow kinetic assay with the off-target hCA I and the glaucoma-associate isoforms hCA II, IV, and XII (Table 4).[282]

Table 4. Inhibition data of human CA isoforms CA I, II, IV, and XII with sulfonamides **A1-7**, **A18-50** reported here and the standard sulfonamide inhibitor acetazolamide (**AAZ**) by a stopped-flow CO_2 hydrase assay.[282]

Cmpd	n	R₁	R₂	R₃	K_I^a (nM)			
					CA I	CA II	CA IV	CA XII
A1	-	C_6H_5	-	-	95.3	98.4	2854.4	65.4
A2	-	$4\text{-}NO_2\text{-}C_6H_4$	-	-	224.3	120.9	1685.3	77.4
A3	-	$4\text{-}F\text{-}C_6H_4$	-	-	112.8	78.5	1196.7	60.1
A4	-	2-Naph	-	-	458.1	87.1	6248.1	78.6
A5	-	Fu	-	-	68.4	62.8	1584.5	55.4
A6	-	CH_2CN	-	-	105.3	153.7	5547.2	113.2
A7	-	$CH_2C_6H_5$	-	-	278.4	89.1	3587.4	104.3
A18	1	C_6H_5	CH_2CH_3	CH_2CH_3	786.6	8.3	4147.5	43.9
A19	1	C_6H_5	CH_2CH_3	$CH_2C_6H_5$	4210.4	391.6	>10000	82.6
A20	1	C_6H_5	$CH_2C_6H_5$	$CH_2C_6H_5$	865.9	412.3	>10000	98.8
A21	1	C_6H_5	$(CH_2)_4CH_3$	$(CH_2)_4CH_3$	506.1	124.5	>10000	69.4
A22	1	C_6H_5	$(CH_2)_5CH_3$	$(CH_2)_5CH_3$	878.7	237	>10000	92.8
A23	1	C_6H_5	$(CH_2)_7CH_3$	$(CH_2)_7CH_3$	946.7	843.8	>10000	99.4
A24	2	C_6H_5	CH_2CH_3	CH_2CH_3	184.7	8.9	3928.8	61.1
A25	2	C_6H_5	CH_2CH_3	$CH_2C_6H_5$	544.3	79.6	>10000	90.4
A26	2	C_6H_5	$CH_2C_6H_5$	$CH_2C_6H_5$	692.3	559.2	4640.8	302.5
A27	2	C_6H_5	$(CH_2)_4CH_3$	$(CH_2)_4CH_3$	563.6	522.6	3244.8	100.3
A28	2	C_6H_5	$(CH_2)_5CH_3$	$(CH_2)_5CH_3$	308.2	578.4	3455.4	77.8
A29	2	C_6H_5	$(CH_2)_7CH_3$	$(CH_2)_7CH_3$	209.3	778.8	>10000	280
A30	2	$CH_2C_6H_5$	$(CH_2)_5CH_3$	$(CH_2)_5CH_3$	518.4	780.8	3413.2	62.5
A31	2	Fu	$(CH_2)_5CH_3$	$(CH_2)_5CH_3$	220.1	60.4	3153.7	9.7
A32	1	2-Naph	$(CH_2)_5CH_3$	$(CH_2)_5CH_3$	541.4	4562.9	>10000	61.7
A33	1	CH_2CN	$(CH_2)_5CH_3$	$(CH_2)_5CH_3$	395.9	52.5	3478.3	8.6
A34	1	$CH_2C_6H_5$	$(CH_2)_2C_6H_5$	$(CH_2)_2CN$	777.3	368.5	>10000	75.5
A35	1	Fu	$(CH_2)_2C_6H_5$	$(CH_2)_2CN$	300.8	73.2	457.4	8.7
A36	1	$4\text{-}F\text{-}C_6H_4$	$(CH_2)_2C_6H_5$	$(CH_2)_2CN$	676.4	133	4133.8	9.8
A37	1	2-Naph	$(CH_2)_2C_6H_5$	$(CH_2)_2CN$	685	247.5	3812.9	64.9
A38	1	$4\text{-}NO_2\text{-}C_6H_4$	$(CH_2)_2C_6H_5$	$(CH_2)_2CN$	407.5	264.2	2421.5	89.5
A39	1	CH_2CN	$(CH_2)_2C_6H_5$	$(CH_2)_2CN$	61.6	0.7	726.6	8.9

A40	1	$CH_2C_6H_5$	$(CH_2)_2C_6H_5$	$(CH_2)_3NH_2$	242.4	367.3	2149.2	83.7
A41	1	Fu	$(CH_2)_2C_6H_5$	$(CH_2)_3NH_2$	246.7	57	374.1	42.7
A42	1	$4\text{-}F\text{-}C_6H_4$	$(CH_2)_2C_6H_5$	$(CH_2)_3NH_2$	451.4	30.4	365.3	0.6
A43	1	2-Naph	$(CH_2)_2C_6H_5$	$(CH_2)_3NH_2$	506.7	5.6	819.2	10.5
A44	1	$(CH_2)_2NH_2$	$(CH_2)_5CH_3$	$(CH_2)_5CH_3$	435.8	2924.8	913.9	32.5
A45	1	$CH_2C_6H_5$	$(CH_2)_2C_6H_5$	$(CH_2)_2COOH$	203.5	72	2330.5	29.7
A46	1	Fu	$(CH_2)_2C_6H_5$	$(CH_2)_2COOH$	79.5	2.4	335.5	7.1
A47	1	$4\text{-}F\text{-}C_6H_4$	$(CH_2)_2C_6H_5$	$(CH_2)_2COOH$	95.8	23.5	419.3	8.8
A48	1	2-Naph	$(CH_2)_2C_6H_5$	$(CH_2)_2COOH$	197	72.5	680.6	6.8
A49	1	CH_2COOH	$(CH_2)_5CH_3$	$(CH_2)_5CH_3$	285.5	585.7	45.8	9.9
A50	1	Fu	$(CH_2)_2C_6H_5$	$(CH_2)_2CONHoleyl$	737.9	132	1807.1	5.5
AAZ	-	-	-	-	250	12	74	5.7

a. Mean from three different assays, by a stopped-flow technique (errors were in the range of $\pm5-10\%$ of the reported values). Fu = furyl; Naph = naphthyl

Generally, the inhibition data reported in Table 4 highlighted that mono-tailed compounds **A1-7** were medium to high nanomolar inhibitors of CA I (K_I = 68.4 - 458.1 nM), II (K_I = 62.8 - 153.7 nM) and XII (K_I = 55.4-113.2 nM), and weak inhibitors of CA IV with inhibition constant (K_I) values in the low micromolar range (1.1 - 6.2 μM).

In detail, compounds **A1** ($R_1 = C_6H_5$) and **A5** (R_1 = Fu) inhibited the off-target CA I in the medium nanomolar range (K_I = 95.3 and 68.4 nM, respectively), while compounds **A2**, **A4** and **A7** acted as weaker inhibitors (K_I = 224.3 - 458.1 nM). In fact, the introduction of bulky substituents (**A2**, and **A4**, K_Is of 224.3 and 458.1 nM) or the elongation of the chain (**7**, K_I of 278.4 nM) in R_1 decreased the action against CA I when compared to compound **A1**.

The aryl-tailed compounds **A1-6** acted as medium nanomolar inhibitors (K_I = 62.8 - 120.9 nM) against CA II, with compound **A5** (R_1 = Fu) being the single-tail isoform inhibitor. Compound **A7** ($R_1 = CH_2CN$) reported instead the worst inhibition of action against hCA II (K_I = 153.7 nM).

hCA IV was the least inhibited by compounds **A1-7**. In this context, derivatives **A2** (K_I = 1.6 μM), **A3** (K_I = 1.1 μM) and **A5** (K_I = 1.5 μM) resulted to be significantly better inhibitors than the bulkier derivative **A4** (R_1 = 2-Naph, K_I value of 6.2 μM).

CA XII was inhibited almost similarly by the single-tail compounds **A1-7**. Nonetheless, again derivative **A5** (R_1 = Fu) stood out as the best inhibitor (K_I = 55.4 nM), whereas the cyanoalkyl- and phenethyl-tailed compounds **A6** and **A7** exhibit K_Is above 100 nM.

Data in Table 4 showed that the development of **A1-7** upon inclusion of two other tails to synthesize compounds **A18-50**, significantly impacted the inhibition profiles against the panel of CA isoforms. In fact, **TTIs** showed lightly decreased or markedly improved inhibition of CA XII (K_Is = 0.6 - 302.5 nM). CA IV remained the less inhibited isozyme, though inhibition improvement of one or two orders of magnitude was testified for some compounds (K_Is = 45.8 - >10000 nM). On the whole, no significant improvement of CA I inhibition was detected with **TTIs** (K_Is = 79.5 - 4210.4 nM). CA II showed the inhibition profiles most affected, both positively and negatively, upon the inclusion of additional tails on the scaffold of **A1-7** (K_Is = 0.7 - 4562.9 nM).

To better discuss **TTIs** structure-activity relationship (SAR) from Table 4, compounds and related data were distinguished in five subsets: (**i**) **A18-29** (with R_1 = C_6H_5), (**ii**) **A30-33, A44, A49** (with R_2 = R_3 = $(CH_2)_5CH_3$), (**iii**) **A34-39** (R_2 = $(CH_2)_2C_6H_5$ and R_3 = $(CH_2)_2CN$), (**iv**) **A40-43** (R_2 = $(CH_2)_2C_6H_5$ and R_3 = $(CH_2)_3NH_2$), and (**v**) **A45-48** (R_2 = $(CH_2)_2C_6H_5$ and R_3 = $(CH_2)_2COOH$).

(**i**) In the first subset, compounds **A18** and **A20-29** were high nanomolar inhibitors of the ubiquitous off-target hCA I with K_I values between 184.7 and 946.7 nM, while derivative **A24** (R_2 = R_3 = CH_2CH_3) showed the best inhibitory profile (K_I = 184.7 nM). Instead, compound **A19** (R_2 = CH_2CH_3 and R_3 = $CH_2C_6H_5$) resulted in the worst hCA I inhibitor among all synthesized compounds (K_I = 4210.4 nM).

The glaucoma-implicated isoform CA II was inhibited in the nanomolar range (K_I = 8.3 - 843.8 nM) and, in particular, the introduction of R_2 = R_3 = CH_2CH_3 for compounds **A18** (n = 1) and **A24** (n = 2) and R_2 = CH_2CH_3 and R_3 = $CH_2C_6H_5$ for derivative **A25** (n = 2) increased the inhibition profile against this isoform (K_I = 8.3, 8.9 and 79.6 nM, respectively). Thus, derivative **A18** is the most CA II selective compound (CA I/ CA II = 94).

Only compounds **A18**, **A24**, and **A26-28** inhibited CA IV with K_I values in the range of 3.2 - 4.6 μM, while the other compounds of this series showed no activity below 10 μM.

All derivatives potently inhibited the other glaucoma-associated isoform, CA XII, with K_I values below 100 nM, except for compounds **A26** and **A29** that were also the worst inhibitors among all the synthesized compounds against this isoform (K_I = 280.0 and 302.5 nM). Compound **A18** showed the best inhibitory profile of this series (K_I = 43.9 nM).

The importance of the linker length (n =1,2) is pointed out from the activity analysis of this first subset. In fact, the elongation of the chain between R_1 and R_2/R_3 increased the activity against hCA I, II and IV which possess the smallest binding cavities, as a longer linker (n=2) can shift the tails R_2/R_3 towards the outer rim of the active site, removing the ligand-target steric encumbrance. On the other hand, the larger active sites of CA XII are able to host bulky substituents and the introduction of the linker n=2, which drives the tails R_2/R_3 out from the active site, may decrease the activity by weakening the ligand-target interactions.

(ii) Comparing the second subset (A30-33, A44, A49 with $R_2 = R_3 = (CH_2)_5CH_3$) compounds) with the first subset R_2/R_3-analogues A22 and A28, it was highlighted that the introduction of a furyl ring (Fu) and CH_2CN in R_1 increased the activity against the off-target CA I and CA II, such as observed in compounds A31 (CA I K_I = 220.1 nM; CA II K_I = 60.4 nM) and A33 (CA I K_I = 395.9 nM; CA II K_I = 52.5 nM). On the other hand, for $R_1 = CH_2C_6H_5$ (A30) and 2-Naph (A32), the activity on CA II strongly decreased for both substituents (K_I = 780.8 nM and 4.5 µM, respectively), while a weak increase in inhibition was observed for compound A30 (K_I = 518.4 nM) and a decrement for A32 (K_I = 541.4 nM) against CA I.

CA IV was weakly inhibited by A30-32 with K_I values in the micromolar range of 3.1 - 3.4 µM. Furthermore, the tail R_1 = CH_2CN reduction of compounds A33 into amine A44 decreased the activity on hCA II of 55 times (K_I = 2.9 µM) and increased the activity on CA IV of 3 times (K_I = 913.9 nM). Instead, the swap of A33 nitrile into carboxylic acid A49 worsened the activity against CA II by 11 times (K_I = 585.7 nM), but increased the inhibition profile against CA IV by 76 times (K_I = 45.8 nM), obtaining the most potent and selective compounds against this isozyme (CA I/ CA IV = 6.2).

In the case of CA XII, all compounds showed good activity against the target and, in particular, compounds A31 (K_I = 9.7 nM), A33 (K_I = 8.6 nM) and A49 (K_I = 9.9 nM) inhibited this isoform with K_I in the low nanomolar range while A30, A32, and A44 acted as medium nanomolar inhibitors (K_I = 32.5 - 62.5 nM).

Generally, for this subset it was observed that the concomitant presence of $R_2 = R_3 = (CH_2)_5CH_3$ with a 2-Naphthyl ring in R_1 (A32) worsened the activity by 19 times against CA II (K_I = 4.5 µM) and increased the activity by 1.5 times against hCA XII (K_I = 61.7 nM) with respect to the analog A22 ($R_1 = C_6H_5$), improving the CA II/ CA XII selectivity from 2.5 to

74 times. Of note, the presence of a potentially charged moiety in R_1 such as $(CH_2)_2NH_2$ (**A44**) or better CH_2COOH (**A49**) increased the activity against CA IV, which possesses a wider hydrophilic half in the active site with respect to the other hCAs with many acidic/basic residues at the middle rim of the cavity.

(**iii**) The third subset (**A34-39**) is characterized by the introduction of a hydrophobic tail R_2 = $(CH_2)_2C_6H_5$, a polar one R_3 = $(CH_2)_2CN$ and a variable pendant R_1. Only compound **A39** (R_1 = (CH_2CN) was a medium nanomolar inhibitor (K_I = 61.6 nM), which resulted to be the most potent agent against the off-target CA I, whereas **A34-38** acted in the high nanomolar range (K_I = 300.8 - 777.3 nM).

The glaucoma-associated CA II was potently inhibited by derivative **A39** with a K_I in the subnanomolar range (0.7 nM), resulting in the most potent and third selective inhibitor against this isozyme (CA I/ CA II = 88.0), while **A35** (R_1 = Fu) acted in the medium nanomolar range with K_I = 73.2 nM and derivatives **A34**, **A36-38** showed K_I values between 133.0 - 368.5 nM.

The best inhibitors against CA IV within this subset were **A35** and **A39** with K_I in the high nanomolar range (457.4 and 726.6 nM, respectively) whereas **A36-38** were low micromolar inhibitors with K_I values between 2.4-4.1 μM and derivative **A34** (R_1 = $CH_2C_6H_5$) acted with K_I > 10 μM.

The target hCA XII was strongly inhibited by all compounds of the subset with compounds **A35**, **A36** and **A39** acting in a low nanomolar range (K_I = 8.7, 9.8 and 8.9 nM, respectively), while **A34**, **A37** and **A38** were medium nanomolar inhibitors (K_I = 75.5, 64.9 and 89.5 nM, respectively). In this case, derivative **A36** resulted in the third most selective inhibitor against hCA XII (CA I/ CA XII = 69.8).

The comparison of compounds **A37** and **A39** from subset **iii** with the second subset analogs **A32** and **A33** (R_2 = R_3 = $(CH_2)_5CH_3$) pointed out that the substitution of R_2 and R_3 with the tails $(CH_2)_2C_6H_5$ and $(CH_2)_2CN$, respectively, generally increased the activity against CA II and IV, with the opposite effect against CA I and no significant effect against CA XII.

(**iv**) The fourth series (**A40-43**) was obtained by reducing R_3 = $(CH_2)_2CN$ to obtain primary amine tails in the aforesaid derivatives **A34-37**, introducing a potentially positively charged pendant. This structural modification led to a general increment of the activity against hCA

I, II, IV, and XII, suggesting that a strong polar interaction is favorable for the binding and might take place in all four active sites.

In detail, the four compounds resulted to be high nanomolar inhibitors of CA I with K_I in the 242.4-506.7 nM range. Moreover, it is observed that $A40$ ($R_1 = CH_2C_6H_5$) and $A41$ ($R_1 =$ Fu) inhibited this isoform with a two-fold potency ($K_I = 242.4$ and 246.7 nM, respectively) with respect to $A42$ ($R_1 = 4$-F-C_6H_5) and $A43$ ($R_1 = 2$-Naph), which showed a K_I of 451.4 and 506.7 nM, respectively.

Derivatives $A40$-43 were good inhibitors of the glaucoma-associated CA II with K_Is in the high nanomolar for $A40$ ($K_I = 367.3$ nM), medium nanomolar for $A41$ and $A42$ ($K_I = 57.0$ and 30.4 nM, respectively) and low nanomolar range for $A43$ ($K_I = 5.6$ nM), which was the second most selective obtained inhibitor against this isoform (CA I/ CA II = 90.5).

Interestingly, it was observed that the introduction of a positively charged tail increased the activity against CA IV at least 4 times for $A40$ ($K_I = 2.1$ μM), 1.2 times for $A41$ ($K_I = 374.1$ nM), 11 times for $A42$ ($K_I = 365.3$ nM), and 4.5 times for $A43$ ($K_I = 819.2$ nM) with respect to their analogs of the third subset ($A34$-37).

The glaucoma-related CA XII was strongly inhibited by $A42$ with a subnanomolar K_I of 0.6 nM that makes it the most potent and selective compound against this isoform (selectivity ratio CA I/ CA XII = 752.3), whereas $A40$ ($K_I = 83.7$ nM), $A41$ ($K_I = 42.7$ nM) and $A43$ ($K_I = 10.5$ nM) acted with a K_I in the medium nanomolar range.

(**v**) The fifth subset ($A45$-48) obtained by the introduction of a potentially negatively charged tail in R_3 showed a general increment of the inhibition activity against CA I, II, IV, and XII compared to their analogs $A34$-37.

In detail, compounds $A46$ ($K_I = 79.5$ nM) and $A47$ ($K_I = 95.8$ nM) acted as medium nanomolar inhibitors against the off-target CA I, whereas the introduction of a more encumbering R_1 ($CH_2C_6H_5$ and 2-Naphthalene), such as in $A45$ and $A48$, lightly decreased the activity to the high nanomolar range ($K_I = 203.5$ and 197.0 nM, respectively).

The target CA II was inhibited in the low nanomolar range by compound $A46$ ($K_I = 2.4$ nM), the second most potent inhibitor against this isozyme, and in the medium nanomolar range by $A45$ ($K_I = 72.0$ nM), $A47$ ($K_I = 23.5$ nM) and $A48$ ($K_I = 72.5$ nM).

The inhibition profile against hCA IV was in the high nanomolar range for derivatives **A46-47** (K_I = 335.5, 419.3 and 680.6 nM, respectively) and decreased for compound **A45** with a K_I value of 2.3 μM.

Moreover, derivatives **A46-48** were low nanomolar inhibitors of CA XII (K_I = 7.1, 8.8 and 6.8 nM, respectively), whereas **A48** and **A46** resulted to be the second and third most potent inhibitors of this glaucoma-associated isoform, while compound **A45** acted with a K_I of 29.7 nM.

Comparing the fourth (**A40-43**) and the fifth subset (**A45-48**), it was detected that the presence of R_3 = $(CH_2)_2COOH$ in place of amine tails shifted the activity against CA I.

Finally, the loss of the hydrophilic tail R_3 in **50** decreased the activity against CA I (K_I = 737.9 nM), II (K_I = 132.0 nM) and IV (K_I = 1.8 μM) without effects against CA XII (K_I = 5.5 nM), obtaining the second most potent and selective compound against this isoform (CA I/ CA XII = 134.2).

As pointed out by data in Table 4, single-tail inhibitors **A1-7** showed rather flat inhibition profiles against all tested hCAs and no marked isoform selectivity was detected. In contrast, the selectivity of action is often enhanced with TTIs **A18-50** (Table 5).

Table 5. Selective index (*SI*) for the single-tail compounds **A1-7** and **TTIs A18-50** calculated as ratio between $K_{I\,CA1}$ and $K_{I\,CA2}$

Cmpd	R_1	R_2	R_3	*SI*					
				CA I/II	CA I/IV	CA II/IV	CA I/XII	CA II/XII	CA IV/XII
A1	C_6H_5	-	-	1.0	0.03	0.03	1.5	1.5	43.6
A2	$4\text{-}NO_2\text{-}C_6H_4$	-	-	1.9	0.1	0.07	2.9	1.6	21.4
A3	$4\text{-}F\text{-}C_6H_4$	-	-	1.4	0.09	0.06	1.9	1.3	19.9
A4	2-Naph	-	-	5.3	0.07	0.01	5.8	1.1	79.5
A5	Fu	-	-	1.1	0.04	0.04	1.2	1.1	28.6
A6	CH_2CN	-	-	0.7	0.02	0.03	0.9	1.4	49.0
A7	$CH_2C_6H_5$	-	-	3.1	0.08	0.02	2.7	0.9	34.4
A18	C_6H_5	CH_2CH_3	CH_2CH_3	94.8	0.2	0.002	17.9	0.2	94.5
A19	C_6H_5	CH_2CH_3	$CH_2C_6H_5$	10.7	<0.4	<0.04	51.0	4.7	>121.1
A20	C_6H_5	$CH_2C_6H_5$	$CH_2C_6H_5$	2.1	<0.09	<0.04	3.7	8.8	>101.2
A21	C_6H_5	$(CH_2)_4CH_3$	$(CH_2)_4CH_3$	4.1	<0.05	<0.01	7.3	1.8	>144.1
A22	C_6H_5	$(CH_2)_5CH_3$	$(CH_2)_5CH_3$	3.7	<0.09	<0.02	2.6	9.5	>107.8
A23	C_6H_5	$(CH_2)_7CH_3$	$(CH_2)_7CH_3$	1.1	<0.09	<0.08	9.5	8.5	>100.6

A24	C_6H_5	CH_2CH_3	CH_2CH_3	20.7	0.04	0.002	3.0	0.1	64.3
A25	C_6H_5	CH_2CH_3	$CH_2C_6H_5$	6.8	<0.05	<0.008	6.0	0.9	>110.6
A26	C_6H_5	$CH_2C_6H_5$	$CH_2C_6H_5$	1.2	0.2	0.1	2.3	1.8	15.3
A27	C_6H_5	$(CH_2)_4CH_3$	$(CH_2)_4CH_3$	1.1	0.2	0.2	5.6	5.2	32.4
A28	C_6H_5	$(CH_2)_5CH_3$	$(CH_2)_5CH_3$	0.5	0.09	0.2	4.0	7.4	44.4
A29	C_6H_5	$(CH_2)_7CH_3$	$(CH_2)_7CH_3$	0.3	<0.02	<0.08	0.7	2.8	>35.7
A30	$CH_2C_6H_5$	$(CH_2)_5CH_3$	$(CH_2)_5CH_3$	0.7	0.2	0.2	8.3	12.5	54.6
A31	Fu	$(CH_2)_5CH_3$	$(CH_2)_5CH_3$	3.6	0.07	0.02	22.7	6.2	325.1
A32	2-Naph	$(CH_2)_5CH_3$	$(CH_2)_5CH_3$	0.1	<0.05	<0.5	8.8	74.0	>162.1
A33	CH_2CN	$(CH_2)_5CH_3$	$(CH_2)_5CH_3$	7.5	0.1	0.02	46.0	6.1	404.5
A34	$CH_2C_6H_5$	$(CH_2)_2C_6H_5$	$(CH_2)_2CN$	2.1	<0.08	<0.04	10.3	4.9	>132.5
A35	Fu	$(CH_2)_2C_6H_5$	$(CH_2)_2CN$	4.1	0.7	0.2	34.6	8.4	52.6
A36	$4-F-C_6H_4$	$(CH_2)_2C_6H_5$	$(CH_2)_2CN$	5.1	0.2	0.1	69.8	13.6	421.8
A37	2-Naph	$(CH_2)_2C_6H_5$	$(CH_2)_2CN$	2.8	0.2	0.03	10.5	3.8	58.8
A38	$4-NO_2-C_6H_4$	$(CH_2)_2C_6H_5$	$(CH_2)_2CN$	1.5	0.2	0.06	4.6	3.0	27.1
A39	CH_2CN	$(CH_2)_2C_6H_5$	$(CH_2)_2CN$	88.0	0.08	0.001	6.9	0.08	81.6
A40	$CH_2C_6H_5$	$(CH_2)_2C_6H_5$	$(CH_2)_3NH_2$	0.7	0.1	0.2	2.9	4.4	25.7
A41	Fu	$(CH_2)_2C_6H_5$	$(CH_2)_3NH_2$	4.3	0.7	0.2	5.8	1.3	8.8
A42	$4-F-C_6H_4$	$(CH_2)_2C_6H_5$	$(CH_2)_3NH_2$	14.9	1.2	0.08	752.3	50.7	608.8
A43	2-Naph	$(CH_2)_2C_6H_5$	$(CH_2)_3NH_2$	90.5	0.6	0.007	48.3	0.5	78.0
A44	$(CH_2)_2NH_2$	$(CH_2)_5CH_3$	$(CH_2)_5CH_3$	0.2	0.5	3.2	13.4	90.0	28.1
A45	$CH_2C_6H_5$	$(CH_2)_2C_6H_5$	$(CH_2)_2COOH$	2.8	0.09	0.03	6.9	2.4	78.5
A46	Fu	$(CH_2)_2C_6H_5$	$(CH_2)_2COOH$	33.1	0.2	0.007	11.2	0.3	47.3
A47	$4-F-C_6H_4$	$(CH_2)_2C_6H_5$	$(CH_2)_2COOH$	4.1	0.2	0.06	10.9	2.7	47.6
A48	2-Naph	$(CH_2)_2C_6H_5$	$(CH_2)_2COOH$	2.7	0.3	0.1	29.0	10.7	100.1
A49	CH_2COOH	$(CH_2)_5CH_3$	$(CH_2)_5CH_3$	0.5	6.2	12.8	28.8	59.2	4.6
A50	Fu	$(CH_2)_2C_6H_5$	$(CH_2)_2CONHoleyl$	5.6	0.4	0.07	134.2	24.0	328.6

For instance, starting from compound **A1** (R_1 = C_6H_5; *SI* CA I/ CA II = 1.0; CA I/ CA XII = 1.5; CA II/ CA XII = 1.5; CA IV/ CA XII = 43.6), the introduction of various lipophilic pendants in R_2 and R_3 (as in **A18-29**) decreased the activity against all isoforms, except for derivatives **A18** and **A24** where the inhibition profile against CA II and XII was increased. Interestingly, CA I/ CA II selectivity of **A18-27** was improved up to a *SI* of 94.8 for compound **A18**. Compound **A28** and **A29** (CA I/ CA II = 0.5 and 0.3, respectively) were instead the most selective CA I inhibitors of this subset.

Derivatives **A18-28** also exhibited improved selectivity for CA XII over CA I (*SI* 2.3 - 51.0), whereas **A29** showed a greater action against CA I (*SI* I/XII = 0.7). Moreover, derivatives **A19**-**23** and **A26-29** showed an increased selectivity for CA XII over CA II (*SI* 1.8 - 9.5), in contrast with **A24** and **A25** more active against CA II (*SI* 0.14 and 0.9). Within this subset, improved selectivity profiles for CA IV over CA I and II were not detected. CA IV/ XII selectivity increased up to 64.3 - >144.1 for the subset **A18-25.**

In comparison to the single-tail derivative **A2**, compound **A38** (R_1 = 4-NO_2-C_6H_4, R_2 = $(CH_2)_2C_6H_5$, R_3 = $(CH_2)_2CN$) showed an increased selectivity for CA XII over CA I, II and IV (*SI* I/XII 4.6, II/XII 3.0, IV/XII 27.1), while I/II selectivity showed a decrease (*SI* 1.5).

While derivative **A3** (R_1 = 4-F-C_6H_4) showed *SI*s equal to I/II 1.4, I/ IV 0.1, I/ XII 1.9, II/XII 1.3, IV/ XII 19.9, the addition in R_2 of $(CH_2)_2C_6H_5$ and $(CH_2)_2CN$ (**A36**), $(CH_2)_3NH_2$ (**A42**) and $(CH_2)_2COOH$ (**A47**) in R_3 led to remarkable results in terms of selectivity of action. In detail, selectivity was increased for CA II over CA I and for CA XII over CA I, II and IV for compounds **A36** (I/ II = 5.1, I/XII = 69.8, II/XII = 13.6, IV/XII = 421.8), **A47** (I/ II = 4.1, I/ XII = 10.9, II/XII = 2.7, IV/XII = 47.6) and even more in derivative **A42** (I/ II = 14.9, I/XII = 753.3, II/XII = 50.7, IV/XII = 608.8). Notably, the introduction of an amine moiety in R_3 significantly shifted the selectivity toward CA XII making compound **A42** 752.3 times more active against the glaucoma-associated isoform CA XII than the off-target hCA I. **A42** also showed the best CA IV/ CA XII selectivity index with a ratio of 608.8. The nature of R_3 can also be assumed to be responsible for a >1 *SI* for CA IV over CA I.

Variable outcomes in terms of selectivity of action were observed appending R_2 and R_3 tails on the 2-Naph single-tail **A4** (*SI*s CA I/ CA II = 5.3, CA I/ CA XII = 5.8, CA II/ CA XII = 1.1, CA IV/ CA XII = 79.5) yielding **A32** (R_2 = R_3 $(CH_2)_5CH_3$, R_3), **A37** (R_2 = $(CH_2)_2C_6H_5$, R_3 = $(CH_2)_2CN$), **A43** (R_2 = $(CH_2)_2C_6H_5$, R_3 = $(CH_2)_3NH_2$) and **A48** (R_2 = $(CH_2)_2C_6H_5$, R_3 = $(CH_2)_2COOH$). In fact, I/II selectivity decreased for derivative **A37** (I/II *SI* 2.8) and **A48** (I/II *SI* 2.7) up to the inversion displayed by **A32** (*SI* 0.1). In contrast it strongly increased with amine **A43** (I/II *SI* 90.5). I/XII selectivity was improved for all these derivatives in the order **A32** (I/XII *SI* = 8.8), **A37** (I/XII *SI* = 10.6), **A48** (I/XII *SI* = 29.0) **A43** (I/XII *SI* = 48.3). The lipophilic **TTI A32** showed great selectivity for CA XII over CA II and CA IV (*SI* = 74.0 and > 162.1, respectively). Likewise acted carboxylic acid **A48** (*SI* II/ XII = 10.7, IV/ XII =

100.1). A low II/XII *SI* increase was observed for nitrile **A37** (*SI* 3.8), while an inversion was detected for amine **A43** (*SI* II/XII = 0.5). The latter also showed an improved I/IV *SI* value (0.6) with respect to **A4** (0.07).

The **TTI** development of derivative **A5** (*SI*s I/II = 1.1, I/IV = 0.04, I/XII = 1.2, II/XII = 1.1, IV/XII = 28.6), to give **A31** (R_2 = R_3 (CH_2)$_5$$CH_3$, R_3), **A35** (R_2 = (CH_2)$_2$$C_6H_5$, R_3 = (CH_2)$_2$CN), **A41** (R_2 = (CH_2)$_2$$C_6H_5$, R_3 = (CH_2)$_3$$NH_2$), **A46** ($R_2$ = (CH_2)$_2$$C_6H_5$, R_3 = (CH_2)$_2$COOH) and **A50** (R_2 = (CH_2)$_2$$C_6H_5$, R_3 = (CH_2)$_2$CONHoleyl), overall increased the selectivity for CA II over CA I (3.6, 4.1, 4.3, 33.1 and 5.6, respectively). CA I/IV *SI*s were overall improved (0.2-0.7) with respect to **A5** (except **A31**) but not reversed. Interestingly, the reduction of nitrile **A35** into amine **A41** did not lead to variations in the I/IV selectivity, while the hydrolysis to carboxylic acid **A46** decreased it by 3 times. I/IV *SI* increased instead twice upon formation of amide **A50**.

The selective index for CA XII over CA I increased for all five derivatives, greatly with **A31** (*SI* 22.7), nitrile **A35** (*SI* 34.6) and amide **A50** (*SI* 134.1), less with amine **A41** (*SI* 5.8) and carboxylic acid **A46** (I/XII = 11.2). These compounds also showed selectivity for CA XII over CA II with *SI* of 6.2 (**A31**), 8.4 (**A35**), 1.3 (**A41**), 24.0 (**A24**), except for the carboxylic acid **A46** (*SI* 0.3).

Except for derivative **A41** (*SI* 8.8), selectivity for CA XII over IV ratio was enhanced for compound **A31** (*SI* 325.1), **A35** (*SI* 52.6), **A46** (*SI* 47.3) and **A50** (*SI* 328.6) respect to the lead **A5**.

The functionalization of **A6** (I/ II = 0.7, I/IV = 0.02, II/IV = 0.03, I/XII = 0.9, II/XII = 1.4, IV/XII = 49.0) with R_2 and R_3 produced derivatives **A33** (R_2 = R_3 (CH_2)$_5$$CH_3$) and **39** ($R_2$ = (CH_2)$_2$$C_6H_5$, R_3 = (CH_2)$_2$CN), that acted 7.5 and 88.0 times more efficiently against CA II over CA I. Moreover, compound **A33** showed an increment of *SI* I/XII (46.0), II/XII (6.1) and IV/XII (404.5). Instead, derivative **A39** showed a drastically improved action against CA II over CA XII (CA II/ CA XII = 0.1), and improved *SI*s I/XII (6.9) and IV/XII (81.6). The reduction and hydrolysis of the nitrile of derivative **A33** to give amine **A44** and carboxylic acid **A49** led to a selectivity against CA I over CA II (CA I/ CA II = 0.2 and 0.5, respectively). Interestingly, **A49** was the first-in-class selective CA IV inhibitor over CA I (*SI* 6.2) and hCA

II (*SI* 12.8) and also showed the lowest IV/XII *SI* (4.6). Finally, amine and carboxylic acid **A44** and **A49** showed increased II/XII *SI* (90.0 and 59.2, respectively).

The R_2/R_3 development of compound **A7** ($R_1 = CH_2C_6H_5$, I/II = 3.1, I/XII = 2.7, II/XII = 0.9, IV/ XII = 34.4) to give **A30** ($R_2 = R_3$ ($CH_2)_5CH_3$, R_3), **A34** ($R_2 = (CH_2)_2C_6H_5$, $R_3 = (CH_2)_2CN$), **A40** ($R_2 = (CH_2)_2C_6H_5$, $R_3 = (CH_2)_3NH_2$) and **A45** ($R_2 = (CH_2)_2C_6H_5$, $R_3 = (CH_2)_2COOH$) decreased I/II selectivity up to a total inversion with derivatives **A30** (*SI* 0.7) and **A40** (*SI* 0.7). On the contrary, an improvement was detected in the selectivity against CA XII over CA I (*SI* 2.9 - 10.3), hCA II (*SI* 2.4 - 12.5) and CA IV (*SI* 54.6 - >137.5), except for compound **A45** that showed a worsening in the IV/XII selectivity (*SI* 25.9) when compared to the lead **A7**.

Five selected three-tailed inhibitors (**A34**, **A41**, **A42**, **A46**, and **A48**) were crystallized in complex with hCA II with resolutions between 1.30-1.45 Å, by the research group of Prof. Robert McKenna from the University of Florida (Figure 31).
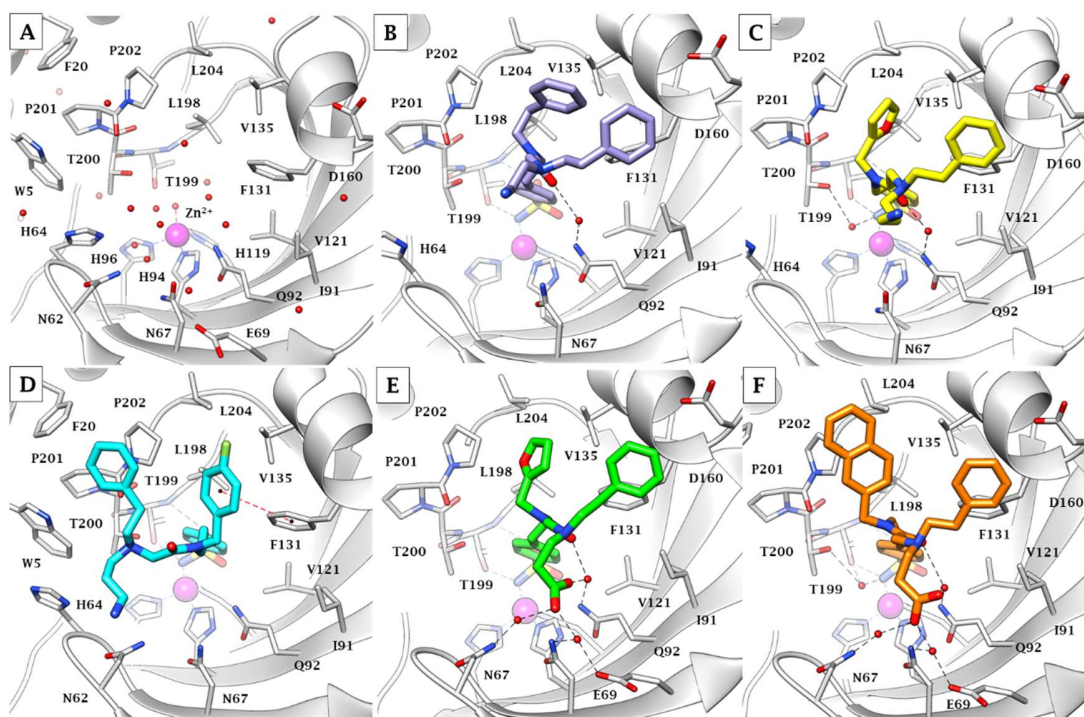
Figure 31. X-ray crystallography: active site view of hCA II in adduct with A) no inhibitor (PDB 3KKX; 2.00 Å), B) **A34** (PDB 6WQ4; 1.35 Å), C) **A41** (PDB 6WQ5; 1.30 Å), D) **A42** (PDB 6WQ7; 1.30 Å), E) **A46** (PDB 6WQ8; 1.41 Å)**,** and F) **A48** (PDB 6WQ9 ; 1.30 Å). H-bonds and π-π stackings are represented as black and red dashed lines, respectively. Water molecules involved in water-bridged H-bonds are shown as red spheres.

The crystallographic screening was complemented with docking calculations in order to gain insight into the binding properties of the studied compounds within the hCA I, IV, and XII isoforms.

The *in silico* study was performed on the single-tail derivatives **A1-7** and, among **TTIs**, on the most potent compounds against each isoform (**A39** and **A49**). In addition, the cocrystallized ligands (**A34**, **A41**, **A42**, **A46** and **A48**) were considered in the docking against hCA II in order to assess the accuracy of the used docking protocol. The binding orientations resulting from docking were refined with an MM-GBSA method simulating a water media (VSGB method) for improving the comparison with the crystallographic outcomes. The efficiency of the adopted protocol with three-tail compounds was validated by application to the crystallographic target/inhibitor adducts described above. Despite the absence of water molecules, crystallographic/simulated ligand RMSDs were computed below 1.0 Å, with the main deviation at the level of aliphatic tails (e.g. the carboxylate pendant in compound **A46**; Figure 32).
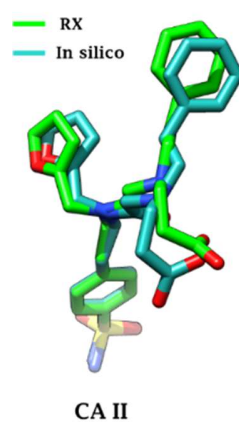
Figure 32. Superimposition of crystallographic (green)/predicted (cyan) binding orientations of compound **A46** in CA II active site.

As expected, derivatives **A1-7** showed interactions within the hCA I, II and XII active sites limited to a portion of the hydrophobic half of the cavity (Figure 33), that produce inhibition profiles devoid of selectivity and thus promiscuous.
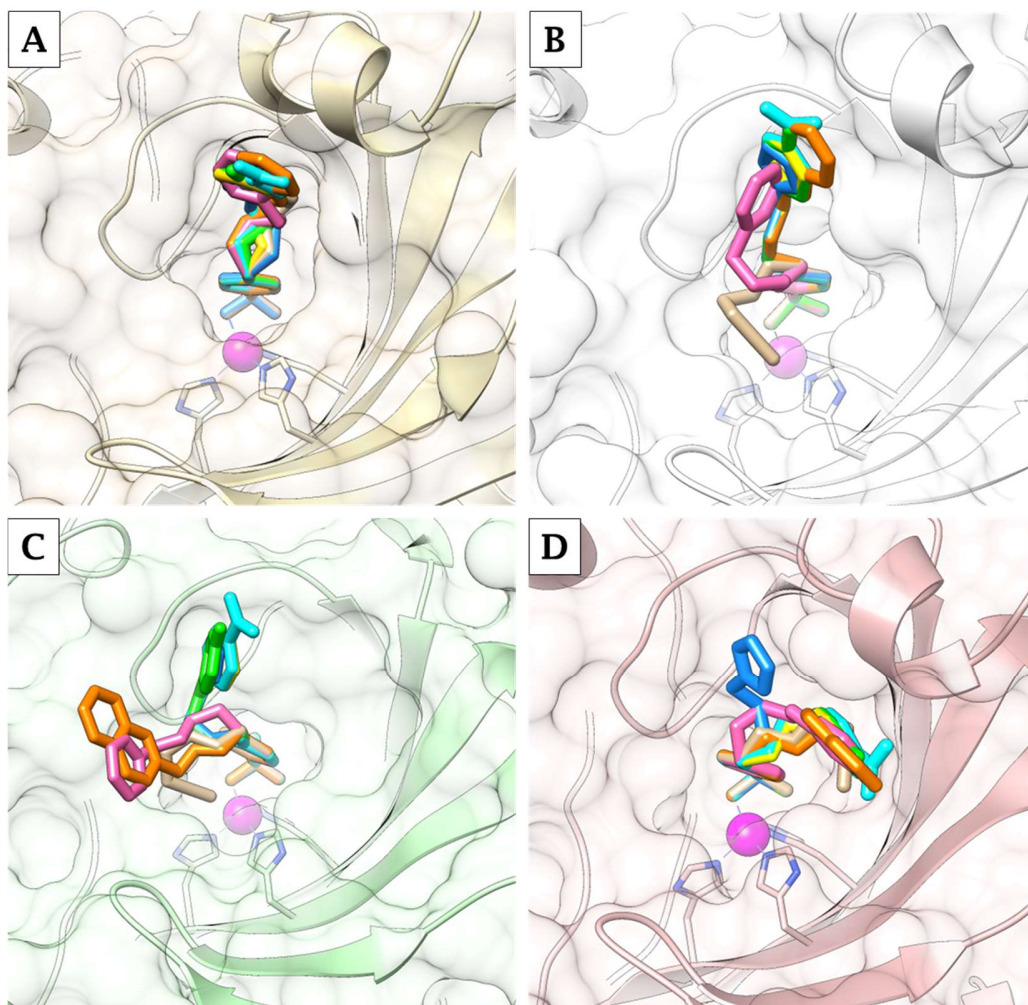
Figure 33. Superimposition of docked orientations of **A1** (yellow), **A2** (cyan), **A3** (green), **A4** (orange), **A5** (blue), **A6** (tan), **A7** (pink) within the active site of A) CA I, B) CA II, C) CA VI and D) CA XII.

The absence of a hydrophobic half in the active site of hCA IV led the tails of **A1-7** towards alternative pockets according to the nature of the pendants, and on the whole, reduces the inhibition efficacy up to a micromolar range.

Panels A and B of Figure 34 depict the predicted binding mode of **A39** to hCA I and II, respectively, as the most active inhibitor against these two isoforms. hCA I shows a narrower active site than hCA II because of specific amino acid mutations such as T/H200, N/H67, L/Y204 and, mostly, I/F91 (Figure 34A,B).
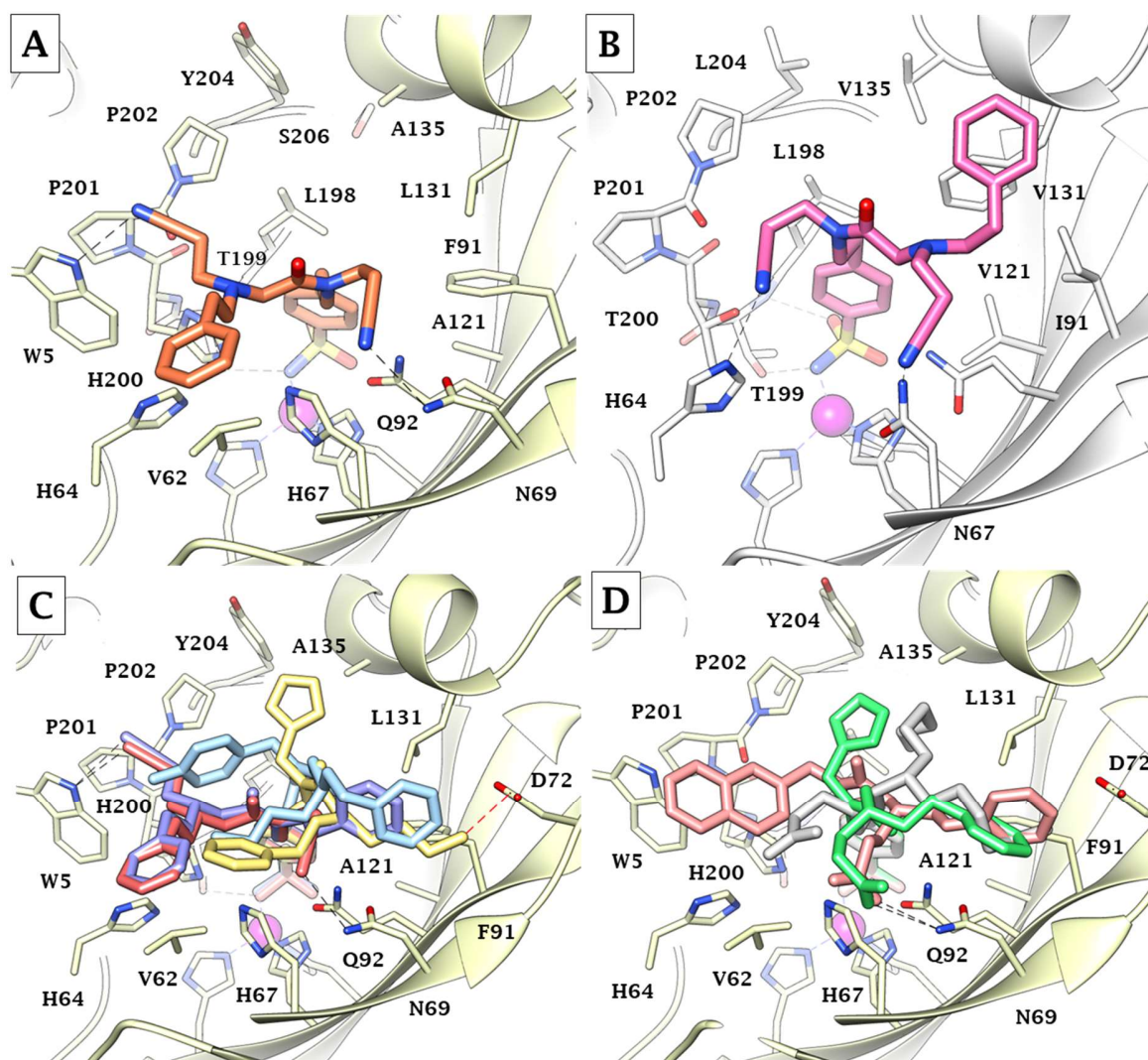
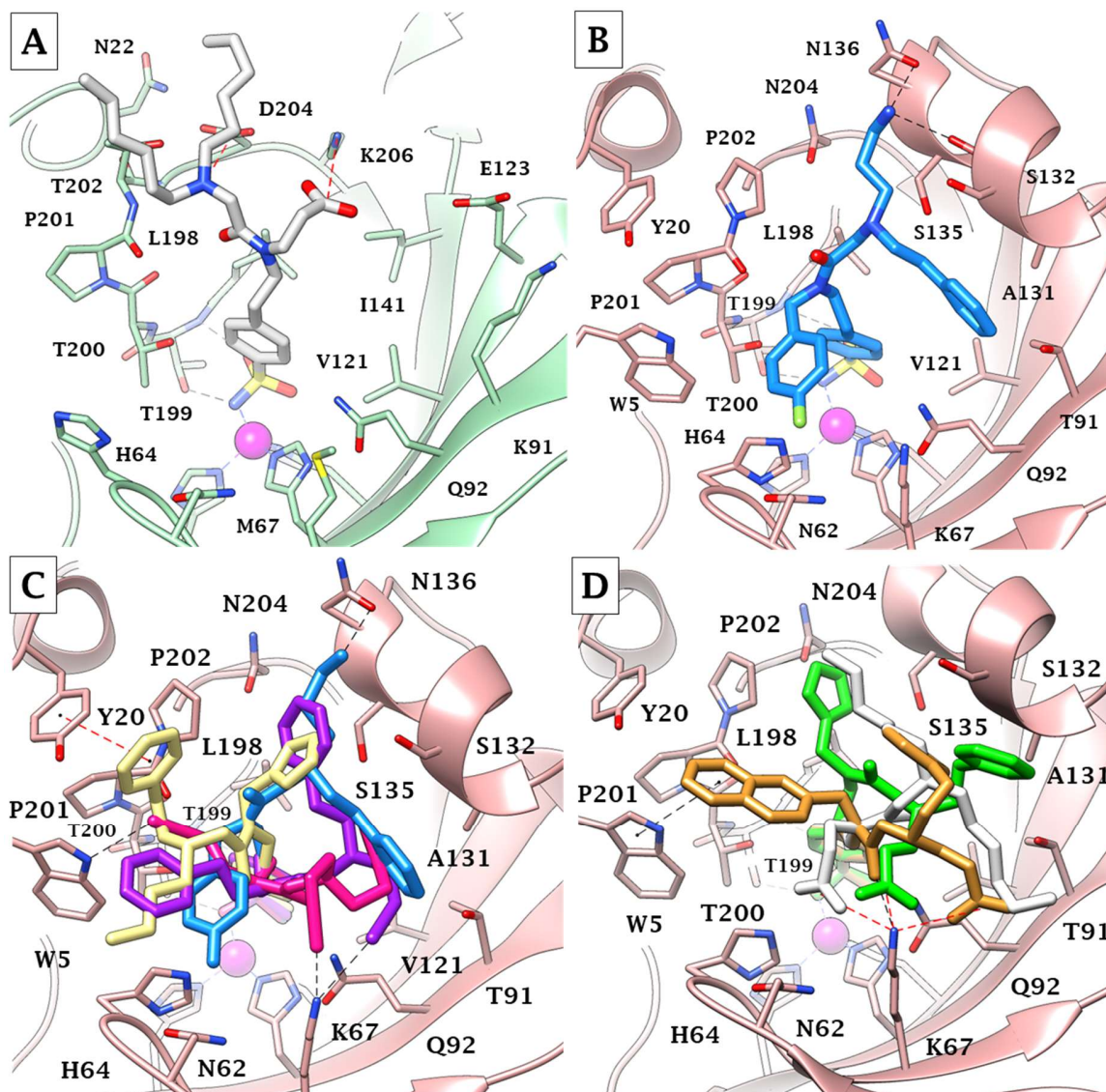**Figure 34.** *In silico* predicted binding conformations for the adducts A) **A39**/hCA I and B) **A39**/hCA II; predicted binding conformations of C) **A34** (light purple), **A39** (light red), **A41** (light yellow), **A42** (light blue) and D) **A46** (green), **A48** (peach), **A49** (light grey) in CA I active site. H-bond and salt bridge interactions are depicted as black, and red dashed lines, respectively.

As a main result of the latter mutation, T_2 and T_3 are shifted towards the lipophilic pocket lined by W5, V62 (solely present in hCA I), H64, and P201, where the cyanoethyl moiety receives an H-bond by W5 NH. The cyanoethyl in T_1 engages interactions with the hydrophilic half of the binding cavity among which it forms an H-bond with N69. As for hCA II, the tail of the ligand occupies on the whole a region nearer to the hydrophobic half of the active site. In fact, the phenethyl in T_2, as observed in crystallography with similar

ligands, lies above F131 interacting with residues 13-135 of the α-helix. The position of the two cyanoethyl portions is almost inverted when compared to hCA I: the moiety in T_1 receives H-bond by H64 NH, whereas the nitrile group in T3 is in H-bond distance with N67. As compound **A39** uniquely possesses, among the selected derivatives (Figure 35), two aliphatic, partially polar but non-protic tails (cyanoethyl), it can be supposed to possess a favorable complementarity with the narrow and rather lipophilic active sites of hCA I and II, which drives the most potent action here reported against the two ubiquitous isoforms (K_{IS} of 61.6 and 0.7 nM respectively).
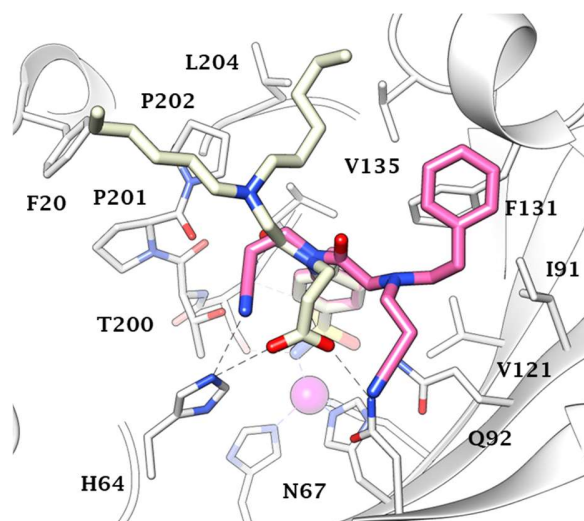
Figure 35. *In silico* predicted binding conformations of **A39** (fuchsia) and **A49** (white) in CA II active site. H-bond and salt bridge interactions are depicted as black, and red dashed lines, respectively.

In fact, the greater steric hindrance produced by another phenethyl in T_1 (compound **A34**, Figure 31B and 35) lowered the inhibition potency by 10 and 500 times against hCA I and II, respectively. Solely the presence of a carboxyethyl tail in T_3 of compound **A46** (but not **A48**, presumably because of the unwieldy naphthyl ring in T_1) leads the inhibitor action against isoform I (K_I of 79.5 nM) and II (K_I of 2.4 nM) to the level of compound **A39**, likely because of the interactions of the carboxylate with the hydrophilic portion of the binding cavity (Figures 31E-F and 35B).

The active site of hCA IV is the most particular among those of hCAs as largely losing the hydrophobic/hydrophilic division common to most other catalytically active isoforms. In

fact, α-helix 130-135 is absent and replaced by an extended loop that protrudes to bulk solvent. At the same time, the hydrophobic half of the binding cavity is replaced by a region rich in polar amino acids such as K91, E123, T202, D204, K206, and E138 (Figure 36 and 37C).
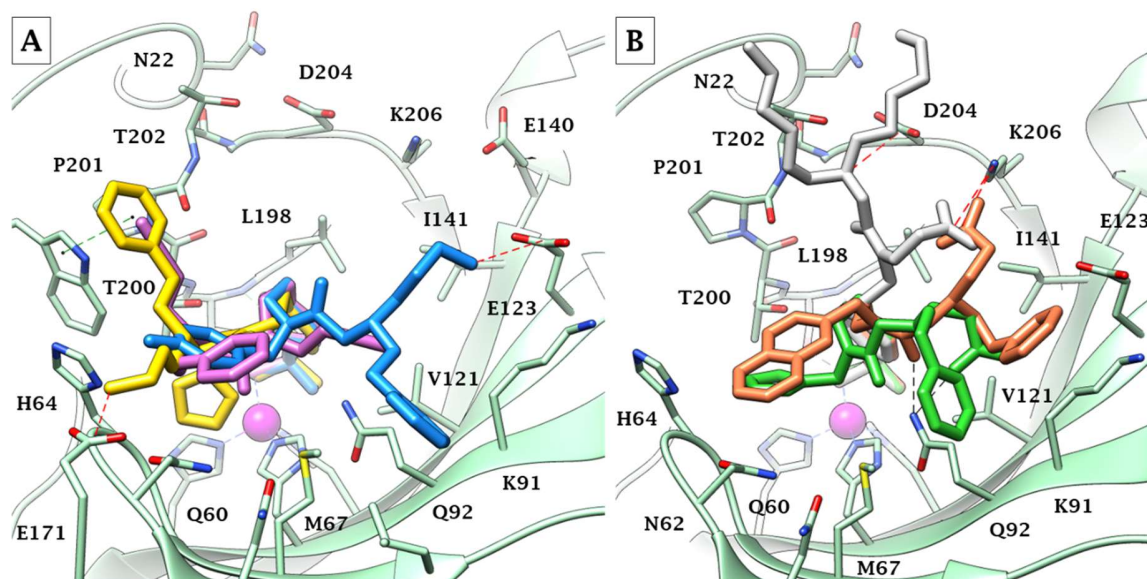
Figure 36. *In silico* predicted binding conformations of A) **A39** (magenta), **A41** (yellow), **A42** (blue) and B) **A46** (green), **A48** (orange), **A49** (light grey) in CA IV active site. H-bond, π-π and salt bridge interactions are depicted as black, green and red dashed lines, respectively.

As a result, this isoform is the less inhibited by **TTIs**, with K_{IS} above 100 nM, except for derivative **A49**, which solely possesses a carboxylate function in T_1. As shown in Figure 37A, the latter forms a salt bridge with K206, and this conformation also leads the protonated T_2/T_3 N branching atom in a salt bridge with D204. Other ligands, such as **A41**, **A42** and **A48**, were also predicted to form salt bridges within the hCA IV active site (Figure 36), but involving carboxylate or amine moieties in T_3. As a result, the ligands adopt conformation which do not allow the formation of two salt bridges with the polar pocket of the active site, as observed for **A49**. As the latter shows a K_I of 45.8 nM despite two hexyl groups protruding to bulk solvent (Figure 37A), it can be supposed that their replacement with less lipophilic groups might even increase the inhibition efficiency of this membrane-associated CA.

Figure 37. *In silico* predicted binding conformations for the adducts A) **A49**/hCA IV, and B) **A42**/hCA XII; predicted binding conformations of C) **A34** (purple), **A39** (magenta), **A41** (light yellow), **A42** (blue) and D) **A46** (green), **A48** (orange), **A49** (white) in CA XII active site. H-bond, π-π and salt bridge interactions are depicted as black, green and red dashed lines, respectively.

Isoform CA XII maintains an overall hydro/lipophilic partition in its wide active site (F/A131 with respect to CA II), but specific mutations with respect to CA II, that are N/K67, I/T91, G/S132, V/S135, and L/N204, significantly enhance the hydrophilicity of the binding cavity (Figure 37B-D). It should be noted that compound **A42** shows the unique subnanomolar K_I value against a tumor-associated CA XII (K_I = 0.6 nM). The peculiar active site architecture

of CA XII indeed drives a favorable disposition of the three tails of the ligands: the T_1 4-F-phenyl accommodates in the pocket lined by W5, H64, N62, and K67; the T_2 phenethyl lies over the most lipophilic cleft of the binding pocket, made by V121, T91 and A131; the propylamine pendant in T_3 is involved in a bifurcated H-bonds system with the side chain N136 and S132 backbone CO (Figure 37B). In contrast, compound **A41**, having a furyl ring in place of the 4-F-phenyl of **A42**, exhibits a very different binding orientation in the CA XII active site (Figure 37C,D), as it occurred with CA II as well (Figure 31 and 37).

For a first pharmacological application of the proposed approach, we selected the inhibitors showing the best concomitant action against CA II, IV and XII (**A39**, **A46** and **A47**) for evaluating their intraocular pressure (IOP) lowering activity in a rabbit model of glaucoma (Figure 38).
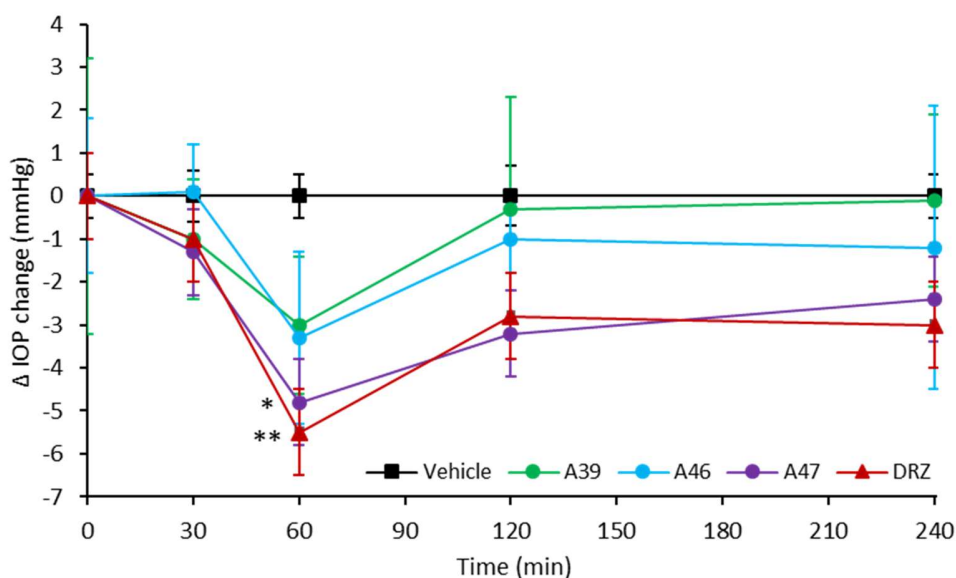
Figure 38. Drop of intraocular pressure (ΔIOP, mmHg) versus time (min) in hypertonic saline induced ocular hypertension in rabbits, treated with 50 μL of 1% solution of compounds **A39**, **A46** and **A47,** and **DRZ** as the standard. Hydroxypropylcellulose at 0.05% was used as vehicle. Data are analyzed with 2-way ANOVA followed by Bonferroni multiple comparison test. * $p < 0.05$ **A47** *vs* vehicle at 60'; ** $p < 0.01$ **DRZ** *vs* vehicle at 60'.

The compounds showed a sufficient water solubility to be formulated as 1% eye drops and **DRZ** hydrochloride 1% was used as reference compound and hydroxypropyl cellulose 0.05%

as vehicle in the experimental setting. The compounds were formulated and administered as 1% eye drops to rabbits with high IOP, induced by the injection of 0.05 mL of hypertonic saline solution (5% in distilled water) into the vitreous of both eyes. As depicted in Figure 4, at 30 min post-instillation only compounds **A39** and **A47** decreased the IOP by 1.0 and 1.3 mmHg, respectively such as **DRZ** (-1.0 mmHg), while **A46** was inactive. At 60 min after administration, all compounds triggered the maximum IOP reduction, where **A39** and **A46** showed a maximal IOP lowering activity of 3.0 and 3.3 mmHg, respectively. Instead, compound **A47** resulted in the most effective, decreasing the IOP of 4.8 mmHg in a comparable manner of **DRZ** (-5.4 mmHg). After 120 min, a decrement of the effect was observed for all compounds with **A39** and **A46** that decreased IOP by 0.3 and 1.0 mmHg, while the standard **DRZ** showed to be less effective than **A47** (-3.2 mmHg) with an IOP reduction of 2.8 mmHg. Uniquely, compounds **A46** (-1.2 mmHg) and **A47** (-2.4 mmHg) protracted their action at 240 min post-instillation, whereas compound **A39** was inactive. In particular, **A47** showed a similar profile to the standard **DRZ** (-3.0 mmHg).

The experimental procedures are reported in Chapter 7 and the data and results of this research were published in Bonardi, A., et al. *J. Med. Chem.* **2020**, *63*, 7422-7444.[283]

3.2 Development of H2S donors-carbonic anhydrase inhibitor hybrids for the treatment of inflammatory diseases and tumors (Series B)

Rheumatoid arthritis (RA) and Juvenile idiopathic arthritis (JIA) are inflammatory diseases that mainly affect people over sixty and under sixteen years old, respectively. The patients have chronic inflammation of the synovial membrane, leading to the articular cartilage and juxta-articular bone destruction with deformity as a final consequence.[284-286]
The pathophysiology of RA and JIA is unknown to date. It is supposed that activation of endothelial cells induces new blood vessel growth and a hyperplastic expansion of the synovial membrane that invades the periarticular bone at the cartilage-bone junction, leading to bony erosions and cartilage degradation.[284-286]

This process promotes the migration in loco of macrophages and leukocytes (T cells, B cells, and monocytes) that release pro-inflammatory cytokines, such as the tumor necrosis factor (TNF) and interleukin-6 (IL-6), stimulating the production of several secondary modulators: the nuclear factor κB ligand (RANKL), which is responsible for the osteoclast differentiation and osteoblasts apoptosis, prostaglandins and matrix metalloproteinases that mediate the symptoms of the disease, including pain, swelling and degradation of cartilage and bone.[284,285,287]

Important evidence is that the patients with RA show the concomitant presence of a lower pH (6.5) in the synovial fluid, with respect to healthy patients or affected by osteoporosis, which is also linked to the inflammatory reaction and direct damage to the cartilage and tissue around the joint.[39,288-295] Furthermore, it was demonstrated that the synovial fluid became acidic as the intensity of the inflammatory response increased and the more intense is the inflammatory reaction more acid became the synovial fluid pH, provoking pain.[288-289]

Several isoforms of carbonic anhydrases are identified in articular diseases.[1,2] In detail, hCA I was found to be over-expressed in the synovium of the patients with ankylosing spondylitis (AS), and transgenic mice that over-expressed hCA I showed aggravated joint inflammation and destruction.[296,297] Antibodies to hCA III and IV have been in RA while a significant increase of hCA IX and hCA XII protein and activity are recognized in biological specimens from JIA patients.[38,39] Furthermore, hCA IX and XII have been found in hypoxic tumors, as crucial for cancer survival and development.

Hypoxia is a key feature of many tumors as responsible for the Warburg effect, the metabolic switch of cancer cells from glycolytic metabolism to fermentation.[298-303] The inadequate supply of oxygen is primarily a pathophysiological consequence of structurally and functionally disturbed microcirculation and deteriorated oxygen diffusion processes. [298-304] Tumor hypoxia appears to be strongly associated with the propagation, malignant progression, and resistance to chemotherapy and radiotherapy of tumors.[298-304] In hypoxic conditions the hypoxia-inducible factor 1 (HIF1) triggers a signaling cascade that regulates the expression of several genes, including hCA IX and XII isozymes (Figure 39A).[298-307] The hCA IX and XII expression is strongly increased in many types of tumors, such as gliomas/ependymomas,[299] mesotheliomas,[299] papillary/follicular carcinomas,[299] carcinomas

of the bladder,[308] uterine cervix,[309,310] nasopharyngeal carcinomas,[311] head and neck,[312] breast,[306,313,314] esophagus,[299] lungs,[315] brain,[299] vulva,[299] squamous/basal cell carcinomas,[299] and kidney tumors,[316] among others and is downregulated by the wild-type von Hippel-Lindau tumor suppressor protein (pVHL).[298-307] In some cancer cells, the VHL gene is mutated leading to the strong upregulation of tumor-associated CA isoforms as a consequence of constitutive HIF activation.[299,304,313] In order to survive in hypoxic conditions and acidosis due to fermentative metabolism, which could promote mitochondrial damage and induce cell apoptosis, tumors express the transmembrane CA IX and XII, and more other proteins, responsible to maintain an intracellular pH of 7.2 acidifying the extracellular pH to 6.8 (Figure 39B).
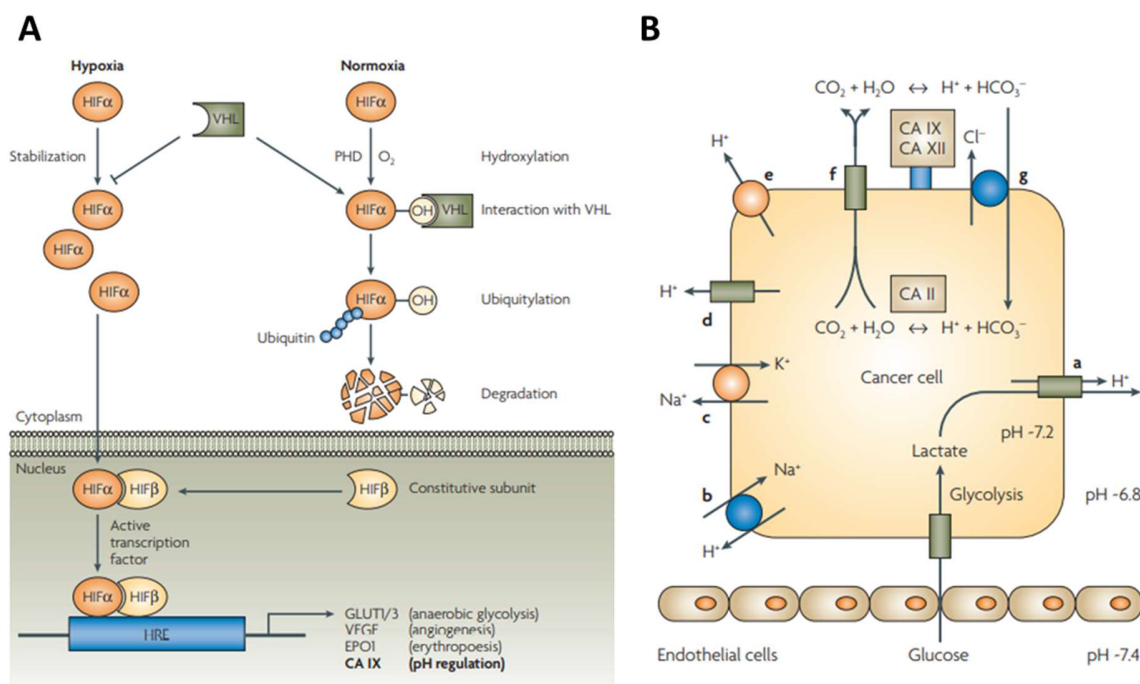
Figure X1. A) Mechanism of hypoxia-induced gene expression mediated by the HIF transcription factor. B) Proteins and processes involved in pH regulation within the tumor cell. CO_2 hydration to bicarbonate and protons is catalyzed in these cells by the transmembrane isozymes, CA IX and XII, possessing an extracellular active site. Other involved proteins include (a) monocarboxylate carrier, (b) Na^+/H^+ antiporter, (c) ATP-dependent Na^+/K^+ antiporter, (d) H^+ channels, (e) plasma-membrane proton pump H^+/ATPase, (f) aquaporins, and (g) anion exchangers.

Hydrogen sulfide (H_2S) is a gasotransmitter of the human body - together with nitric oxide (NO), and carbon monoxide (CO) – and has been widely investigated in the last three decades.[317] Its endogenous synthesis is attributed to three enzymes with different subcellular and tissue distribution called cystathionine-β-synthase (CBS), cystathionine-γ-lyase (CSE), and 3-mercaptopyruvate sulfurtransferase (3-MST), that use as L-cysteine, L-homocysteine, and 3-mercaptopyruvate, respectively as substrate.[317-320] Once synthesized by a cell, this ubiquitous small gaseous signaling molecule performs a paracrine action that involves at least 200 neighboring cells, according to its lipophilic nature which allows the crossing of membranes.[321] Hydrogen sulfide has not a specific receptor or signaling pathway, but it triggers many cellular effectors in a cell/tissue/species-dependent way, being it involved in various and important physiological processes such as modulator of vascular tone and blood pressure, neurotransmission and nociception, angiogenesis, cardiac function, various leukocytic functions, penile erectile function, scavenger action, ATP synthesis stimulator and other.[317,321]

Several studies demonstrated that the pathogenesis of many diseases such as inflammatory ones is also related to the deficiencies of hydrogen sulfide and the treatment with H_2S releaser improves the symptoms.[317,322-331] On the other hand, other studies have confirmed the toxicity of this gasotransmitter against tumors, in which the CA IX and XII are also involved.[332]

Basing on these considerations we developed H_2S releaser-CAI hybrids, to combine the hydrogen sulfide activity and the inhibition of proper hCA isoforms for the treatment of inflammation and tumors.

Thus, the inhibition of specific CAs, whose activity is abnormal on the synovial membrane, could repristinate the normal pH of the synovial fluid, alleviating the RA and JIA symptoms (pain, cartilages, and bony erosion).[333] On the other hand, the released H_2S suppresses the inflammatory process on several levels improving symptoms such as redness, swelling, heat, pain, and loss of function, blocking leucocyte adhesion, promoting neutrophils apoptosis, analgesia, and reparation of the damage.[317,322-324] Moreover, H_2S prevents the formation of the complex RANKL-RANK, blocking the transcription of pro-inflammatory cytokines, osteoclasts differentiation, and osteoblast apoptosis, protecting by bony erosion.[287,325,333,334]

The same approach could be successful also in the context of hypoxic tumors, where the inhibition of the overexpressed CA IX and XII prevents their growth, invasion, and metastasis formation, while the release of hydrogen sulfide blocks tumor proliferation, stopping the cell replication in the G_2 and M phase, and also promotes apoptosis.[332]

The design of H_2S releaser - CAI hybrids has to be guided by the knowledge that hydrogen sulfide is a toxic gas. In fact, if inhaled at high concentrations (> 20ppm) it enters the bloodstream and tissues determining the blockage of the cell respiratory chain by binding the cytochrome C oxidase iron, inducing oxidative stress and blocking the synthesis of ATP, which can be fatal (ppm = 1000).[318] Basing on this evidences, it is important to control the H_2S release to have its optimal concentration and achieve only the therapeutic effect. In literature, a large variety of H_2S donor scaffolds is reported and classified according to the H_2S release trigger mechanisms and by the H_2S concentration released during the time (Figure 40).[335]
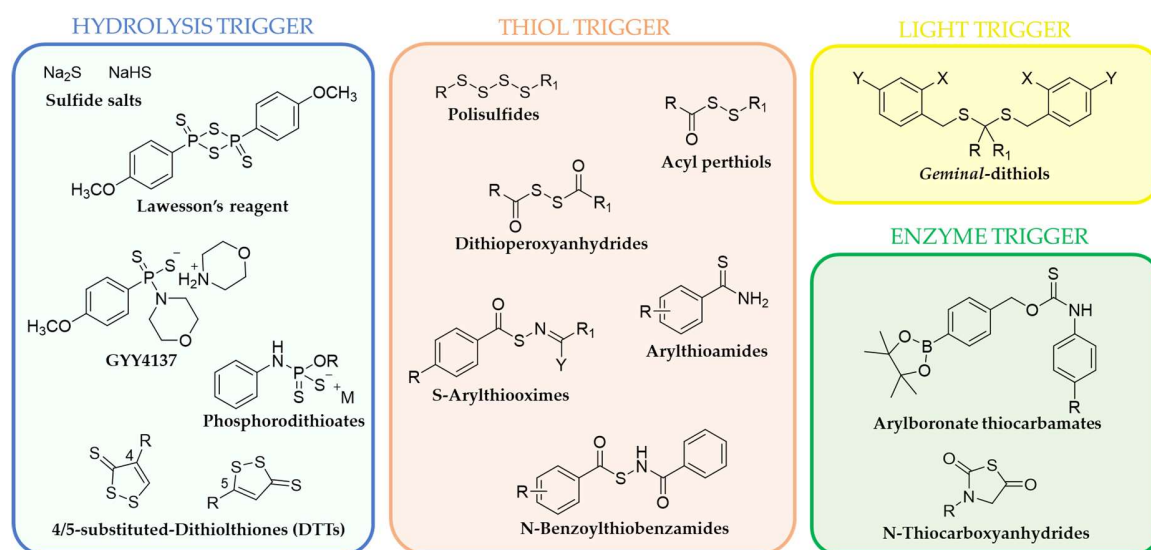
Figure 40. Some H_2S releaser scaffolds distinguished by the H_2S release trigger mechanisms.

On the basis of the therapeutic application as anti-inflammatory/antitumor drugs and the rate of H_2S release, we started our investigations adopting a 4-substituted dithiolthione (**DTTs**) scaffold as hydrogen sulfide releaser (Figure 40).[336] The latter was previously identified as hydrolysis triggered H_2S releaser, though in a paper by Li, L., et al. a metabolic activation

was observed as needed.[337] Benzenesulfonamides were used as CAI fragments to achieve a potent CA inhibition.
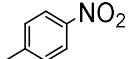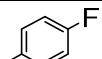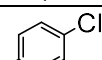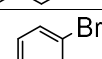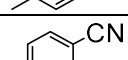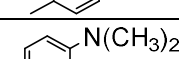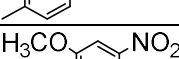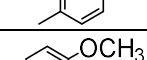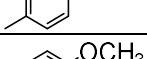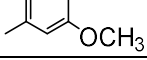
The synthesis of the H2S releaser - CAI hybrids is reported in *Scheme 4* and it starts with the preparation of the 4-substituted **DTT** nucleus through three reactions. Initially, the 4-isopropylbenzoic acid is protected through the formation of the ethyl ester **B1**, using $SOCl_2$ in dry EtOH. Then the **DTT** nucleus is obtained by reaction of the derivative **B1** in melted sulfur at 220 °C, obtaining the intermediate **B2** which is hydrolyzed in CH_3COOH and H_2SO_4 9M, CH_3COOH at 100 °C, to give the carboxylic acid **B3**. The secondary amines **A1-3**, and **B4-13** were synthesized starting from 4-(2-aminoethyl)benzenesulfonamide, applying a reductive amination in presence of aromatic aldehydes and sodium borohydride in dry MeOH or, alternatively, a nucleophilic substitution with the appropriate halides in dry DMF to obtain **A6**, and **A7**. Finally, the coupling reaction between the carboxylic acid **B3** with the prepared amines (**A1-3**, **A6**, **A7**, and **B4-13**), in presence of DIPEA and PyBOP in dry DMF, gave the desired hybrids **B14-28**.


A1, B14: R=C_6H_5
A2, B15: R=4-NO_2-C_6H_4
A3, B16: R=4-F-C_6H_4
B4, B17: R=4-Cl-C_6H_4
B5, B18: R=4-Br-C_6H_4
B6, B19: R=4-CN-C_6H_4
B7, B20: R=4-$N(CH_3)_2$-C_6H_4
B8, B21: R=2-OCH_3,4-NO_2-C_6H_4

B9, B22: R=4-OCH_3-C_6H_4
B10, B23: R=3,4-OCH_3-C_6H_4
B11, B24: R=4-SCH_3-C_6H_4
B12, B25: R=1-Naph
B13, B26: R=3-Thionaph
A6, B27: R=CH_2CN
A7, B28: R=$CH_2C_6H_5$
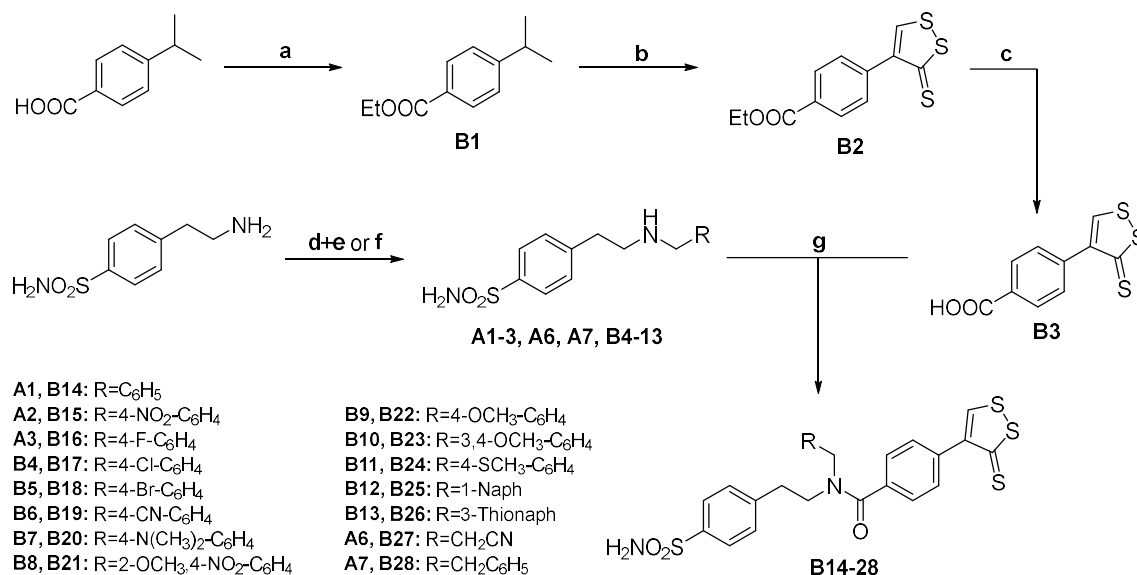
Scheme 4. Reagents and conditions: a) $SOCl_2$, dry EtOH, 0 → 60 °C, 6 h; b) S_8, 135 → 220 °C, 6-8 h; c) H_2SO_4 9M, CH_3COOH, 100 °C, 4 h; d) RCHO, dry MeOH, reflux, 4 h; e) $NaBH_4$, dry MeOH, reflux, 0.5-2 h; f) R-X, dry DMF, r.t or 60 °C, 0.5-6 h; g) DIPEA, PyBOP, dry DMF; r.t, o.n.

The synthesized compounds **B14-28** were submitted to a stopped-flow kinetic assay against five hCAs that are I, II, IV, IX and XII, using acetazolamide (AAZ) as standard.[282] The cytosolic enzymes hCA I and II are considered the off-target isoforms for most CAIs therapeutic applications, but are also involved in articular inflammation (hCA I) and bone resorption (hCA I and II).[1,296,297,336] Isoforms hCA IV, IX and XII were recently identified to be overexpressed on the synovial membrane and linked to inflamed conditions.[333,282] Moreover, as stated above, hCA IX and XII are validated antitumor targets.

In Table 6 the K_I values (nM) for all compounds **B14-28** are reported. These bulky derivatives reported promising CA inhibition profiles when considering anti-inflammatory and antitumor applications.

Table 6. Inhibition data of hCA isoforms hCA I, II, IV, IX, and XII with sulfonamides **B14-28** reported here and the standard sulfonamide inhibitor acetazolamide (AAZ) by a stopped-flow CO_2 hydrase assay.[282]

Cmpd	R	K_I (nM)[a]				
		CA I	CA II	CAIV	CA IX	CA XII
B14		770.7	479.9	4339.7	43.0	9.7
B15	NO2	7452.9	918.7	>10000	36.6	32.9
B16	F	5324.1	599.8	>10000	46.3	65.3
B17	Cl	5504.9	2974.1	430.1	24.0	9.8
B18	Br	7703.9	3660.6	1042.1	19.1	12.9
B19	CN	>10000	4826.4	46.2	40.3	8.8
B20	N(CH3)2	4260.7	995.4	3412.3	22.7	9.5
B21	H3CO NO2	6697.4	2950.5	4092.6	4.1	7.7
B22	OCH3	2214.8	589.1	1586.2	50.3	76.4
B23	OCH3 OCH3	890.3	218.5	292.6	18.6	8.5
B24	SCH3	7210.5	9645.8	403.8	46.2	8.4
B25		>10000	4464.3	244.2	15.6	7.0

B26		>10000	2481.7	48.0	2.4	8.3
B27	⌐CN	429.2	60.4	523.1	28.7	9.5
B28		4387.0	660.9	243.2	125.7	9.5
AAZ	-	250.0	12.5	74	25.0	5.7

a. Mean from three different assays, by a stopped-flow technique (errors were in the range of $\pm 5-10\%$ of the reported values).

In fact, the derivatives mostly display a weak inhibition of the off-target CA I (in the micromolar range), except for derivatives **B14** and **B23** that inhibited this isoform in the high nanomolar range ($K_I = 770.7$, and 890.3 nM, respectively), and a lightly better inhibition against the most physiologically relevant hCA II. Against the latter, a subset of derivatives (**B14**, **B15**, **B22**, **B23**, **B28**) acts in the high nanomolar range ($K_I = 218.5$-660.9 nM). When a less bulky R substituent was incorporated (R = CH_2CN), the efficacy against I and II increases as in compound **B27** (CA I $K_I = 429.2$ nM; CA II $K_I = 60.4$ nM), obtaining the most active compound against both off-target isoforms.

As for CA IV, the *p*-CN **B19** ($K_I = 46.2$ nM) and the 3-benzothiophene **B26** ($K_I = 48.0$ nM) derivatives exhibited K_I values below 100 nM, resulting in the most potent and also the first (CA II / CA IV = 104) and the second (CA II / CA IV = 52) selective compounds against this isoform, respectively. Moreover, compounds **B17**, **B23-25**, **B27**, **B28** showed an inhibition profile in the range of the high nanomolar ($K_I = 243.2$-523.1 nM) versus CA IV, while the remaining compounds were weak inhibitors acting in the micromolar range ($1.0 \geq K_I > 10.0$ µM).

Interestingly, CA IX and XII, which possess a rather roomier active site for accommodating these bulky substituents, were the most inhibited CAs. The K_{I}s were in a narrow range against both isoforms (CA IX $K_I = 2.4$-125.7 nM and CA XII $K_I = 5.7$-76.4 nM).

In particular, compounds **B26** and **B21** were the most potent and selective inhibitors (CA II / CA IX = 1034 and 719, respectively) with a K_I of 2.4 nM and 4.1 nM, respectively, while the elongation of the linker as in **B28** reduced the K_I to over 100 nM ($K_I = 125.7$ nM). All the other hybrids resulted in CA IX inhibitors in the medium nanomolar range with K_I values between 15.6-50.3 nM.

Instead, isoform CA XII is strongly inhibited by a subset of compounds (**B14**, **B17**, **B19-21**, and **B23-28)** with K_I values in a low nanomolar range (K_I = 7.0-9.8 nM). Among these, derivatives **B25** (K_I = 7.0 nM) and **B21** (K_I = 7.7 nM) were the most potent CA XII inhibitors, while **B24** (K_I = 8.4 nM) and **B25** (K_I = 7.0 nM) resulted in the most selective compounds against this isoform (CA II / CA XII = 1148 and 637, respectively). Compounds **B15**, **B16**, **B18**, and **B22** inhibited CA XII in the medium nanomolar range with K_I values between 12.9-76.4 nM.

Despite the evidence of the H_2S release properties of the adopted scaffold,[337] a specific assay is being carried out to verify whether the CAI incorporation influences such a release. Indeed, according to the paper mentioned above,[337] no H_2S release was observed upon simple hydrolysis. Thus to detect the release of H_2S, compounds (100 μM) will be incubated (37°C) for timed intervals (0–90 or 180 min) with rat plasma, phosphate buffer, or fresh or boiled (1 min) rat liver homogenate (430 μl), in presence of pyridoxal 5′-phosphate (2 mM; 20 μl) and physiological saline (50 μl). The concentration of H_2S released will be measured spectrophotometrically using the methylene blue assay, injecting zinc acetate (1% w/v, 250 μl) to trap generated H_2S, followed by trichloroacetic acid (10% w/v, 250 μl) to precipitate protein and thus stop the reaction. Baseline H_2S concentration will be determined in incubates in which trichloroacetic acid (10% w/v, 250 μl) was added directly to the tissue homogenate before the addition of L-cysteine and subsequent incubation as described above. Subsequently, N,N-dimethyl-p-phenylenediamine sulfate (20 μM; 133 μl) in 7.2 M HCl will be added followed by $FeCl_3$ (30 μM; 133 μl) in 1.2 M HCl, and absorbance (670 nm) of aliquots of the resulting solution (300 μl) will be determined 10 min thereafter. The H_2S concentration of each sample will be calculated against a calibration curve of Na_2S (3.125–250 μM) and results will be expressed as nmol H_2S formed/mg soluble protein.[337]

The effects of the most selective compounds for CA IV, IX, and XII over CA I and II (**B21**, **B24-26**) were evaluated in a rat model of rheumatoid arthritis induced by the intra-articular injection of Complete Freund's Adjuvant (CFA) in the Paw Pressure and Incapacitance tests, in the framework of a collaboration study with the research group of Professor Carla Ghelardini from University of Florence. Moreover, the synthetic precursors of compound

B25 (**B3**, **B12**) were tested to evaluate the efficacy of the hybrid with respect to the single drugs.

The Paw Pressure test measured the hypersensitivity to a mechanical noxious stimulus after oral administration dose of the compounds at 1, 10 and 30 mg/kg (Figure 41).
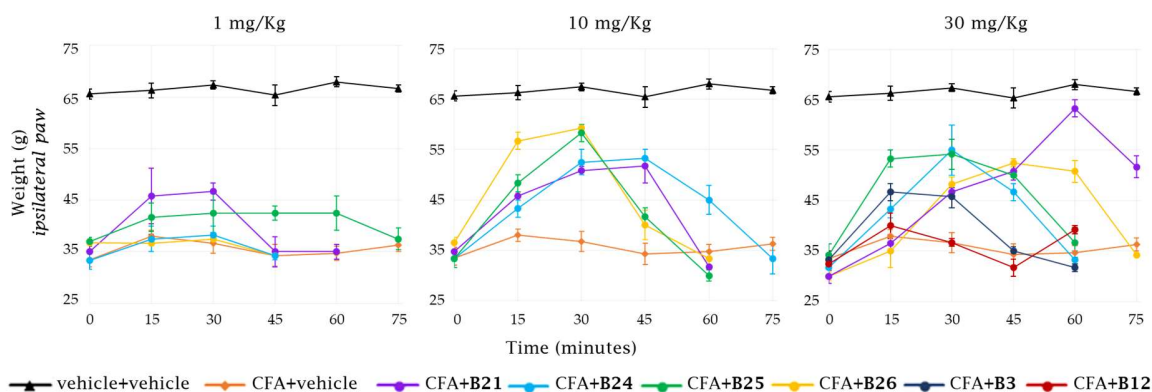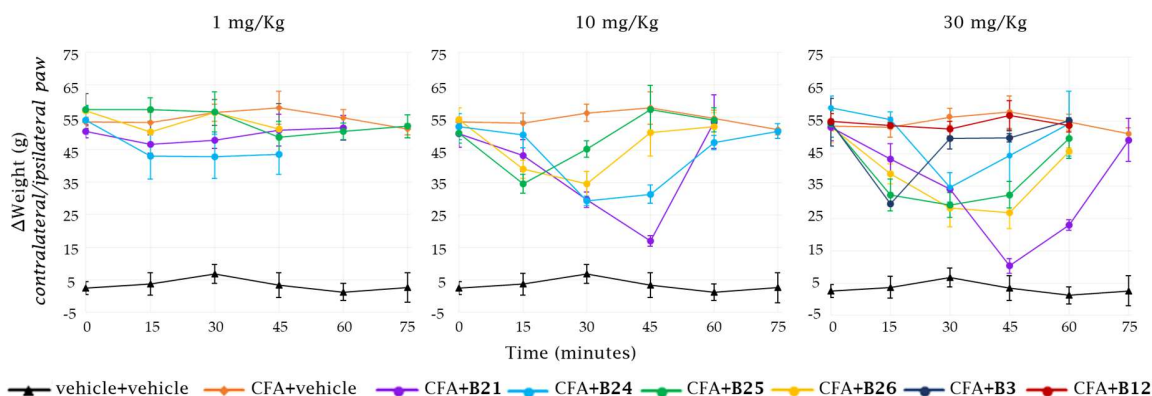

Figure 41. Acute pain-relieving effect of hybrids **B21**, **B24**, **B25** and **B26** respect to the single drugs **B3** and **B12** in a rat model of rheumatoid arthritis induced by CFA intra-articular injection measured through Paw Pressure Test.

In the group treated with CFA (orange line), the weight tolerated on the ipsilateral paw decreased to 33 g in comparison to the control value of 65 g (black line). All orally administered compounds evoked an anti-hypersensitivity effect in a dose-dependent manner; the dose of 30 mg per Kg increased the pain threshold of the ipsilateral paw above 47 g at 30 min after treatment with all tested hybrids. In detail, **B25** and **B26** show the maximum efficacy at 30 min. That of **B24** increases till 45 min, while **B21** interestingly shows a maximum action at 60 min post-administration. The H_2S releaser portion **B3** shows a feeble maximum action at 15 min, while the CA inhibitor **B12** oddly did not report activity.

The Incapacitance test evaluated the postural unbalanced weight related to spontaneous pain (Figure 42).

Figure 42. Acute pain-relieving effect of hybrids **B21**, **B24**, **B25** and **B26** respect to the single drugs **B3** and **B12** in a rat model of rheumatoid arthritis induced by CFA intra-articular injection measured through Incapacitance Test.

The difference between the weight on the contralateral and the ipsilateral paw was significantly increased to 55 g (orange line) in animals treated with CFA in comparison to the 2 g of the control group (black line). As in the paw pressure test, all orally administered compounds reduced the Δ weight value in a dose-dependent manner. In particular, for all tested hybrids the dose of 30 mg per Kg restores the postural unbalance up to 35 g at 30 min after treatment, and moreover down to 10 g after 45 min of treatment with derivative **B21** (purple line). Again, **B25** and **B26** show their maximum efficacy at 30 min. Again, the action of **B24** reached a maximum at 45 min, and **B21** reported a peak of efficacy after 45 min. The H$_2$S releaser portion **B3** shows a comparable action with **B26** at 15 min, while the CA inhibitor **B12** did not show activity.

On the other hand, a subset of compounds are being also tested as antiproliferative derivatives to have insights on the antitumor properties of CAI/H$_2$S releaser hybrids with respect to the single components.

In conclusion, we reported a series of H$_2$S releaser-CAI hybrids with potent and selective inhibitory action against the CAs overexpressed in inflammatory tissues and tumors. Because these compounds seem to be H$_2$S releaser subsequently to enzyme trigger and not hydrolysis trigger such as reported in the literature, the assay to measure the H$_2$S released by these compounds has been scheduled by a different protocol, that is in rat liver and kidney homogenate.[337] To date, only the pain-relieving action of these hybrid derivatives was

evaluated *in vivo* in a rat model of RA. Promising data was measured by the Paw Pressure and Incapacitance tests. A comparison study between the *in vivo* action of the most active compound **B21** and the co-administration of the single entities is currently ongoing to point out a multi-target effect.

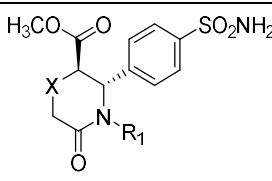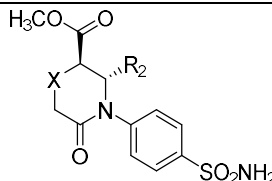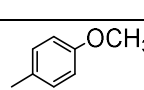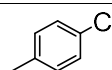The experimental procedures are reported in Chapter 7.
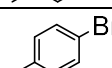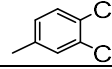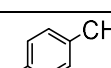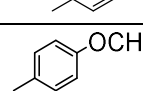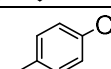
3.3 From random to rational: a discovery approach to selective subnanomolar inhibitors of human carbonic anhydrase IV based on the Castagnoli-Cushman multicomponent reaction (Series C)

As aforementioned in the preceding paragraph 3.2, CAs in general have been considered important regulators of tumor cell pH by modulating the balance of protons and bicarbonate anions necessary to cell survival and proliferation. Of the fifteen human CA isoforms, however, only hCA IX and XII have been considered valid drug targets for cancer.[338] Other isoforms may also be considered as cancer targets, but little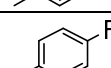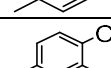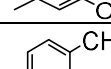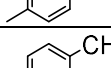 is known about their specific function even though there is evidence of their expression and upregulation in tumors.[339] The tumor-associated potential of hCA IV (particularly in brain tumors) is little studied. However, it is known that hCA IV mRNA expression is elevated in gliomas, renal cell carcinomas, thyroid cancers, and melanomas.[339-341] The recently noted disconnect between inhibition of hCA IX and XII and antiproliferative activity on cancer cells[342] also suggests that other isoforms can be implicated in the overall cellular activity.

Thus, the development of selective hCA IV inhibitors could to better define the role of this isoform in the progression and survival of brain tumors such as gliomas.

The development of CA IV selective inhibitors was carried out on the basis of a series of CAIs synthesized in the group of Prof. Mikhail Krasavin (Saint Petersburg State University) basing on the Castagnoli-Cushman reaction (CCR). Among these, compound **C2d** strongly inhibited CA IV in the low nanomolar range with K_I of 9.6 (Table 7). Despite that, derivative **C2d** was also a potent inhibitor against the off-target CA I (9.2 nM) and II (3.7 nM), and it acted with K_I of 34.0 nM against the CA VII (a target for neuropathic pain).[279]

Table 7. Inhibitory profile of compounds of the first series (**C1a-h**, **C2a-h**) against hCA I, II, IV and VII.[279]

Cmpd	X	R₁	R₂	K_I (nM)[a]			
				CA I	CA II	CA IV	CA VII
C1a	direct bond	(4-OCH₃ benzyl)	-	441.4	18.4	885.6	43.3
C1b	direct bond	(4-Cl benzyl)	-	501.7	153.8	8695.3	28.6
C1c	direct bond	(4-Br benzyl)	-	798.8	8.7	974.4	30.4
C1d	direct bond	(propyl)	-	764.2	38.2	542.9	48.1
C1e	direct bond	(isobutyl)	-	729.9	27.9	433.2	56.4
C1f	NMs	(isobutyl)	-	479.4	94.4	433.8	85.4
C1g	NMs	(3,4-diCl benzyl)	-	816.3	5.2	521.3	85.4
C1h	O	(isobutyl)	-	618.4	9103.9	9719.5	55.0
C2a	direct bond	-	(4-CH₃ phenyl)	51.0	4.8	71.7	49.4
C2b	direct bond	-	(phenyl)	81.5	61.7	958.0	78.8
C2c	direct bond	-	(4-OCH₃ phenyl)	9.1	4.9	443.6	81.7
C2d	direct bond	-	(4-Cl phenyl)	9.2	3.7	9.6	34.0
C2e	direct bond	-	(4-F phenyl)	351.7	2.6	80.5	86.3
C2f	NMs	-	(3,4-diCl phenyl)	513.5	65.0	713.3	65.1
C2g	NMs	-	(4-CH₃ phenyl)	91.3	56.4	778.4	79.2
C2h	O	-	(4-CH₃ phenyl)	8.9	3.8	607.9	78.7
AAZ	-	-	-	250.0	12.5	74.0	2.5

a. Mean from 3 different assays, by a stopped-flow technique (errors were in the range of ± 5e10% of the reported values); Ms = mesyl group.

Considering the shortage and the lack of selectivity of CA IV inhibitors,[343] compound **C2d** was considered a promising lead to use in a structure-based drug design and optimization campaign.

Once the binding mode of C2d was defined, a series of congeners were designed in order to increase the interaction with amino acid residues that are unique to hCA IV. Both enantiomers **(R,R)-C2d** and **(S,S)-C2d** were docked into the CA IV X-ray solved structure using the induced-fit docking procedure followed by refinement with the MM-GBSA (molecular mechanics/generalized Born surface area continuum solvation) method[344] (see Experimental Section, Chapter 7). The minimum-energy docking poses thus obtained are shown in Figure 43.
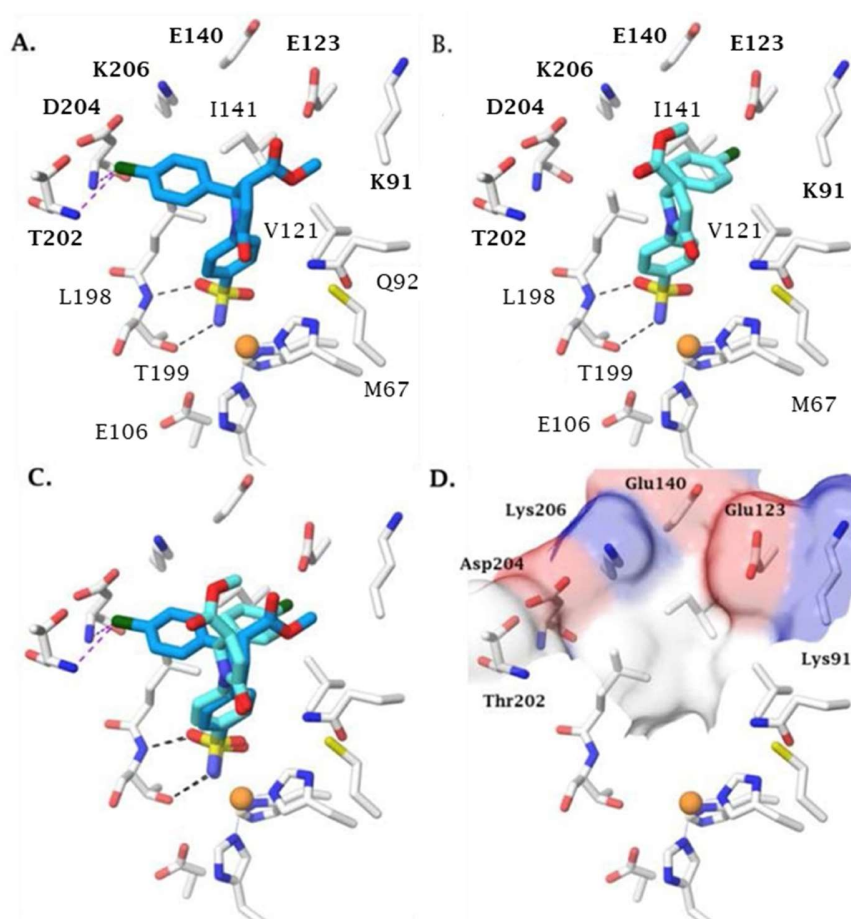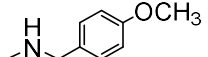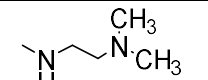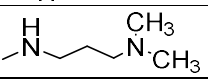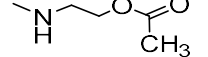

Figure 43. Predicted binding orientation of A) **R,R-C2d**, B) **S,S-C2d** and C) superposition of both enantiomers in the hCA IV active site; D) surface representation of the hCA IV targeted (pocket A).
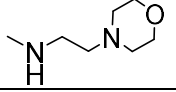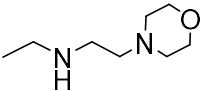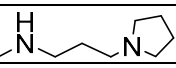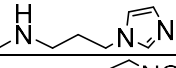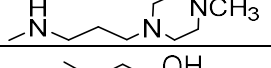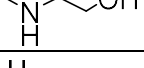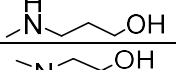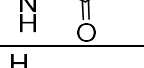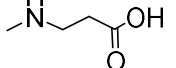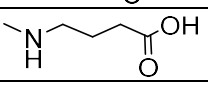
For both enantiomers, the orientation of the benzenesulfonamide motif is the same as for the majority of such ligands in the hCA active site, providing anchoring to the prosthetic zinc metal ion.[345] In particular, the sulfonamide group coordinates to the zinc ion *via* the negatively charged nitrogen atom, and establishes two H-bonds with the residue T199, as shown in Figure 43. Likewise, the pyrrolidin-2-one scaffold adopts a fully superimposable disposition in both enantiomers. The position of the 4-chlorophenyl fragment is distinctly different in the two enantiomers. In **(R,R)-C2d**, this substituent points towards T202 and D204 forming weak H-bonds through the chlorine atom with the backbone NH of both residues and further vdW contacts with their side chains. Additionally, the benzene ring forms π-alkyl interactions with the L198 side chain. The methyl ester moiety did not appear to be involved in significant contacts with the binding site residues, though pointing to the hydrophilic/charged area of hCA IV active site (Figure 43A).

For **(S,S)-C2d**, less favorable and more hindered binding was displayed by the 4-chlorophenyl portion. It accommodates at the edge between the lipophilic pocket lined by L198, I141 and V121, and the "middle" hydrophilic area of the binding site (Figure 43B). Such positioning is likely driven by hydrophobic contacts of the aromatic portion with L198 and I141 side chains and vdW interactions with the E123 carboxylate moiety. Similarly to the other enantiomer (Figure 43C), the methyl ester group in **(S,S)-C2d**, points to the outer edge of the active site, towards the same hydrophilic area of the cavity (termed herein 'pocket A'). The main structural feature of hCA IV active site that distinguishes it from that of the other hCAs, is the presence of a strongly hydrophilic/charged area ("pocket A" formed by K91, E132, E140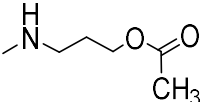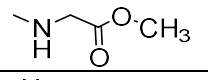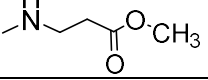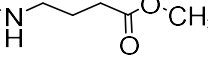, K206, D204 and T202 residues) which partially replaces the hydrophobic cleft typical of other α-CAs (Figure 43D). Considering that in both enantiomers of **C2d**, the methoxycarbonyl group points towards this area and that the group is not involved in contacts with the target counterpart, the core of **C2d** was decorated by attaching hydrogen bond donor/acceptor (HBD/HBA) moieties as well as ionizable carboxylic acid groups via a carboxamides linkage. Thus, the fruitful collaboration with the research group of Saint Petersburg State University continued and the group worked on synthesizing the **C2d**-derivatives (**C4a-w**) designed by our *in silico* approach (Table 8).[279]

All compounds were tested in CO_2 hydration stopped-flow biochemical assay[282] against the same hCA isoforms as the first-iteration lead **C2d** to produce the inhibition data (K_I) summarized in Table 8.

Tabella 8. Inhibitory profile of compounds **C3** and **C4a-w** against hCA I, II, IV and VII.[279]

Cmpd	R	K_I (nM)[a]			
		CA I	CA II	CA IV	CA VII
C3	-	350.4	44.8	25.1	48.3
C4a	NH₂	941.1	57.3	68.7	69.0
C4b	−N (pyrrolidine)	3285	30.0	84.8	96.4
C4c	−N__O (morpholine)	314.1	7.8	31.3	33.9
C4d	−N__S (thiomorpholine)	256.4	4.6	21.9	18.9
C4e	−N__NCH₃	819.3	4.5	4.7	58.0
C4f	N-CH₂-C₆H₄-OCH₃	2125	1.6	2.1	5.8
C4g	NH-CH₂CH₂-N(CH₃)CH₃	285.5	19.8	1.2	18.1
C4h	NH-CH₂CH₂CH₂-N(CH₃)CH₃	960.2	8.9	0.52	9.5
C4i	NH-CH₂CH₂-O-C(O)CH₃	1066	13.3	0.59	46.8
C4j	NH-CH₂CH₂CH₂-O-C(O)CH₃	5093	8.5	1.8	85.5
C4k	NH-CH₂-C(O)-O-CH₃	495.5	3.4	2.40	4.8
C4l	NH-CH₂CH₂-C(O)-O-CH₃	649.0	7.5	1.0	46.3
C4m	NH-CH₂CH₂CH₂-C(O)-O-CH₃	105.1	34.9	6.5	69.3

C4n		517.7	5.9	0.61	5.6
C1o		101.8	6.7	1.5	70.2
C4p		720.3	40.6	0.89	174.5
C4q		7797	32.6	0.66	304.1
C4r		748.1	9.5	0.39	34.6
C4s		369.6	4.8	0.9	62.8
C4t		6092	7.9	0.22	80.6
C4u		87.3	5.8	0.65	3.0
C4v		886.7	26.3	0.31	41.3
C4w		737.1	37.3	1.8	52.2
C2d	-	9.2	3.7	9.6	34.0

a. Mean from 3 different assays, by a stopped-flow technique (errors were in the range of ± 5e10% of the reported values).

Examination of the data in Table 8 clearly reveals the positive outcome of the undertaken modifications for improving the inhibitory potency and selectivity toward CA IV isoform. The single-digit nanomolar inhibition of CA I by **C2d** was apparently weakened by 2-3 orders of magnitude throughout the second generation analogs. At the same time, some analogs displayed one order of magnitude loss in potency against CA II and VII (e. g., **C4p-q**) while gaining potency by about the same factor against the target CA IV isoform (**C4i**, **C4n**, **C4p-v**). Clearly, the modification introduced in the second-iteration, aimed at building contacts with the HBA, HBD and positively changed side-chain residues in 'pocket A' which is unique to CA IV, resulted in many subnanomolar inhibitors of that isoform, thereby attesting the soundness of the design strategy. Among these subnanomolar CA IV inhibitors, compounds **C4i**, **C4p**, **C4q**, **C4r**, **C4t**, and **C4v** showed the best selectivity profiles, particularly, against CA II ubiquitously inhibited by a wide range of primary sulfonamides.

The best selectivity improvement in the second iteration was apparently achieved with compounds **C4p-q** and **C4v** having drastically different side chains. This, on one hand, justified the correctness of the unbiased "HBD/HBA" approach to targeting both types of interactions in "pocket A" as well potential electrostatic (salt bridge) contact which is likely the case with carboxylic acid **C4v**. On the other hand, we were intrigued whether if these hypothetical binding modes were predicted as the low-energy complex via docking.

Thus, compounds **C4p**, **C4q**, and **C4v**, which are turned out as the most selective for CA IV over the ubiquitous CA I and II as well as CA VII, were subject to *in silico* studies to show the interactions driving their subnanomolar inhibition efficacy for the target (hCA IV) isoform. Induced-fit docking procedures were used to allow the movement of the active site residues, particularly those of pocket A that are more exposed to the solvent. Both enantiomers of the three compounds were evaluated and the poses were submitted to MM-GBSA-based refinements (Figure 44).

The benzenesulfonamide fragments held the same orientation depicted for the lead molecule (**C2d**), not affected by the incorporation of bulkier amide residues at the methyl ester site of **C2d**. While the S,S-enantiomers of **C4p**, **C4q** and **C4v** all showed a **S,S-C2d**-like positioning for pyrrolidin-2-one and 4-chlorophenyl motifs, different lodging and interactions arose for the R,R-enantiomers compared to those earlier identified for **R,R-C2d**. In the R,R-enantiomers, the pyrrolidin-2-one core is partially rotated, the amide carbonyl group forms an H-bond with Q92, and the 4-chlorophenyl group is oriented towards W5 and H64 whose side-chain NH donate a weak H-bond to the chlorine atom.

Most importantly, both enantiomers of **C4p**, **C4q**, and **C4v** orient the charged hydrophilic HBA/HBD groups towards pocket A for both enantiomers likely driven by H-bonds and salt-bridge interactions Figure 44.

It is notable, however, that while the R,R-enantiomer's orientation enables these charged hydrophilic moieties to easily reach and interact with the pocket A amino acid residues, an evident torsion of the amidic linker is required in the case of S,S-enantiomers, which influences the set of interactions the charged groups can form with the protein. In particular, the positively charged imidazole ring of compound **C4q**, in both conformations, forms a salt bridge with the carboxylate side chains of E123 and E140 and a π-cation interaction with the

NH$_3^+$ of K206 (Figure 44A,B). The carboxylate group in the side chains of **R,R-/S,S-C4v** forms a salt bridge contact with the side chain of K206 in two different modes depending on the ligand absolute configuration (Figure 44C,D). The protonated pyrrolidine moiety of **R,R-C4p** is engaged in a salt-bridge contact with the carboxylates of E123 and E140 while the same pyrrolidine moiety in **S,S-C4p** forms an interaction only with E123 (Figure 44E,F).
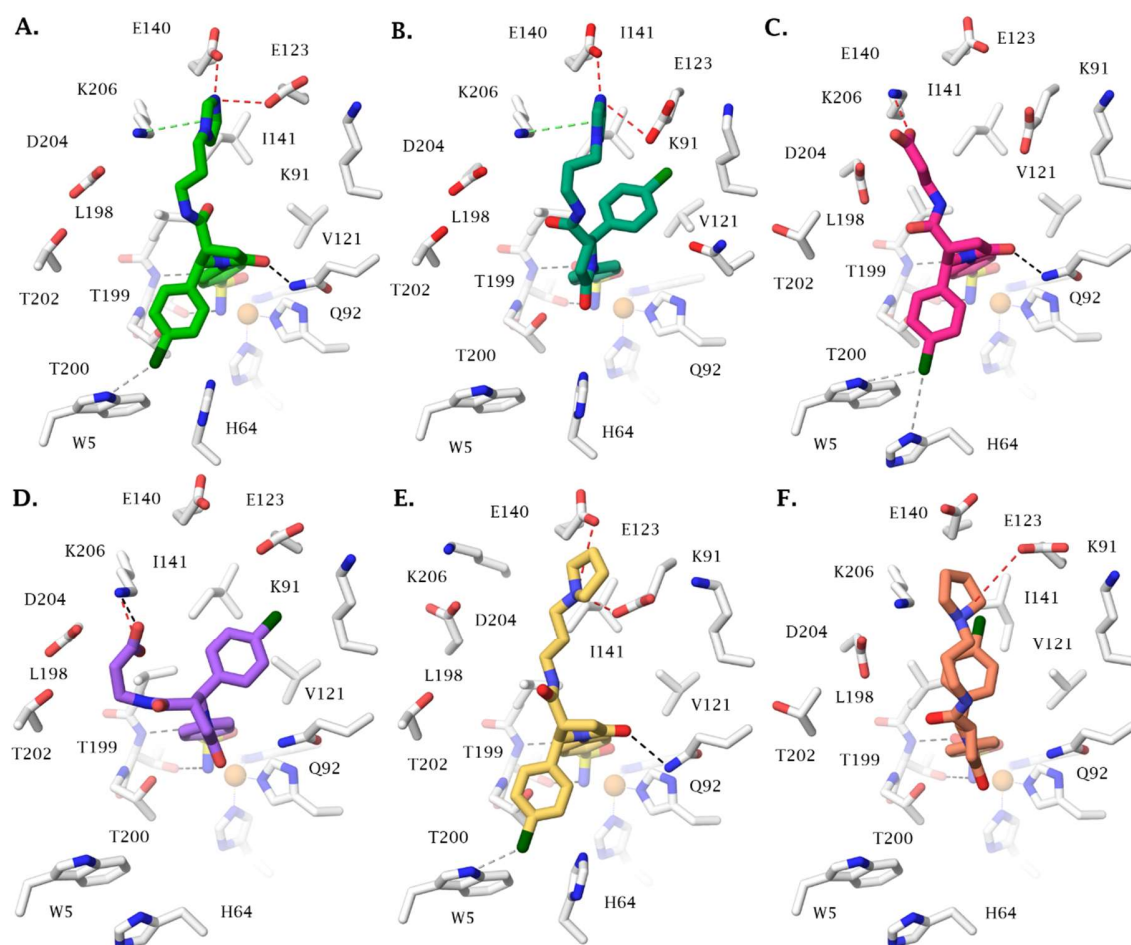
Figure 44. Induced-Fit docking of A) **R,R-C4q**, B) **S,S-C4q**, C) **R,R-C4v**, D) **S,S-C4v**, E) **R,R-C4p**, F) **S,S-C4p** in the hCA IV active site. Hydrogen bonds are represented as black dashed lines (weak ones in grey). Salt bridges are represented as red dashed lines. π-cation interactions are represented as green dashed lines.

Among the second iteration inhibitors, the derivatives **C4i**, **C4p**, **C4q**, **C4r**, **C4t**, and **C4v** showed selective, dose-dependent cytotoxicity against human glioma T98G cell line under

chemically induced hypoxia conditions. This effect may be related to the inhibition of CA IV by these compounds, considering the experimentally established increased mRNA expression of this enzyme under the hypoxic conditions. These findings substantially enrich the arsenal of available tool compounds to further elucidate the role of hCA IV as a drug target, particularly for the treatment of glioma.

The experimental procedures are reported in Chapter 7 and the data and results of this research were published in Kalinin S., et al. *Eur. J. Med. Chem.* **2019**, *182*, 111642.[279]

3.4 The antibiotic furagin and its derivatives are isoform-selective human carbonic anhydrase inhibitors (Series D)

Another strategy to overcome the lack of selectivity of primary sulfonamides was the research of isoform-selective CAI classes. A multitude of new chemotypes as well as novel CA inhibition mechanisms, other that the first discovered zinc-binding mechanism, (see paragraph 1.4.3) were reported in the last decades.[346-352] That has highly enriched our understanding of these enzymes and also allowed obtaining of isoform-selective CAIs targeting physiologically relevant isoforms.[346-352] Among the new chemotypes, which also exhibited the highest levels of isoform selectivity, were the coumarins,[352] the sulfocoumarins,[348-351] and their congeners, homosulfocoumarins (3H-1,2-benzoxathiepine 2,2-dioxides),[353] and saccharin derivatives.[354-356] Because this last chemotype was somewhat chemically similar to hydantoin (imidazolidine-2,4-dione) that may serve as a zinc-binding group (ZBG) we investigated the clinically used antibiotic **furagin**, also known under names Furazidine, Furamags, or Furazidin, that contains hydantoin moiety[357,358] as well as its derivatives **D1-16** prepared by the research group of Prof. Raivis Žalubovskis (Latvian Institute of Organic Synthesis, Riga) as CAIs against therapeutically relevant isoforms.

The furagin derivatives **D1-16** were prepared by reaction of 1-aminohydantoin hydrochloride with proper aldehydes, and their (and **furagin**) inhibitory profiles were evaluated by applying a stopped-flow carbon dioxide hydrase assay,[282] in comparison to acetazolamide (AAZ) as a

standard CAI against four physiologically significant isoforms CA I, II, IX, and XII (Table 9).[281]

Table 9. Inhibition data of hCA I, II, IX, and XII with aminohydantoines (**D1-15**, **furagin**) using **AAZ** as a standard inhibitor.[281]

Cmpd	R	K_I (nM)[a]			
		CA I	CA II	CA IX	CA XII
D1	C_6H_5	39600	900	3500	5600
D2	$4\text{-}OCH_3\text{-}C_6H_4$	57600	6400	1200	4700
D3	$4\text{-}NO_2\text{-}C_6H_4$	>100000	11100	7400	2800
D4	$4\text{-}(COCH_3)\text{-}C_6H_4$	>100000	8300	4900	930
D5	$4\text{-}(OCH_2C_6H_5)\text{-}C_6H_4$	>100000	540	350	910
D6	$CHCH(CO_2C_2H_5)$	45900	23600	810	440
D7	$CHC(CH_3)_2$	28800	16500	2900	880
D8	$CHCH(4\text{-}OCH_3\text{-}C_6H_4)$	>100000	3100	400	360
D9	$2,4\text{-}(OH)_2\text{-}C_6H_3$	>100000	59900	5800	150
D10	$4\text{-}(B(OH)_2)\text{-}C_6H_4$	90700	14200	7300	230
D11	3-furanyl	16000	710	850	1700
D12	2-pyridyl	51800	4200	4500	1300
D13	3-pyridyl	45600	620	2300	3200
D14	4-pyridyl	26600	3300	1600	810
D15	5-imidazolyl	9600	12400	560	350
D16	-	19000	4000	1100	160
furagin	-	>100000	9600	260	57
AAZ	-	250	12	25	5.7

a. Mean from 3 different assays, by a stopped-flow technique (errors were in the range of ± 5–10% of the reported values).

All the tested aminohydantoins exhibited a weak inhibitory effect on the slow cytosolic isoform, CA I, where the binding affinity constant (K_I) values fluctuating in the thousands nM range (K_I 16 800->100 000 nM).

The physiologically relevant isoform, CA II, was better inhibited by most of the tested compounds (K_{IS}: 620-59 000 nM). It is observed that the aminohydantoin compounds (**D1**, **D5**, **D11**, and **D13**) were more potent CA II inhibitors with K_{IS} in the range from 540-900 nM. These compounds have unsubstituted phenyl ring or heteroaryl moieties. The rest of the compounds showed a weaker inhibitory effect of CA II with K_{IS} in the range from 3100–59900 nM. It is interesting to note, that compound **D9** having dihydroxyphenyl substituent stood out by nearly three times weaker inhibition in comparison to the second weakest inhibitor **D6**.

The tumor-associated isoform CA IX was inhibited in the nanomolar range by compounds **D5**, **D6**, **D8**, **D11**, **D15**, and **furagin** (K_{IS}: 260–850 nM), where the strongest inhibition was observed for **furagin**. Other aminohydantoin derivatives showed one order weaker inhibition with K_{IS} in the range from 1100-7300 nM. Certain pattern can be observed, where better CA IX inhibition can be observed for compounds with vinyl substituents (**D6**, **D8**, **D14**, and **furagin**) or small hetaryl substituents (**D11**, and **D15**), with the exception of compound **D5**, containing ester moiety on phenyl ring.

The other tumor-associated isoform CA XII was best inhibited among all isoforms studied. The best compound of this series was **furagin** with K_I of 57 nM, followed by vinyl substituted aminohydantoin derivatives **D16**, **D6**, and **D7** with K_{IS} of 160, 360, and 880 nM, respectively. One order weaker CA XII inhibition compare to **furagin** was also observed for aryl (**D4**, **D5**, and **D9**) and hetaryl (**D14**, and **D15**) derivatives ranging K_{IS} from 150 to 930 nM. In general, good selectivity against cancer-associated CA isoforms (hCA IX and XII) compare to off-target ones (CA I and II) was observed for three compounds **furagin**, **D6**, and **D9**.

Docking studies were used to investigate the binding mode of **furagin** and aminohydantoines **D1-16** within the active site of hCA II (pdb 5LJT),[276] IX (pdb 5FL4),[359] and XII (pdb 1JD0).[30] Similarly to benzenesulfonamides (pK_a = 10.1) which bind to the Zn ion of the CA active site in the deprotonated form, the imidic nitrogen of the hydantoin nucleus as well was considered negatively charged (pK_a = 9.16)[360] in the experiments and resulted to coordinate the zinc ion in all the obtained poses with hCAs II, IX, and XII. Furthermore, the oxygen atom of the C=O in position 4 of the hydantoin core acts as a bifurcated acceptor, establishing

two H-bonds with T199, whereas the heterocycle forms vdW contacts with residues H94, H96, H119, L198, T200, and W209 (Figure 45).
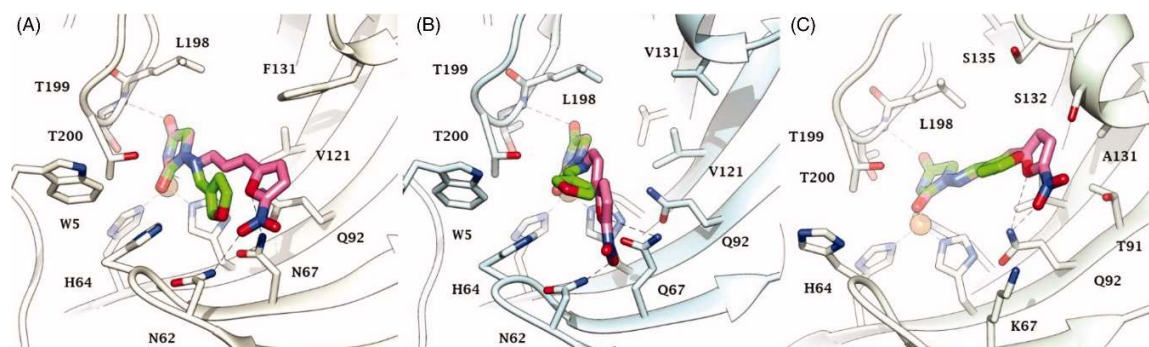
Figure 45. Predicted docking orientations of **D11** (green) and **furagin** (pink) to (A) CA II, (B) CA IX and (C) CA XII.

In hCA II and CA IX, the N1 pendants of all ligands are oriented towards a hydrophilic cleft defined by H4, W5, N62, N67 (Figure 46A,B), and H64, except **D5** and **D6** in CA II, whose N1 tails are housed, into a hydrophobic pocket formed by I91, V121, and F131. Amino acids T91, Q92, A131, S132, and S135 are instead targeted by the pendants on the aminohydantoin of the ligands in all docking solutions with CA XII (Figure 45C). The docking procedure was complemented with 100 ns long molecular dynamic (MD) simulations on the predicted binding conformations of **furagin** and **D9**, the most potent CA XII inhibitors also showing significant CA XII over CA II selectivity. The structure of the three investigated CA isoforms was stable during the computation with the backbone atom RMSDs exhibiting small fluctuations over the 100 ns (Figures 46 and 48).
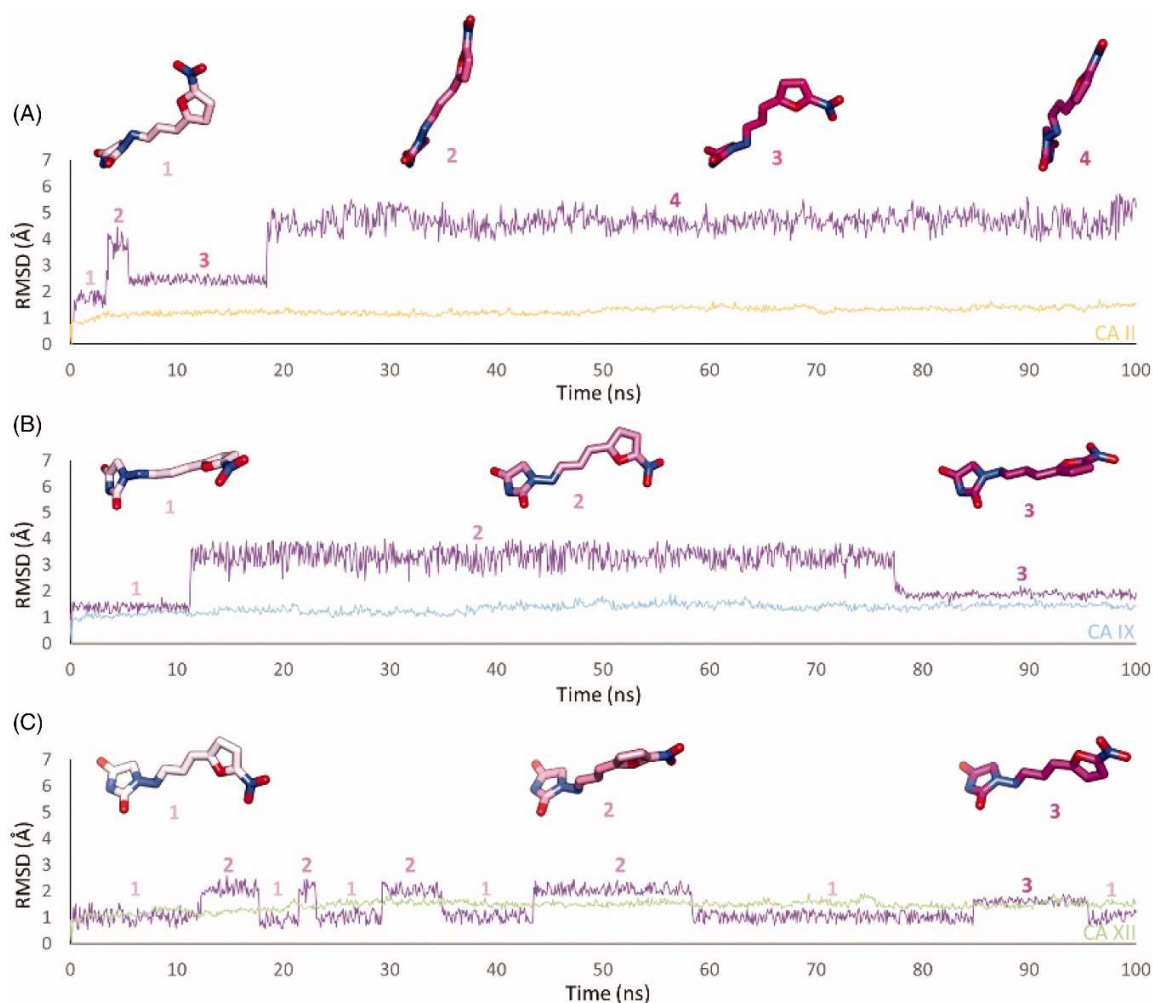
Figure 46. RMSD analysis of **furagin** heavy atoms and (A) CA II, (B) CAIX, and (C) CA XII backbone over the 100 ns MD simulation. The ligand color darkens over the dynamic simulation.

Additionally, the ZBG of the ligands remains stably anchored to the metal ion all over the MD, with the hydantoin core receiving H-bonds by the amidic NH and side chain OH of T199 (Figures 47 and 49).

After an initial equilibration, mainly occurring in CA II and IX, the molecular tail of **furagin** undergoes minor conformational fluctuations during simulation, approaching to stable binding conformations within the three hCA isoforms (Figures 46 and 47).
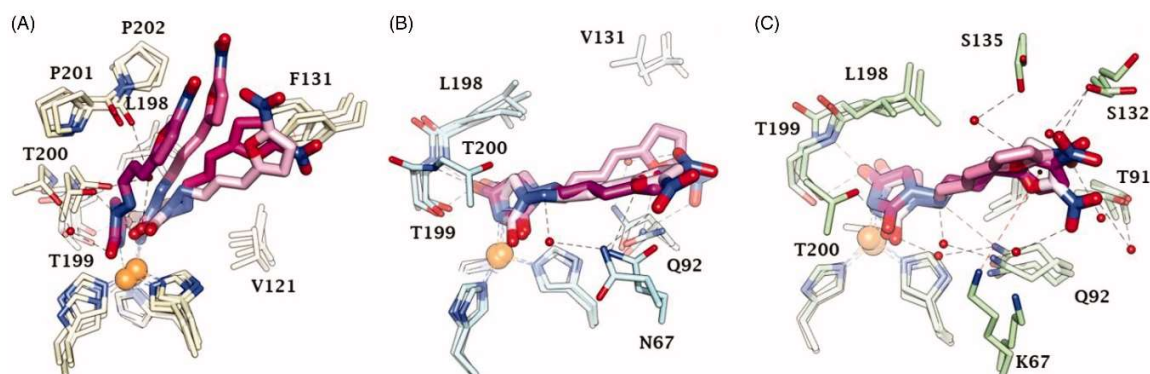
Figure 47. Dynamics evolution of the binding mode of **furagin** to (A) CA II, (B) CA IX, and (C) CA XII over the course of 100 ns. Water molecules are represented as red spheres. The ligand color darkens over the dynamic simulation.

In CA IX and XII, the ligand accommodates the N1-pendant in the hydrophilic half of the active sites where it makes vdW contacts and both direct and water-mediated H-bond interactions with the enzymes (Figure 47B,C). In the CA II, the ligand-bound conformation of **furagin** orients the tail towards the hydrophobic area of the target and does not form persistent H-bond interactions over the 100 ns (Figure 47A). The hydrogen bond persistence within the three CA isoforms is in good agreement with the inhibitory profile of the ligand (hCAXII > hCA IX > hCA II).

An ensemble of few conformations is representative of the binding of **D9** within hCA II and IX (Figures 48 and 49).
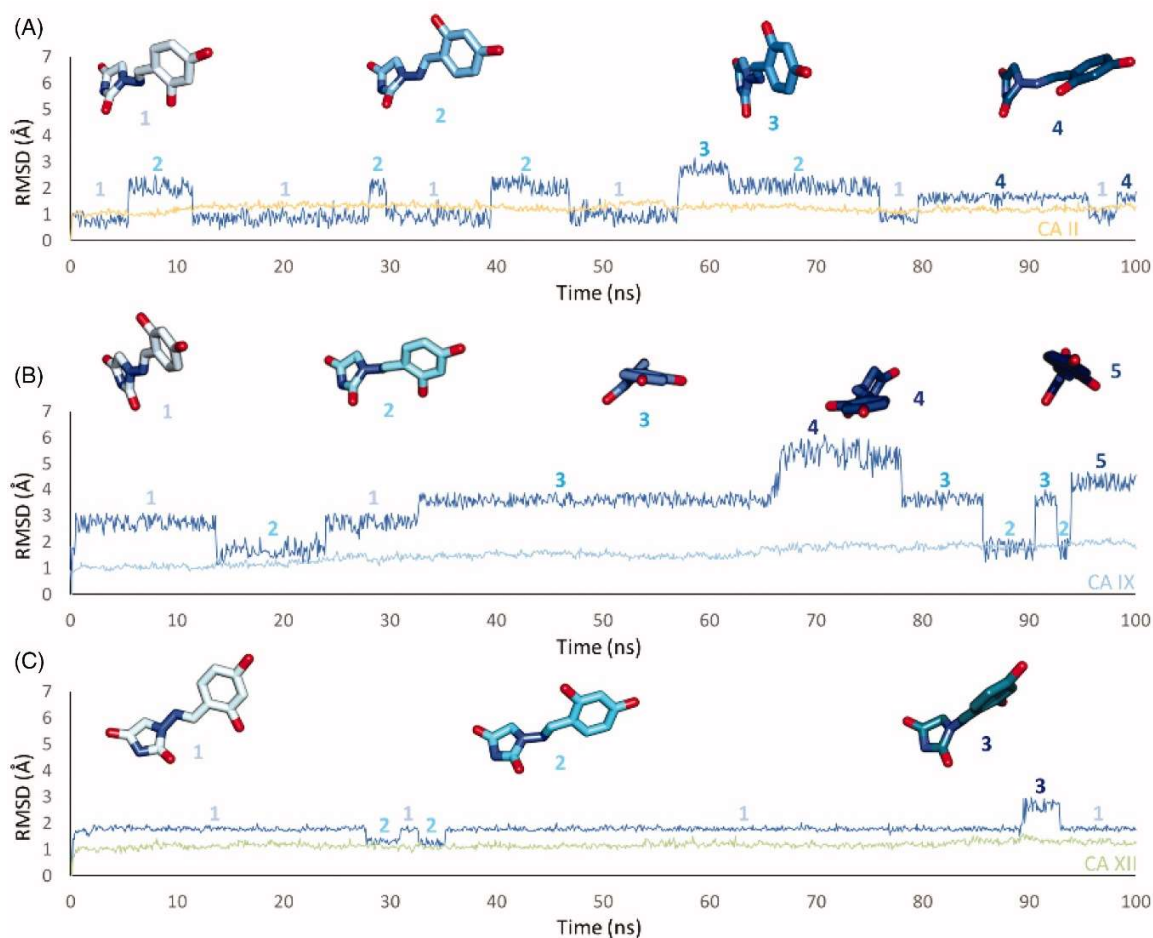
Figure 48. RMSD analysis of **D9** heavy atoms and (A) CA II, (B) CAIX, and (C) CA XII backbone over the 100 ns MD simulation. The ligand color darkens over the dynamic simulation.

Here, the ligand approaches the hydrophobic regions of the enzymes and, coming next to the end of the simulation, the N1 tails lose direct or water-bridged H-bonds with glutamine and asparagine residues, progressively moving towards T199 or T200, that is, the area of the enzyme that undergoes to the greatest residue displacement. In CA XII, the docked pose of **D9** remains firmly anchored to the residues of the hydrophilic portion of the enzyme throughout the dynamic. A wide network of direct and water-mediated H-bonds stabilize the binding of the ligand. This is consistent with the inhibition profile exhibited by **D9** in hCA XII as compared with the other two CA isoforms.
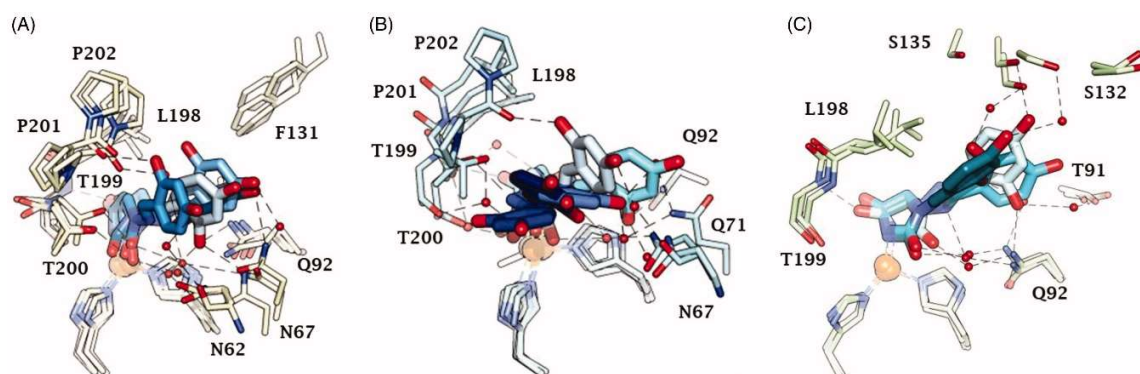
Figure 49. Dynamics evolution of the binding mode of **D9** to (A) CA II, (B) CA IX, and (C) CA XII over the course of 100 ns. Water molecules are represented as red spheres. The ligand color darkens over the dynamic simulation.
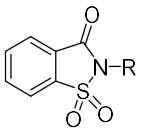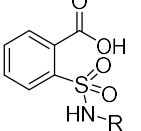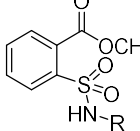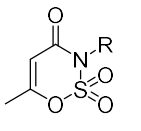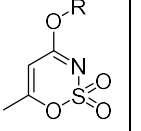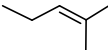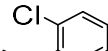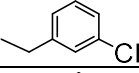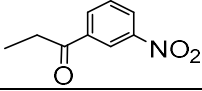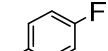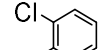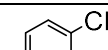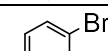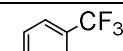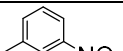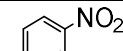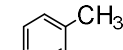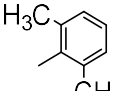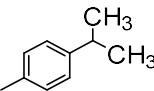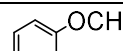
The experimental procedures are reported in Chapter 7 and the data and results of this research were published in Pustenko A., et al. *J. Enzyme Inhib. Med. Chem.* **2020**, *35*, 1011-1020.[281]
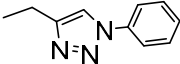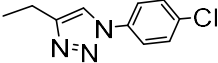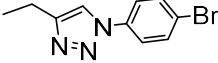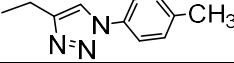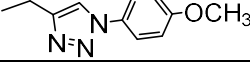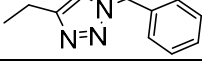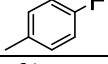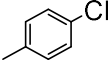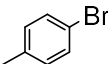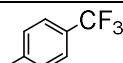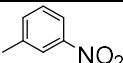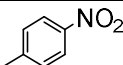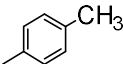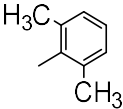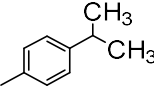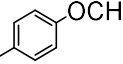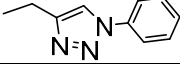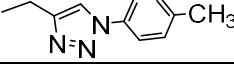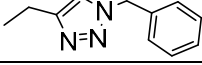
3.5 Novel insights on saccharin- and acesulfame-based carbonic anhydrase inhibitors: design, synthesis and biological activity (Series E)
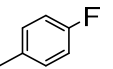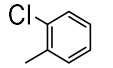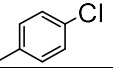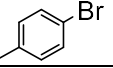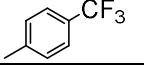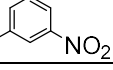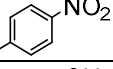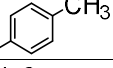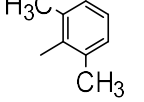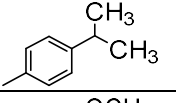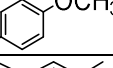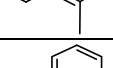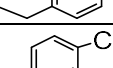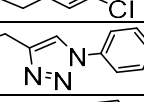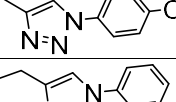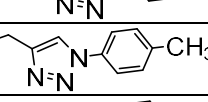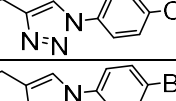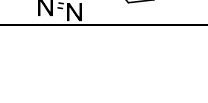
Saccharin and acesulfame scaffolds have great importance for the development of "non-classical" inhibitors of hCAs and since the discovery of their inhibitory activity against these enzymes,[361-364] they caught the attention as valuable hit compounds for the design of novel molecules acting against hCAs.
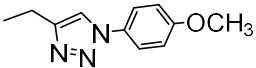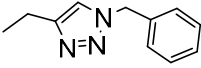
In this context, the research group of Prof. Daniela Secci (Sapienza University of Rome), developed these scaffolds using different approaches,[365-369] leading to a variety of derivatives. (Table 10). All the synthesized compounds were submitted to stopped-flow kinetic assay to evaluate their inhibitory activity (Table 10) against the off-targets (hCA I, and II), and the tumor-associated isoforms (hCA IX, and XII).[371] Albeit these compounds were less effective than others reported in previous works,[129,130,363,364] some of them retained nanomolar activity and selectivity against targets, observing that the inhibitory activity of the compounds of series **E1-5** is strictly influenced by the substituent group/linker bound to the saccharin and acesulfame cores.

Table 10. Inhibition data of hCA I, II, IX, and XII with saccharin- (**E1-3**) and acesulfame-based derivatives (**E4,5**) using **AAZ** as a standard inhibitor.[371]

Cmpd	R	K_I (µM)[a]			
		CA I	CA II	CA IX	CA XII
E1a		> 1000	> 1000	0.39	0.23
E1b		> 1000	> 1000	0.30	0.22
E1c		> 1000	> 1000	0.10	1.3
E1d		> 1000	> 1000	> 1000	0.41
E1e		> 1000	> 1000	> 1000	> 1000
E1f		> 1000	> 1000	> 1000	> 1000
E1g		> 1000	477.8	640.0	> 1000
E1h		> 1000	> 1000	> 1000	> 1000
E1i		> 1000	> 1000	869.1	> 1000
E1j		> 1000	> 1000	> 1000	> 1000
E1k		> 1000	> 1000	> 1000	> 1000
E1l		> 1000	> 1000	443.5	> 1000
E1m		> 1000	> 1000	> 1000	> 1000
E1n		> 1000	> 1000	> 1000	> 1000
E1o		> 1000	> 1000	> 1000	> 1000
E1p		> 1000	> 1000	> 1000	> 1000

E1q		> 1000	> 1000	> 1000	> 1000
E1r		> 1000	80.8	758.6	> 1000
E1s		> 1000	76.4	537.6	> 1000
E1t		> 1000	> 1000	669.6	> 1000
E1u		> 1000	> 1000	666.1	> 1000
E1v		> 100	> 100	20.9	7.4
E2a		> 1000	> 1000	46.5	> 1000
E2b		> 1000	> 1000	45.8	> 1000
E2c		> 1000	> 1000	> 1000	> 1000
E2d		> 1000	> 1000	> 1000	> 1000
E2e		> 1000	> 1000	72.8	> 1000
E2f		> 1000	> 1000	84.8	> 1000
E2g		> 1000	> 1000	> 1000	> 1000
E2h		> 1000	66.9	0.24	> 1000
E2i		> 1000	> 1000	> 1000	> 1000
E2j		> 1000	> 1000	> 1000	> 1000
E2k		> 1000	> 1000	> 1000	> 1000
E2l		> 1000	> 1000	> 1000	> 1000
E2m		> 1000	> 1000	926.9	> 1000
E2n		> 1000	> 1000	> 1000	> 1000
E2o		> 100	> 100	1.9	4.5

E3a	(phenyl)	> 1000	> 1000	59.6	> 1000
E3b	(4-F-phenyl)	> 1000	> 1000	261.8	> 1000
E3c	(2-Cl-phenyl)	> 1000	> 1000	427.5	> 1000
E3d	(4-Cl-phenyl)	> 1000	> 1000	955.3	> 1000
E3e	(4-Br-phenyl)	> 1000	688.7	6.7	> 1000
E3f	(4-CF₃-phenyl)	> 1000	> 1000	562.6	> 1000
E3g	(3-NO₂-phenyl)	> 1000	> 1000	> 1000	> 1000
E3h	(4-NO₂-phenyl)	> 1000	> 1000	62.8	> 1000
E3i	(4-CH₃-phenyl)	> 1000	> 1000	68.2	> 1000
E3j	(2,3-dimethylphenyl)	> 1000	> 1000	39.7	> 1000
E3k	(4-isopropylphenyl)	> 1000	> 1000	57.6	> 1000
E3l	(4-OCH₃-phenyl)	> 1000	> 1000	93.3	> 1000
E4a	(alkene)	> 1000	> 1000	0.33	0.24
E4b	(ethylbenzene)	> 1000	> 1000	2.7	0.27
E4c	(dichloro ethylbenzene)	> 1000	> 1000	0.47	2.0
E4d	(triazole-phenyl)	> 1000	> 1000	> 1000	> 1000
E4e	(triazole-4-Cl-phenyl)	> 1000	> 1000	> 1000	> 1000
E5a	(triazole-phenyl)	> 1000	> 1000	> 1000	> 1000
E5b	(triazole-4-CH₃-phenyl)	> 1000	> 1000	> 1000	> 1000
E5c	(triazole-4-Cl-phenyl)	> 1000	> 1000	> 1000	> 1000
E5d	(triazole-4-Br-phenyl)	> 1000	> 1000	> 1000	> 1000

E5e		> 1000	> 1000	> 1000	> 1000
E5f		> 100	> 100	1.1	> 100
AAZ	-	250	12	25	5.7

a. Mean from 3 different assays, by a stopped-flow technique (errors were in the range of ± 5–10% of the reported values).

A subset of CAIs, namely compounds **E1b**, **E1v**, **E2o**, and **E4b**, endowed with the best CA IX and XII inhibitory profiles, was selected to study the interaction mechanism driving the inhibition profiles reported in Table 10.[371] A computational protocol, consisting of joint docking procedure and MD simulations, was used to investigate the compounds binding mode within CAs IX and XII (see Experimental Section, Chapter 7). The derivatives were treated as CAIs anchoring to zinc-bound water molecule basing on a number of considerations: 1) zinc-binder CAI chemotypes, such as primary sulfonamides, sulfamates and sulfamides, mono- and dithiocarbamates, or hydroxamates, mainly act in the deprotonated form, as anions, straightly coordinating the Zn(II) ion from the enzyme active site[20]; 2) saccharin (**E1a-v**) and acesulfame (**E4a-e**, and **E5a-f**) derivatives bearing a tertiary sulfonamide moiety cannot interact with the targets in the deprotonated form; 3) although the deprotonation of the secondary sulfonamide group of hydrolysed saccharin derivatives (**E2a-o**, and **E3a-l**) is possible, but its internal position in the molecules does not allow it to coordinate the Zn ion due to the steric hindrance of the groups surrounding the negatively charged sulfonamide; 4) crystallographic evidence showed that deprotonated sulfonate moieties, which possess similar features as the SO_2 group of the here reported saccharin and acesulfame compounds, drive CA inhibition by anchoring to the zinc-bound water molecule/hydroxide ion (not by coordination to the zinc ion).[370] This led us to consider in our *in silico* studies the nucleophile mediated anchoring mechanism for derivatives **E1b**, **E1v**, and **E4b**. Likewise, crystallographic evidence showed that carboxylic acids as **E2o**, except for few cases, act as CAIs anchoring to the zinc-bound nucleophile.[370] Thus, dockings were performed including the Zn-bound water molecule in the target and the reliability of poses for derivatives **E1b**, **E1v**, **E2o**, and **E4b** within CA IX and XII active sites (Figures 50 and 52) assessed with MD simulations. The MD trajectories showed the stability of the

anchorage to the zinc-bound water molecule that persists for >70–80% of the simulation time; moreover, the ligands maintain constant hydrophobic contacts with different portions of the active sites. In both CA IX and XII saccharin derivatives **E1b**, and **E1v** are H-bond anchored by one S=O group to the metal-coordinated water that is, in turn, H-bonded to side chain hydroxyl group of T199 (Figure 50).
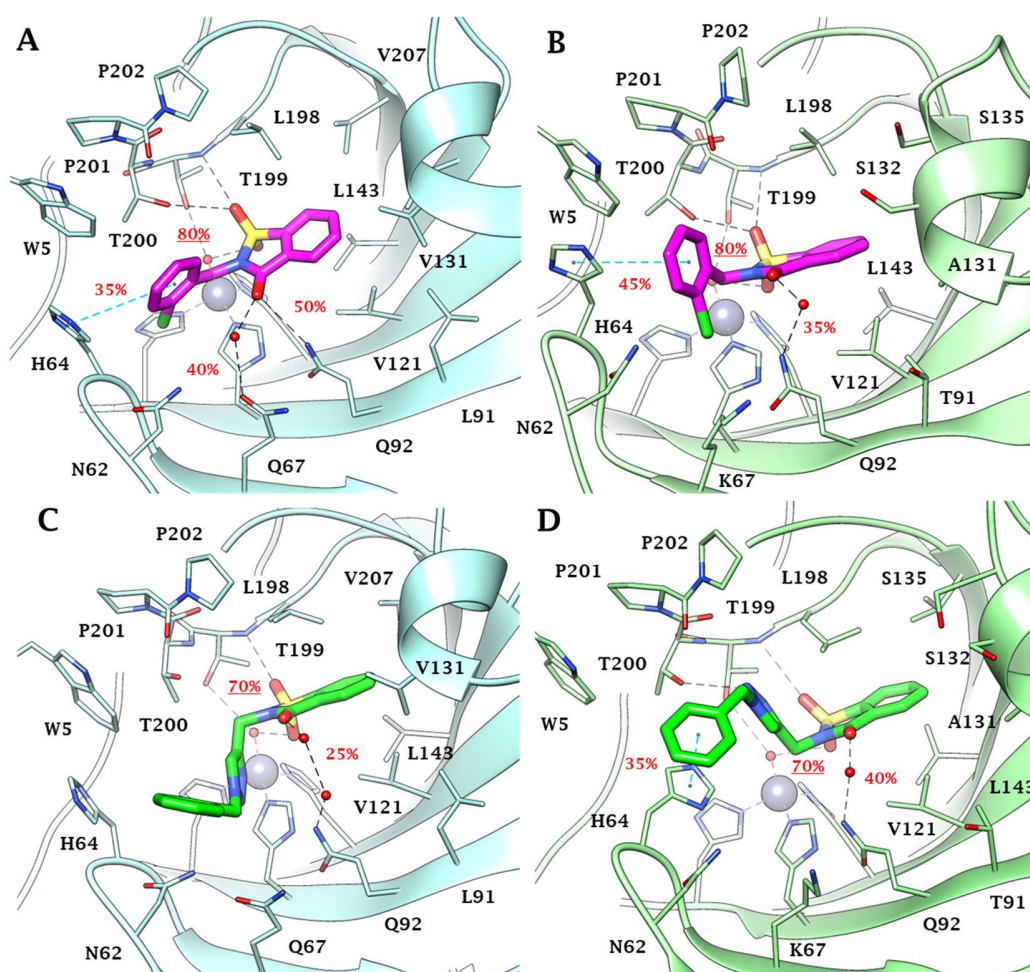
Figure 50. Predicted binding mode of compounds **E1b** and **E1v** into (A, C) CA IX and (B, D) CA XII active site. H-bonds and π-π stackings are represented as black and blue dashed lines, respectively. Dashed bonds occupancy over the MD simulation is indicated as percentage, among which underlined is the occupancy of the anchorage to the zinc-bound water. Water molecules are shown as red spheres.

The other S=O group of both ligands accepts one H-bond by T199 backbone NH, but just **E1b** also engages in hydrogen bonding with the side chain hydroxyl group of T200 (OH-O Y200). Of note, this H-bonds network persists for most MD simulations mainly contributing

to the pose stability. Moreover, the C=O group of the ligands engages direct or water bridged H-bonds with Q67 and Q92 which fluctuate over the MD computations. The N-benzyl group of derivative **E1b** accommodates in the pocket lined by W5, H64, and N62 forming vdW contacts and π-π interactions with the aromatic residues. This cleft is only partially occupied by the 1-benzyl-1,2,3-triazol-4-yl N-pendant of derivative **E1v** over the MD course making the docking poses less stable, and thereby providing a plausible explanation of the worst CA IX and XII inhibitory profile of **E1v** compared to **E1b** (Figure 50).

The interaction mode of **E1b** and **E1v** within both CA IX and XII can explain the lower up to absent CAs inhibition observed for the N-phenyl saccharin derivatives **E1e-p** and 1-phenyl-1,2,3-triazole **E1q-u**. In fact, the lack of a methylene spacer between the heterocycle and the aromatic pendant (as in **E1e-p**) or between the triazole and the outer aromatic ring (as in **E1q-u**) hampers a suitable ligand/target complementarity interaction and stable accommodation of the pendant in the pocket formed by W5, H64, and N62 (Figure 51).
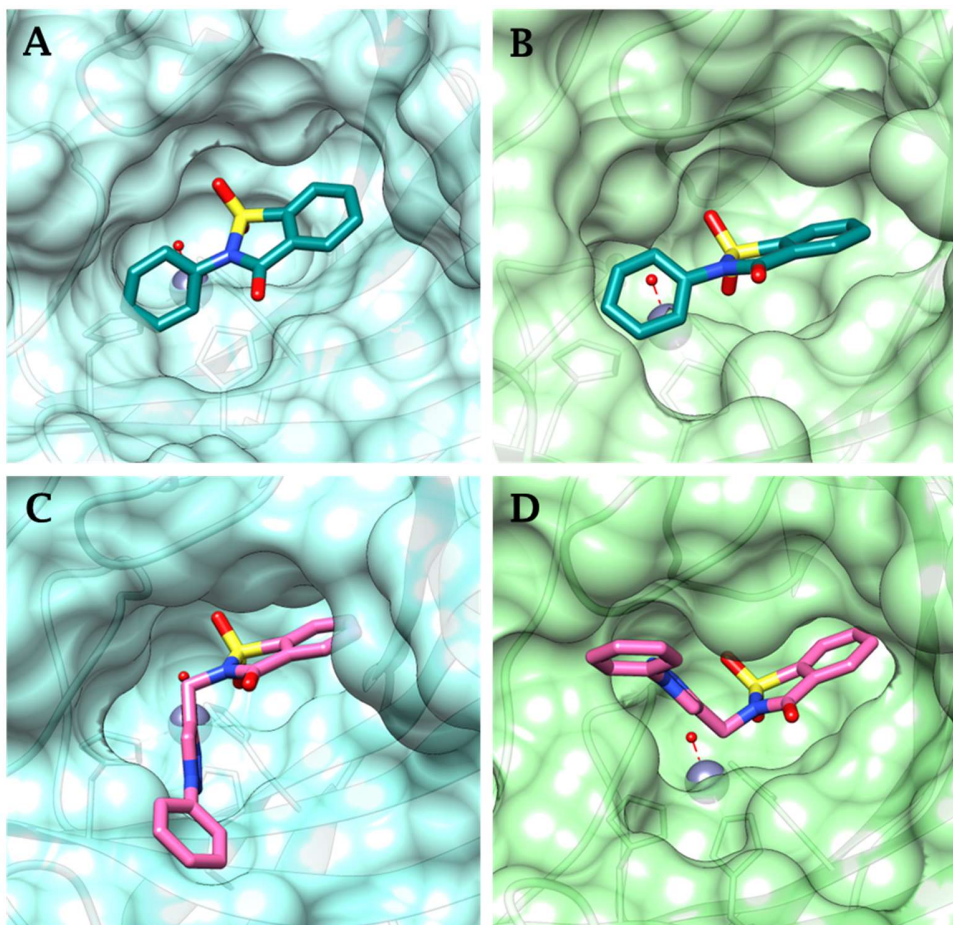
Figure 51. Replacement of the benzyl moiety of **E1b** and **E1v** with a phenyl ring (to give **E1e** and **E1q**, respectively) within the ligand/target complexes found by docking. Compound **E1e** in the active site of A) CA IX and B) CA XII; compound **E1q** in the active site of C) CA IX and D) CA XII. All graphical representations point out significant protein-ligand clashes.

Both in CA IX and XII active sites, the hydrolyzed saccharin **E2o** anchors to the zinc-bound water molecule by the carboxylate group, which also engages one H-bond with T199 backbone NH (Figure 52A,B). Its negatively charged sulfonamide group SO_2NH- takes part in a network of H-bonds involving multiple residues of the binding cavity: Q92 by a fluctuating water-bridged H-bond (N-H···(H)OH···Q92) and Y200 (N-H···O-T200). In CA IX, the hydroxyl side chain of T200 is also in H-bond contact with the ligand triazole N3 atom, and π-π contacts are formed by the indole moiety of W5 and the outer phenyl ring of **E2o**. In contrast, the placing of the 1-benzyl-1,2,3-triazol-4-yl N-pendant within the pocket formed by W5, H64, and N62 in CA XII is less stable over the MD course with respect to CA IX, as

well as the water bridged H-bond formed by the triazole NH and N62 and the π-π interactions (Figure 52B).
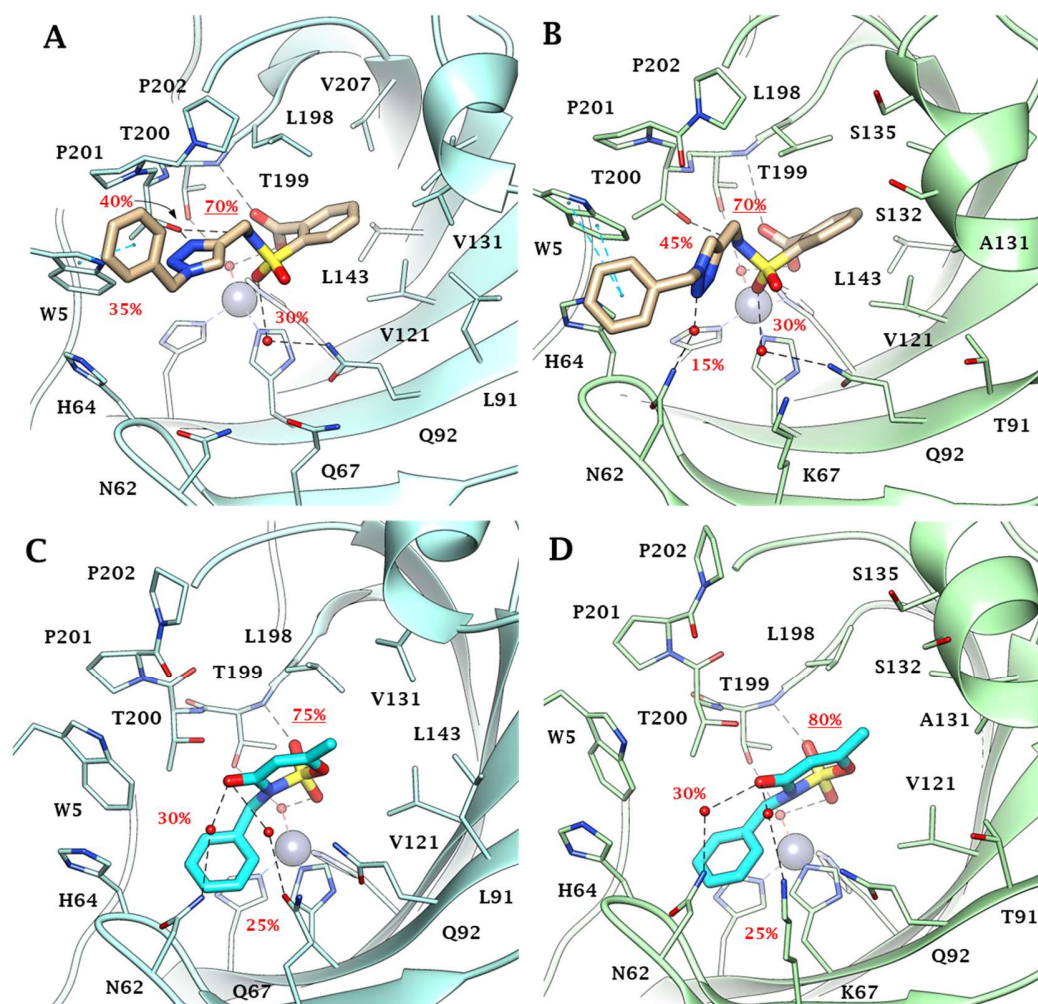
Figure 52. Predicted binding mode of compounds **E2o** and **E4b** into (A, C) CA IX and (B, D) CA XII active site. H-bonds and π-π stackings are represented as black and blue dashed lines, respectively. Dashed bonds occupancy over the MD simulation is indicated as a percentage, among which underlined is the occupancy of the anchorage to the zinc-bound water. Water molecules are shown as red spheres.

Again, the absence of a methylene spacer between the sulfonamide and the aromatic N-pendant, as in the methyl esters **E3a-l** and carboxylic acids **E2a-l**, translates into a lower CA IX and XII inhibition activity of these derivatives when compared to **E2o**. However, the drop of efficacy was lower than that observed with saccharin analogs most likely because of the greater conformational flexibility and adaptation capability within the active site of the

hydrolyzed ligands than cyclized compounds. Surprisingly, while a total loss of CA XII inhibition activity was observed for **E2a-l**, and **E3a-l**, their medium micromolar profile against CA IX is likely to be related to the hydrophobic features of the CA IX active site and to the larger size of its cleft able to host the benzoate group when the triazole ring brings both a phenyl and benzyl moiety. As already observed for **E2m**, and **E2n** the absence of the methylene spacer between the triazole and the outer aromatic ring, produced a whole loss of action against CAs. Likewise, in both CA IX and XII, acesulfame **E4b** anchors to the zinc-bound water molecule through the sulfimide S=O (Figures 5(C,D)) and the anchorage strengthened by another H-bond occurring between the other S=O group and T199 backbone NH. The carbonyl group of **E4b** is involved in a network of water/bridged H-bond with N62, Asn/Lys67 (CA IX/XII) and Q92. Interestingly, the N-benzyl moiety stably accommodates (>65% MD) within the pocket formed by W5, Y7, H64, N62, and H96 engaging vdW contacts. On the basis of the depicted binding mode, a 1-phenyl-1,2,3-triazol-4-yl N- or O-pendant drops the inhibitory action of acesulfame derivatives **E4d**, **E4e**, and **E5a-e** because of steric hindrance reasons in CA IX and XII active sites. Consistently to the inhibition profile in Table 10, the binding mode predicted for **E1b**, **E1v**, **E2o**, and **E4b** in CA IX and XII is likely not allowed in the narrower and hindered active site of CA I and II (Figure 53), in which the used computational protocol was not able to find reliable solutions.[58]
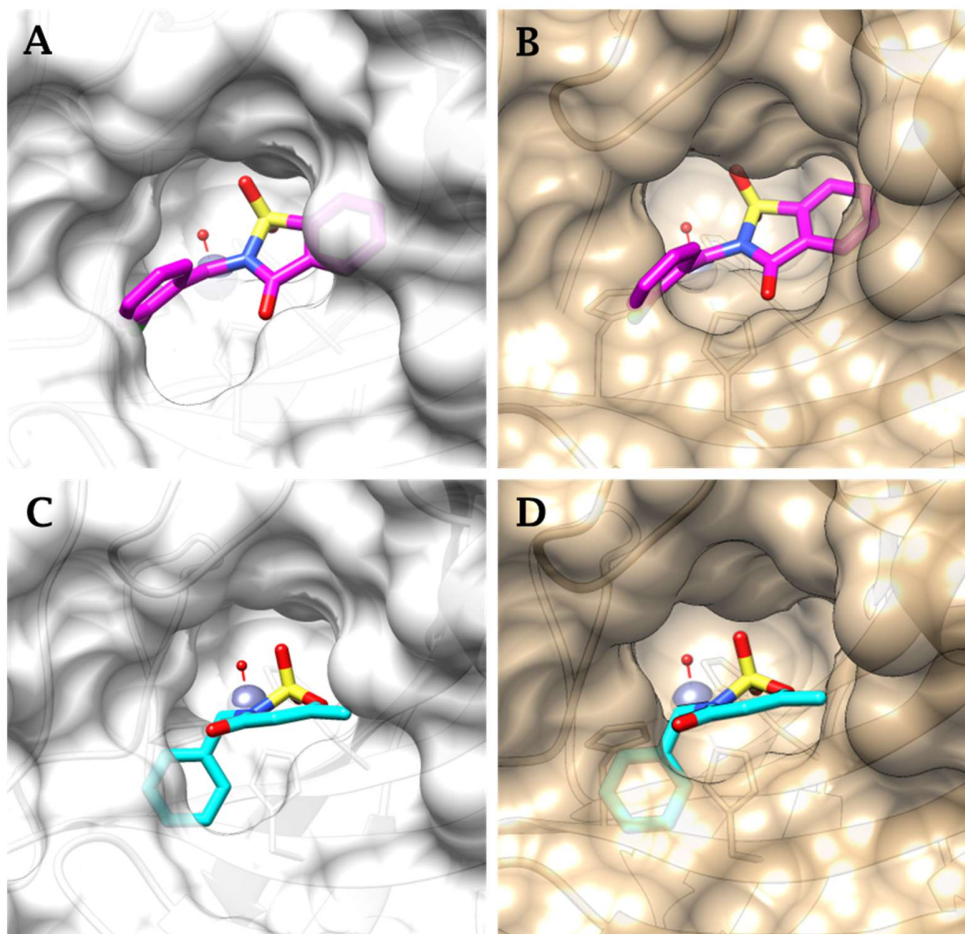
Figure 53. Representation of the CA IX predicted binding mode of **E1b** and **E4b** in CA I and CA II after isoforms overlay. (A) **E1b**-CA I, (B) **E1b**-CA II, (C) **E4b**-CA I and (D) **E4b**-CA II. All graphical representations point out significant protein-ligand clashes.

In silico studies underlined the importance of the flexibility for the correct distribution of the molecular fragments inside the hCA IX, and XII active site. Indeed, the removal of the methylene group in the N-benzyl saccharins to obtain the N-phenyl analogs elicited detrimental effects, with the only exception of the opened-saccharin derivative **E2h**. Similarly, for the triazole bearing derivatives, the insertion of a second methylene group separating the triazole moiety from the outer phenyl ring (**E2o**, and **E5f**) improved the activity. By docking and MD studies the most probable binding mode of the four most active compounds (**E1b**, **E1v**, **E2o**, and **E4b**) was described based on the anchoring to zinc-bound

water, confirming and explaining the correlation between inhibitory activity and the ability to occupy sites in order to establish interactions that influenced the binding affinity.

The experimental procedures are reported in Chapter 7 and the data and results of this research were published in Guglielmi P., et al. *J. Enzyme Inhib. Med. Chem.* **2020**, *35*, 1891-1905.[371]

During my three-year Ph.D. cycle, some other collaborations were carried on, where *in silico* investigations (docking, MM-GBSA and MD) contributed to clarify the ligand-target interaction mode:

a) "*2-Benzylpiperazine: A new scaffold for potent human carbonic anhydrase inhibitors. Synthesis, enzyme inhibition, enantioselectivity, computational and crystallographic studies and in vivo activity for a new class of intraocular pressure-lowering agents*" in collaboration with Prof. Maria Novella Romanelli from the University of Florence, in which a docking study was carried out with benzenesulfonamide CAIs as inhibitors of the glaucoma-related isoform CA II and IV.[372]

b) "*Dual-tail aryl sulfone-based benzenesulfonamides differently match the hydrophobic and hydrophilic halves of human carbonic anhydrases active sites: Selective inhibitors for the tumor-associated hCA IX isoform*" in collaboration with Prof. Hany S. Ibrahim from Egyptian Russian University, studying *in silico* dual-tailed benzenesulfonamide as CA II and XII inhibitors.[373]

c) "*Steroids interfere with human carbonic anhydrase activity by using alternative binding mechanisms*" in collaboration with Prof. Antimo Gioiello from the University of Perugia, studying *in silico* different steroids acting as zinc-binders (i.e. hyocholic and cholic acids)

and derivatives anchoring to the zinc-bound water molecule/hydroxide ion (i.e. estradiol, and tauroursodeoxycholic acid) toward hCA II.[374]

d) *"Synthesis, computational studies and assessment of in vitro inhibitory activity of squalene derivatives as carbonic anhydrase inhibitors"* in collaboration with Dr. Mariana Pinteala from "Petru Poni" Institute of Macromolecular Chemistry (Romania), in which a docking study was carried out on squalene-benzene sulfonamide CAIs against hCA II and IV.[375]

The long and continuous collaboration with Prof. Wagdy M. Eldehna from Kafrelsheikh University led to several publications, where *in silico* studies were performed on benzenesulfonamide CAIs within the off-target hCA II and tumor-associated hCA IX and XII active sites:

e) *"Enhancement of the tail hydrophobic interactions within the carbonic anhydrase IX active site via structural extension: Design and synthesis of novel N-substituted isatins-SLC-0111 hybrids as carbonic anhydrase inhibitors and antitumor agents"*.[376]

f) *"Novel diamide-based benzenesulfonamides as selective carbonic anhydrase ix inhibitors endowed with antitumor activity: Synthesis, biological evaluation and in silico insights"*.[377]

g) *"Synthesis, biological evaluation and in silico studies with 4-benzylidene-2- phenyl-5(4H)-imidazolone-based benzenesulfonamides as novel selective carbonic anhydrase IX inhibitors endowed with anticancer activity"*.[378]

h) *"3-Hydrazinoisatin-based benzenesulfonamides as novel carbonic anhydrase inhibitors endowed with anticancer activity: Synthesis, in vitro biological evaluation and in silico insights"*.[379]

i) *"Sulfonamide-based ring-fused analogues for CAN508 as novel carbonic anhydrase inhibitors endowed with antitumor activity: Design, synthesis, and in vitro biological evaluation"*.[380]

j) *"3-Methylthiazolo[3,2-a]benzimidazole-benzenesulfonamide conjugates as novel carbonic anhydrase inhibitors endowed with anticancer activity: Design, synthesis, biological and molecular modeling studies"*.[381]

k) *"Synthesis, biological and molecular dynamics investigations with a series of triazolopyrimidine/triazole-based benzenesulfonamides as novel carbonic anhydrase inhibitors"*.[280]

Taken as an example of the lasting and fruitful collaboration, here following the *in silico* investigation carried out on the triazolopyrimidine/triazole-based benzenesulfonamide compounds (project k) is reported.

3.6 Synthesis, biological and molecular dynamics investigations with a series of triazolopyrimidine/triazole-based benzenesulfonamides as novel carbonic anhydrase inhibitors (Series F)

A literature survey regarding several hCA inhibitors revealed that triazole and fused triazole-linked benzenesulfonamides are important classes of potent CAIs with high selectivity against the tumor-associated isoforms (hCA IX and XII) over the ubiquitously expressed isoforms CA I and II.[366,382-384] Furthermore, the triazole moiety was found to enhance the solubility of the molecules,[383] while fused triazoles revealed better hydrophilic/hydrophobic ratio to improve solubility and CA receptor fitting in both hydrophilic and hydrophobic pockets.[366,384] Carrying on our previous works[376-378] in the search for potent and selective CA IX and CA XII inhibitors, the development of new sets of triazolopyrimidine (**F1a-d**) and triazole-based benzenesulfonamides (**F2a-h**, **F3a-c**, **F4a,b**, **F5a,b**, and **F6a-g**) was undertaken, applying the tail approach. A joint *in silico* and synthetic approach led to obtain a set of compounds featured by a different functionalized linker connecting the triazole/triazolopyrimidine benzenesulfonamide scaffold to an aril tail (Table 11). Such linkers were selected to donate different levels of flexibility to the aryl tail and impart the possibility for the new compounds to adopt a diversity of orientations that may allow the specific interactions between the tail and the most variable amino acidic residues at the entrance of hCA active site. Furthermore, the aryl was designed to ensure different electronic, hydrophilic and lipophilic environments to explore a valuable SAR. The synthesized sulfonamides were assessed for their inhibitory activities against hCA I, II, IX and XII isoforms (Table 11).

Table 11. Inhibition data of hCA isoforms I, II, IX and XII with sulfonamides (**F1a-d**, **F2a-h**, **F3a-c**, **F4a,b**, **F5a,b** and **F6a-g**), using **AAZ** as a standard inhibitor.

F1a-d   F2a-h (R=H)   F4a,b (X=O)   F6a-g
         F3a-c (R=CH₃)   F5a,b (X=S)

Cmpd	Ar	K_I (nM)[a]			
		CA I	CA II	CA IX	CA XII
F1a	4-OCH₃-C₆H₄	2381.9	324.6	63.2	38.3
F1b	4-(4-methylpiperazin-1-yl)-C₆H₄	4953.5	837.6	85.0	26.2
F1c	2-pyridyl	3721.8	536.9	47.9	59.3
F1d	4-pyridyl	2481.0	456.2	24.6	45.3
F2a	C₆H₅	771.4	86.4	41.1	105.0
F2b	4-F-C₆H₄	494.9	65.2	31.5	29.5
F2c	4-Cl-C₆H₄	702.7	6.9	73.2	8.2
F2d	4-NO₂-C₆H₄	1536.5	24.7	34.4	10.2
F2e	4-OH-C₆H₄	334.6	8.8	8.3	7.8
F2f	4-piperidinyl-C₆H₄	824.6	95.4	33.0	17.6
F2g	4-morpholinyl-C₆H₄	987.7	64.2	19.7	49.7
F2h	3-pyridyl	476.5	74.2	6.6	34.4
F3a	C₆H₅	633.1	8.9	41.3	23.8
F3b	4-pyridyl	295.2	8.5	5.8	26.0
F3c	4-morpholinyl-C₆H₄	793.4	53.9	31.7	9.9
F4a	C₆H₅	306.9	70.5	4.9	16.2
F4b	4-Cl-C₆H₄	537.1	10.9	16.4	48.2
F5a	C₆H₅	368.2	9.7	40.2	31.0
F5b	4-Cl-C₆H₄	597.5	11.1	16.7	21.9
F6a	C₆H₅	442.3	9.8	8.2	8.1
F6b	4-F-C₆H₄	94.4	65.5	7.8	17.6
F6c	4-Cl-C₆H₄	403.3	9.5	43.3	73.6
F6d	4-CH₃-C₆H₄	312.6	42.8	3.9	23.8
F6e	4-OCH₃-C₆H₄	694.9	126.6	3.3	9.8
F6f	4-SO₂NH₂-C₆H₄	676.6	78.7	28.6	4.4
F6g	4-COOH-C₆H₄	507.4	9.6	15.3	19.9

AAZ	-	250	12	25	5.7

a. Mean from 3 different assays, by a stopped-flow technique (errors were in the range of ± 5–10% of the reported values).

Among the synthesized triazolopyrimidine- and triazole-based benzenesulfonamides, the most selective compounds for the cancer-associated hCAs over the ubiquitous isozymes, **F1d** (*SI* CAI / CA IX = 100.85; *SI* CAI / CA XII = 54.77; *SI* CAII / CA IX = 18.54; *SI* CAII / CA XII = 10.07) and **F6e** (*SI* CAI / CA IX = 210.58; *SI* CAI / CA XII = 70.91; *SI* CAII / CA IX = 38.36; *SI* CAII / CA XII = 12.92), were selected and docked into the active site of CAs II, IX and XII. Poses showing the best scoring values and favorable binding interactions were subjected to an MM-GBSA based refinement (Figure 54) and, limited to CA IX and XII, to a cycle of 100 ns molecular dynamics (MD; Figures 55-57).

According to the X-ray solved structures reported in the literature,[3] benzenesulfonamide fragment of **F1d** and **F6e** coordinates around the zinc ion, adopting superimposable binding orientations within the three active sites (Figures 54, 56 and 57).
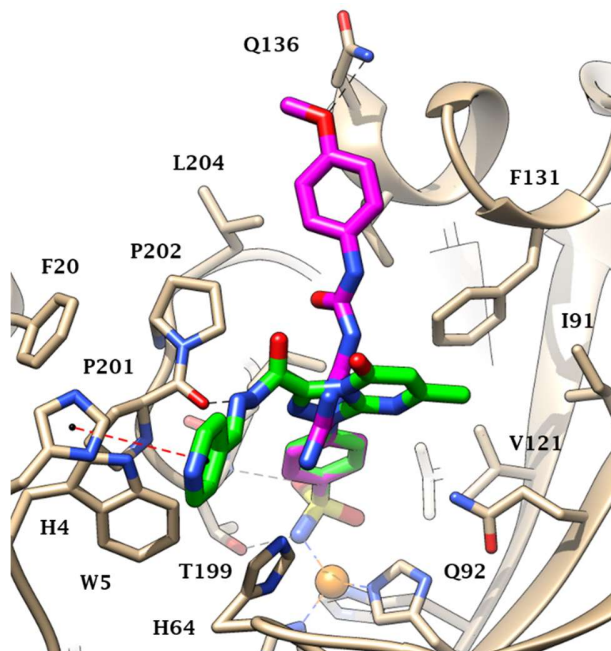
Figure 54. Docked poses of **F1d** (green) and **F6e** (purple) in the active site of hCA II. H-bonds and π-π interactions are depicted as black and red dashed lines, respectively.

As a result, the observed specificity of action of the selected compounds needed to be sought in the interactions established by the tails of **F1d** and **F6e** with the enzymatic counterparts. While the triazolopyrimidine of **F1d** occupied a central position within the CA II binding pocket, its arylidenehydrazide tail accommodated into the cleft formed by W5, H64 and H4, establishing a π-π contact with the latter (Figure 54).

Also, the 5-amino- 1,2,4-triazole portion of **F6e** was positioned in a middle position of the CA II active site, whereas the 4-methoxyphenylureido tail accommodated in the pocket lined by L204, V135, F131 receiving an H-bond by the Q136 side chain. The MD simulations of **F1d** and **F6e** within CA IX and XII showed the overall stability of the ligand/target adducts over the tested 100 ns, with the interactions involving the benzenesulfonamide core being steady during the computations (Figures 56 and 57). In contrast, movements of the tails of **F1d** and **F6e** in relation to the active site residues resulted in root-mean-square deviation (RMSD) values in the 2.5-3 Å range for CA IX and 4-6 Å range for CA XII (Figure 55).
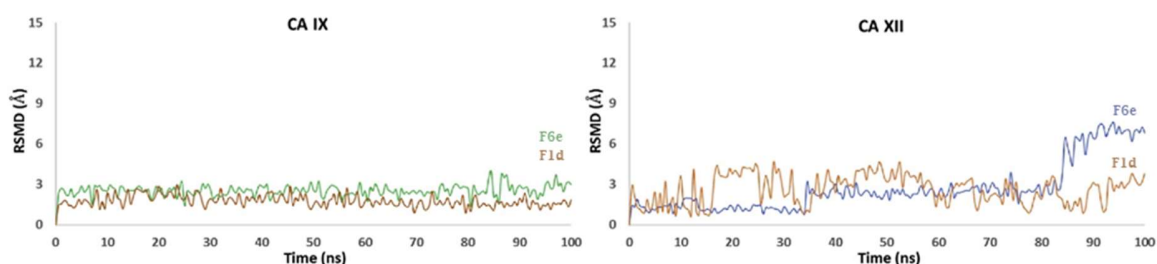
Figure 55. RMSD analysis of the ligands heavy atoms over the 100 ns MD in CA IX and XII.

Figure 56 depicts the main binding orientations reported by **F1d** (panel A) and **F6e** (panel B) within the binding site of CA IX. The arylidenehydrazide tail of **F1d** was found to stably occupy the pocket formed by V20, W5, P201 and P202 where intense hydrophobic contacts persist over the MD course (Figure 56A). Additionally, interesting water bridges connecting the pyridine N atom and V20 carbonyl group and the inner hydrazide N atom and P201 C=O, were found for approximately 20% of the simulation time. The 4-methoxyphenylureido pendant of **F6e** was oriented towards a small cleft lined by L91, Q92 and T73 and was stabilized by H-bonds persisting for over 90% of the time between Q92 side chain and the

N2 atom of the triazole and the ureido C=O (Figure 56B). Further, two water molecules bridged the oxygen atom of the methoxy group and the A90 and L74 residues. The binding orientations of the molecular tails of **F1d** and **F6e** within the CA XII active site were predicted to be less stable in comparison to the CA IX/ligand interactions (Figure 56).
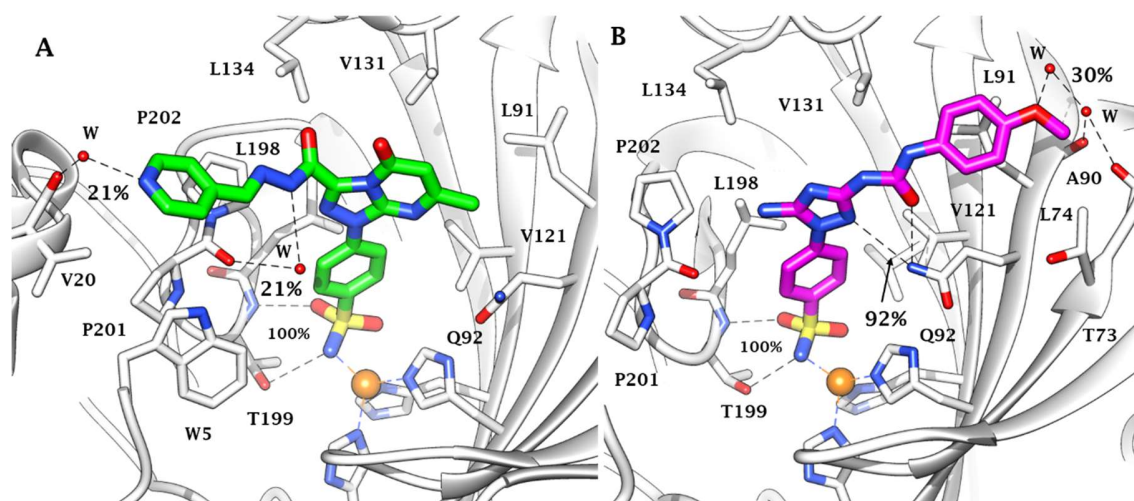
Figure 56. Principal predicted orientation produced over a cycle of 100 ns MD for A) **F1d** and B) **F6e** bound in the CA IX active site. H-bonds are depicted as black dashed lines. The bond occupancies over 100 ns are reported as a percentage.

The arylidenehydrazide tail of **F1d** established vdW contacts with Y20, P201, and P202, but it did not firmly position into the pocket because of the V20 (CA IX)/Y20 (CA XII) mutation which increases the steric hindrance on the enzymatic counterpart (Figure 57A). As a result, during the MD simulation the arylidenehydrazide tail was found to move within the area comprised from Q136 to W5. The position of the triazolopyrimidine ring was stabilized by π-cation interactions with the ammonium group of K67 (30% of the simulation time) whereas a water-mediated interaction between the hydrazido moiety and Q136 side chain persisted for 20% of the MD time (Figure 57A).

As far as the adduct of **F6e** with CA XII is concerned, the RMSD value plotted as a function of time (Figure 55) indicated that important changes in the ligand-binding orientation occurred at approximately 35 and 85 ns of MD (Figure 57B). Indeed, while initially the phenylureido pendant showed to form an H-bond through its ureido C=O with Q92 (32% of

MD time) and a water bridge with T91 (with occasional π-cation interaction with K67), after 35 ns the molecular tail shifted toward the α-helix 131-135 only maintaining the water-mediated interaction with T91. Approaching the end of the MD, the phenylureido tail significantly moved away from the original position likely because of H-bonds established by the urea with S135 side chain and by the methoxy group with Y20 (Figure 57B).
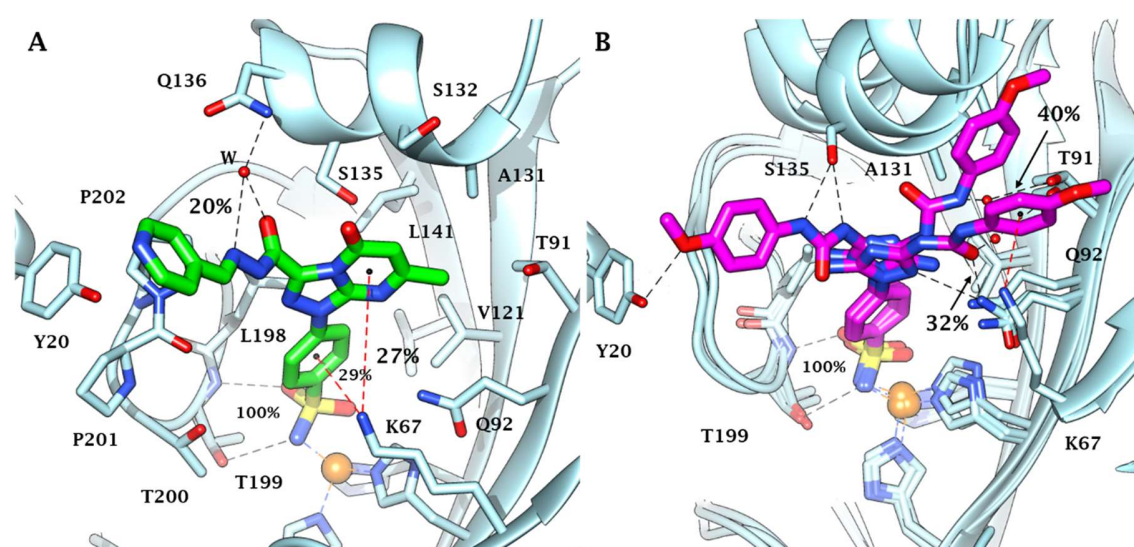
Figure 57. A) Principal predicted orientation produced over a cycle of 100 ns MD for **F1d** bound in the CA XII active site. B) Principal predicted orientations extrapolated from the 100 ns MD of **F6e** bound in the CA XII active site. H-bonds and π-cation interactions are depicted as black and red dashed lines, respectively. The bond occupancies over 100 ns are reported as a percentage. The latter are below 10% when not indicated.

The different binding orientations predicted for both ligands within CA II, IX and XII, allow their good selectivity values to be argued. The greater efficacy of **F1d** against CA IX than the other isozymes is likely related to the accommodation and strong interaction of the arylidenehydrazide moiety with the aforesaid hydrophobic pocket (V20, W5, P201, and P202). In fact, the V20/F20 (CA IX/CA II) and the V20/Y20 (CA IX/CA XII) mutations reduced such an intense binding. Nonetheless, in CA XII π-cation interactions of K67 with both the benzene and pyridinone rings, not present in CA II, likely led to the increase of K_I values up to a low nanomolar range (Table 11). In the case of **F6e**, the phenylureido tail occupied a different binding pocket in the CA II compared to CA IX and XII (Figures 54, 56 and 57), most likely due to owing to the presence of a phenylalanine residue in position 131

which sterically prevent the binding nearby the region where the ligand, in the tumor-associated CAs, bound to Q92 and L91 (CA IX) and T91 and K67 (CA XII).

The experimental procedures are reported in Chapter 7 and the data and results of this research were published in Said, M.A., et al. *Eur. J. Med. Chem.* **2020**, *185*, 1118-1143.[280]

Chapter 4. Carbonic anhydrase inhibitors as antimicrobial agents: synthesis, and *in silico* investigations.

Nowadays, the growing drug resistance to antimicrobial drugs is a major problem in the treatment of infectious diseases caused by pathogens such as bacteria, fungi, and protozoa, which are the second leading cause of death in the world.[385,386]

This issue has raised massive scientific interest expressly for discovering new molecular targets essential for the life cycle/growth of the pathogens and developing a feasible plan for the realization of novel antibacterial drugs, possibly effective as next-generation antibiotics. Microbes express their pathogenicity through their virulence, which determines the ability of pathogens to enter a host, evade host defenses, grow in the host environment, counteract its immune responses, assimilate iron or other nutrients from the host, or sense environmental changes.[387-389] The main classes of clinically used antibiotics inhibit bacterial growth by interfering with the biosynthesis of proteins (tetracyclines, macrolides, lincosamides, erythromycin, phenicols, aminoglycosides, and fusidic acid), nucleic acids (quinolones, novobiocin, ansamycins, benzylpyrimidines, imidazole, nitrofurans), folate metabolism (sulfonamides), or the formation of the microbe cell wall (β-lactams, glycopeptides, lipoglycopeptide, and fosfomycin).[390-392]

In recent decades, the revolution of modern medicine, especially in surgery and chemotherapy, also has led to an increase in the numbers of immunocompromised patients with resistance to the already limited therapeutic options for the treatment of systemic fungal infections.[393] Immunosuppression is mainly due to the extensive use of antibiotics, anticancer drugs, corticosteroids, increased transplant frequency, central venous catheter application, and acquired immunodeficiency syndrome (AIDS), and has resulted in an increase in the number of invasive fungal infections (IFIs) in patients, which are normally prevented by a healthy immune system. To date, fungi have shown resistance towards the best antifungal drugs such as polyenes, azoles, and echinocandins, that disrupt or block the formation of the peculiar fungal cell wall.

Unlike vaccines and drugs that are available against bacterial and viral pathogens, therapeutic options are limited for the diseases caused by protozoan parasites. In the past, classical antiprotozoal agents were effectively used to control infections caused by pathogenic protozoa. Most of the drugs in use as anti protozoan agents were discovered in the 1950s, and a few drugs discovered thereafter have several limitations, such as high cost, low efficacy, and poor safety. At present, the treatment options are limited and the resistance of parasites to existing antiparasitic agents has necessitated the identification of new therapeutic targets to fight against protozoan diseases.[394] Therefore, there is an urgent need to identify novel targets in common parasitoses, which are currently classified as priority infections by the WHO (category 1: reemerging or uncontrolled infections).[395,396]

One strategy for fighting antibiotics is represented by the upgrade of the current clinical drugs for generating novel antibiotics[397,398] but, as a limitation, the newly created drugs could have a limited life span for the possible resistance they would develop sooner or later. An interesting strategy to overcome antibiotic resistance is to discover and use novel enzymes essentially involved in central microbial metabolism. In Table 12, are reported some enzymes that are responsible for the pathogen virulence, acting against host components and contributing to the damage of host tissues.

Table 12. List of enzymes used as drug targets, which are traditionally used as molecular targets and the clinically used drugs against these molecular targets.

Enzyme	Clinical drug
Carbonic anhydrase	Acetazolamide
Angiotensin-converting enzyme	Captopril
Neuraminidase	Oseltamivir
HIV-1 protease	Saquinavir, Indinavir
Guanine phosphoribosyltransferase	Allopurinol
Dihydrofolate reductase	Methotrexate
Inosine 5'-monophosphate dehydrogenase	Tiazofurin
Cyclooxygenase	Diclofenac, Indometacin
Thymidylate synthase	Tomudex
Dihydropteroate synthase	Sulfanilamide, Sulfathiazole

Indeed, the interconversion of CO_2 and HCO_3^- is spontaneously and precisely balanced from the living organisms to maintain the equilibrium between dissolved inorganic carbon dioxide (CO_2), carbonic acid (H_2CO_3), bicarbonate (HCO_3^-), and carbonate (CO_3^{2-}), by carbonic anhydrases.[399-404] Thus, the survival of microorganisms could be compromised by restricting the access of the pathogen to the important metabolites, which are essential for microbe biosynthesis and energy metabolism, using CAIs.[405]

In particular, in bacteria are expressed the α-, β-, and γ-CAs classes, in fungi there are only α-, and β-CAs, while in protozoa are identified α-, β-, and η-CAs.

4.1 N-Nitrosulfonamides as carbonic anhydrase inhibitors: a promising chemotype for targeting Chagas disease and Leishmaniasis (Series G)

World Health Organization (WHO) included Chagas disease (American trypanosomiasis) and leishmaniasis in the list of neglected tropical diseases (NTDs). Parasites of the kinetoplastidae family are responsible for these infections, both belonging to the vector-borne diseases affecting 20 million people and killing more than 50000 every year.[406]

Trypanosoma cruzi is naturally transmitted by kissing bugs (mainly belonging to the genera *Triatoma* and *Rhodnius*), which primarily diffuse in Latin America. The disease evolves producing potentially fatal lesions to organs in the cardiac, digestive or neurological systems.[406]

Leishmaniasis is transmitted by the bite of an infected phlebotomine and works out skin or visceral aches that could turn out to be fatal if untreated. Among the NTDs, leishmaniasis is the first-in-class in terms of mortality and morbidity.[406]

Available pharmacological treatments for the majority of NTDs are limited in terms of cost and toxicity and ineffective, and resistance phenomena constantly increase throughout the world.[407-409] Pharmaceutical industry shows poor interest in searching for new effective drugs for the treatment of NTDs due to high costs and expected low financial return. It is urgent to find new therapeutic targets for these parasitoses, which WHO classifies as priority infections.[407,410] Novel targets have been identified driven by large-scale analysis on the completely known genome sequence of both protozoans. Indeed, endeavors to enrich the

therapeutic arsenal against Chagas disease and leishmaniasis based on enzymatic inhibition have been starting in many laboratories with synthetic drugs representing a valuable source for new treatments.[411,412]

The metalloenzymes carbonic anhydrases recently identified in these protozoans are novel promising targets for chemotherapeutic interventions.[25,411,413] CAs from *Trypanosoma cruzi* (TcCA) and *Leishmania donovani chagasi* (LdcCA) were cloned and characterized in 2013,[414-416] resulting in the design of the novel antiprotozoal agents that act by a totally new mechanism of action and lack cross-resistance to existing drugs. The α-CA TcCA is endowed with a very high catalytic activity for the CO_2 hydration reaction and was shown to be inhibited in the nanomolar range by many types of CA inhibitors (CAIs) such as aromatic/heterocyclic sulphonamides,[414,417,418] sulfamates,[414] thiols,[414] anions,[419] dithiocarbammates,[419] hydroxamates,[420] and benzoxaboroles.[421] Thiols and hydroxamates exhibited *in vitro* anti-trypanosomal activity, inhibiting the three phases of the pathogen's life cycle.[414,420] The β-CA LdcCA also features an effective catalytic activity and was shown to be efficiently inhibited by sulfonamides and heterocyclic thiols with nanomolar inhibition constants.[416,422] Some such thiols derivatives displayed *in vitro* anti-leishmania activity in preliminary assays being able to reduce parasites growth and causing their death.[416] Identification of new protozoans CAIs with effective anti-trypanosomal or anti-leishmanial activities is more than ever worth of endeavor due to such targets remarkable druggability.

Nifurtimox and benznidazole have been the first effective drugs for treating acute-phase human Chagas infection, with the first being no longer available on the market because of undesirable side effects.[423] They feature heteroaromatic nitro moieties that are pivotal for the anti-protozoa mechanism of action. Parasite resistance arisen with benznidazole drove the development of alternative therapies. Indeed, combined treatment of benznidazole with drugs with different mechanisms of action such as azoles, nitric oxide, or clomipramine could be a strategy to improve the pharmacotherapy efficacy.[411]

Noteworthy, a new chemotype able to afford α- and β-CAs inhibition was reported by Nocentini et al. in 2016, namely N-nitrosulfonamides.[424] Interestingly, these latter were shown to inhibit ubiquitous, off-targets isoforms, such as CA II, feebler than lead

sulfonamides though holding remarkable submicromolar inhibition of the human tumor-associated CA IX (α-CA) and the β-CA from the pathogen fungus *Malassezia Globosa.*

Considering the above, the set of N-nitrosulfonamides was extended and screened on a wider pattern of human and pathogen (from protozoa and fungi) CAs, among which the target α-TcCA and β-LdcCA.

Furthermore, we produced silver salts of all such derivatives based on the marked effects against viruses, bacteria, fungi, and protozoa that silver salts have been shown to possess.[424] The anti-microbial behaviors of silver, silver ions, and silver-containing compounds have long been investigated with various anti-microbial mechanisms of action having been proposed to date.[425-428] The biologically active silver ion (Ag^+) irreversibly damages key enzyme systems in the cell membranes of pathogens. Conversely, silver exhibits low toxicity in the human body, and minimal risk is expected due to clinical exposure.[425] Recently, silver nanoparticles (Ag-NPs) were demonstrated to produce reactive oxygen species to which *Leishmania* parasites are very sensitive.[428] Moreover, the commercially available antibiotic silver sulfadiazine shares a wealth of features with silver N-nitrosulfonamides. These latter derivatives are thus endowed with multiple potential anti-protozoa entities to be synergistically exploited to overcome resistance issues displayed by single-targeted therapy. The general synthetic strategy proposed by Minksztym[428] for the chemoselective mononitration of aminosulfonamides was applied to a set of ten starting compounds being commercially available (**G1-3**, **G7**, **G8**) or yielded by methylation (**G4-6**) or deacetylation (**G17**, **G19**) reactions (*Scheme 5* and *6*).

Quenching and work-up of the NH_4NO_3/H_2SO_4 based nitration reaction was switched for the most unstable derivatives **G16**, **G18** and **G20** from water to NH_4OH (aq) to generate the stable ammonium salts instead of the zwitterion forms of N-nitrosulfonamides (*Scheme 5* and *6*).[429,430]
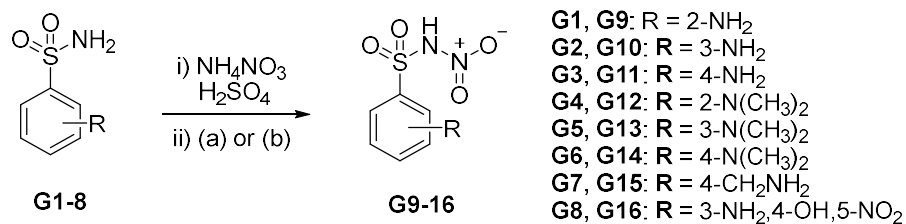
Scheme 5. Synthesis of aromatic N-nitrosulfonamides. (a) H_2O; (b) $NH_4OH(aq)$
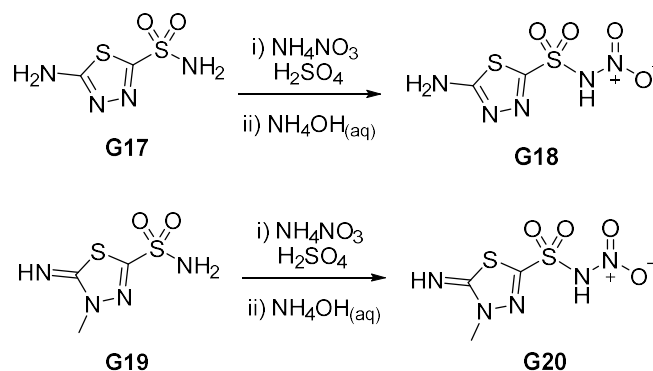
Scheme 6. Synthesis of heteroaromatic N-nitrosulfonamides.

The production of the silver salts of the derivatives was achieved by different methods depending on the nature of the compound or the form it was produced in the previous step. Silver carbonate was used as base (to remove the proton) and source of silver ion in an aqueous phase in the case of zwitterion of amino aromatic compounds. $NaOH/AgNO_3$ were used for the zwitterion of the amino aliphatic compound **G15** and ammonium salts **G16**, **G18**, **G20** (*Scheme 7*).
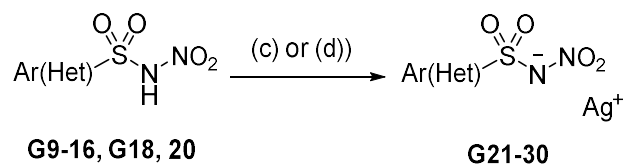
Scheme 7. Synthesis of silver salts of N-nitrosulfonamides. (c) Ag_2CO_3, H_2O; (d) NaOH, $AgNO_3$, H_2O.

All silver salts compounds precipitated in aqueous phases were therefore recrystallized by the same solvent. All the obtained derivatives were properly characterized by means of ^{1}H-NMR, ^{13}C-NMR, and MS (see Experimental section, Chapter 7).

The inhibition profiles of the N-nitrosulfonamide derivatives were evaluated against six α-CAs and three β-CA isoforms in addition to acetazolamide (**AAZ**) as a standard inhibitor, by a stopped-flow CO_2 hydrase assay.[282]

Five human CA isoforms, among which the ubiquitous CA I and II (involved in many physio-pathological processes) and the membrane-associated CA IV (involved in ocular aches, stroke, and arthritis), IX and XII (over-expressed in hypoxic tumors) were included in the kinetic study to work out thorough SAR and selectivity profiles.[1] Along with the target TcCA and LdcCA, the activity of two additional β-CA isoforms from pathogenic fungi was studied with the reported inhibitors, namely MgCA from *Malassezia globosa* (responsible for the production of dandruff)[80] and Can2 from *Cryptococcus neoformans* (that can cause fungal meningitis and encephalitis).[31] The inhibitory efficacy against nine such isoforms was also assessed with the silver salts of all derivatives to verify whether the monovalent metal ion affects the enzymatic activities. The inhibition constants (K_Is) of these latter do not show significant variations out of the error ranges, witnessing no significant action of the Ag^+ ion to each CA activity. Tables 13 gather the inhibition data of silver salts **G21-30**.

Table 13. Inhibition data of hCA I, II, IV, IX, XII and pathogen TcCA, LdcCA, MgCA, Can2 with N-nitrosulfonamide silver salts **G21-30** and the standard sulfonamide inhibitor acetazolamide (**AAZ**) by the stopped-flow CO_2 hydrase assay.[282]

Cmpd	R	K_I [a] (μM)								
		CA I	CA II	CA IV	CA IX	CA XII	TcCA	LdcCA	MgCA	Can2
G21	2-NH$_2$	29.0	60.9	39.2	0.52	0.75	3.2	4.7	0.52	7.4
G22	3-NH$_2$	54.7	7.7	4.3	5.4	2.6	0.15	0.49	1.7	0.25
G23	4-NH$_2$	67.4	53.4	23.6	9.4	2.0	0.10	0.23	0.76	0.40
G24	2-N(CH$_3$)$_2$	80.6	6.2	32.2	8.0	3.6	5.0	4.8	32.2	4.3
G25	3-N(CH$_3$)$_2$	45.9	18.1	4.5	6.8	5.7	1.4	0.50	4.5	1.1
G26	4-N(CH$_3$)$_2$	58.3	64.2	11.0	4.5	3.9	0.43	0.65	0.30	0.42
G27	4-CH$_2$NH$_2$	39.6	55.8	3.1	5.4	0.65	0.47	0.71	7.1	1.0
G28	3-NH$_2$,4-OH,5-NO$_2$	19.8	45.0	1.9	5.2	0.55	0.85	1.0	0.57	0.35
G29	-	7.3	2.9	1.4	0.84	0.92	0.35	0.52	4.1	0.76
G30	-	4.9	2.2	4.8	0.23	0.76	0.32	0.44	2.7	2.3
AAZ	-	0.25	0.012	0.075	0.025	0.006	0.06	0.09	0.076	0.01

[a] Mean from 3 different assays, by a stopped-flow technique (errors were in the range of ± 5-10 % of the reported values).

According to preliminary data reported in literature,[424] N-nitro aromatic sulfonamides exhibited low CA I and II inhibitory effectiveness, with K_Is spanning in a low to a medium micromolar range (2.2-80.6 µM). Heteroaromatic derivatives **G29** and **G30** turned out as the most potent inhibitors against these ubiquitous hCAs. Whereas CA IV was targeted by all derivatives in a low micromolar range (1.4-39.2 µM), a wealth of submicromolar K_Is values against CA IX and XII (0.23-9.4 µM) confirmed the favorite efficacy of N-nitrosulfonamides against the tumor-associated isoforms. CA XII was the most affected isozyme among the considered cluster, though the greatest inhibition was measured with the thiadiazole derivative **G30** with CA IX (K_I of 0.23 µM). It should be noted that CA XII features more threonine and serine residues in the active site than other hCAs. Likely extended H-bond networks between N-nitrosulfonamide moieties and such hydrophilic residues could justify the reported low K_I values. Noteworthy, TcCA turned out to be the most affected α-CA among those studied. Most derivatives inhibited TcCA in a medium nanomolar range (0.10-0.85 µM), except for compounds bearing 2-NH_2, 2-$N(CH_3)_2$ or 3-$N(CH_3)_2$ moieties at the phenyl ring (K_Is in the range 1.4-5.0 µM). The incorporation of primary amino groups at the meta or para position of the phenyl ring confers to **G22** and **G23** the greatest TcCA inhibitory efficacies as well as the strongest CA inhibition properties of the study. In agreement with the inhibition data previously reported,[424] β-CAs were generally more efficiently inhibited by N-nitrosulfonamides than α-CAs. Indeed, most K_Is shown in Table 13 for LdcCA, MgCA and Can2 lie in a submicromolar range. While the first isozyme is undoubtedly the most affected one among the three (K_Is in the range 0.23-4.8 µM), equally efficient inhibitions were measured against the fungal MgCA and Can2. The 4-NH_2-phenyl derivative **G23** arose again as the most potent one against the target LdcCA (K_I of 0.23 µM). Unlike against TcCA, **G22** inhibited the isozyme comparably with the heterocyclic derivatives **G29** and **G30** (K_Is of 0.49, 0.52 and 0.44 µM, respectively).

Striking target/off-target CAs selectivity profiles can be ascribed to many N-nitrosulfonamide derivatives. As a general trend, the designed compounds acted one to more than two orders of magnitude more potently against TcCA and LdcCA than ubiquitous h isoforms CA I and II; *e.g.* derivative **G23** showed a TcCA/CA II and LdcCA/CA II inhibition ratios of 540 and 230, respectively.

The *in vitro* inhibition results of N-nitrosulfonamides against TcCA and LdcCA isoforms were carried on by studying the inhibitory activity of some such inhibitors against various *Trypanosoma cruzi* and *Leishmania* forms. Compounds **G22** and **G23** demonstrated the most potent and selective inhibition against the target CAs and were furthered in the study in the silver salt forms.

The percentage of inhibition of the *Trypanosoma cruzi* epimastigote forms at different concentrations of synthetic compounds are shown in Table 14.

Table 14. Minimum inhibitory concentration (MIC) and concentration which reduced the proliferation of epimastigotes by 50% (IC_{50}) values derived from growth inhibition assays of *T. cruzi* Dm28c clone and Y strain. Determination of cytotoxicity (CC_{50}) and the selectivity index (SI_{50}) of **G22** and **G23** was done using RAW 264.7 macrophages.

	MIC (µM)		IC_{50} (µM)			Selectivity index (SI) *	
Cmpd	Epimastigotes forms *T. cruzi* Dm28c	Epimastigotes forms *T. cruzi* Y	Epimastigotes forms *T. cruzi* Dm28c (µM)	Epimastigotes forms *T. cruzi* Y (µM)	Raw 267.4 cells toxicity CC_{50} (µM)	Epimastigotes forms *T. cruzi* Dm28c	Epimastigotes forms *T. cruzi* Y
Benznidazole	32	32	29.12 ± 3.03	17.00± 0.64	137.54± 12.05	4.77 ± 0.91	8.09± 0.40
G22	16	32	5.03±0.95	12.00±1.06	29.28± 0.38	5.87±1.14	2.47± 0.41
G23	32	8	11.99±0.14	2.51±0.40	34.89± 3.47	2.32±0.79	11.58± 2.72

Average values of three independent experiments ± standard deviations; SI = IC_{50} Raw 267.4 cells/IC_{50} epimastigote forms of *T. cruzi* Dm28c *and T. cruzi* Y

The experiments, performed by the research group of Professor Alane Beatriz Vermelho from the Federal University of Rio de Janeiro, showed that compounds **G22** and **G23** possess better activity than the reference drug benznidazole (Bnz) against the epimastigotes forms of *Trypanosoma cruzi* in both Dm28c clone and Y strain. At the concentration of 5.03 ±0.95 µM compound **G22** inhibited by 50% (IC_{50}) the proliferation of *T. cruzi* Dm28c. For *T. cruzi* Y, IC_{50} values were reached at the concentrations of 12.00±1.06 and 2.51 ±0.40 µM for **G22** and **G23**, respectively. Anyhow, the two derivatives possess higher toxicity than Bnz for Raw 267.4 macrophage cells (Table 14). As a result, only **G22** shows a better *SI* (5.87±1.14) than benznidazole (4.77±0.91) for *T. cruzi* Dm28c, whereas uniquely **G23** display a higher *SI* for the Y strain of the parasite 11.58± 2.72 concerning the standard (8.09±0.40). Compounds **G22** and **G23** were also screened against both *T. cruzi* forms relevant to human infection. Table 15 summarizes the trypanocidal activity against the non-replicative (trypomastigotes) and replicative (amastigotes) stages of *T. cruzi*, Dm28c-Luc clone. Both inhibitors **G22** and

G23 showed potent activity against trypomastigotes, reaching IC_{50} values of 4 to 19.5 folds better than Bnz, respectively. For intracellular amastigotes, **G22** ($IC_{50} = 5.2 \pm 1.1$) and **G23** ($IC_{50} = 8.3 \pm 1.5$) showed lower efficacy than Bnz ($IC_{50} = 1.7 \pm 0.3$). The higher toxicity than Bnz against Vero cells found for compounds **G22** and **G23** resulted in a reduced selectivity index with respect to the reference drug (Table 15).

Table 15. Analysis of cytotoxicity and trypanocidal effect of compounds.

| Cmpd | IC_{50} (µM) | | Vero cells toxicity CC_{50} (µM) | Selectivity index (*SI*)* | |
	Trypomastigotes	Intracellular amastigotes		Trypomastigotes	Intracellular amastigotes
Benznidazole	15.6 ± 1.9	1.7 ± 0.3	>500	>32	>294.1
G22	0.8 ± 0.3	5.2 ± 1.1	21.1 ± 2.8	26.4	4.1
G23	3.9 ± 1.1	8.3 ± 1.5	24.1 ± 3.6	6.2	2.9

Average values of three independent experiments ± standard deviations; $SI = IC_{50}$ Vero cells/IC_{50} Trypomastigote and intracellular amastigote forms of *T. cruzi,* Dm28c-Luc clone.

Minimum inhibitory concentrations (MIC) of **G22** and **G23** against *Leishamnia infantum* and *L.amazonensis* are shown in Table 16, whereas IC_{50}, CC_{50} and *SI* values are represented in Figure 58. While compound **G22** shows MIC values of 25 against both Leishmania spp, **G23** exhibits a two-fold greater activity against *L. amazonensis* than *L. infantum* (Table 16). These values are higher than the reference drug Amphotericin B (AMP).

Table 16. Minimum inhibitory concentration (MIC) assays of *L. amazonensis* and *L. infantum*

| Compound | MIC (µM) | |
	Promastigotes forms *L. amazonensis*	Promastigotes forms *L. infantum*
Amphotericin B	8	8
G22	25	25
G23	12.5	25

Average values of three independent experiments ± standard deviations.

Derivatives **G22** and **G23** respectively display IC_{50} of 16.61 and 8.43 µM against the promastigotes forms of *L. amazonensis* and 16.64 and 17.67 µM for *L. infantum* (Figure 59A). The standard AMP is more effective with IC_{50} values of 1.65 and 1.77 µM against the two Leishmania sp. Nonetheless, the concentration of AMP which reduced 50% of RAW

267.4 macrophages cells viability (CC_{50}) is very low (1 μM), whereas inhibitors **G22** and **G23** possess lower toxicity (CC_{50} values of 29.28 μM and 34.89 μM respectively (Figure 58B). As a result of these latter, whereas the *SI* of the reference compound AMP was more than two-fold higher than **G22** against both Leishmanias, **G23** showed a better selectivity profile than AMP against *L. amazonensis* (Figure 58C).
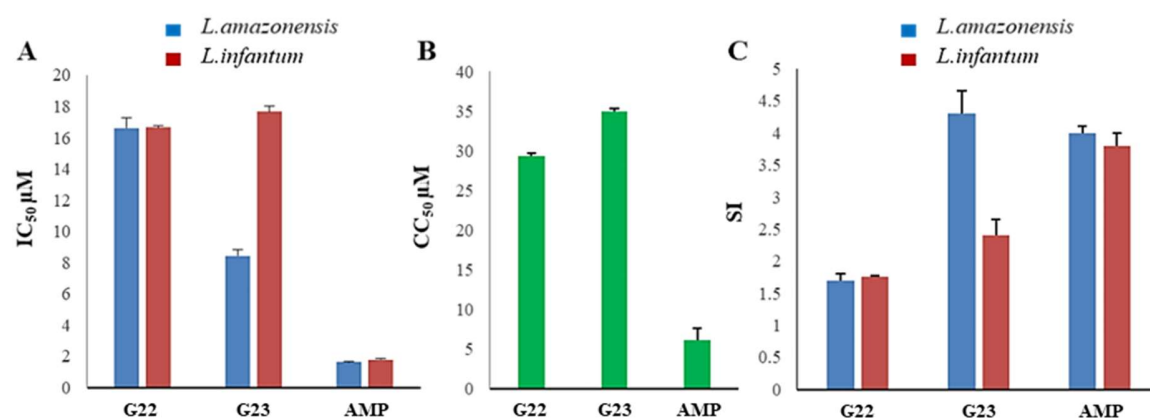
Figure 58. A) Concentration which reduced the proliferation of promastigotes by 50 % (IC_{50} μM); B) cytotoxic concentration which reduced 50% of RAW 267.4 cells (CC_{50} μM); C) selectivity index: RAW 267.4 cells (CC_{50})/ IC_{50} against *L. amazonensis* and *L. infantum.*

The present results make N-nitrosulfonamides innovative chemotypes to yield the selective inhibition of the target pathogens CAs over human isoforms. The reported *in vitro* assays against various strains of *T. cruzi* and *L. donovani* are of remarkable interest in the field of NTDs and represent a new interesting starting point to the rational CAIs optimization for the treatment of Chagas disease and leishmaniasis.

The experimental procedures are reported in Chapter 7 and the data and results of this research were published in Bonardi, A., et al. *ACS Med. Chem. Lett.* **2019**, *10*, 413-418.[431]

4.2 Benzoxaboroles: new potent inhibitors of the carbonic anhydrases from the pathogenic bacterium Vibrio cholerae (Series H)

Vibrio spp. are bacteria present in freshwater, estuarine and marine environments, that prefer warm and brackish water.[432] Among the ~12 pathogenic species for humans of the >100 described *Vibrio* spp., *Vibrio cholerae* is the unique rod shape Gram Negative bacterium that provokes cholera, a disease endemic in low-income countries.[432,433] Annually, cholera affects more than 2-4 million people worldwide with 21,000-143,000 deaths, half of them being children under 5 years old.[434-436] The infection occurs mainly by the fecal-oral route through contaminated food, or poorly sanitized water,[337,338] or person-to-person close contact.[339,340] *V. cholerae* enters in the gastrointestinal tract and reaches the small intestine.[441] Several intestinal environmental factors such as bicarbonate,[442] bile, unsaturated fatty acids, and reduced oxygen levels promote the co-transcription of toxin-co-regulated pilus (Tcp), cholera toxin (CT) and other colonization-associated genes (all encoded by regulon *toxT*), that allow the pathogen proliferation.[443] Using the filamentous surface appendage Tcp, *V. cholerae* is able to bind the same adjacent bacterial cells and to tightly adhere to enterocytes without disrupting the mucosal integrity.[441,444,445] Instead, the pathogen-secreted toxin CT, composed of two subunits *ctxA* and *ctxB*, recognizes and binds the sialylated glycosphingolipid GM1 on the cytoplasmatic membrane of enterocytes with the pentameric *ctxB* subunit.[446] After endocytosis, CT enters in the endoplasmic reticulum (ER) via a retrograde transport, where the subunits are dissociated.[446] The enzymatic *ctxA* subunit released in the cytosol, upon allosteric activation by ADP ribosylation factor 6 (ARF6), is able to trigger the G-protein coupled receptor and consequently the adenylyl cyclase (AC).[446] The high levels of produced cAMP stimulate the protein kinase A (PKA)-dependent phosphorylation of the cystic fibrosis transmembrane receptor (CFTR), responsible for the efflux of water and ions into the lumen of the small intestine, leading to diarrhea.[446] The profuse watery diarrhea, together with vomiting and gastroenteritis, are the main clinical symptoms of cholera disease that, if untreated, results in death due to dehydration within 1-2 days.[446,448] To date, the long-term solutions to prevent cholera are the surveillance, sanitization of the water, good hygiene

practices, social mobilization monitoring, and oral cholera vaccines.[449,450] On the other hand, the infection is treated by prompt administration of oral/intravenous rehydration solution (ORS),[451-453] appropriate antibiotics (such as azithromycin and ciprofloxacin)[454,455] and zinc.[456] While the administration of ORS is a fundamental but symptomatic therapy, the use of antibiotics is important to eradicate the cause of the illness. However, the spreading drug resistance to antimicrobial agents is threatening the efficacy of current chemotherapy, making the development of new antibiotic drugs with different mechanisms of action essential.[385]

Bicarbonate is an important virulence factor for *V. cholerae* as it is a positive effector for *toxT* activity, promoting the transcription of genes that encode for Tcp, CT and other proteins implicated in proliferation.[442,457-459] These gene expression is significatively reduced by the addition of carbonic anhydrase inhibitors (CAIs).[457-459] Thus, it is probable that *V.cholerae* uses the carbonic anhydrases system to accumulate bicarbonate into the cell for activating its virulence, as the bicarbonate levels are very high in the upper small intestine colonized by the pathogen and this bacterium does not encode bicarbonate transporter proteins in its genome.[457-459]

Such evidence make CAs interesting targets to prevent *V. cholerae* proliferation, offering the possibility to develop antibacterial drugs with an innovative mechanism of action to contrast the disease.

In particular, the genome of *V. cholerae* encodes for three CAs, VchCA, VchCAβ, and VchCAγ respectively belonging to the α-, β- and γ-class, suggesting an important role of these enzymes in the pathogen physiology.[457,460,461]

To date, only the 3D structure of VchCAβ was solved by X-ray crystallography in 2015 revealing a tetrameric type II β-CA, while structural information was not collected for VchCA and VchCAγ.

Kinetic parameters in Table 17 show that VchCA (K_{cat} = 8.2 x 10^5 s^{-1}) is more active than VchCAγ (K_{cat} = 7.4 x 10^5 s^{-1}) and VchCAβ (K_{cat} = 3.3 x 10^5 s^{-1}), and all of them are more active than hCA I (K_{cat} = 2.0 x 10^5 s^{-1}).[461-465]
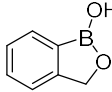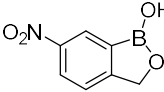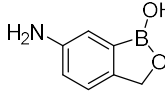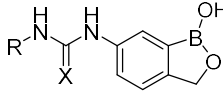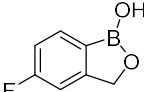
Table 17. Kinetic parameters for the CO_2 hydration reaction of α-CAs human cytosolic isozymes hCA I and II and VchCA measured at 20°C and pH 7.5 in 10 mM HEPES buffer and 20 mM Na_2SO_4, and VchCAβ and VchCAγ measured at 20°C, pH 8.3 in 20 mM TRIS buffer and 20 mM $NaClO_4$.[461-465]

Enzyme	Species	Class	Activity level	K_{cat} (s⁻¹)	K_M (M)	k_{cat}/k_m M⁻¹ x s⁻¹	K_I AAZ (nM)
hCA I	Human	α	Moderate	2.0×10^5	4.0×10^{-3}	5.0×10^7	250
hCA II	Human	α	Very high	1.4×10^6	9.3×10^{-3}	1.5×10^8	12
VchCA	*V. cholerae*	α	Moderate	8.2×10^5	11.7×10^{-3}	5.4×10^7	6.8
VchCAβ	*V. cholerae*	β	Moderate	3.3×10^5	8.1×10^{-3}	1.9×10^6	4512
VchCAγ	*V. cholerae*	γ	Moderate	7.4×10^5	11.5×10^{-3}	6.4×10^7	473

In recent studies, searching for new CAIs chemotypes acting as antiinfectives, benzoxaborole derivatives that demonstrated potent inhibitory activity fungi and parasites CAs were developed.[110, 421, 466-469] Therefore, the purpose of this project was to provide new information about the potential of benzoxaboroles as potential inhibitors of the three CAs-classes of *Vibrio cholerae*, with a main focus on VchCAγ, as no benzoxaborole derivative has been assayed to date for the inhibition of this CA class. A stopped-flow kinetic assay[282] against VchCAs of α-, β-, and γ-classes was therefore applied to a set of benzoxaborole derivatives (**H1–23**) previously synthesized by the research group of Prof. Jean-Yves Winum from the University of Montpellier (Table 18). Noteworthy, at the time when the study was undertaken, no molecular modeling investigation on γ-class CA, were known. The kinetic study includes acetazolamide (**AAZ**), a clinically used sulfonamide inhibitor, that was used as standard and tavaborole (**TVB**), a benzoxaborole commercially used as topical antifungal medication. Inhibitory profiles were displayed as inhibition constants (K_{IS}) in comparison with those against the main physiological human isoform CA II, off-target in this study (Table 18).

Generally, the inhibitory activity resulted in more intense against VchCA (α-CA) compared to VchCAγ, which, in turn, showed an inhibition more potent respect to VchCAβ. Moreover, selective benzoxaborole derivatives were detected against α-VchCA with a high selective index against the off-target CA II and, in particular, compound **H18** exhibited a selective inhibitory action against all VchCAs over hCA II (*SI* CA II / VchCA > 125.0; *SI* CA II / VchCAβ > 10.7; *SI* CA II / VchCAγ > 14.6).

Table 18. Inhibition data of hCA II, VchCA (α-CA) VchCAβ and VchCAγ with benzoxaboroles **H1-23**, **TVB** and the standard sulfonamide inhibitor **AAZ** by a stopped flow CO2 hydrase assay.[282]

Cmpd	X	R	K_I (nM)[a]			
			VchCA	VchCAβ	VchCAγ	CA II
H1		-	319	70313	2837	8180
H2		-	142	8866	818	504
H3		-	165	21830	1168	590
H4	O	$CH_2C_6H_5$	90	42143	1874	439
H5	O	CH_2-(3-Cl,5-CH_3- C_6H_5)	53	61318	718	276
H6	O	C_6H_5	117	56351	705	730
H7	O	4-Cl-C_6H_5	56	19532	650	707
H8	O	CH_2-fur-2-yl	164	79946	1229	841
H9	O	4-F-C_6H_5	48	28046	644	480
H10	O	4-CF_3-C_6H_5	46	55124	957	456
H11	O	2,4,6-Cl-C_6H_5	76	84459	895	272
H12	O	2-OCH_3,5-CH_3-C_6H_5	556	67286	410	89
H13	O	4-$COCH_3$-C_6H_5	103	65084	1128	797
H14	S	$CH_2CH_2C_6H_5$	102	18372	554	1547
H15	S	4-CH_3-C_6H_5	109	2586	1762	1253
H16	S	napht-2-yl	603	25994	2974	1148
H17	S	4-OCH_3-C_6H_5	165	2297	874	1250
H18	S	4-NO_2-C_6H_5	80	933	687	>10000
H19	S	$CH_2C_6H_5$	96	30408	3955	1305
H20	S	4-F-C_6H_5	112	6350	544	1500
H21	S	CH_2-fur-2-yl	220	31939	1996	2230
H22	S	4-CF_3-C_6H_5	72	1253	1919	1838
H23	S	C_6H_5	1204	19128	834	1625
TVB		-	157	97278	841	462
AAZ		-	6.8	451	473	12

a. Mean from 3 different assays, by a stopped-flow technique (errors were in the range of ± 5–10% of the reported values).

A computational protocol consisting of joint docking, MMGBSA, and MD simulations was undertaken to explore in-depth the inhibitory profiles of benzoxaboroles **H1-23** towards VchCA, VchCAβ, and VchCAγ. Benzoxaboroles were shown to act as zinc-binder CAIs

against hCA II in the form of their conjugated Lewis base. Compounds **H1**, **H4**, **H6**, **H12**, **H19,** and **H23** were observed in the tetrahedral anionic B(OH)$_2^-$ form as tetra- and/or penta-coordinated around the metal atom in hCA II active site,[110] while *in silico* study showed that the same benzoxaborole derivatives coordinate the zinc ion in a tetrahedral coordination geometry in the narrower active site of β-CAs from fungi.[466] Thus, docking studies were performed considering the benzoxaborole B(OH)$_2^-$ anion form.

All ligands were submitted to QM geometry optimization (B3LYP/6-31G^{*+}) and ESP charges computation prior to dock the molecules into the homology-built models of VchCA (α-CA), VchCAβ, and VchCAγ and to verify the adducts stability by MD simulations. In fact, the pdb database only contains the 3D coordinates for VchCAβ that however is present in type II or "closed" form of the enzyme (PDB 5CXK),[470] thus not suitable for docking aims. The HM models were respectively developed using as templates the solved coordinates of α-CA from *Photobacterium profundum* (5HPJ), type-I β-CA from *Pseudomonas aeruginosa* (6D2N), and γ-CA from *Escherichia coli* (3TIO). The templates show the highest sequence identity percentage with the targets, namely 53%, 52%, and 61% respectively. The best scored HM-built models were used to figure out the binding mode of representative benzoxaboroles within VchCAs active sites. ΔG binding energy was computed by an MM-GBSA method and the stability of the predicted ligand/target adducts was evaluated by 100 ns molecular dynamic (MD) simulations. The structure of the three investigated CA isoforms was stable during the computation with the backbone atom root mean square deviations (RMSDs), exhibiting small fluctuations over the course of the dynamic. As well, all docked binding orientations showed significant stability along the MD, and the Zn coordination being firmly maintained. Despite the structural differences between VchCA (α-CA) and hCA II (i.e. the hCA II α-helix structural motif residues ranging from 129 to 135 is replaced in VchCA by a short coil formed by residues 128-132), benzoxaboroles derivatives share similar interaction features within the bacterial and human isozymes.

In fact, the predicted binding modes for the unsubstituted benzoxaborole **H1** in VchCA strictly resembles the interaction mode within hCA II[110] and two main binding solutions, featured by almost the same interaction energy values with the target, were found with

different coordination geometry, namely a tetrahedral (**t**, Figure 59A) and a trigonal bipyramid (**p**, Figure 59B).
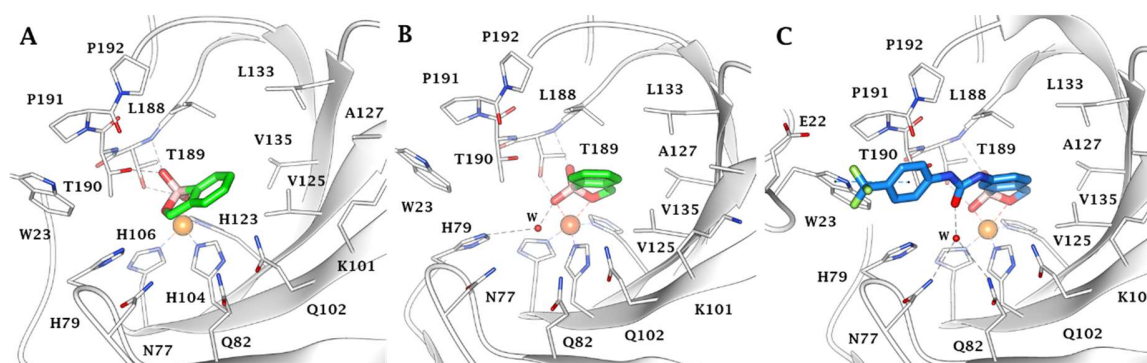
Figure 59. Predicted binding mode of **H1** (green) and **H10** (blue) within VchCA (α-CA) active site. A) Tetrahedral (**t**); B) and C) trigonal bipyramid (**p**) coordinated poses of compounds **H1** and **H10**, respectively. H-bonds and π-π interactions are shown as black and blue dashed lines, respectively. Water molecules are represented as red spheres.

In the tetra-coordinated form, the fourth coordination position about the metal ion is occupied by one hydroxyl group on the boron atom, which also forms an H-bond with T189 side chain (95% stable along the MD); the other BOH is involved in a bifurcated H-bond with T189 backbone NH (92%) and the side chain hydroxyl group of T190 (81%).

In the penta-coordinated pose, the cyclic oxygen atom additionally binds the Zn^{2+} and similar H-bonds as above only occur with T189, involving the residue side chain OH (97%) and the backbone NH (94%) groups, respectively. Moreover, a 65% stable water bridged H-bond occurs between the coordinating OH and H79. The position of the heterocycle in both orientations is further stabilized by hydrophobic interactions with residues from the lipophilic half of the binding cavity (V125, V135, L133, L188, P192).

The introduction of a bulky substituent at the 6 position of the benzoxaborole scaffold, as in derivative **H10**, the most potent VchCA inhibitor, only enables a **p**-like binding mode, with the formation of H-bonds of stability comparable to those of derivative **H1**. The 4-CF$_3$-phenyl-ureido pendant accommodates into the pocket formed by W23, H79, and P191, establishing π-π (43%) and vdW interactions (Figure 59C). Water bridged H-bond network

occurring between the ureido oxygen atom and N77 (53%) and Q82 (32%) side further stabilizes the adduct.

The binding site of the active VchCAβ dimer, as the other members of the β-CAs family, locates at the interface and is composed of amino acids from the two monomers forming the dimer (Figure 60). The zinc ion is coordinated by a histidine and two cysteine residues belonging to the same monomer.
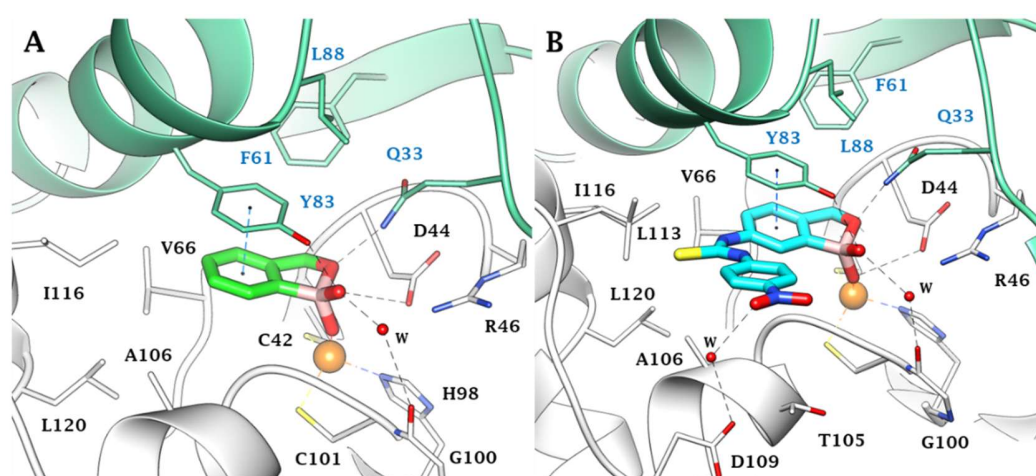
Figure 60. Predicted binding mode for **H1** and **H18** within type-I VchCAβ active site. Tetrahedral (**t**) coordinated poses of compounds (A) **H1** and (B) **H18**. H-bonds and π-π interactions are shown as black and blue dashed lines, respectively. Water molecules are represented as red spheres. The labels of amino acids from different chains are colored differently.

The *in silico* insights showed that the narrow active site of VchCAβ can accommodate benzoxaborole derivatives only as stably tetra-coordinated (**t**) around the Zn(II) ion (Figure 60). The binding orientation is stabilized by multiple interactions with Y83: a Y83-OH···O-B interaction involving the second OH group of the ligand (that not coordinated to the Zn^{2+}) and the hydroxyl group of the residue (67%), a π-π stacking interaction between the benzene ring of **H1** and the phenyl ring of the amino acid (75%). In addition, the same OH group donates an H-bond to D44 side chain carboxylate (69%) and is in H-bond contact with G100 (43%) through a bridged water molecule whereas the benzoxaborole endocyclic oxygen acts as an acceptor forming another H-bond with Q33 side chain (58%). Moreover, the binding

pose is further stabilized by vdW interactions with F61, V66, I116 and L120 (Figure 60A). However, the dynamic behavior of this adduct highlighted an overall reduced stability of the pose over the 100 ns long simulation. This might be probably related to the enclosed, restricted active site of VchCAβ, when compared to other β-CAs (e.g. Can2),[466] that prevents a consistent pose stabilization and induces the lower inhibitory profile of the benzoxaboroles against VchCAβ compared to VchCA, VchCAγ, and Can2 (fungi CA of *Saccharomyces cerevisiae*).

The predicted interaction mode for compound **H18**, the most effective VchCAβ inhibitor in Table 18, highlighted how the flexibility of the (thio)ureido linker allows the pendant in position 6 to accommodate in the lipophilic pocket formed by A106, L113, I116 (Figure 60B). MD simulations pointed out that the persistence of the H-bonds involving the zinc-binding group is enhanced by 10-15%, as well as the pose stability over the MD, with respect to derivative **H1**. The lodging of the X ureido atom in the inner portion of the aforesaid lipophilic cleft can support the more effective inhibitory action of thioureido over ureido derivatives. The p-NO$_2$ group in **H18** (and presumably the CF$_3$ in **H22**, the second most potent VchCAβ inhibitor) favors water bridged H-bonds with residues at the outer rim of the binding cavity such as D109 (38%).

Likewise, the active site of the trimer VchCAγ, as other γ-CAs, locates at the interface and is composed of amino acids belonging to two distinct monomers (Figures 61).
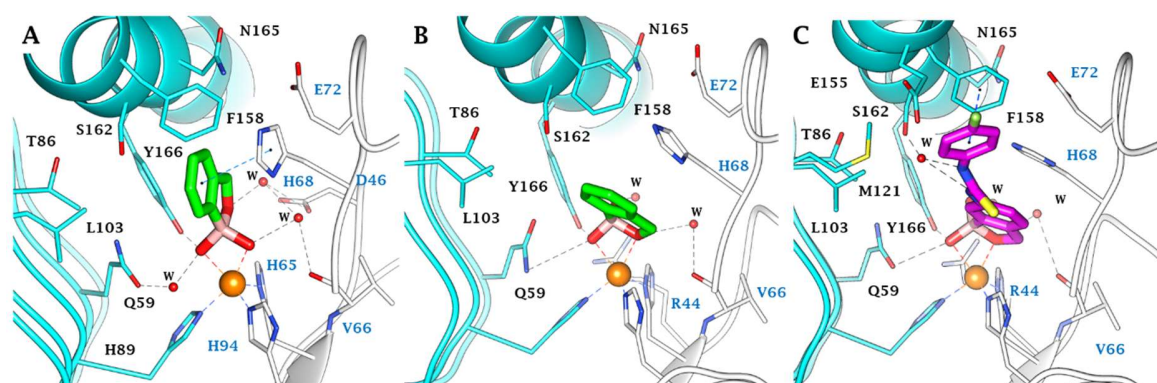
Figure 61. Predicted binding poses of **H1** and **H20** in VchCAγ active site: (A) **p1** and (B) **p2** of derivative **H1** and (C) compound **H20**. H-bonds and π-π interactions are shown as black and blue dashed lines, respectively. Water molecules are represented as red spheres. The labels of amino acids from different chains are colored differently.

In the case of VchCAγ, the zinc ion is coordinated by three histidine residues belonging to distinct chains. Unlike VchCAβ, the active site of VchCAγ is roomy enough to accommodate two alternative stable penta-coordinated orientations (**p1** and **p2**) for benzoxaborole **H1**. In **p1**, the dual coordination around Zn^{2+} occurs by both OH groups of the ligand, with one also involved in a direct and a water-mediated H-bond with the phenolic group of Y166 (74%) and the Q59 side chain (48%). The other OH and the endocyclic oxygen atom are water bridged with V66 backbone C=O (37%) and D46 (32%) side chain carboxylate (Figures 61A). Additionally, the benzene ring of **H1** is sandwiched between H68 and T86, forming π-π (56%) and π-alkyl interactions with these residues. In **p2**, the endocyclic oxygen atom and an OH group of the ligand coordinate around the zinc ion. The **p2** binding orientation is stabilized by two H-bonds with the phenolic group of Y166 and the amide side chain of Q59 (72% and 61% stable respectively). The other OH and the cyclic oxygen atom are involved in 42% and 21% stable water bridges with V66 backbone C=O and the R44 side chain (Figures 61B). Moreover, it is in hydrophobic contact with T67, H68, and H94 (Figure 61B). From an energetical point of view, the **p2** binding mode is favored over **p1** (dG -52.34 kcal/mol vs -46.83 kcal/mol). Interestingly, the 6-ureido derivatives bind in the active site by a **p2**-like mode (Figure 62C), conserving a similarly stable H-bond network as described for derivative **H1**. The 4-F-phenylureido group of inhibitor **H20**, the most active against VchCAγ extends towards the lipophilic half of the active site, interacting through a π-π interaction (45%) and vdW contacts with L103, M121, and F158. Further, the ureidic NH is commonly implicated in a water bridge with S162 side chain (approximately 55% stable).

The above findings indicate that benzoxaboroles represent an interesting chemotype worth developing as innovative antibacterial agents since they possess a new mechanism of action and isoform selectivity preferentially against the bacterial expressed CAs. This study enriches the inhibitory profiles database for the different *Vibrio cholerae* CA-classes. Furthermore, it furnishes suggestions for the rational design of new potent and selective inhibitors targeting *V. cholerae* CAs over human off-target ones.

The experimental procedures and sequence alignment of the homology built models with relative templates are reported in Chapter 7. The data and results of this research were published in Bonardi, A., et al. *ACS Med. Chem. Lett.* **2020**, *DOI: 10.1021/acsmedchemlett.0c00403.*[471]

Chapter 5. *In silico* studies on different GABA$_A$ receptor subtypes: homology modeling, mutagenesis, docking, and molecular dynamics studies.

This project is the result of a collaboration with Prof. Arias of the Oklahoma State University and focuses on an *in silico* analysis to clarify the binding site and the interaction mode of the alkaloids (+)-catharanthine within the GABA$_A$ receptor. The study is supported by electrophysiological and [^{3}H]-Flunitrazepam displacement experiments able to suggest a loreclezole-like mechanism of (+)-catharanthine for the modulation of GABA$_A$Rs. Many of the experimental results of this study are at the moment unpublished. Therefore, only, docking, MD and Homology model results will be discussed.

5.1 (+)-Catharanthine potentiates GABA$_A$ receptors by interacting with a site shared with loreclezole and (+)-etomidate: an electrophysiological and molecular modeling study

Coronaridine congeners, including natural compounds (-)-ibogaine and its metabolite noribogaine, (-)-coronaridine, and (+)-catharanthine, and the synthetic derivative 18-methoxycoronaridine (18-MC) (Figure 62), decrease self-administration of many different drugs of abuse in animal models and reduce drug craving and relapse in humans, making them significant lead compounds for anti-addictive therapies.[472] The current notion is that its anti-addictive activity is mediated by selective inhibition of $\alpha_3\beta_4$-containing nicotinic acetylcholine receptors (AChRs) expressed in the habenula.[268,472-475]

Animal studies showed that coronaridine congeners have, in addition to anti-addictive activity, antidepressant, anxiolytic, anti-obesity, sedative, and anti-neuropathic activity.[268,476-480] This variety of behavioral effects might be related to the pharmacological promiscuity exhibited by these congeners. For instance, coronaridine congeners may inhibit, in addition to AChRs,[474,475] several receptors and voltage-gated channels as well as potentiate γ-aminobutyric acid type A receptors (GABA$_A$Rs).[268]
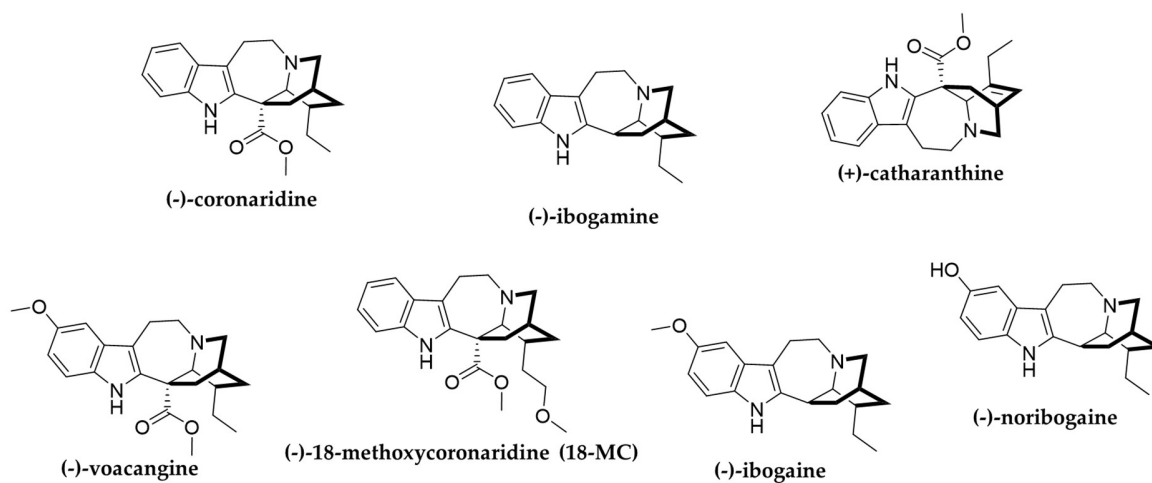
Figure 62. Chemical structure of some coronaridine congeners.

GABA$_A$Rs are composed of five subunits belonging to different classes but the majority of these receptors are assembled by one γ2, two α, and two β subunits.

To date, the binding site of coronaridins and congeners in the GABA$_A$Rs has not been identified. Displacement studies specifically designed for this study, using the radioligand [^{3}H]-Flunitrazepam, shown that (+)-catharanthine and many other coronaridins (e.g., (-)-ibogaine, (-)-noribogaine, and (-)-ibogamine) do not affect the binding of the radioligand. Moreover, studies with HEK293 cells expressing GABA$_A$Rs without the γ-subunit, which indeed is important for BDZ binding, suggested that the coronaridins bind at the β(+)-α(-) interface, in an allosteric site other than that of BDZ.

Nowadays, the Protein Data Bank database contains several X-ray and Cryo-EM solved structures of human GABA$_A$Rs receptors both in Apo form or in complex with ligands. However, all these structures are not suitable for the in silico investigation due to the lack, in some cases, of some important structural elements, such as α-helices, and in others due to problems in the positioning of the γ subunit. In 2019 the structure of hα1β3γ2 GABA$_A$R (PDB: 6HUJ)[481] was released in which all the above drawbacks were overcome.

Thus, this structure was used as template to obtain the homology models of the GABA$_A$R subtypes, useful to investigate the binding mode of (+)-catharanthine, (+)-etomidate, and loreclezole.

As a part of collaboration with Prof. Arias, the homology models of the following GABA$_A$Rs were built, four of which were mutants GABA$_A$Rs: h$\alpha_2\beta_1\gamma_2$, h$\alpha_1\beta_2\gamma_2$, and h$\alpha_2\beta_3\gamma_2$, $\alpha_1\beta_2$(N265S)γ_2, $\alpha_1\beta_2$(M286C)γ_2, $\alpha_1\beta_2$(R269A)γ_2, and $\alpha_1\beta_2$(D282A)γ_2. Figure 63 shows the sequence alignment of $\alpha_{1/2}$ and $\beta_{1/2/3}$ subunits for residues comprising the binding site. While the α_1 and α_2 subunits show a 100% identity in the transmembrane M1-M2 domains, the β_1 and $\beta_{2/3}$ subunits differ by only two residues. It is noteworthy that the $\beta_{2/3}$-N265S mutation produces a homologous β_1-S265 receptor (Figure 63).
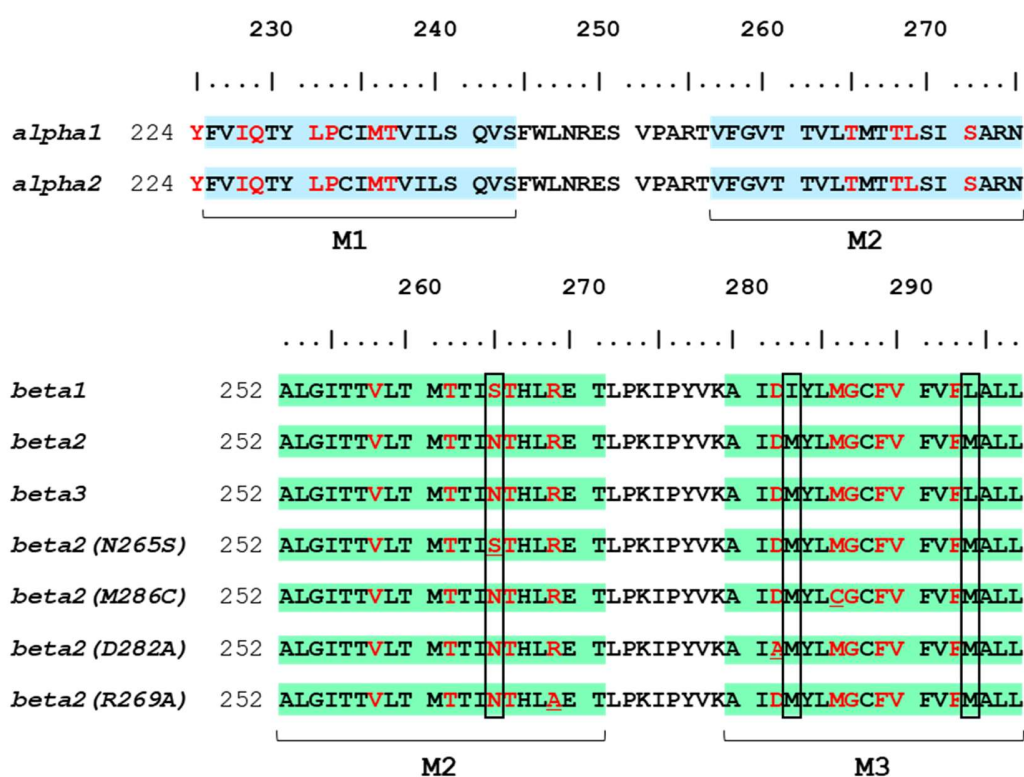
Figure 63. Sequence alignment of the TM residues (in red) forming ligands binding sites. The black squares highlight the differences among amino acids of the native receptors. The mutated residues are underlined.

Docking results carried out on $\alpha_1\beta_2\gamma_2$ and $\alpha_2\beta_1\gamma_2$ GABA$_A$R models indicated that (+)-catharanthine, (+)-etomidate, and loreclezole interact with an overlapping binding site located in the β_2(+)/α_1(-) interface formed by both β_2-M2/M3 and α_1-M1/M2 domains of the h$\alpha_1\beta_2\gamma_2$ GABA$_A$R model (Figure 64A,B). The interactions that take place between the ligands and the residues of the built GABA$_A$R models are reported in Table 19.

Table 19. Residues involved in the docking of (+)-catharanthine, (+)-etomidate, and loreclezole to different wild-type and mutant GABA$_A$R models.

Ligand	GABA$_A$R model	$\alpha_{1/2}$-Subunit Residues (TMD)	$\beta_{1/2/3}$-Subunit Residues (TMD)
(+)-Etomidate	h$\alpha_1\beta_{2/3}\gamma_2$	I228, Q229, L232, P233, and M236 (M1) T265 and L269 (M2)	V258 and **N265** (M2) M286, *F289*, V290, and F293 (M3)
	h$\alpha_2\beta_1\gamma_2$	I228, L232, P233, and M236 (M1) T265 and L269 (M2)	V258 (M2) M286, *F289*, V290, and F293 (M3)
	h$\alpha_1\beta_2$(N265S)γ_2	I228, L232, P233, and M236 (M1) T265 and L269 (M2)	V258 (M2) M286, *F289*, V290, and F293 (M3)
	h$\alpha_1\beta_2$(M286C)γ_2	I228, L232, P233, and M236 (M1) T265 and L269 (M2)	V258 and **N265** (M2) *F289*, V290, and F293 (M3)
Loreclezole	h$\alpha_1\beta_{2/3}\gamma_2$	Q229, P233, and T237 (M1) T265, and L269 (M2)	V258, T262, **N265**, and **R269** (M2) *F289* (M3)
	h$\alpha_2\beta_1\gamma_2$	Q229, P233, and T237 (M1) T265, and L269 (M2)	V258, T262, S265*, and **R269** (M2) *F289* (M3)
	h$\alpha_1\beta_2$(N265S)γ_2	Q229, P233, and T237 (M1) T265, and L269 (M2)	V258, T262, S265*, and **R269** (M2) *F289* (M3)
(+)-Catharanthine	h$\alpha_1\beta_{2/3}\gamma_2$	Y225 (pre-M1) I228 and Q229 (M1)	**N265**, L268, and **R269** (M2) L272, P273, K274, and **K279** (M2-M3 loop) **D282** and L285 (M3)
	h$\alpha_2\beta_1\gamma_2$	Y225 (pre-M1) I228 and Q229 (M1) S272 (M2)	S265*, L268, and **R269** (M2) L272, P273, K274 and **K279** (M2-M3 loop) **D282** and L285 (M3)
	h$\alpha_1\beta_2$(N265S)γ_2	Y225 (pre-M1) I228 and Q229 (M1)	S265*, L268, and **R269** (M2) L272, P273, K274 and **K279** (M2-M3 loop) **D282** and L285 (M3)
	h$\alpha_1\beta_2$(D282A)γ_2	Y225 (pre-M1) I228, Q229, and P233 (M1)	**N265**, L268, and **R269** (M2) L272, P273, K274, and **K279** (M2-M3 loop) A282* and L285 (M3)
	h$\alpha_1\beta_2$(R269A)γ_2	Y225 (pre-M1) I228 and Q229 (M1)	**N265**, L268, and A269* (M2) L272, P273, K274, and **K279** (M2-M3 loop) **D282** and L285 (M3)

TMD = transmembrane domain; residues in **bold** form H-bonds; residues in *italics* form π-π interactions; * residues β2-S265 and β2-A269 still form VdW interactions in the respective mutants.
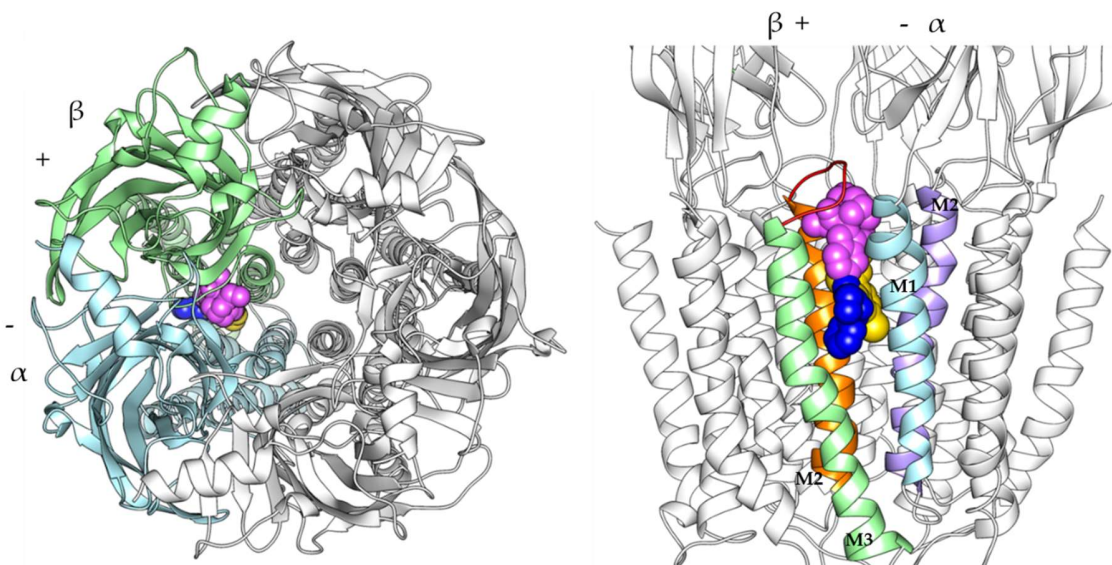
Figure 64. (A) Extracellular, and (B) transmembrane view of the overlapped binding sites of (+)-catharanthine (magenta), loreclezole (yellow), and (+)-etomidate (blue).

The stability of the poses was assessed by 100 ns long MD simulations. The stability of each ligand is greater in the β_2-containing GABA$_A$R model than that in the β_1-containing GABA$_A$R. For instance, the smaller RMSD values for (+)-etomidate/h$\alpha_1\beta_2\gamma_2$ complex indicate a longer and more stable interaction time compared to its interaction with the h$\alpha_1\beta_2$(N265S)γ_2 mutant (homologous to the wild-type h$\alpha_1\beta_1\gamma_2$ GABA$_A$R; Figure 65D). Nevertheless, differences among ligand sites were also found. For instance, the binding site for (+)-etomidate is located deeper in the transmembrane domain with respect to the other two ligands, whereas the binding position of (+)-catharanthine is closer to the extracellular/transmembrane junction, lined by β_2-M2/M3 and α_1-M1 domains, and the β_2-M2/M3 loop (Figure 64).

In the (+)-etomidate site, the ligand's imidazole ring formed a π-π stacking with β_2-F289 (at M3), and accepted an H-bond from the amide NH$_2$ of the β_2-N265 side chain (at M2) (Figure 65A; Table 19), which persisted for almost the entire duration (78%) of the MD simulation (100 ns) in the h$\alpha_1\beta_2\gamma_2$ GABA$_A$R (Figure 65D).
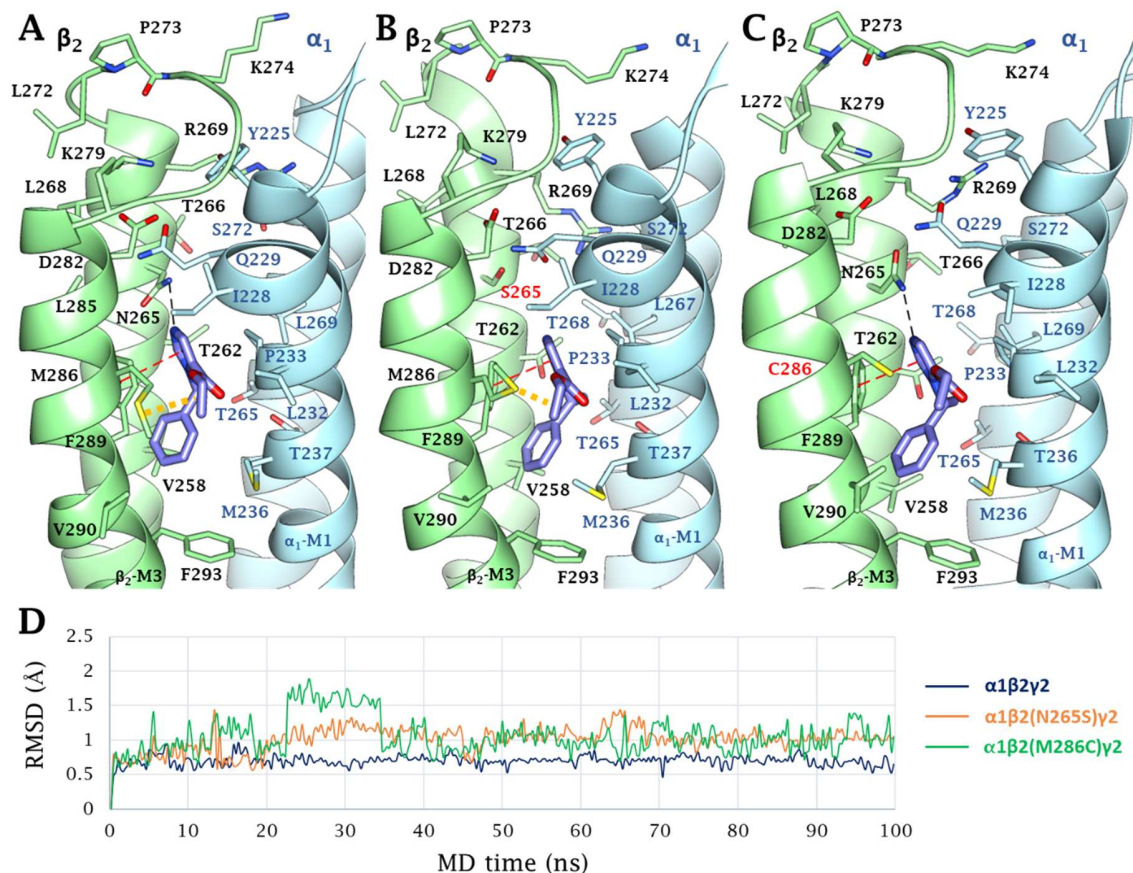
Figure 65. Predicted binding mode of (+)-etomidate (blue) to the respective (A) $h\alpha_1\beta_2\gamma_2$, (B) $h\alpha_1\beta_2(N265S)\gamma_2$, and (C) $h\alpha_1\beta_2(M286C)\gamma_2$ GABA$_A$R models. (D) RMSD plots for the MD simulations (100 ns) of (+)-etomidate docked to the wild-type $h\alpha_1\beta_2\gamma_2$ GABA$_A$R (dark blue), and $h\alpha_1\beta_2(N265S)\gamma_2$ (light brown) and $h\alpha_1\beta_2(M286C)\gamma_2$ (green) mutants. H-bonds, π-π stacking, and vdW contacts with M286 are depicted as a black, red, and yellow dashed line, respectively.

The latter interaction was seen neither in the $h\alpha_2\beta_1\gamma_2$ (Table 19) nor in $h\alpha_1\beta_2(N265S)\gamma_2$ mutant (Fig. 65B), and the stability of the above-mentioned H-bond decreased from 78% to 55% in the mutant $\alpha_1\beta_2(M286C)\gamma_2$ (Figure 65C), concomitant with larger RMSD fluctuations (Fig. 65D). The docking pose of (+)-etomidate is also stabilized by lipophilic interactions with α_1-M1 (i.e., I228, Q229, L232, and P233), α_1-M2 (i.e., T265 and L269), β_2-M2 (i.e., V258), and β_2-M3 (i.e., F293) residues (Fig. 65A; Table 19). In addition, the ethyl ester moiety of (+)-etomidate is accommodated between four lipophilic residues from β_2-M3 (i.e., M286 and V290) and α_1-M1 (i.e., L232 and M236) (Fig. 65A; Table 19), forming stable van der Waals (vdW) interactions. The interaction with β_2-M286 was stable for almost the entire

duration (76%) of the MD simulations (Fig. 65D) but was present for only 22% of the simulation with the β_2-C286 mutant (Fig. 65D; Table 19). Interestingly, vdW contacts with β_2-M286 also decreased from 76% in the $\alpha_1\beta_2\gamma_2$ wild-type to 64% in the $\alpha_1\beta_2(N265S)\gamma2$ mutant. These results further support the pivotal role of both β_2-N265 (at M2) and β_2-M286 (at M3) residues in the etomidate-receptor interaction.

In the case of loreclezole, the dichlorophenyl ring of the ligand engaged in π-π stacking interactions with β_2-F289 (at M3), and established vdW interactions with α_1-M1 (i.e., I228, P233, and T237), α_1-M2 (i.e., T265 and L269), and β_2-M2 (i.e., V258 and T262) residues (Figure 66A; Table 19). The ligand's haloolefine moiety also formed hydrophobic contacts with α_1-P233 (at M1) and α_1-L269 (at M2) side chains, whereas its triazole ring formed two H-bonds with the NH_2 side chains of the β_2-N265 and β_2-R269 residues (at M2). These two H-bonds were stable for practically the whole MD simulation (69% and 76%, respectively; Figure 66C), indicating that the ligand is stable in this site. In both $\alpha_2\beta_1\gamma_2$ (Table 19) and $\alpha_1\beta_2(N265S)\gamma_2$ (Figure 66B) models, however, a partial loss of triazole interactions with α_1-M1 (i.e., I228, Q229, and P233) and β_2-M2 (i.e., N265) residues was observed, as determined by a decreased stability (from 69% to 55%) in the mutant (Figure 66C), whereas the H-bond with β_2-R269 was maintained (Table 19). Although loreclezole did not interact with β_2-M286 (Figure 66A; Table 19), the stability of other important interactions with this ligand was assessed in the h$\alpha_1\beta_2$(M286C)γ_2 mutant (Figure 66C). The results indicated that the observed H-bonds with β_2-N265 and β_2-R269 are held over the MD course with stability comparable (71% and 74%, respectively) to that in the wild-type h$\alpha_1\beta_2\gamma_2$ receptor.
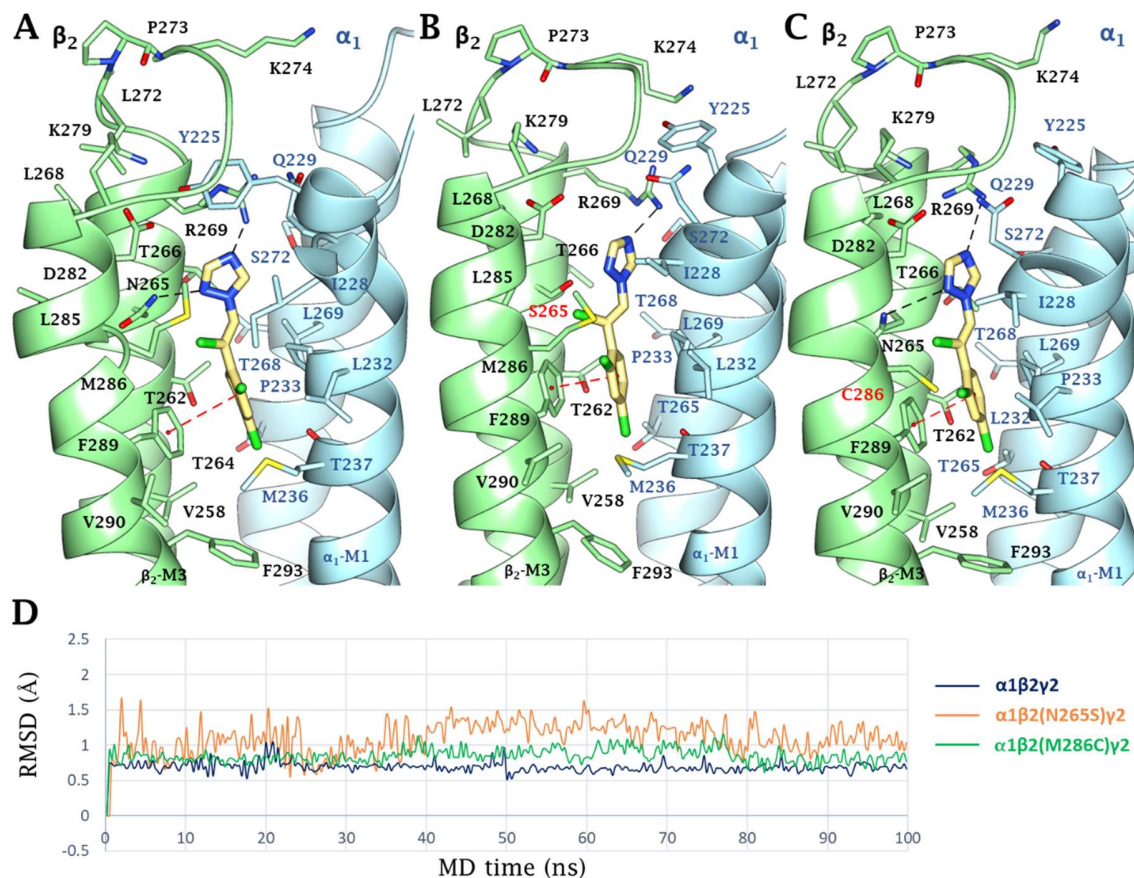
Figure 66. Predicted binding mode of loreclezole (yellow) to the respective (A) $h\alpha_1\beta_2\gamma_2$, (B) $h\alpha_1\beta_2(N265S)\gamma_2$, and (C) $h\alpha_1\beta_2(M286C)\gamma_2$ GABA$_A$R models. (D) RMSD plots for the MD simulations (100 ns) of (+)-etomidate docked to the wild-type $h\alpha_1\beta_2\gamma_2$ GABA$_A$R (dark blue), and $h\alpha_1\beta_2(N265S)\gamma_2$ (light brown) and $h\alpha_1\beta_2(M286C)\gamma_2$ (green) mutants. H-bonds and π-π stacking interactions are depicted as black and red dashed lines, respectively.

The binding of (+)-catharanthine was stabilized by four H-bonds, instead of two or one H-bond as in the case of loreclezole and (+)-etomidate, respectively. The tertiary amine N atom and the indolic NH of the alkaloid formed H-bonds with the β_2-R269 side chain NH$_2$ group (at M2) and with the β_2-D282 side chain carboxylic moiety (at M3), respectively (Figure 67A; Table 19). Another two H-bonds were observed between the C=O and the O atoms of the ligand's methyl ester and the NH$_2$ of β_2-N265 (at M2) and β_2-K279 (in the M2-M3 loop).
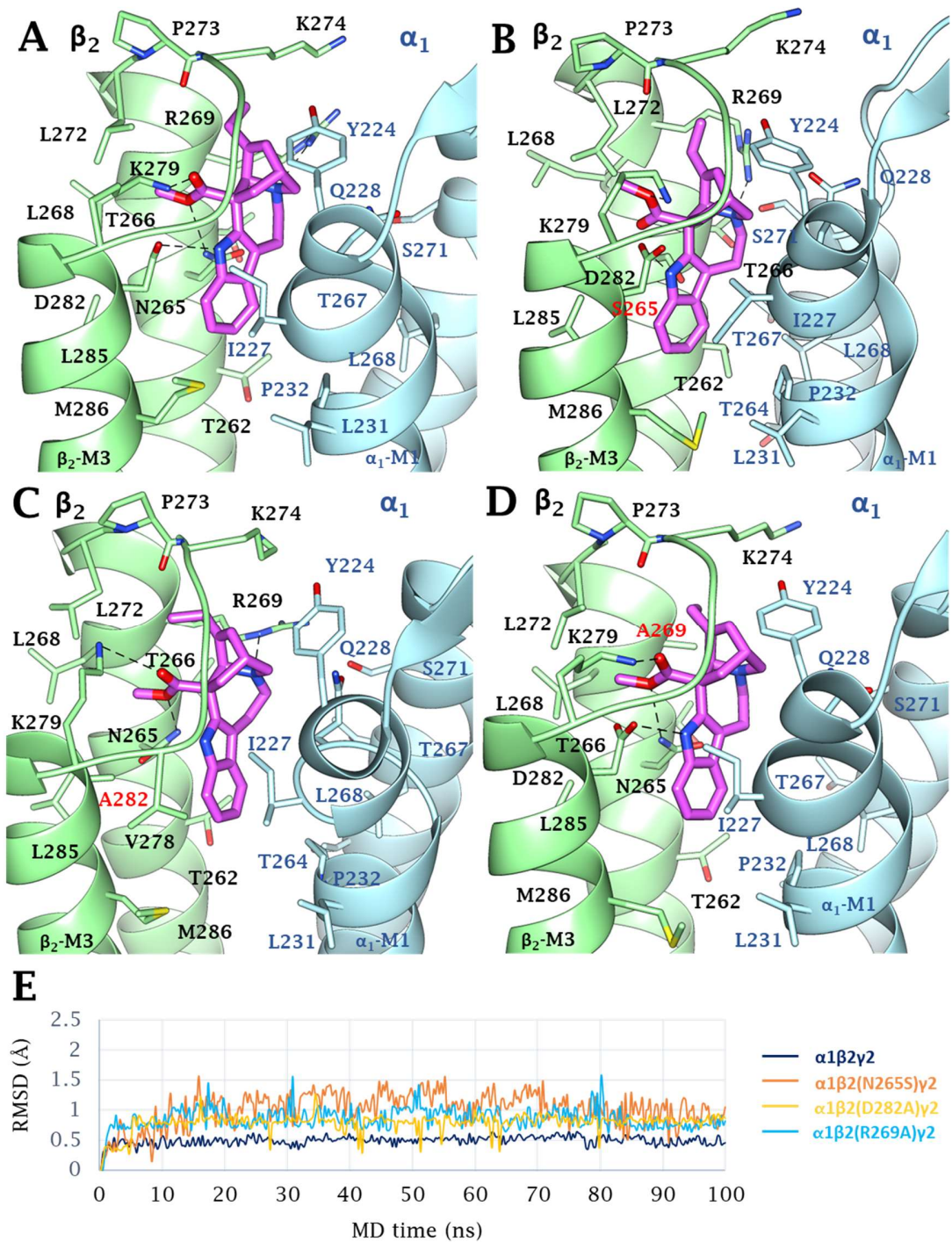
Figure 67. Predicted binding mode of (+)-catharanthine (magenta) to the respective (A) $h\alpha_1\beta_2\gamma_2$, (B) $h\alpha_1\beta_2(N265S)\gamma_2$, (C) $h\alpha_1\beta_2(D282A)\gamma_2$, and (D) $h\alpha_1\beta_2(R269A)\gamma_2$ GABA$_A$R models. (E) RMSD plots for the MD simulations (100 ns) of (+)-etomidate docked to the wild-type $h\alpha_1\beta_2\gamma_2$ GABA$_A$R (dark blue), and $h\alpha_1\beta_2(N265S)\gamma_2$ (light brown), $h\alpha_1\beta_2(D282A)\gamma_2$ (yellow), and $h\alpha_1\beta_2(R269A)\gamma_2$ (cyan) mutants. H-bonds and π-π stacking interactions are depicted as black and red dashed lines, respectively.

152

The stability of the H-bonds at N265 (80%), D282 (61%), R269 (73%), and K279 (68%) was maintained during most of the MD course in the wild-type $h\alpha_1\beta_2\gamma_2$ (Figure 67E). Interestingly, each particular H-bond was not only lost in the respective $\alpha_1\beta_2(N265S)\gamma_2$ (Figure 67B), $\alpha_1\beta_2(D282A)\gamma_2$ (Figure 67C), and $\alpha_1\beta_2(R269A)\gamma_2$ (Figure 67D) mutant, but also decreased the stability of the other three H-bonds. For example, the $\beta_2(N265S)$ mutation also decreased the respective interactions with R269 (from 73% to 60%), D282 (from 61% to 42%), and K279 (from 68% to 45%). These results support the importance of N265, R269, D282, and K279 residues in (+)-catharanthine's stability. A wide network of hydrophobic interactions was also observed between the indole-azepinic ring of (+)-catharanthine and α_1-M1 (i.e., I228 and Q229) and β_2-M3 (i.e., D282 and L285) residues as well as between the tricycle and α1-Y225 aromatic ring (located in pre-M1), the methyl ester and β_2-L268/L272 (at M2), and the ethyl moiety and β_2-P273/K274 (located in the M2/M3 extracellular loop) (Figure 67A; Table 19).

This *in silico* study not only supported the electrophysiological results, but also added structural details in terms of similitudes and differences in the interaction of (+)-catharanthine, (+)-etomidate, and loreclezole with different GABA$_A$R models. The studied ligands showed more stable interactions with $\beta_2/3$- compared to β_1-containing GABA$_A$R models, supporting the observed receptor subtype preference in the potentiating activity of (+)-catharanthine in comparison with other ligands.[478,479,482] In particular, (+)-catharanthine interacted with a pocket formed by β_2(+)M2/M3, α_1(-)M1, including the pre-M1 segment and β_2-M2/M3 loop, therefore located relatively close to the extracellular/transmembrane junction of the GABA$_A$R. Interestingly, both pre-M1 segment and M2/M3 loop have been functionally involved in the gating process.[483,484] In contrast, (+)-etomidate and loreclezole occupied a binding cavity, formed by β_2-M2/M3 and α_1-M1/M2 domains, located slightly deeper within the transmembrane domain. This relatively different location of the binding site allows us to propose two different PAM mechanisms, where only (+)-catharanthine might potentiate GABA$_A$Rs by preserving an open configuration after interacting with the extracellular/transmembrane junction.

Although overlapping binding sites were observed for (+)-etomidate, loreclezole, and (+)-catharanthine in the wild-type $\alpha_1\beta_2\gamma_2$ GABA$_A$R model, differences can also be addressed. In

particular, (+)-etomidate interacted with β_2-N265 and β_2-M286, both residues located within the $\beta_2(+)/\alpha_1(-)$ interface, whereas loreclezole and (+)-catharanthine interacted with the β_2-N265, but not the β_2-M286, residue. The stability of each interaction was subsequently studied by MDs simulations (100 ns). The results indicated that the interaction of (+)-etomidate with C286 in the $\alpha_1\beta_2(M286C)\gamma_2$ mutant is significantly reduced with respect to M286 in the $\alpha_1\beta_2\gamma_2$ model, and all three ligands showed decreased interactions with the $\alpha_1\beta_2(N265S)\gamma_2$ mutant. These results supported a pivotal role for $\beta_{2/3}$-N265 (at M2) for all ligands, and of $\beta_{2/3}$-M286 (at M3) for R(+)-etomidate. Our docking experiments with (+)-etomidate are in excellent alignment with the photolabeling studies: in both cases, α-M236 and β-M286 were identified as critical for (+)-etomidate binding.[485]

Additional structural differences were also observed among ligand interactions. For instance, (+)-etomidate and loreclezole, but not (+)-catharanthine, established a π-π interaction with β_2-F289 (at M3). In addition, both (+)-catharanthine and loreclezole formed H-bonds with β_2-R269 (at M2), whereas (+)-etomidate was the only ligand that made contact with α_1-M236 (at M1) and $\beta2$-V290 (at M3). Previous mutational studies showed that β_3-R269A (valerenic acid), β_2-F289S (valerenic acid and loreclezole), and α_1-M236W (valerenic acid and (+)-etomidate) mutations decreased the activity of these ligands, supporting a structural and functional role for these residues.[253] Interestingly, (+)-catharanthine was the only ligand that formed an H-bond with β_2-D282 (at M3). To determine the structural role of the H-bonds formed with β_2-R269 and β_2-D282, additional *in silico* mutational experiments were performed using GABAARs containing either the β_2-R269A or β_2-D282A mutation. Although each mutation produced a loss in the respective H-bond interaction, the R269A mutation induced a more substantial ligand destabilization than that in the D282A mutation, probably because in the latter the ligand is still stabilized by the adjacent H-bond with K279, located in the middle of the M2/M3 loop. This particular residue has an important role in the process of agonist-induced GABA$_A$R gating,[484] and thus, might be involved in the positive allosteric mechanism elicited by (+)-catharanthine.[486]

Radioligand, mutational, and molecular docking studies helped delineate the binding site for (+)-catharanthine. Although this site is partially shared with loreclezole and (+)-etomidate, it

also has unique structural features such as the interaction with residues in the β_2-M3 domain and β_2-M2/M3 loop.

Chapter 6. Ph.D. internship at the Department of Pharmaceutical Chemistry in Vienna

During the three-year Ph.D. cycle, I attended a stage in the organic chemistry laboratory of Prof. Vittorio Pace at the University of Vienna. There, I was involved in the investigation of reductive lithiation arene-catalyzed of imines (electrophiles) as a new method for the synthesis of amino alcohols and I improved my know-how on lithium chemistry and reactions conducted under an inert atmosphere at -78 °C.

Chapter 7. Experimental section

7.1 General Protocols

CHEMISTRY

Anhydrous solvents and all reagents were purchased from Sigma-Aldrich, Alfa Aesar, and TCI. All reactions involving air- or moisture-sensitive compounds were performed under a nitrogen atmosphere using dried glassware and syringes techniques to transfer solutions. Nuclear magnetic resonance (^{1}H-NMR, ^{13}C-NMR, ^{19}F-NMR) spectra were recorded using a Bruker Advance III 400 MHz spectrometer in DMSO-d_6 or CDCl$_3$. Chemical shifts are reported in parts per million (ppm) and the coupling constants (J) are expressed in Hertz (Hz). Splitting patterns are designated as follows: s, singlet; d, doublet; t, triplet; q, quadruplet; sept, septet; m, multiplet; bs, broad singlet; dd, double of doubles, appt, apparent triplet, appq, apparent quartet. The assignment of exchangeable protons (OH and NH) was confirmed by the addition of D$_2$O. Analytical thin-layer chromatography (TLC) was carried out on Merck silica gel F-254 plates. Flash chromatography purifications were performed on Merck Silica gel 60 (230-400 mesh ASTM) as the stationary phase and ethyl acetate/n-hexane or MeOH/DCM were used as eluents. Melting points (m.p.) were measured in open capillary tubes with a Gallenkamp MPD350.BM3.5 apparatus and are uncorrected. HPLC was performed by using a Waters 2690 separation module coupled with a photodiode array detector (PDA Waters 996) and a column, a Nova-Pak C18 4 μm 3.9 mm × 150 mm (Waters), silica-based reverse-phase column. The sample was dissolved in acetonitrile 10%, and an injection volume of 45 μL was used. The mobile phase, at a flow rate of 1 mL/min, was a gradient of water + trifluoroacetic acid (TFA) 0.1% (A) and acetonitrile + TFA 0.1% (B), with steps as follows: (A% : B%), 0−10 min 90:10, 10−25 min gradient to 60:40, 26:28 min isocratic 20:80, 29−35 min isocratic 90:10. TFA 0.1% in water as well in acetonitrile was used as a counterion. All compounds reported here were >96% HPLC pure. The solvents used in MS measures were acetone, acetonitrile (Chromasolv grade), purchased from Sigma-Aldrich (Milan - Italy), and mQ water 18 MΩ, obtained from Millipore's Simplicity system (Milan-Italy). The mass spectra were obtained using a Varian 1200L triple quadrupole

system (Palo Alto, CA, USA) equipped by Electrospray Source (ESI) operating in both positive and negative ions. Stock solutions of analytes were prepared in acetone at 1.0 mg mL^{-1} and stored at 4°C. Working solutions of each analyte were freshly prepared by diluting stock solutions in a mixture of mQ H$_2$O/ACN 1/1 (*v/v*) up to a concentration of 1.0 µg mL^{-1} The mass spectra of each analyte were acquired by introducing, via syringe pump at 10 µL min^{-1}, of its working solution. Raw-data were collected and processed by Varian Workstation, version 6.8 software.

CARBONIC ANHYDRASE INHIBITION

- α-CAs. An Applied Photophysics stopped-flow instrument has been used for assaying the CA catalyzed CO$_2$ hydration activity.[282] Phenol red (at a concentration of 0.2 mM) has been used as a pH indicator, working at the absorbance maximum of 557 nm, with 20 mM Hepes (pH 7.5) as the buffer, and 20 mM Na$_2$SO$_4$ (for maintaining constant the ionic strength), following the initial rates of the CA-catalyzed CO$_2$ hydration reaction for a period of 10-100 s at 25°C.[169] The CO$_2$ concentrations ranged from 1.7 to 17 mM for the determination of the kinetic parameters and inhibition constants. For each inhibitor, at least six traces of the initial 5-10% of the reaction have been used for determining the initial velocity. The uncatalyzed rates were determined in the same manner and subtracted from the total observed rates. Stock solutions of inhibitor (0.1 mM) were prepared in distilled-deionized water and dilutions up to 0.01 nM were done thereafter with the assay buffer. Inhibitor and enzyme solutions were preincubated together for 15 min (sulfonamides) or 6h (coumarins) at room temperature before the assay, in order to allow for the formation of the E-I complex. The inhibition constants were obtained by non-linear least-squares methods using PRISM 3 and the Cheng-Prusoff equation, as reported earlier,[282] and represent the mean from at least three different determinations. All hCA isoforms were recombinant ones obtained in-house as reported earlier,[1,2] while the α-CA SpiCA3, was obtained and purified by a diverse procedure as the one reported earlier in the thesis.

- β-CAs. An Applied Photophysics stopped-flow instrument has been used for assaying the CA catalyzed CO$_2$ hydration activity.[282] Bromothymol blue (at a concentration of 0.2 mM)

has been used as a pH indicator, working at the absorbance maximum of 557 nm, with 10–20 mM TRIS (pH 8.3) as buffer, and 20 mM $NaBF_4$ for maintaining constant the ionic strength, following the initial rates of the CA catalyzed CO_2 hydration reaction for a period of 10–100 s at 25°C. The CO_2 concentrations ranged from 1.7 to 17 mM for the determination of the kinetic parameters and inhibition constants. For each inhibitor, at least six traces of the initial 5–10% of the reaction have been used for determining the initial velocity. The uncatalyzed rates were determined in the same manner and subtracted from the total observed rates. Stock solutions of inhibitor (10 mM) were prepared in distilled-deionized water and dilutions up to 0.01M were done thereafter with the assay buffer. Inhibitor and enzyme solutions were preincubated together for 15 min (sulfonamides) or 30 min (anions) at room temperature prior to assay, in order to allow for the formation of the E-I complex. The inhibition constants were obtained by non-linear least-squares methods using the Cheng-Prusoff equation whereas the kinetic parameters for the uninhibited enzymes from Lineweaver-Burk plots, as reported earlier,[282] and represent the mean from at least three different determinations. *Entamoeba histolytica* was a protein, obtained and purified by a diverse procedure as the one reported below in the thesis.

MODELING

- Hardware. Workstation SO Linux (32 processors)

- Distribution: Linux version 4.15.0-122-generic gcc version 7.5.0 (Ubuntu 7.5.0-3)
- Intel® Xeon® Silver 4110 CPU @ 2.10 GHz (1200 MHz)
- System memory (16 DIMM slots):
  - Memory Capacity: Up to 4TB 3DS ECC DDR4-2933MHz RDIMM/LRDIMM
  - Memory Type: 2933/2666/2400/2133MHz ECC DDR4 RDIMM/LRDIMM
  - Memory Voltage: 1.2V
  - DIMM Sizes: RDIMM: 64GB; LRDIMM: 64GB; 3DS LRDIMM: 128GB
- Graphic card: Nvidia Quadro P5000; 16GB GPU dedicated

- *Software.* Schrödinger Suite Release 2019-1, Schrödinger, LLC, New York, NY, 2019 www.schroedinger.com[487]

- Maestro v.11.9; [487a]
- Epik, v.4.7;[487b]
- Impact, v.8.2; [487c]
- Prime, v.5.5; [487d]

- Macromodel v. 12.3;[487e]
- Glide, v.8.2; [487f]
- Jaguar, v.10.3;[487g]
- Desmond, 5.7;[487h]

- **Other** *softwares.* Swiss-PdbViewer, v. 4.1; BioEdit, v.7.2; Chimera.

Experimental protocol

a. Protein Preparation

All crystal structures or homology-built models used for computational studies were prepared using the Protein Preparation Wizard tool implemented in the Schrödinger suite, assigning bond orders, adding hydrogens, deleting water molecules, and optimizing H-bonding networks. The energy minimization protocol with a Root Mean Square Deviation (RMSD) value of 0.30 Å was applied using an Optimized Potentials for Liquid Simulation (OPLS3e) force field.[487-490]

This procedure was applied to the following structures:

- X-Ray solved structures (PDB ID): 2MNX, 5LJT, 1ZNC, 5FL4, 5DVX, 1JD0 and 1JCZ;
- Cryo-EM solved structures (PDB ID): 6HUJ;
- homology built models and mutants: VchCA, VchCAβ, VchCAγ, hα$_2$β$_1$γ$_2$, hα$_1$β$_2$γ$_2$, hα$_2$β$_3$γ$_2$, hα$_1$β$_2$(M286C)γ$_2$, hα$_1$β$_2$(N265S)γ$_2$, hα$_1$β$_2$(D282A)γ$_2$, and hα$_1$β$_2$(R269A)γ$_2$.

b. Ligand preparation

The 3D ligand structures were prepared by Maestro (v.11.9)[487a] and evaluated for their ionization states at pH 7.4 ± 0.5 with Epik (v.4.7).[487b] The conjugate gradient method in Macromodel (v.12.3)[487g] was used for energy minimization (maximum iteration number: 2500; convergence criterion: 0.05 Kcal/mol/Å^2).

For compounds of the series **H** the atomic electrostatic charges of the ligands were computed with Jaguar (v.10.3)[487g] fitting them to an electrostatic potential calculated at the B3LYP/ 6–31G*[+] level of theory. ESP atomic charges were used in docking simulations.

c. Grid generation

Grids for docking were centered in the centroid of the complexed ligand (for compounds of series **A**, **C**, **D**, **E**, **F** and **H**) or on the β(+)/α(-) interfacial site of GABA$_A$ receptor (for (+)-catharanthine, loreclezole, and etomidate; Chapter 5).

d. Docking studies

For molecular docking studies the software Glide SP (v.8.2; default settings)[487f] was used. In this regard, grids were centered on the β(+)/α(-) interfacial site for (+)-etomidate and loreclezole (Forman, 2011). The standard precision (SP) mode of the GlideScore function was applied to evaluate the predicted binding poses.

The Induced Fit Docking protocol in Schrödinger, used for compounds of series **C**, consists of a Glide SP docking[487f] followed by a Prime refinement of the residue side chains within 5 Å and then by a final Glide XP docking of the ligand into the receptor in the refined conformation.

e. MM-GBSA calculations

The best three poses for each compound was refined with Prime MM-GBSA calculations (v.5.5)[487d] with a VSGB (Variable Surface Generalized Born) solvation model considering the target flexible within 3 Å around the ligand.[109]

f. MD protocol

Molecular dynamics (MD) simulations were performed using Desmond Molecular Dynamics System (v.5.7.)[487h] (Schrödinger suite) and OPL3e force field. Only in the case of GABAARs (Chapter 5), each receptor model was embedded in a model membrane of POPC (1-palmitoyl-2-oleoyl-sn-glycero-3-phosphocholine) (at 300 K), to better simulate the

physiological environment. For simulations in the CA active sites, the partial charge of the zinc ion was set to 0.8 and in the case of zinc-binders, the zero bound order was considered between the ligands coordinating atom and the metal. All systems were solvated in an orthorhombic box using simple point charge water molecules extended 15 Å away from any protein atom around the transmembrane domain helices. The system was neutralized with 0.15 M Cl$^-$ and Na$^+$ ions. The simulation protocol included a starting relaxation step followed by a final production phase of 50 ns. In particular, the relaxation step comprised the following: (a) a stage of 100 ps at 10 K retaining the harmonic restraints on the solute heavy atoms (force constant of 50 Kcal/mol/Å^2) using the NPT ensemble with Brownian dynamics; (b) a stage of 12 ps at 10 K with harmonic restraints on the solute heavy atoms (force constant of 50 Kcal/mol/Å^2), using the NVT ensemble and Berendsen thermostat; (c) a stage of 12 ps at 10 K and 1 atm, retaining the harmonic restraints and using the NPT ensemble and Berendsen thermostat and barostat; (f) a stage of 12 ps at 300 K and 1 atm, retaining the harmonic restraints and using the NPT ensemble and Berendsen thermostat and barostat; (g) a final 24 ps stage at 300 K and 1 atm without harmonic restraints, using the NPT Berendsen thermostat and barostat. The final production phase of MD was run using a canonical NPT Berendsen ensemble at 300 K. During the MD simulation, a time step of 2 fs was used while constraining the bond lengths of H atoms with the M-SHAKE algorithm. The atomic coordinates of the system were saved every 100 ps along the MD trajectory. Protein RMSD, ligand RMSD/RMSF (Root Mean Square Fluctuation) ligand torsions evolution and occurrence of intermolecular H-bonds and hydrophobic contacts were provided by the Simulation Interaction Diagram (SID) implemented in Maestro along with the production phase of the MD simulation. The tool reads the MD trajectory file and identifies ligand/target interactions repeatedly occurring during the simulation time (for instance, a 60% value suggests that the interaction is maintained for the 60% of the MD).

Figures were generated with Maestro and Chimera.[487a]

7.2 Sulfonamide inhibitors of human carbonic anhydrases designed through a three-tails approach: improving ligand/isoform matching and selectivity of action (Series A)

7.2.1 Chemistry.

The general chemistry protocols are reported at the beginning of the experimental section.

General Synthetic Procedures for preparation of 4-(2-(arylalkyl)amino)ethyl)benzenesulfonamides (A1-7). *Procedure 1*. To a solution of 4-(2-aminoethyl)benzenesulfonamide (9.99 mmol, 1.0 equiv) in dry MeOH (40 mL), the appropriate aldehyde (1.1 equiv) was added and the mixture was heated at reflux temperature under stirring for 0.5-4h.[491] Sodium borohydride (1.6 equiv) was added portion-wise at 0°C and the reaction mixture was stirred at reflux temperature for 0.5-3 h. The solvent was evaporated under *vacuum*, and water was added (25 mL). pH was taken to 7 with HCl 1M. The suspension was filtered, and the collected powder was purified with flash silica chromatography (5% MeOH in DCM) to give compounds **A1-5**.

Procedure 2. To a solution of 4-(2-aminoethyl)benzenesulfonamide (9.99 mmol, 1.0 equiv) in dry DMF (5 mL), triethylamine (1.2 equiv) and the appropriate halide (1.1 equiv) were added at room temperature and the mixture was stirred at room temperature for 0.5 h (**A6**) or 60°C for 8 h (**A7**). The reaction mixture was quenched by the addition of water (20 mL) and extracted with DCM (30 mL x 3). The organic layer was collected, washed with brine (40 mL x 3), dried over Na_2SO_4, filtered and evaporated under *vacuum* to give compounds **A6-7** as powders.

4-(2-(Benzylamino)ethyl)benzenesulfonamide (A1). Compound **A1** was obtained according the general procedure 1 earlier reported using 4-(2-aminoethyl)benzenesulfonamide 9.99 mmol, 1.0 equiv) and benzaldehyde (1.1 equiv) in dry MeOH (40 mL). The reaction mixture was initially stirred at reflux temperature for 4h and after the addition of sodium borohydride (1.6 equiv) it was stirred at reflux temperature for other 2 h. Yield 96%; mp 173-175 °C; silica gel TLC R_f 0.08 (TFA/MeOH/DCM 3/5/92% *v/v*). δH (400 MHz, DMSO-d6): 7.76 (d, J = 8.1 Hz, 2H, Ar-*H*), 7.42 (m, 7H, Ar-*H*), 7.32 (s,

2H, exchange with D$_2$O, SO$_2$NH_2, overlap with signal at 7.42), 4.04 (s, 2H, CH_2), 3.07 (m, 2H, CH_2), 2.97 (m, 2H, CH_2). δC (100 MHz, DMSO-d6): 145.87, 142.74, 141.80, 129.99, 129.05, 128.86, 127.46, 126.55, 53.77, 50.91, 36.50. ESI-MS (m/z) [M+H]$^+$: calculated for C$_{15}$H$_{19}$N$_2$O$_2$S 291.1; found 291.2.

4-(2-((4-Nitrobenzyl)amino)ethyl)benzenesulfonamide (A2). Compound **A2** was obtained according the general procedure 1 earlier reported using 4-(2-aminoethyl)benzenesulfonamide (9.99 mmol, 1.0 equiv) and 4-nitrobenzaldehyde (1.1 equiv) in dry MeOH (40 mL). The reaction mixture was initially stirred at reflux temperature for 1h and after the addition of sodium borohydride (1.6 equiv) it was stirred at reflux temperature for 3 h. Yield 94%; mp 166-168 °C; silica gel TLC R_f 0.17 (TFA/MeOH/DCM 3/5/92% v/v). δH (400 MHz, DMSO-d6): 8.16 (d, J = 8.6 Hz, 2H, Ar-H), 7.72 (d, J = 8.2 Hz, 2H, Ar-H), 7.57 (d, J = 8.6 Hz, 2H, Ar-H), 7.39 (d, J = 8.2 Hz, 2H, Ar-H), 7.26 (s, 2H, exchange with D$_2$O, SO$_2$NH_2), 3.84 (s, 2H, CH_2), 2.82 (m, 2H, CH_2), 2.73 (m, 2H, CH_2), 2.40 (bs, 1H, exchange with D$_2$O, NH). δC (100 MHz, DMSO-d6): 150.49, 147.34, 145.84, 142.88, 130.12, 129.84, 126.69, 124.29, 53.05, 51.00, 36.63. ESI-MS (m/z) [M+H]$^+$: calculated for C$_{15}$H$_{18}$N$_3$O$_4$S 336.1; found 336.1.

4-(2-((4-Fluorobenzyl)amino)ethyl)benzenesulfonamide (A3). Compound **A3** was obtained according the general procedure 1 earlier reported using 4-(2-aminoethyl)benzenesulfonamide (9.99 mmol, 1.0 equiv) and 4-fluorobenzaldehyde (1.1 equiv) in dry MeOH (40 mL). The reaction mixture was initially stirred at reflux temperature for 2 h and after the addition of sodium borohydride (1.6 equiv) it was stirred at reflux temperature for other 2 h. Yield 95%; mp 145-147 °C; silica gel TLC R_f 0.21 (TFA/MeOH/DCM 3/5/92% v/v). δH (400 MHz, DMSO-d6): 7.73 (d, J = 8.2 Hz, 2H, Ar-H), 7.38 (m, 4H, Ar-H), 7.28 (s, 2H, exchange with D$_2$O, SO$_2$NH_2, overlap with signal at 7.38), 7.12 (t, J = 8.8 Hz, 2H, Ar-H), 3.73 (s, 2H, CH_2), 2.79 (m, 4H, 2 x CH_2). δF (376 MHz, DMSO-d6): -116.18. δC (100 MHz, DMSO-d6): 145.61, 142.94, 131.06, 130.98, 130.10, 126.73, 115.96, 115.75, 52.74, 50.62, 36.18. ESI-MS (m/z) [M+H]$^+$: calculated for C$_{15}$H$_{18}$FN$_2$O$_2$S 309.1; found 309.1.

4-(2-((Naphthalen-2-ylmethyl)amino)ethyl)benzenesulfonamide (A4). Compound **A4** was obtained according the general procedure 1 earlier reported using 4-(2-aminoethyl)benzenesulfonamide (9.99 mmol, 1.0 equiv) and 2-naphthaldehyde (1.1 equiv) in dry MeOH (40 mL). The reaction mixture was initially stirred at reflux temperature for 0.5 h and after the addition of sodium borohydride (1.6 equiv) it was stirred at reflux temperature for other 0.5 h. Yield 86%; mp 186-188 °C; silica gel TLC R_f 0.04 (TFA/MeOH/DCM 3/5/92% v/v). δH (400 MHz, DMSO-d6): 7.85 (m, 2H, Ar-*H*), 7.76 (s, 1H, Ar-*H*), 7.70 (d, J = 8.2 Hz, 2H, Ar-*H*), 7.48 (m, 4H, Ar-*H*), 7.38 (d, J = 8.1 Hz, 2H, Ar-*H*), 7.19 (s, 2H, exchange with D_2O, SO_2NH_2), 3.87 (s, 2H, C*H*$_2$), 2.79 (m, 4H, 2 x C*H*$_2$), 2.21 (bs, 1H, exchange with D_2O, N*H*). δC (100 MHz, DMSO-d6): 145.85, 142.88, 142.83, 139.55, 133.94, 133.08, 130.05, 128.57, 128.48, 127.73, 126.97, 126.88, 126.58, 126.40, 53.85, 51.01, 36.57. ESI-MS (m/z) [M+H]$^+$: calculated for $C_{19}H_{21}N_2O_2S$ 341.1; found 341.1.

4-(2-((Furan-2-ylmethyl)amino)ethyl)benzenesulfonamide (A5). Compound **A5** was obtained according the general procedure 1 earlier reported using 4-(2-aminoethyl)benzenesulfonamide (9.99 mmol, 1.0 equiv) and 2-furaldehyde (1.1 equiv) in dry MeOH (40 mL). The reaction mixture was initially stirred at reflux temperature for 4 h and after the addition of sodium borohydride (1.6 equiv) it was stirred at reflux temperature for other 3h. Yield 88%; mp 133-135 °C; silica gel TLC R_f 0.19 (TFA/MeOH/DCM 3/5/92% v/v). δH (400 MHz, DMSO-d6): 7.71 (d, J = 8.3 Hz, 2H, Ar-*H*), 7.56-7.49 (m, 1H, Ar-*H*), 7.37 (d, J = 8.3 Hz, 2H, Ar-*H*), 7.24 (s, 2H, exchange with D_2O, SO_2NH_2), 6.35 (dd, J = 3.1, 1.9 Hz, 1H, Ar-*H*), 6.20 (d, J = 3.1 Hz, 1H, Ar-*H*), 3.67 (s, 2H, C*H*$_2$), 2.75 (m, 4H, 2 x C*H*$_2$), 2.04 (bs, 1H, exchange with D_2O, N*H*). δC (100 MHz, DMSO-d6): 155.36, 145.73, 142.62, 129.93, 126.49, 126.48, 111.13, 107.47, 50.67, 46.21, 36.29. ESI-MS (m/z) [M+H]$^+$: calculated for $C_{13}H_{17}N_2O_3S$ 281.1; found 281.1.

4-(2-((2-Cyanoethyl)amino)ethyl)benzenesulfonamide (A6). Compound **A6** was obtained according the general procedure 2 earlier reported using 4-(2-aminoethyl)benzenesulfonamide (9.99 mmol, 1.0 equiv) and 3-chloropropionitrile (1.1 equiv) in dry DMF (5 mL) and a rt stirring of 0.5 h. Yield 85%; mp 85-87 °C; silica gel TLC

R_f 0.15 (TFA/MeOH/DCM 3/5/92% v/v). δH (400 MHz, DMSO-d6): 7.72 (d, J = 8.0 Hz, 2H, Ar-H), 7.41 (d, J = 8.0 Hz, 2H, Ar-H), 7.27 (s, 2H, exchange with D$_2$O, SO$_2$NH_2), 2.76 (m, 6H, 3 x CH_2), 2.57 (t, J = 6.6 Hz, 2H, CH_2). δC (100 MHz, DMSO-d6): 145.72, 142.88, 130.14, 126.68, 121.19, 50.83, 45.66, 36.59, 18.88. ESI-MS (m/z) [M+H]$^+$: calculated for C$_{11}$H$_{16}$N$_3$O$_2$S 254.1; found 254.0.

4-(2-(Phenethylamino)ethyl)benzenesulfonamide (A7). Compound **A7** was obtained according the general procedure 2 earlier reported using 4-(2-aminoethyl)benzenesulfonamide (9.99 mmol, 1.0 equiv) and (2-bromoethyl)benzene (1.1 equiv) in dry DMF (5 mL) and a 60°C stirring of 8h. Yield 73%; mp 213-215 °C; silica gel TLC R_f 0.02 (TFA/MeOH/DCM 3/5/92% v/v). δH (400 MHz, DMSO-d6): 7.78 (d, J = 8.2 Hz, 2H, Ar-H), 7.44 (d, J = 8.2 Hz, 2H, Ar-H), 7.34 (m, 4H, Ar-H), 7.26 (s, 2H, exchange with D$_2$O, SO$_2$NH_2, overlap with signal at 7.25), 7.25 (m, 1H, Ar-H), 2.89 (m, 8H, 4 x CH_2). δC (100 MHz, DMSO-d6): 145.71, 142.27, 141.02, 130.04, 129.47, 129.26, 126.88, 126.59, 51.35, 50.91, 36.29, 36.05. ESI-MS (m/z) [M+H]$^+$: calculated for C$_{16}$H$_{21}$N$_2$O$_2$S 305.1; found 305.1.

General Synthetic Procedure for preparation of Chloro-amides (A8-17). To a suspension of 4-(2-(arylalkyl)amino)ethyl)benzenesulfonamide **A1-7** (6.89 mmol, 1.0 equiv) and K$_2$CO$_3$ (1.2 equiv) in acetone (40 mL) cooled to 0°C, the appropriate chloroacylchloride (1.2 equiv) was added dropwise and the mixture was stirred for 0.5 h. The solvent was evaporated under *vacuum*, then slush (50 mL) was added and the basic suspension was neutralized with HCl 1M. The precipitate was collected by filtration and purified with flash chromatography (1% MeOH in DCM) to give compounds **A8-17**.

N-Benzyl-2-chloro-N-(4-sulfamoylphenethyl)acetamide (A8). Compound **A8** was obtained according the general procedure earlier reported using 4-(2-(benzylamino)ethyl)benzenesulfonamide **A1** and 2-chloroacetyl chloride (1.2 equiv). Yield 91%; mp 122-124 °C; silica gel TLC R_f 0.32 (TFA/MeOH/DCM 3/5/92% v/v). δH (400 MHz, DMSO-d6): 7.74 (t, J = 8.7 Hz, 2H, Ar-H), 7.35 (m, 7H, Ar-H), 7.27 (s, 2H, exchange with

D$_2$O, SO$_2$NH_2, overlap with signal at 7.35), 4.58 (s, 2H, CH_2), 4.42 (s, 1.2H, CH_2), 4.40 (s, 0.8H, CH_2), 3.46 (m, 2H, CH_2), 2.96 (m, 1H, CH_2), 2.82 (m, 1H, CH_2). δC (100 MHz, DMSO-d6): 167.23, 144.15, 143.63, 143.50, 143.28, 138.55, 137.89, 130.43, 130.15, 129.83, 129.55, 128.62, 128.23, 128.14, 126.89, 49.33, 49.08, 48.26, 43.19, 43.11, 34.80, 33.62. ESI-MS (m/z) [M+H]$^+$: calculated for C$_{17}$H$_{20}$ClN$_2$O$_3$S 367.1; found 367.0.

N-Benzyl-3-chloro-N-(4-sulfamoylphenethyl)propanamide (A9). Compound **A9** was obtained according the general procedure earlier reported using 4-(2-(benzylamino)ethyl)benzenesulfonamide **A1** and 3-chloropropionyl chloride (1.2 equiv). Yield 93 %; mp 151-153 °C; silica gel TLC R_f 0.36 (TFA/MeOH/DCM 3/5/92% v/v). δH (400 MHz, DMSO-d6): 7.73 (t, J = 7.2 Hz, 2H, Ar-H), 7.32 (m, 7H, Ar-H), 7.25 (s, 2H, exchange with D$_2$O, SO$_2$NH_2, overlap with signal at 7.32), 4.56 (s, 2H, CH_2), 3.79 (m, 2H, CH_2), 3.47 (m, 3H, 2 x CH_2), 2.86 (m, 3H, 2 x CH_2). δC (100 MHz, DMSO-d6): 170.61, 170.55, 144.41, 143.79, 143.39, 143.13, 138.89, 138.40, 130.43, 130.19, 129.82, 129.52, 128.65, 128.43, 128.16, 127.65, 126.89, 126.85, 51.60, 48.93, 48.76, 48.41, 41.94, 41.68, 36.60, 36.05, 34.93, 34.05. ESI-MS (m/z) [M+H]$^+$: calculated for C$_{18}$H$_{22}$ClN$_2$O$_3$S 381.1; found 381.0.

2-Chloro-N-(4-nitrobenzyl)-N-(4-sulfamoylphenethyl)acetamide (A10). Compound **A10** was obtained according the general procedure earlier reported using 4-(2-((4-nitrobenzyl)amino)ethyl)benzenesulfonamide **A2** and 2-chloroacetyl chloride (1.2 equiv). Yield 89 %; mp 204-206 °C; silica gel TLC R_f 0.28 (TFA/MeOH/DCM 3/5/92% v/v). δH (400 MHz, DMSO-d6): 8.20 (d, J = 8.7 Hz, 2H, Ar-H), 7.77 (m, 3H, Ar-H), 7.49 (m, 4H, Ar-H), 7.31 (s, (s, 2H, exchange with D$_2$O, SO$_2$NH_2), 4.76 (s, 0.6 H, CH_2), 4.71 (s, 1.4 H, CH_2), 4.47 (s, 1.4 H, CH_2), 4.38 (s, 0.6 H, CH_2), 3.55 (m, 2H, CH_2), 2.97 (m, 1.5H, CH_2), 2.84 (m, 0.5H, CH_2). δC (100 MHz, DMSO-d6): 166.50, 164.81, 146.66, 145.78, 144.58, 142.46, 142.41, 140.51, 131.32, 131.13, 129.42, 129.13, 128.40, 128.17, 125.99, 125.82, 123.81, 123.57, 50.32, 49.22, 48.96, 48.16, 47.53, 44.25, 42.06, 33.84. ESI-MS (m/z) [M+H]$^+$: calculated for C$_{17}$H$_{19}$ClN$_3$O$_5$S 412.1; found 412.0.

2-Chloro-N-(4-fluorobenzyl)-N-(4-sulfamoylphenethyl)acetamide **(A11).** Compound **A11** was obtained according the general procedure earlier reported using 4-(2-((4-fluorobenzyl)amino)ethyl)benzenesulfonamide **A3** and 2-chloroacetyl chloride (1.2 equiv). Yield 86 %; mp 167-169 °C; silica gel TLC R_f 0.30 (TFA/MeOH/DCM 3/5/92% *v/v*). δH (400 MHz, DMSO-d6): 7.74 (t, J = 8.6 Hz, 2H, Ar-*H*), 7.32 (m, 6H, Ar-*H*), 7.30 (s, 2H, exchange with D_2O, SO_2NH_2, overlap with signal at 7.32), 4.56 (s, 2H, C*H*$_2$), 4.41 (s, 2H, C*H*$_2$), 3.45 (m, 2H, C*H*$_2$), 2.95 (t, J = 7.4 Hz, 1.2H, C*H*$_2$), 2.78 (m, 0.8H, C*H*$_2$). δF (376 MHz, DMSO-d6): -114.96, -115.41. δC (100 MHz, DMSO-d6): 167.31, 143.60, 143.47, 142.79, 134.74, 130.74, 130.66, 130.44, 130.15, 129.80, 126.89, 116.68, 116.39, 116.18, 51.23, 49.32, 48.44, 48.10, 43.15, 43.07, 34.79, 33.57. ESI-MS (m/z) [M+H]$^+$: calculated for $C_{17}H_{19}ClFN_2O_3S$ 385.0; found 385.0.

2-Chloro-N-(naphthalen-2-ylmethyl)-N-(4-sulfamoylphenethyl)acetamide **(A12).** Compound **A12** was obtained according the general procedure earlier reported using 4-(2-((naphthalen-2-ylmethyl)amino)ethyl)benzenesulfonamide **A4** and 2-chloroacetyl chloride (1.2 equiv). Yield 54 %; mp 181-183 °C; silica gel TLC R_f 0.34 (TFA/MeOH/DCM 3/5/92% *v/v*). δH (400 MHz, DMSO-d6): 7.91 (m, 3H, Ar-*H*), 7.73 (m, 3H, Ar-*H*), 7.40 (m, 5H, Ar-*H*), 7.30 (s, 2H, exchange with D_2O, SO_2NH_2, overlap with signal at 7.40), 4.75 (s, 2H, C*H*$_2$), 4.47 (s, 1.2H, C*H*$_2$), 4.46 (s, 0.8H, C*H*$_2$), 3.52 (t, J = 7.5 Hz, 2H, C*H*$_2$), 3.01 (m, 2H, C*H*$_2$), 2.84 (m, 2H, C*H*$_2$). δC (100 MHz, DMSO-d6): 167.33, 144.15, 143.64, 143.50, 143.29, 136.15, 135.55, 134.99, 134.01, 133.95, 133.44, 133.32, 130.44, 130.17, 129.50, 129.24, 128.80, 128.62, 127.49, 127.35, 127.09, 126.98, 126.87, 126.49, 126.41, 52.08, 49.33, 49.27, 48.35, 43.29, 43.21, 34.83, 33.67. ESI-MS (m/z) [M+H]$^+$: calculated for $C_{21}H_{22}ClN_2O_3S$ 417.1; found 417.0.

2-Chloro-N-(furan-2-ylmethyl)-N-(4-sulfamoylphenethyl)acetamide (A13). Compound **A13** was obtained according the general procedure earlier reported using 4-(2-((furan-2-ylmethyl)amino)ethyl)benzenesulfonamide **A5** and 2-chloroacetyl chloride (1.2 equiv). Yield 75 %; mp 141-143 °C; silica gel TLC R_f 0.27 (TFA/MeOH/DCM 3/5/92% *v/v*). δH (400 MHz, DMSO-d6): 7.74 (t, J = 7.6 Hz, 2H, Ar-*H*), 7.67 (s, 0.5H, Ar), 7.61 (s, 0.5H, Ar-

H), 7.44 (d, *J* = 8.0 Hz, 1H, Ar-*H*), 7.37 (d, *J* = 8.1 Hz, 1H, Ar-*H*), 7.30 (s, 2H, exchange with D$_2$O, SO$_2$N*H$_2$*)$_,$ 6.45 (m, 1.5H, Ar-*H*), 6.38 (m, 0.5H, Ar-*H*), 4.57 (s, 2H, C*H$_2$*), 4.51 (s, 1H, C*H$_2$*), 4.38 (s, 1H, C*H$_2$*), 3.48 (dd, *J* = 14.0, 6.3 Hz, 2H, C*H$_2$*), 2.90 (t, *J* = 7.7 Hz, 1H, C*H$_2$*), 2.75 (m, 1H, C*H$_2$*). δC (100 MHz, DMSO-d6): 166.74, 166.66, 151.48, 151.18, 151.07, 144.24, 144.11, 143.97, 143.86, 143.66, 143.50, 143.36, 143.13, 130.33, 130.05, 126.78, 126.74, 111.62, 111.54, 110.64, 109.83, 109.70, 49.13, 48.21, 45.07, 43.19, 43.09, 42.37, 34.57, 33.47. ESI-MS (m/z) [M+H]$^+$: calculated for C$_{15}$H$_{18}$ClN$_2$O$_4$S 357.0; found 357.0.

3-Chloro-N-(furan-2-ylmethyl)-N-(4-sulfamoylphenethyl)propanamide (A14). Compound **A14** was obtained according the general procedure earlier reported using 4-(2-((furan-2-ylmethyl)amino)ethyl)benzenesulfonamide **A5** and 3-chloropropionyl chloride (1.2 equiv). Yield 71 %; mp 113-115 °C; silica gel TLC *R$_f$* 0.31 (TFA/MeOH/DCM 3/5/92% *v/v*). δH (400 MHz, DMSO-d6): 7.74 (m, 2H, Ar-*H*), 7.64 (s, 0.5H, Ar-*H*), 7.60 (s, 0.5H, Ar-*H*), 7.40 (m, 2H, Ar-*H*), 7.29 (s, 2H, exchange with D$_2$O, SO$_2$N*H$_2$*), 6.42 (m, 1.5H, Ar-*H*), 6.34 (s, 0.5H, Ar-*H*) 4.55 (s, 1H, C*H$_2$*), 4.54 (s, 1H, C*H$_2$*), 3.81 (t, *J* = 6.5 Hz, 1H, C*H$_2$*), 3.76 (t, *J* = 6.4 Hz, 1H, C*H$_2$*), 3.48 (m, 2H, C*H$_2$*), 2.97 (t, *J* = 6.5 Hz, 1H, C*H$_2$*), 2.79 (m, 3H, 2 x C*H$_2$*). δC (100 MHz, DMSO-d6): 170.08, 169.94, 151.94, 151.67, 144.21, 144.03, 143.61, 143.50, 143.33, 143.07, 130.29, 130.04, 126.77, 126.73, 111.54, 111.52, 109.47, 109.28, 48.75, 47.96, 44.98, 41.87, 41.59, 41.43, 36.49, 35.98, 34.73, 33.82. ESI-MS (m/z) [M+H]$^+$: calculated for C$_{16}$H$_{20}$ClN$_2$O$_4$S 371.1; found 371.1.

2-Chloro-N-(2-cyanoethyl)-N-(4-sulfamoylphenethyl)acetamide (A15). Compound **A15** was obtained according the general procedure earlier reported using 4-(2-((2-cyanoethyl)amino)ethyl)benzenesulfonamide **A6** and 2-chloroacetyl chloride (1.2 equiv). Yield 71 %; mp 199-201 °C; silica gel TLC *R$_f$* 0.04 (TFA/MeOH/DCM 3/5/92% *v/v*). δH (400 MHz, DMSO-d6): 7.77 (d, *J* = 7.4 Hz, 2H, Ar-*H*), 7.51 (d, 7.3 Hz, 2H, Ar-*H*), 7.29 (s, 2H, exchange with D$_2$O, SO$_2$N*H$_2$*), 4.46 (s, 1H, C*H$_2$*), 4.36 (s, 1H, C*H$_2$*), 3.59 (s, 4H, 2 x C*H$_2$*), 2.86 (m, 4H, 2 x C*H$_2$*). δC (100 MHz, DMSO-d6): 167.37, 167.13, 144.04, 143.50, 143.24, 130.54, 130.29, 126.85, 124.09, 120.03, 95.68, 49.92, 47.96, 44.16, 43.20, 43.02,

42.82, 34.99, 33.62, 18.01, 16.44. ESI-MS (m/z) [M+H]$^+$: calculated for C$_{13}$H$_{17}$ClN$_3$O$_3$S 330.0; found 330.0.

2-Chloro-N-phenethyl-N-(4-sulfamoylphenethyl)acetamide (A16). Compound **A16** was obtained according the general procedure earlier reported using 4-(2-(phenethylamino)ethyl)benzenesulfonamide **A7** and 2-chloroacetyl chloride (1.2 equiv). Yield 92 %; mp 178-180 °C; silica gel TLC R_f 0.29 (TFA/MeOH/DCM 3/5/92% v/v). δH (400 MHz, DMSO-d6): 7.75 (d, J = 7.1 Hz, 2H, Ar-*H*), 7.44 (dd, J = 15.3, 8.2 Hz, 2H, Ar-*H*), 7,29 (s, 2H, exchange with D$_2$O, SO$_2$N*H*$_2$, overlap with signal at 7.26), 7.26 (m, 5H, Ar-*H*), 4.29 (s, 0.9H, C*H*$_2$), 4.18 (s, 1.1H, C*H*$_2$), 3.47 (m, 4H 0.9H, C*H*$_2$), 2.92 (m, 1H, C*H*$_2$), 2.85 (t, J = 7.5 Hz, 2H, C*H*$_2$), 2.77 (m, 1H, C*H*$_2$). δC (100 MHz, DMSO-d6): 167.49, 144.74, 144.06, 143.60, 143.25, 140.38, 139.73, 130.85, 130.66, 130.32, 130.12, 129.92, 129.81, 127.94, 127.67, 127.18, 127.12, 50.73, 50.37, 48.96, 48.41, 43.08, 43.05, 35.57, 35.33, 34.26, 33.98. ESI-MS (m/z) [M+H]$^+$: calculated for C$_{18}$H$_{22}$ClN$_2$O$_3$S 381.1; found 381.0.

3-Chloro-N-phenethyl-N-(4-sulfamoylphenethyl)propanamide (A17). Compound **A17** was obtained according the general procedure earlier reported using 4-(2-(phenethylamino)ethyl)benzenesulfonamide **A7** and 3-chloropropionyl chloride (1.2 equiv). Yield 54 %; mp 181-183 °C; silica gel TLC R_f 0.34 (TFA/MeOH/DCM 3/5/92% v/v). δH (400 MHz, DMSO-d6): 7.74 (d, J = 8.1 Hz, 2H, Ar-*H*), 7.43 (dd, J = 12.1, 8.2 Hz, 2H, Ar-*H*), 7.30 (s, 2H, exchange with D$_2$O, SO$_2$N*H*$_2$, overlap with signal at 7.24), 7.24 (m, 5H, Ar-*H*), 3.75 (t, J = 6.4 Hz, 1H, C*H*$_2$), 3.70 (t, J = 6.4 Hz, 1H, C*H*$_2$), 3.46 (s, 4H, 2 x C*H*$_2$), 2.85 (m, 5H, 3 x C*H*$_2$), 2.64 (t, J = 6.4 Hz, 1H, C*H*$_2$). δC (100 MHz, DMSO-d6): 169.88, 169.79, 144.48, 143.65, 143.32, 143.01, 140.18, 139.57, 130.32, 130.08, 129.88, 129.64, 129.35, 129.28, 127.32, 127.09, 126.66, 49.89, 49.53, 48.28, 47.81, 41.71, 36.00, 35.43, 35.17, 34.28, 33.98. ESI-MS (m/z) [M+H]$^+$: calculated for C$_{19}$H$_{24}$ClN$_2$O$_3$S 395.1; found 395.1.

Synthesis of 3-(phenethylamino)propanenitrile. To a solution of phenethylamine (16,5 mmol, 1.0 equiv) in dry DMF (5 mL), triethylamine (1.2 equiv) and 3-chloropropionitrile (1.1 equiv) were added and the mixture was stirred at room temperature for 0.5 h. The

reaction was quenched by addition of water (20 mL) and extracted with EtOAc (30 mL x 3). The organic layer was collected, washed with brine (40 mL x 3), dried over Na_2SO_4, filtered-off and evaporated under *vacuum* to give 3-(phenethylamino)propanenitrile as an orange oil. Yield 92 %; silica gel TLC R_f 0.42 (TFA/MeOH/DCM 1.5/1.5/97% *v/v*). 7.23 (m, 5H, Ar-*H*), 2.85 (m, 6H, 3 x C*H$_2$*), 2.57 (t, J = 6.6 Hz, 2H, C*H$_2$*), 1.89 (bs, 1H, exchange with D_2O, N*H*). δC (100 MHz, DMSO-d6): 141.30, 129.64, 129.28, 126.90, 120.99, 51.41, 45.80, 37.04, 18.99. ESI-MS (m/z) [M+H]$^+$: calculated for $C_{11}H_{15}N_2$ 175.1; found 175.0.

General synthetic procedure for preparation of three-tail compounds A18-39. To a solution of chloroalkylamide **A8-17** (0.69 mmol, 1.0 equiv) and triethylamine (1.2 equiv) in MeCN dry (5 mL), the proper secondary amine (1.1 equiv) was added and the mixture was heated at reflux temperature for 4-24h under stirring. The solvent was evaporated under vacuum and the crude was treated with $NaHCO_3$ saturated solution (5 mL) and extracted with EtOAc (10 mL x 3). The organic layer was dried over Na_2SO_4, filtered and evaporated under vacuum. The obtained residue was purified by flash chromatography (1% MeOH in DCM) to give the compounds **A18-39** as an oil or powder.

N-Benzyl-2-(diethylamino)-N-(4-sulfamoylphenethyl)acetamide (A18). Compound **A18** was obtained according the general procedure earlier reported using N-benzyl-2-chloro-N-(4-sulfamoylphenethyl)acetamide **A8** and diethylamine (1.1 equiv) in dry MeCN (5 mL) and stirring for 4h at reflux temperature. The sticky residue was purified by flash chromatography (1% MeOH in DCM) to give **A18** as a powder. Yield 71 %; mp 93-95 °C; silica gel TLC R_f 0.12 (TFA/MeOH/DCM 3/5/92% *v/v*). δH (400 MHz, DMSO-d6): 7.74 (t, J = 7.5 Hz, 2H, Ar-*H*), 7.31 (m, 7H, Ar-*H*), 7.27 (s, 2H, exchange with D_2O, SO_2NH_2), 4.70 (s, 0.9H, C*H$_2$*), 4.56 (s, 1.1H, C*H$_2$*), 3.57 (m, 1H, C*H$_2$*), 3.44 (m, 1H, C*H$_2$*), 3.16 (s, 1H, C*H$_2$*), 3.13 (s, 1H, C*H$_2$*), 2.94 (m, 1H, C*H$_2$*), 2.78 (m, 1H, C*H$_2$*), 2.46 (m, 4H, 2 x C*H$_2$*), 0.90 (m, 6H, 2 x C*H$_3$*). δC (100 MHz, DMSO-d6): 170.22, 143.34, 143.10, 142.34, 142.13, 138.18, 137.82, 129.25, 129.09, 128.69, 128.42, 127.54, 127.19, 127.00, 126.77, 125.80, 125.72, 56.33, 56.25, 50.03, 47.71, 47.15, 46.76, 46.72, 46.42, 33.89, 32.72, 11.38. ESI-HRMS (m/z) [M+H]$^+$: calculated for $C_{21}H_{30}N_3O_3S$ 404.2007; found 404.2012.

N-Benzyl-2-(benzyl(ethyl)amino)-N-(4-sulfamoylphenethyl)acetamide (A19). Compound **A19** was obtained according the general procedure earlier reported using N-benzyl-2-chloro-N-(4-sulfamoylphenethyl)acetamide **A8** and N-ethylbenzylamine (1.1 equiv) in dry MeCN (5 mL) and stirring for 16h at reflux temperature. The sticky residue was purified by flash chromatography (1% MeOH in DCM) to give **A19** as an oil. Yield 65 %; silica gel TLC R_f 0.27 (TFA/MeOH/DCM 3/5/92% v/v). δH (400 MHz, DMSO-d6): 7.75 (t, J = 8.5 Hz, 2H, Ar-H), 7.37 (m, 11H, Ar-H), 7.28 (s, 2H, exchange with D$_2$O, SO$_2$NH_2, overlap with signal at 7.37), 7.13 (d, J = 7.2 Hz, 1H, Ar-H), 4.62 (s, 1H, CH_2), 4.60 (s, 1H, CH_2), 3.64 (s, 1H, CH_2), 3.60 (s, 1H, CH_2), 3.55 (m, 1H, CH_2), 3.45 (m, 1H, CH_2), 3.25 (s, 1H, CH_2), 3.15 (s, 1H, CH_2), 2.84 (m, 2H, CH_2), 247 (m, 2H, CH_2), 0.98 (m, 3H, CH_3). δC (100 MHz, DMSO-d6): 171.12, 144.35, 143.83, 143.39, 143.22, 139.72, 139.03, 138.56, 130.40, 130.26, 130.12, 129.67, 129.42, 129.25, 129.22, 128.62, 128.20, 128.09, 127.69, 126.80, 126.78, 58.40, 56.64, 55.97, 51.10, 48.37, 48.12, 47.70, 34.76, 33.82, 16.77, 13.76, 12.53. ESI-HRMS (m/z) [M+H]$^+$: calculated for C$_{26}$H$_{32}$N$_3$O$_3$S 466.2164; found 466.2169.

N-Benzyl-2-(dibenzylamino)-N-(4-sulfamoylphenethyl)acetamide (A20). Compound **A20** was obtained according the general procedure earlier reported using N-benzyl-2-chloro-N-(4-sulfamoylphenethyl)acetamide **A8** and dibenzylamine (1.1 equiv) in dry MeCN (5 mL) and stirring for 15h at reflux temperature. The sticky residue was purified by flash chromatography (MeOH 1%/DCM) to give **A20** as a white powder. Yield 68 %; mp 98-100 °C; silica gel TLC R_f 0.38 (TFA/MeOH/DCM 3/5/92% v/v). δH (400 MHz, DMSO-d6): 7.67 (t, J = 8.1 Hz, 2H, Ar-H), 7.28 (m, 15H, Ar-H), 7.24 (s, 2H, exchange with D$_2$O, SO$_2$NH_2, overlap with signal at 7.28), 6.94 (m, 2H, Ar-H), 4.54 (s, 1.1H, CH_2), 4.43 (s, 0.9H, CH_2), 3.68 (s, 2.3H, 2 x CH_2), 3.59 (s, 1.7H, 2 x CH_2), 3.41 (m, 2H, CH_2), 3.23 (s, 1H, CH_2), 3.08 (s, 1H, CH_2), 2.79 (t, J = 7.3 Hz, 0.9H, CH_2), 2.61 (t, J = 6.8 Hz, 1.1H, CH_2). δC (100 MHz, DMSO-d6): 170.96, 170.84, 144.38, 143.48, 143.28, 143.16, 139.69, 139.61, 139.04, 138.39, 130.13, 129.98, 129.91, 129.57, 129.44, 129.36, 129.29, 128.64, 128.22, 128.10,

127.45, 126.79, 126.71, 58.48, 58.42, 55.73, 55.42, 50.99, 48.13, 47.99, 34.58, 33.91. ESI-HRMS (m/z) [M+H]$^+$: calculated for C$_{31}$H$_{34}$N$_3$O$_3$S 528.2321; found 466. 528.2317.

N-Benzyl-2-(dipentylamino)-N-(4-sulfamoylphenethyl)acetamide (A21). Compound **A21** was obtained according the general procedure earlier reported using N-benzyl-2-chloro-N-(4-sulfamoylphenethyl)acetamide **A8** and dipentylamine (1.1 equiv) in dry MeCN (5 mL) and stirring for 16h at reflux temperature. The sticky residue was purified by flash chromatography (1% MeOH in DCM) to give **A21** as an oil. Yield 70 %; silica gel TLC R_f 0.14 (TFA/MeOH/DCM 3/5/92% v/v). δH (400 MHz, DMSO-d6): 7.73 (t, *J* = 7.8 Hz, 2H, Ar-*H*), 7.34 (m, 7H, Ar-*H*), 7.28 (s, 2H, exchange with D$_2$O, SO$_2$N*H$_2$*, overlap with signal at 7.34), 4.73 (s, 0.7H, C*H$_2$*), 4.58 (s, 1.3H, C*H$_2$*), 3.61 (m, 0.9H, C*H$_2$*), 3.46 (m, 1.1H, C*H$_2$*), 3.15 (m, 2H, C*H$_2$*), 2.95 (m, 1.1H, C*H$_2$*), 2.81(m, 0.9H, C*H$_2$*), 2.43 (m, 4H, 2x C*H$_2$*), 1.21 (m, 12H, 6 x C*H$_2$*), 0.81 (m, 6H, 2 x C*H$_3$*). δC (100 MHz, DMSO-d6): 167.34, 144.32, 144.01, 143.73, 143.45, 143.22, 138.70, 130.29, 130.08, 129.73, 129.40, 128.79, 128.62, 128.22, 128.14, 127.68, 126.82, 54.91, 54.85, 51.87, 51.13, 49.31, 48.49, 48.24, 47.90, 43.11, 34.74, 33.88, 30.18, 22.95, 22.75, 16.34, 15.05, 14.73. ESI-HRMS (m/z) [M+H]$^+$: calculated for C$_{27}$H$_{42}$N$_3$O$_3$S 488.2947; found 488.2942.

N-Benzyl-2-(dihexylamino)-N-(4-sulfamoylphenethyl)acetamide (A22). Compound **A22** was obtained according the general procedure earlier reported using N-benzyl-2-chloro-N-(4-sulfamoylphenethyl)acetamide **A8** and dihexylamine (1.1 equiv) in dry MeCN (5 mL) and stirring for 16h at reflux temperature. The sticky residue was purified by flash chromatography (1% MeOH in DCM) to give **A22** as an oil. Yield 72 %; silica gel TLC R_f 0.34 (TFA/MeOH/DCM 3/5/92% v/v). δH (400 MHz, DMSO-d6): 7.73 (t, *J* = 7.5 Hz, 2H, Ar-*H*), 7.33 (m, 7H, Ar-*H*), 7.26 (s, 2H, exchange with D$_2$O, SO$_2$N*H$_2$*, overlap with signal at 7.33), 4.73 (s, 0.9H, C*H$_2$*), 4.56 (s, 1.1H, C*H$_2$*), 3.62 (m, 1H, C*H$_2$*), 3.42 (m, 1H, C*H$_2$*), 3.14 (m, 1H, C*H$_2$*), 2.94 (m, 1.1H, C*H$_2$*), 2.82 (m, 0.9H, C*H$_2$*), 2.41 (m, 4H, 2x C*H$_2$*), 1.26 (m, 16H, 8 x C*H$_2$*), 0.83 (m, 6H, 2 x C*H$_3$*). δC (100 MHz, DMSO-d6): 170.65, 170.49, 143.73, 143.43, 142.85, 142.63, 138.61, 138.23, 129.62, 129.41, 129.07, 128.74, 128.18, 127.58, 127.46, 127.04, 126.21, 65.33, 58.19, 57.91, 54.32, 54.21, 50.55, 47.89, 47.69, 47.35, 47.31,

34.32, 33.32, 31.63, 31.17, 27.03, 26.99, 26.80, 26.75, 26.11, 26.00, 22.52, 22.32, 15.65, 14.32, 14.27. ESI-HRMS (m/z) [M+H]$^+$: calculated for $C_{29}H_{46}N_3O_3S$ 516.3260; found 516.3264.

N-Benzyl-2-(dioctylamino)-N-(4-sulfamoylphenethyl)acetamide (A23). Compound **A23** was obtained according the general procedure earlier reported using N-benzyl-2-chloro-N-(4-sulfamoyl-phenethyl)acetamide **A8** and dioctylamine (1.1 equiv) in dry MeCN (5 mL) and stirring for 16h at reflux temperature. The sticky residue was purified by flash chromatography (MeOH 1%/DCM) to give **A23** as a powder. Yield 67 %; mp 62-64 °C; silica gel TLC R_f 0.16 (TFA/MeOH/DCM 3/5/92% *v/v*). δH (400 MHz, DMSO-d6): 7.72 (t, *J* = 7.5 Hz, 2H, Ar-*H*), 7.32 (m, 7H, Ar-*H*), 7.27 (s, 2H, exchange with D$_2$O, SO$_2$N*H*$_2$, overlap with signal at 7.32), 4.74 (s, 0.9H, C*H*$_2$), 4.56 (s, 1.1H, C*H*$_2$), 3.61 (m, 1H, C*H*$_2$), 3.38 (m, 1H, C*H*$_2$), 3.14 (m, 1H, C*H*$_2$), 2.95 (m, 1.1H, C*H*$_2$), 2.81 (m, 0.9H, C*H*$_2$), 2.37 (m, 4H, 2x C*H*$_2$), 1.28 (m, 24H, 12 x C*H*$_2$), 0.83 (m, *J* = 6.2 Hz, 6H, 2 x C*H*$_3$). δC (100 MHz, DMSO-d6): 170.23, 170.10, 143.27, 143.01, 142.38, 142.17, 138.18, 137.82, 129.20, 128.99, 128.63, 128.31, 127.74, 127.14, 127.01, 126.60, 125.76, 64.93, 57.81, 57.59, 53.78, 53.70, 50.04, 47.41, 47.14, 46.88, 33.84, 32.86, 31.27, 31.23, 28.91, 28.70, 28.68, 26.93, 26.88, 26.42, 26.35, 22.09, 15.18, 13.94. ESI-HRMS (m/z) [M+H]$^+$: calculated for $C_{33}H_{54}N_3O_3S$ 572.3886; found 572.3881.

N-Benzyl-3-(diethylamino)-N-(4-sulfamoylphenethyl)propanamide (A24). Compound **A24** was obtained according the general procedure earlier reported using N-benzyl-3-chloro-N-(4-sulfamoylphenethyl)propanamide **A9** and diethylamine (1.1 equiv) in dry MeCN (5 mL) and stirring for 16h at reflux temperature. The sticky residue was purified by flash chromatography (1% MeOH in DCM) to give **A24** as an oil. Yield 72 %; silica gel TLC R_f 0.04 (TFA/MeOH/DCM 3/5/92% *v/v*). δH (400 MHz, DMSO-d6): 7.74 (t, *J* = 7.8 Hz, 2H, Ar-*H*), 7.33 (m, 7H, Ar-*H*), 7.30 (s, 2H, exchange with D$_2$O, SO$_2$N*H*$_2$, overlap with signal at 7.33), 4.58 (s, 0.9H, C*H*$_2$), 4.56 (s, 1.1H, C*H*$_2$), 3.49 (t, *J* = 7.4 Hz, 2H, C*H*$_2$), 3,38 (m, 2H, C*H*$_2$), 2.92 (t, *J* = 7.3 Hz, 1,1H, C*H*$_2$), 2.85 (m, 0.9H, C*H*$_2$), 2.72 (m, 2H, C*H*$_2$), 2.45 (m, 4H, 2 x C*H*$_2$), 0.96 (m, 6H, 2 x C*H*$_3$). δC (100 MHz, DMSO-d6): 172.42, 172.16, 144.45, 143.90,

143.42, 143.17, 139.17, 138.88, 130.37, 130.15, 129.76, 129.43, 128.68, 128.28, 128.02, 127.57, 126.84, 126.80, 55.97, 51.78, 49.67, 49.40, 49.00, 48.40, 48.29, 47.39, 47.35, 34.96, 34.30, 34.11, 30.56, 12.48. ESI-HRMS (m/z) [M+H]$^+$: calculated for C$_{22}$H$_{32}$N$_3$O$_3$S 418.2164; found 418.2170.

N-Benzyl-3-(benzyl(ethyl)amino)-N-(4-sulfamoylphenethyl)propanamide (A25). Compound **A25** was obtained according the general procedure earlier reported using N-benzyl-3-chloro-N-(4-sulfamoylphenethyl)propanamide **A9** and N-ethylbenzylamine (1.1 equiv) in dry MeCN (5 mL) and stirring for 20h at reflux temperature. The sticky residue was purified by flash chromatography (1% MeOH in DCM) to give **A25** as a powder. Yield 69 %; mp 77-79 °C; silica gel TLC R_f 0.12 (TFA/MeOH/DCM 3/5/92% v/v). δH (400 MHz, DMSO-d6): 7.73 (t, J = 7.8 Hz, 2H, Ar-*H*), 7.35 (m, 12H, Ar-*H*), 7.33 (s, 2H, exchange with D$_2$O, SO$_2$N*H*$_2$, overlap with signal at 7.35), 4.53 (s, 2H, C*H*$_2$), 4.11 (s, 1H, C*H*$_2$), 3.53 (m, 3H, 2 x C*H*$_2$), 2.86 (m, 3H, 2 x C*H*$_2$), 2.67 (m, 1H, C*H*$_2$), 2.39 (m, 2H, C*H*$_2$), 1.21 (t, J = 7.2 Hz, 2H, C*H*$_2$), 0.95 (m, 3H, 1 x C*H*$_3$). δC (100 MHz, DMSO-d6): 172.27, 171.59, 144.43, 143.82, 143.43, 143.17, 139.16, 138.99, 138.81, 133.37, 130.99, 130.38, 130.12, 129.86, 129.76, 129.68, 129.45, 129.25, 128.71, 128.31, 128.05, 127.63, 126.83, 126.82, 58.05, 51.74, 50.52, 48.99, 48.42, 48.24, 47.94, 47.76, 42.70, 34.95, 34.09, 11.96. ESI-HRMS (m/z) [M+H]$^+$: calculated for C$_{27}$H$_{34}$N$_3$O$_3$S 480.2321; found 480.2315.

N-Benzyl-3-(dibenzylamino)-N-(4-sulfamoylphenethyl)propanamide (A26). Compound **A26** was obtained according the general procedure earlier reported using N-benzyl-3-chloro-N-(4-sulfamoylphenethyl)propanamide **A9** and dibenzylamine (1.1 equiv) in dry MeCN (5 mL) and stirring for 22h at reflux temperature. The sticky residue was purified by flash chromatography (1% MeOH in DCM) to give **A26** as an oil. Yield 64 %; silica gel TLC R_f 0.32 (TFA/MeOH/DCM 3/5/92% v/v). δH (400 MHz, DMSO-d6): 7.67 (m, 2H, Ar-*H*), 7.30 (s, 2H, exchange with D$_2$O, SO$_2$N*H*$_2$, overlap with signal at 7.29), 7.29 (m, 15H, Ar-*H*), 6.93 (m, 2H, Ar-*H*), 4.53 (s, 1.1H, C*H*$_2$), 4.41 (s, 0.9H, C*H*$_2$), 3.67 (s, 0.9H, C*H*$_2$), 3.59 (s, 1.1H, C*H*$_2$), 3.45 (m, 6H, 3 x C*H*$_2$), 3.23 (s, 0.9H, C*H*$_2$), 3.08 (s, 1.1H, C*H*$_2$), 2.77 (m, 1H, C*H*$_2$), 2.60 (t, J = 7.1 Hz, 1H, C*H*$_2$). δC (100 MHz, DMSO-d6): 170.99, 170.87, 144.38, 143.48,

143.28, 143.17, 139.68, 139.61, 139.02, 138.36, 130.53, 130.21, 130.11, 129.97, 129.90, 129.55, 129.42, 129.34, 129.28, 128.64, 128.20, 128.09, 127.46, 126.79, 126.71, 58.50, 58.45, 55.73, 55.45, 51.03, 49.65, 48.15, 48.05, 47.94, 34.60, 33.91, 22.08. ESI-HRMS (m/z) [M+H]$^+$: calculated for $C_{32}H_{36}N_3O_3S$ 542.2477; found 542.2473.

N-Benzyl-3-(dipentylamino)-N-(4-sulfamoylphenethyl)propanamide (A27). Compound **A27** was obtained according the general procedure earlier reported using N-benzyl-3-chloro-N-(4-sulfamoylphenethyl)propanamide **A9** and dipentylamine (1.1 equiv) in dry MeCN (5 mL) and stirring for 16h at reflux temperature. The sticky residue was purified by flash chromatography (1% MeOH in DCM) to give **A27** as an oil. Yield 73 %; silica gel TLC R_f 0.16 (TFA/MeOH/DCM 3/5/92% v/v). δH (400 MHz, DMSO-d6): 7.72 (m, 2H, Ar-*H*), 7.29 (m, 7H, Ar-*H*), 7.27 (s, 2H, exchange with D$_2$O, SO$_2$N*H*$_2$, overlap with signal at 7.29), 4.57 (s, 1.1H, C*H*$_2$), 4.54 (s, 0.9H, C*H*$_2$), 3.46 (m, 2H, C*H*$_2$), 2.89 (m, 1H, C*H*$_2$), 2.82 (m, 1H, C*H*$_2$), 2.63 (s, 4H, 2 x C*H*$_2$), 2.32 (m, 4H, 2 x C*H*$_2$), 1.27 (m, 12H, 6 x C*H*$_2$), 0.84 (m, 6H, 2 x C*H*$_3$). δC (100 MHz, DMSO-d6): 172.97, 172.71, 144.46, 143.82, 143.41, 143.13, 139.21, 138.96, 130.27, 130.13, 129.71, 129.39, 128.66, 128.23, 128.00, 127.39, 126.83, 126.80, 65.98, 54.42, 54.36, 51.91, 51.00, 50.60, 49.18, 49.09, 48.54, 48.42, 35.12, 34.17, 32.30, 32.26, 32.04, 31.23, 30.93, 28.41, 27.78, 27.68, 27.62, 27.57, 27.13, 23.18, 23.04, 16.21, 14.97, 14.94. ESI-HRMS (m/z) [M+H]$^+$: calculated for $C_{28}H_{44}N_3O_3S$ 502.3103; found 502.3098.

N-Benzyl-3-(dihexylamino)-N-(4-sulfamoylphenethyl)propanamide (A28). Compound **A28** was obtained according the general procedure earlier reported using N-benzyl-3-chloro-N-(4-sulfamoylphenethyl)propanamide **A9** and dipentylamine (1.1 equiv) in dry MeCN (5 mL) and stirring for 16h at reflux temperature. The sticky residue was purified by flash chromatography (1% MeOH in DCM) to give **A28** as an oil. Yield 74 %; silica gel TLC R_f 0.20 (TFA/MeOH/DCM 3/5/92% v/v). δH (400 MHz, DMSO-d6): 7.73 (m, 2H, Ar-*H*), 7.32 (m, 7H, Ar-*H*), 7.30 (s, 2H, exchange with D$_2$O, SO$_2$N*H*$_2$, overlap with signal at 7.32), 4.60 (s, 0.9H, C*H*$_2$), 4.56 (s, 1.1H, C*H*$_2$), 3.47 (m, 2H, C*H*$_2$), 3.17 (m, 2H, C*H*$_2$), 2.85 (m, 8H, 4 x C*H*$_2$), 1.55 (m, 4H, 2 x C*H*$_2$), 1.27 (m, 12H, 6 x C*H*$_2$), 0.87 (m, 6H, 2 x C*H*$_3$). δC (100 MHz,

DMSO-d6): 172.90, 172.65, 144.47, 143.82, 143.44, 143.16, 139.27, 139.03, 130.27, 130.12, 129.71, 129.39, 128.66, 128.21, 127.99, 127.40, 126.83, 126.81, 54.44, 54.37, 54.09, 51.89, 51.02, 50.62, 49.73, 49.16, 48.53, 48.43, 36.03, 35.15, 34.20, 32.32, 32.27, 32.19, 31.69, 31.26, 30.95, 30.24, 29.40, 27.84, 27.72, 27.63, 27.59, 27.36, 23.20, 23.11, 14.99. ESI-HRMS (m/z) [M+H]$^+$: calculated for C$_{30}$H$_{48}$N$_3$O$_3$S 530.3416; found 530.3421.

N-Benzyl-3-(dioctylamino)-N-(4-sulfamoylphenethyl)propanamide (A29). Compound **A29** was obtained according the general procedure earlier reported using N-benzyl-3-chloro-N-(4-sulfamoylphenethyl)propanamide **A9** and dioctylamine (1.1 equiv) in dry MeCN (5 mL) and stirring for 16h at reflux temperature. The sticky residue was purified by flash chromatography (1% MeOH in DCM) to give **A29** as an oil. Yield 73 %; silica gel TLC R_f 0.22 (TFA/MeOH/DCM 3/5/92% v/v). δH (400 MHz, DMSO-d6): 7.73 (m, 2H, Ar-H), 7.31 (m, 7H, Ar-H), 7.30 (s, 2H, exchange with D$_2$O, SO$_2$NH_2, overlap with signal at 7.31), 4.60 (s, 0.9H, CH_2), 4.56 (s, 1.1H, CH_2), 3.47 (m, 2H, CH_2), 2.93 (m, 4H, 2 x CH_2), 2.82 (m, 4H, 2 x CH_2), 2.66 (m, 1H, CH_2), 2.57 (m, 1H, CH_2), 1.58 (m, 4H, 2 x CH_2), 1.27 (m, 20H, 5 x CH_2), 0.85 (m, 6H, 2 x CH_3). δC (100 MHz, DMSO-d6): 171.86, 171.61, 143.40, 142.75, 142.41, 142.12, 138.19, 137.95, 129.19, 129.05, 128.64, 128.33, 127.62, 127.16, 126.92, 126.37, 125.79, 125.75, 53.36, 53.31, 50.87, 49.99, 49.63, 49.15, 48.11, 47.47, 47.41, 34.12, 33.15, 31.27, 30.28, 29.91, 29.12, 28.96, 28.95, 28.92, 28.74, 28.73, 28.70, 26.88, 26.85, 26.81, 26.80, 26.72, 22.09, 13.94, 13.92. ESI-HRMS (m/z) [M+H]$^+$: calculated for C$_{34}$H$_{56}$N$_3$O$_3$S 586.4042; found 586.4036.

3-(Dihexylamino)-N-phenethyl-N-(4-sulfamoylphenethyl)propanamide (A30). Compound **A30** was obtained according the general procedure earlier reported using 3-chloro-N-phenethyl-N-(4-sulfamoylphenethyl)propanamide **A17** and dihexylamine (1.1 equiv) in dry MeCN (5 mL) and stirring for 16h at reflux temperature. The sticky residue was purified by flash chromatography (1% MeOH in DCM) to give **A30** as an oil. Yield 68 %; silica gel TLC R_f 0.21 (TFA/MeOH/DCM 3/5/92% v/v). δH (400 MHz, DMSO-d6): 7.75 (m, 2H, Ar-H), 7.35 (m, 7H, Ar-H), 7.30 (s, 2H, exchange with D$_2$O, SO$_2$NH_2, overlap with signal at 7.35), 4.11 (m, 2H, CH_2), 3.49 (m, 2H, CH_2), 3.16 (m, 4H, 2 x CH_2), 2.90 (m,

4H, 2 x C*H₂*), 2.08 (m, 4H, 2 x C*H₂*), 1.60 (m, 4H, 2 x C*H₂*), 1.29 (m, 12H, 6 x C*H₂*), 0.87 (m, 6H, 2 x C*H₃*). δC (100 MHz, DMSO-d6): 170.21, 170.08, 144.37, 143.78, 143.42, 143.22, 140.21, 139.72, 130.56, 130.50, 130.19, 130.05, 129.75, 129.66, 129.44, 127.45, 127.12, 126.82, 65.98, 55.92, 53.01, 49.69, 49.64, 49.07, 48.24, 47.79, 35.36, 35.12, 34.47, 34.14, 31.78, 26.80, 26.39, 23.90, 22.98, 16.22, 14.95, 14.90. ESI-HRMS (m/z) [M+H]⁺: calculated for $C_{31}H_{50}N_3O_3S$ 544.3573; found 544.3578.

3-(Dihexylamino)-N-(furan-2-ylmethyl)-N-(4-sulfamoylphenethyl)propenamide (A31). Compound **A31** was obtained according the general procedure earlier reported using 3-chloro-N-(furan-2-ylmethyl)-N-(4-sulfamoylphenethyl)propenamide **A14** and dihexylamine (1.1 equiv) in dry MeCN (5 mL) and stirring for 16h at reflux temperature. The sticky residue was purified by flash chromatography (1% MeOH in DCM) and to give **A31** as a powder. Yield 68 %; mp 118-120 °C; silica gel TLC *R_f* 0.26 (TFA/MeOH/DCM 3/5/92% *v/v*). δH (400 MHz, DMSO-d6): 7.73 (d, *J* = 8.3 Hz, 2H, Ar-*H*), 7.60 (m, 1H, Ar-*H*), 7.36 (d, *J* = 8.3 Hz, 2H, Ar-*H*), 7.30 (s, 2H, exchange with D₂O, SO₂N*H₂*), 6.40 (m, 2H, Ar-*H*), 4.57 (s, 0.9H, C*H₂*), 4.54 (s, 1.1H, C*H₂*), 3.47 (m, 2H, C*H₂*), 3.16 (m, 2H, C*H₂*), 2.82 (m, 8H, 4 x C*H₂*), 1.56 (m, 4H, 2 x C*H₂*), 1.27 (m, 12H, 6 x C*H₂*), 0.85 (m, 6H, 2 x C*H₃*). δC (100 MHz, DMSO-d6): 152.21, 151.98, 144.38, 144.00, 143.75, 143.51, 143.45, 143.16, 130.30, 130.09, 126.84, 111.62, 111.59, 109.50, 109.25, 54.06, 50.19, 49.65, 49.14, 48.04, 47.80, 45.36, 41.86, 34.96, 33.98, 32.17, 31.91, 31.77, 27.41, 26.71, 26.48, 23.15, 22.94, 14.97, 14.91. ESI-HRMS (m/z) [M+H]⁺: calculated for $C_{28}H_{46}N_3O_4S$ 520.3209; found 520.3215.

2-(Dihexylamino)-N-(naphthalen-2-ylmethyl)-N-(4-sulfamoylphenethyl)acetamide (A32). Compound **A32** was obtained according the general procedure earlier reported using 2-chloro-N-(naphthalen-2-ylmethyl)-N-(4-sulfamoylphenethyl)acetamide **A12** and dihexylamine (1.1 equiv) in dry MeCN (5 mL) and stirring for 16h at reflux temperature. The sticky residue was purified by flash chromatography (1% MeOH in DCM) to give **A32** as an oil. Yield 61 %; silica gel TLC *R_f* 0.16 (TFA/MeOH/DCM 3/5/92% *v/v*). δH (400 MHz, DMSO-d6): 7.89 (m, 3H, Ar-*H*), 7.71 (m, 3H, Ar-*H*), 7.41 (m, 7H, Ar-*H*), 7.29 (s, 2H, exchange with D₂O, SO₂N*H₂*, overlap with signal at 7.41), 4.92 (s, 0.9H, C*H₂*), 4.73 (s, 1.1H,

C*H*₂), 3.68 (m, 1H, C*H*₂), 3.51 (m, 1H, C*H*₂), 3.23 (m, 1.1H, C*H*₂), 3.14 (m, 0.9H, C*H*₂), 2.99 (m, 1H, C*H*₂), 2.85 (m, 1H, C*H*₂), 2.37 (m, 4H, 2 x C*H*₂), 1.29 (m, 4H, 2 x C*H*₂), 1.14 (m, 12H, 6 x C*H*₂), 0.78 (t, J = 6.4 Hz, 6H, 2 x C*H*₃). δC (100 MHz, DMSO-d6): 170.44, 170.23, 143.32, 143.08, 142.36, 142.15, 135.81, 135.53, 133.05, 132.89, 132.22, 129.24, 129.04, 128.27, 127.99, 127.58, 127.46, 126.37, 126.34, 126.24, 126.20, 126.16, 125.85, 125.76, 125.02, 124.61, 64.93, 57.91, 57.48, 53.86, 53.76, 50.17, 47.61, 47.38, 47.08, 34.03, 32.82, 31.17, 26.61, 26.56, 26.38, 22.06, 15.18, 13.89, 13.86. ESI-HRMS (m/z) [M+H]⁺: calculated for $C_{33}H_{48}N_3O_3S$ 566.3416; found 566.3410.

N-(2-Cyanoethyl)-2-(dihexylamino)-N-(4-sulfamoylphenethyl)acetamide **(A33).** Compound **A33** was obtained according the general procedure earlier reported using 2-chloro-N-(2-cyanoethyl)-N-(4-sulfamoylphenethyl)acetamide **A15** and dihexylamine (1.1 equiv) in dry MeCN (5 mL) and stirring for 16h at reflux temperature. The sticky residue was purified by flash chromatography (1% MeOH in DCM) to give **A33** as an oil. Yield 66 %; silica gel TLC R_f 0.08 (TFA/MeOH/DCM 3/5/92% *v/v*). δH (400 MHz, DMSO-d6): 7.75 (d, J = 7.9 Hz, 2H, Ar-*H*), 7.44 (d, J = 8.0 Hz, 2H, Ar-*H*), 7.29 (s, 2H, exchange with D₂O, SO₂N*H*₂), 3.74 (m, 2H, C*H*₂), 3.50 (m, 2H, C*H*₂), 3.27 (s, 1H, C*H*₂), 3.07 (s, 1H, C*H*₂), 2.95 (m, 1H, C*H*₂), 2.85 (m, 2H, C*H*₂), 2.71 (m, 1H, C*H*₂), 2.37 (m, 4H, 2 x C*H*₂), 1.36 (m, 4H, 2 x C*H*₂), 1.22 (m, 12H, 6 x C*H*₂), 0.84 (m, 6H, 2 x C*H*₃). δC (100 MHz, DMSO-d6): 171.58, 171.22, 144.28, 143.93, 143.50, 143.44, 143.24, 130.36, 130.19, 126.81, 126.78, 120.18, 59.14, 58.70, 54.81, 49.27, 47.39, 43.72, 42.10, 35.16, 34.82, 33.81, 32.25, 32.23, 27.66, 27.61, 27.32, 27.23, 23.15, 23.13, 17.86, 16.46, 14.99, 14.96. ESI-HRMS (m/z) [M+H]⁺: calculated for $C_{25}H_{43}N_4O_3S$ 479.3055; found 479.3049.

2-((2-Cyanoethyl)(phenethyl)amino)-N-phenethyl-N-(4-sulfamoylphenethyl)acetamide (A34). Compound **A34** was obtained according the general procedure earlier reported using 2-chloro-N-phenethyl-N-(4-sulfamoylphenethyl)acetamide **A16** and 3-(phenethylamino)propanenitrile (1.1 equiv) in MeCN dry (5 mL) and stirring for 18h at reflux temperature. The sticky residue was purified by flash chromatography (1% MeOH in DCM) to give **A34** as a powder. Yield 68 %; mp 118-120 °C; silica gel TLC R_f 0.26

(TFA/MeOH/DCM 3/5/92% v/v). δH (400 MHz, DMSO-d6): 7.74 (d, J = 6.8 Hz, 2H, Ar-H), 7.42 (d, J = 8.1 Hz, 2H, Ar-H), 7.29 (s, 2H, exchange with D_2O, SO_2NH_2, overlap with signal at 7.23), 7.23 (m, 10H, Ar-H), 3.46 (m, 4H, 2 x CH_2), 3.28 (s, 0.9H, CH_2), 3.16 (s, 1.1H, CH_2), 2.71 (m, 12H, 6 x CH_2). δC (100 MHz, DMSO-d6): 170.49, 170.33, 144.45, 143.98, 143.23, 143.02, 141.07, 140.19, 139.84, 135.53, 130.30, 130.07, 129.95, 129.61, 129.60, 129.57, 129.52, 129.30, 129.25, 129.13, 127.27, 127.05, 126.77, 126.63, 121.05, 56.31, 56.13, 56.06, 55.91, 55.83, 51.24, 50.06, 49.20, 48.93, 47.63, 47.22, 45.60, 36.82, 35.15, 34.98, 34.36, 34.15, 34.10, 33.86, 18.75, 16.72, 16.56. ESI-HRMS (m/z) [M+H]$^+$: calculated for $C_{29}H_{35}N_4O_3S$ 519.2430; found 519.2434.

2-((2-Cyanoethyl)(phenethyl)amino)-N-(furan-2-ylmethyl)-N-(4-sulfamoylphenethyl)acetamide (A35). Compound **A35** was obtained according the general procedure earlier reported using 2-chloro-N-(furan-2-ylmethyl)-N-(4-sulfamoylphenethyl)acetamide **A13** and 3-(phenethylamino)propanenitrile (1.1 equiv) in dry MeCN (5 mL) and stirring for 16h at reflux temperature. The sticky residue was purified by flash chromatography (1% MeOH in DCM) to give **A35** as an oil. Yield 70 %; silica gel TLC R_f 0.20 (TFA/MeOH/DCM 3/5/92% v/v). δH (400 MHz, DMSO-d6): 7.69 (m, 3H, Ar-H), 7.27 (m, 7H, Ar-H), 7.22 (s, 2H, exchange with D_2O, SO_2NH_2, overlap with signal at 7.27), 6.39 (m, 2H, Ar-H), 3.57 (s, 1H, CH_2), 3.49 (m, 2H, CH_2), 3.45 (s, 1H, CH_2), 2.72 (m, 12H, 6 x CH_2). δC (100 MHz, DMSO-d6): 169.56, 169.50, 151.07, 150.90, 143.25, 143.03, 142.96, 142.49, 142.34, 142.12, 140.12, 140.08, 129.33, 129.06, 128.69, 128.67, 128.61, 128.26, 128.22, 125.87, 125.84, 125.77, 120.14, 110.61, 110.54, 108.49, 108.40, 55.52, 55.36, 55.16, 54.96, 49.26, 49.16, 46.74, 44.63, 43.49, 33.64, 33.25, 33.09, 32.76, 30.71, 15.74, 15.63. m/z (ESI positive) 495.3 [M+H]$^+$.

2-((2-Cyanoethyl)(phenethyl)amino)-N-(4-fluorobenzyl)-N-(4-sulfamoylphenethyl)acetamide (A36). Compound **A36** was obtained according the general procedure earlier reported using 2-chloro-N-(4-fluorobenzyl)-N-(4-sulfamoylphenethyl)acetamide **A11** and 3-(phenethylamino)propanenitrile (1.1 equiv) in dry MeCN (5 mL) and stirring for 17h at reflux temperature. The sticky residue was purified by

flash chromatography (1% MeOH in DCM) to give **A36** as an oil. Yield 73 %; silica gel TLC R_f 0.24 (TFA/MeOH/DCM 3/5/92% *v/v*). δH (400 MHz, DMSO-d6): 7.73 (t, *J* = 9.7 Hz, 2H, Ar-*H*), 7.30 (s, 2H, exchange with D$_2$O, SO$_2$N*H*$_2$, overlap with signal at 7.29), 7.29 (m, 11H, Ar-*H*), 4.52 (s, 1.1H, C*H*$_2$), 4.41 (s, 0.9H, C*H*$_2$), 3.43 (m, 2H, C*H*$_2$), 2.74 (m, 12H, 6 x C*H*$_2$). δF (376 MHz, DMSO-d6): -115.54, -115.71. δC (100 MHz, DMSO-d6): 170.92, 170.41, 144.33, 143.98, 143.40, 143.19, 141.13, 130.87, 130.79, 130.47, 130.40, 130.32, 130.12, 130.01, 129.91, 129.84, 129.71, 129.27, 126.91, 126.81, 121.20, 116.30, 116.09, 56.50, 56.26, 56.12, 55.93, 55.52, 50.47, 50.34, 50.21, 49.50, 48.69, 47.81, 34.77, 34.29, 34.08, 33.88, 16.72. ESI-HRMS (m/z) [M+H]$^+$: calculated for C$_{28}$H$_{32}$FN$_4$O$_3$S 523.2179; found 523.2183.

2-((2-Cyanoethyl)(phenethyl)amino)-N-(naphthalen-2-ylmethyl)-N-(4-sulfamoylphenethyl)acetamide (A37).

Compound **A37** was obtained according the general procedure earlier reported using 2-chloro-N-(4-fluorobenzyl)-N-(4-sulfamoylphenethyl)acetamide **A12** and 3-(phenethylamino)propanenitrile (1.1 equiv) in dry MeCN (5 mL) and stirring for 20h at reflux temperature. The sticky residue was purified by flash chromatography (1% MeOH in DCM) to give **A37** as an oil. Yield 73 %; silica gel TLC R_f 0.38 (TFA/MeOH/DCM 3/5/92% *v/v*). δH (400 MHz, DMSO-d6): 7.89 (m, 3H, Ar-*H*)7.73 (t, *J* = 9.7 Hz, 3H, Ar-*H*), 7.30 (m, 10H, Ar-*H*), 7.28 (s, 2H, exchange with D$_2$O, SO$_2$N*H*$_2$, overlap with signal at 7.30), 4.75 (m, 2H, C*H*$_2$), 3.49 (m, 4H, 2 x C*H*$_2$), 2.84 (m, 8H, 4 x C*H*$_2$), 2.58 (m, 2H, C*H*$_2$). δC (100 MHz, DMSO-d6): 171.13, 171.01, 167.33, 144.40, 144.18, 144.04, 143.68, 143.51, 143.44, 143.41, 143.29, 143.16, 141.30, 141.14, 141.09, 136.74, 136.45, 136.16, 135.55, 134.10, 134.00, 133.95, 133.36, 133.25, 130.46, 130.42, 130.18, 130.14, 129.72, 129.67, 129.31, 129.28, 129.23, 129.18, 129.16, 128.71, 128.62, 127.44, 127.36, 127.29, 127.14, 127.08, 126.98, 126.93, 126.90, 126.87, 126.83, 126.48, 126.39, 126.24, 125.90, 121.24, 55.98, 51.34, 50.26, 48.68, 45.71, 43.23, 37.03, 34.77, 34.27, 33.95, 33.64, 31.76, 18.84, 16.79, 16.74, 16.70. ESI-HRMS (m/z) [M+H]$^+$: calculated for C$_{32}$H$_{35}$N$_4$O$_3$S 555.2430; found 555.2425.

2-((2-Cyanoethyl)(phenethyl)amino)-N-(4-nitrobenzyl)-N-(4-sulfamoylphenethyl)acetamide (A38). Compound **A38** was obtained according the general procedure earlier reported using 2-chloro-N-(4-nitrobenzyl)-N-(4-sulfamoylphenethyl)acetamide **A10** and 3-(phenethylamino)propanenitrile (1.1 equiv) in dry MeCN (5 mL) and stirring for 24h at reflux temperature. The sticky residue was purified by flash chromatography (1% MeOH in DCM) to give **A38** as a powder. Yield 51 %; mp 108-110 °C; silica gel TLC R_f 0.09 (TFA/MeOH/DCM 3/5/92% v/v). δH (400 MHz, DMSO-d6): 8.14 (m, 3H, Ar-H), 7.71 (m, 3H, Ar-H), 7.32 (m, 7H, Ar-H), 7.27 (s, 2H, exchange with D$_2$O, SO$_2$NH_2, overlap with signal at 7.32), 4.67 (s, 1.1H, Ar-H), 4.62 (s, 0.9H, CH_2), 3.49 (s, 1H, CH_2), 3.46 (m, 2H, CH_2), 3.26 (s, 1H, CH_2) 2.81 (m, 6H, 3 x CH_2). δC (100 MHz, DMSO-d6): 170.81, 170.36, 144.67, 144.48, 143.87, 142.53, 141.34, 130.88, 130.68, 130.41, 130.29, 130.15, 129.21, 128.43, 126.82, 126.64, 124.73, 124.60, 124.30, 124.26, 121.61, 116.46, 116.17, 56.32, 56.21, 56.07, 55.84, 55.41, 50.59, 50.33, 50.04, 49.72, 48.65, 47.29, 34.72, 34.24, 34.11, 33.66, 16.43. ESI-HRMS (m/z) [M+H]$^+$: calculated for C$_{28}$H$_{32}$N$_5$O$_5$S 550.2124; found 550.2119.

N-(2-Cyanoethyl)-2-((2-cyanoethyl)(phenethyl)amino)-N-(4-sulfamoylphenethyl)acetamide (A39). Compound **A39** was obtained according the general procedure earlier reported using 2-chloro-N-(2-cyanoethyl)-N-(4-sulfamoylphenethyl)acetamide **A15** and 3-(phenethylamino)propanenitrile (1.1 equiv) in MeCN dry (5 mL) and stirring for 14h at reflux temperature. The sticky residue was purified by flash chromatography (1% MeOH in DCM) to give **A39** as an oil. Yield 75 %; silica gel TLC R_f 0.24 (TFA/MeOH/DCM 3/5/92% v/v). δH (400 MHz, DMSO-d6): 7.76 (m, 2H, Ar-H), 7.35 (m, 7H, Ar-H), 7.30 (s, 2H, exchange with D$_2$O, SO$_2$NH_2, overlap with signal at 7.35), 3,55 (m, 6H, 3 x CH_2), 2.82 (m, 10H, 5 x CH_2). δC (100 MHz, DMSO-d6): 167.38, 167.09, 144.29, 144.09, 143.83, 143.50, 143.47, 143.24, 138.62, 130.54, 130.50, 130.43, 130.28, 130.23, 129.77, 129.33, 129.10, 126.84, 126.82, 126.58, 120.21, 120.04, 56.21, 50.23, 49.92, 49.14, 47.96, 47.42, 44.10, 43.46, 43.21, 43.03, 42.82, 42.17, 34.99, 33.84, 21.84, 18.01, 17.88, 16.59, 16.43. ESI-HRMS (m/z) [M+H]$^+$: calculated for C$_{24}$H$_{30}$N$_5$O$_3$S 468.2069; found 468.2073.

General synthetic procedure for preparation of amine derivatives A40-44. To a solution of nitrile derivatives **A33-39** (0.5 mmol, 1.0 equiv) and NaOH$_{(aq)}$ 5M (3.0 equiv) in EtOH (10 mL), Ni/Raney (0.5 mL) was added and the mixture was stirred o.n. under H$_2$ pressure (50 psi). The solution was filtered-off and the solvent was evaporated under *vacuum*. The residue was purified with flash chromatography (5 to 15% MeOH in DCM) to give compounds **A40-44**.

2-((3-Aminopropyl)(phenethyl)amino)-N-phenethyl-N-(4-sulfamoylphenethyl)acetamide (A40). Compound **A40** was obtained according the general procedure earlier reported using 2-((2-cyanoethyl)(phenethyl)amino)-N-phenethyl-N-(4-sulfamoylphenethyl)acetamide **A34**. The obtained residue was purified by flash chromatography to give **A40** as an oil. Yield 26 %; silica gel TLC R_f 0.38 (TFA/MeOH/DCM 3/5/92% *v/v*). δH (400 MHz, DMSO-d6): 7.76 (m, 4H, Ar-*H*), 7.44 (m, 4H, Ar-*H*), 7.23 (s, 2H, exchange with D$_2$O, SO$_2$N*H*$_2$, overlap with signal at 7.20), 7.20 (m, 11H, Ar-*H*), 3.50 (m, 4H, 2 x C*H*$_2$), 3.19 (s, 1.1H, C*H*$_2$), 3.09 (s, 0.9H, C*H*$_2$), 2.75 (m, 10H, 5 x C*H*$_2$), 2.34 (m, 2H, C*H*$_2$), 1.60 (m, 2H, C*H*$_2$). δC (100 MHz, DMSO-d6): 171.90, 171.75, 144.45, 143.88, 143.51, 143.24, 141.28, 141.22, 140.24, 139.80, 130.54, 130.26, 130.16, 129.78, 129.75, 129.50, 129.42, 129.31, 127.49, 127.24, 126.95, 126.81, 126.77, 56.63, 56.40, 55.82, 52.80, 52.70, 49.06, 48.74, 47.95, 47.42, 39.56, 35.12, 34.89, 34.16, 33.88, 33.29, 33.23, 24.57, 23.08. ESI-HRMS (m/z) [M+H]$^+$: calculated for C$_{29}$H$_{39}$N$_4$O$_3$S 523.2743; found 523.2748.

2-((3-Aminopropyl)(phenethyl)amino)-N-(furan-2-ylmethyl)-N-(4-sulfamoylphenethyl)acetamide (A41). Compound **A41** was obtained according the general procedure earlier reported using 2-((2-cyanoethyl)(phenethyl)amino)-N-(furan-2-ylmethyl)-N-(4-sulfamoylphenethyl)acetamide **A35**. The obtained residue was purified by flash chromatography to give **A41** as an oil. Yield 33 %; silica gel TLC R_f 0.42 (TFA/MeOH/DCM 3/5/92% *v/v*). δH (400 MHz, DMSO-d6): 7.75 (t, J = 8.4 Hz, 2H, Ar-*H*), 7.67 (s, 0.5H, Ar-*H*), 7.62 (s, 0.5H, Ar-*H*), 7.29 (m, 7H, Ar-*H*), 7.20 (s, 2H, exchange with D$_2$O, SO$_2$N*H*$_2$, overlap with signal at 7.29), 6.44 (m, 2H, Ar-*H*), 4.60 (m, 2H, C*H*$_2$), 3.57 (s, 2H, C*H*$_2$), 3.49 (m, 2H, C*H*$_2$), 3.26 (s, 2H, C*H*$_2$), 2.75 (m, 7H, 4 x C*H*$_2$), 2.34 (m, 1H, C*H*$_2$), 1.65 (m, 2H,

C*H₂*). δC (100 MHz, DMSO-d6): 172.04, 171,99, 151.83, 151.55, 144.24, 144.20, 143.77, 143.69, 143.56, 143.25, 141.15, 130.50, 130.16, 129.75, 129.34, 129.31, 127.00, 126.88, 126.82, 111.71, 111.67, 109.73, 109.69, 56.71, 56.51, 55.85, 55.67, 53.17, 52.75, 48.22, 47.96, 44.39, 42.03, 39.64, 34.47, 33.78, 33.30, 33.19, 24.31, 24.22. ESI-HRMS (m/z) [M+H]⁺: calculated for $C_{26}H_{35}N_4O_4S$ 499.2379; found 499.2373.

2-((3-Aminopropyl)(phenethyl)amino)-N-(4-fluorobenzyl)-N-(4-sulfamoylphenethyl)acetamide (A42). Compound **A42** was obtained according the general procedure earlier reported using 2-((2-cyanoethyl)(phenethyl)amino)-N-(4-fluorobenzyl)-N-(4-sulfamoylphenethyl)acetamide **A36**. The obtained solid was purified by flash chromatography to give **A42** as an oil. Yield 28 %; silica gel TLC *Rf* 0.37 (TFA/MeOH/DCM 3/5/92% *v/v*). δH (400 MHz, DMSO-d6): 7.77 (m, 2H, Ar-*H*), 7.30 (m, 11H, Ar-*H*), 7.21 (s, 2H, exchange with D₂O, SO₂N*H₂*, overlap with signal at 7.30), 4.60 (m, 2H, C*H₂*), 3.48 (m, 6H, 3 x C*H₂*), 2.83 (m, 7H, 4 x C*H₂*), 2.42 (m, 1H, C*H₂*), 1.68 (m, 2H, C*H₂*). δF (376 MHz, DMSO-d6): -115.42, -115.62. δC (100 MHz, DMSO-d6): 172.31, 163.69, 161.11, 144.28, 143.76, 143.58, 143.26, 141.22, 141.13, 134.99, 134.97, 134.43, 134.41, 130.79, 130.71, 130.50, 130.18, 129.97, 129.89, 129.75, 129.71, 129.31, 126.96, 126.88, 126.82, 116.73, 116.52, 116.40, 116.19, 56.82, 56.47, 55.73, 53.01, 52.80, 50.21, 48.21, 48.00, 39.62, 39.61, 34.52, 33.84, 33.23, 24.54, 24.39. ESI-HRMS (m/z) [M+H]⁺: calculated for $C_{28}H_{36}FN_4O_3S$ 527.2492; found 527.2488.

2-((3-Aminopropyl)(phenethyl)amino)-N-(naphthalen-2-ylmethyl)-N-(4-sulfamoylphenethyl)acetamide (A43). Compound **A43** was obtained according the general procedure earlier reported using 2-((2-cyanoethyl)(phenethyl)amino)-N-(naphthalen-2-ylmethyl)-N-(4-sulfamoylphenethyl)acetamide **A37**. The obtained solid was purified by flash chromatography to give **A43** as an oil. Yield 34 %; silica gel TLC *Rf* 0.42 (TFA/MeOH/DCM 3/5/92% *v/v*). δH (400 MHz, DMSO-d6): 7.91 (m, 3H, Ar-*H*), 7.76 (m, 3H, Ar-*H*), 7.28 (m, 10H, Ar-*H*), 7.20 (s, 2H, exchange with D₂O, SO₂N*H₂*, overlap with signal at 7.28), 4.79 (m, 2H, C*H₂*), 3.52 (m, 4H, 2 x C*H₂*), 2.91 (m, 4H, 2 x C*H₂*), 2.66 (m, 6H, 3 x C*H₂*), 1.70 (m, 2H, C*H₂*). δC (100 MHz, DMSO-d6): 172.58, 172.30, 163.07, 161.66,

144.37, 143.97, 143.60, 143.32, 141.33, 134.21, 134.00, 133.51, 133.34, 130.55, 130.22, 130.16, 129.77, 129.68, 129.57, 129.31, 129.27, 129.19, 128.73, 128.63, 127.53, 127.35, 127.10, 126.96, 126.91, 126.81, 126.17, 126.13, 126.02, 125.27, 56.76, 56.41, 55.89, 55.76, 53.20, 52.91, 52.69, 51.09, 49.69, 49.25, 48.60, 39.62, 33.93, 33.27, 32.59, 32.46, 28.12, 21.21. ESI-HRMS (m/z) [M+H]$^+$: calculated for C$_{32}$H$_{39}$N$_4$O$_3$S 559.2743; found 559.2737.

N-(3-Aminopropyl)-2-(dihexylamino)-N-(4-sulfamoylphenethyl)acetamide (A44). Compound **A44** was obtained according to the general procedure earlier reported using N-(2-cyanoethyl)-2-(dihexylamino)-N-(4-sulfamoylphenethyl)acetamide **A33**. The obtained solid was purified by flash chromatography to give **A44** as an oil. Yield 31 %; silica gel TLC R_f 0.43 (TFA/MeOH/DCM 3/5/92% v/v). δH (400 MHz, DMSO-d6): 7.78 (d, J = 8.0 Hz, 2H, Ar-H), 7.49 (d, J = 8.0 Hz, 2H, Ar-H), 7.35 (s, 2H, exchange with D$_2$O, SO$_2$NH_2), 3.48 (m, 2H, CH_2), 3.20 (m, 2H, CH_2), 2.88 (m, 8H, 4 x CH_2), 1.85 (m, 4H, 2 x CH_2), 1.45 (m, 4H, 2 x CH_2), 1.25 (m, 12H, 6 x CH_2), 0.86 (m, 6H, 2 x CH_3). δC (100 MHz, DMSO-d6): 169.55, 169.26, 143.81, 143.54, 135.94, 133.31, 131.36, 130.47, 130.20, 126.81, 55.06, 55.00, 48.79, 47.51, 37.69, 37.45, 37.41, 34.96, 34.74, 33.94, 33.80, 31.96, 31.94, 28.69, 27.89, 27.31, 27.17, 27.03, 26.88, 26.30, 23.05, 23.02, 14.93, 14.92. ESI-HRMS (m/z) [M+H]$^+$: calculated for C$_{25}$H$_{47}$N$_4$O$_3$S 483.3369; found 483.3374.

General synthetic procedure for preparation of carboxylic acid-derivatives A45-49. To a solution of the appropriate nitrile derivatives **A33-39** (0.5 mmol, 1.0 equiv) in EtOH (5 mL), NaOH$_{(aq)}$ 5M (3.0 equiv) was added and the mixture was heated at reflux temperature under stirring o.n.. The solution was cooled to 0°C and HCl 12M (2.0 equiv) was added dropwise until precipitation of a powder, which was collected by filtration. The solid was purified by flash chromatography (5 to 15% MeOH in DCM) to give the compounds **A45-49**.

3-((2-Oxo-2-(phenethyl(4-sulfamoylphenethyl)amino)ethyl)(phenethyl)amino)propanoic acid (A45). Compound **A45** was obtained according the general procedure earlier reported using 2-((2-

cyanoethyl)(phenethyl)amino)-N-phenethyl-N-(4-sulfamoylphenethyl)acetamide **A34**. The obtained solid was purified by flash chromatography to give **A45** as a powder. Yield 31 %; mp 74-76°C; silica gel TLC R_f 0.35 (TFA/MeOH/DCM 3/5/92% *v/v*). δH (400 MHz, DMSO-d6): 12.05 (brs, 1H, exchange with D_2O, COO*H*), 7.72 (m, 3H, Ar-*H*), 7.27 (m, 16H, Ar-*H*), 7.23 (s, 2H, exchange with D_2O, SO_2NH_2, overlap with signal at 7.27), 3.46 (m, 4H, 2 x C*H*$_2$), 3.14 (s, 0.9H, C*H*$_2$), 3.09 (s, 1.1H, C*H*$_2$), 2.72 (m, 10H, 5x C*H*$_2$), 2.25 (s, 2H, C*H*$_2$). δC (100 MHz, DMSO-d6): 175.20, 175.13, 170.64, 170.52, 167.24, 143.38, 143.18, 142.84, 142.84, 141.41, 141.31, 141.31, 130.43, 130.19, 130.11, 130.05, 129.74, 129.67, 129.65, 129.45, 129.41, 129.29, 127.40, 127.21, 126.89, 126.81, 126.78, 126.65, 57.46, 57.04, 56.40, 51.81, 51.39, 50.34, 49.51, 49.15, 47.86, 47.58, 36.78, 36.48, 35.36, 35.14, 34.17, 33.92, 33.33. ESI-HRMS (m/z) [M+H]$^+$: calculated for $C_{29}H_{36}N_3O_5S$ 538.2376; found 538.2381.

3-((2-((Furan-2-ylmethyl)(4-sulfamoylphenethyl)amino)-2-oxoethyl)(phenethyl)amino)propanoic acid (A46). Compound **A46** was obtained according the general procedure earlier reported using 2-((2-cyanoethyl)(phenethyl)amino)-N-(furan-2-ylmethyl)-N-(4-sulfamoylphenethyl)acetamide **A35**. The obtained solid was purified by flash to give **A46** as a powder. Yield 35 %; mp 33-35°C; silica gel TLC R_f 0.39 (TFA/MeOH/DCM 3/5/92% *v/v*). δH (400 MHz, DMSO-d6): 12.01 (brs, 1H, exchange with D_2O, COO*H*), 7.74 (t, J = 7.3 Hz, 2H, Ar-*H*), 7.64 (s, 0.5H, Ar-*H*), 7.57 (s, 0.5H, Ar-*H*), 7.25 (m, 7H, Ar-*H*), 7.21 (s, 2H, exchange with D_2O, SO_2NH_2, overlap with signal at 7.25), 6.39 (m, 2H, Ar-*H*), 4.54 (m, 2H, C*H*$_2$), 3.48 (s, 2H, C*H*$_2$), 3.38 (m, 2H, C*H*$_2$), 3.27 (s, 2H, C*H*$_2$), 2.76 (m, 6H, 3 x C*H*$_2$), 2.35 (m, 2H, C*H*$_2$). δC (100 MHz, DMSO-d6): 174.69, 174.67, 170.58, 152.17, 152.06, 144.35, 144.06, 144.03, 143.49, 143.38, 143.18, 141.33, 141.22, 130.33, 130.06, 129.70, 129.66, 129.28, 126.86, 111.65, 111.59, 109.46, 109.37, 57.46, 57.32, 56.26, 50.31, 50.16, 48.59, 47.95, 44.57, 41.76, 34.77, 33.80, 33.60, 32.95, 32.87, 31.76. ESI-HRMS (m/z) [M+H]$^+$: calculated for $C_{26}H_{32}N_3O_6S$ 514.2012; found 514.2008.

3-((2-((4-Fluorobenzyl)(4-sulfamoylphenethyl)amino)-2-oxoethyl)(phenethyl)amino)propanoic acid (A47). Compound **A47** was obtained according the general procedure earlier reported using 2-((2-cyanoethyl)(phenethyl)amino)-

N-(4-fluorobenzyl)-N-(4-sulfamoylphenethyl)acetamide **A36**. The obtained solid was purified by flash chromatography to give **A47** as a powder. Yield 33 %; mp 64-66°C; silica gel TLC R_f 0.41 (TFA/MeOH/DCM 3/5/92% v/v). δH (400 MHz, DMSO-d6): 11.82 (brs, 1H, exchange with D_2O, COO*H*), 7.73 (m, 2H, Ar-*H*), 7.24 (m, 11H, Ar-*H*), 7.21 (s, 2H, exchange with D_2O, SO_2NH_2, overlap with signal at 7.24), 4.53 (m, 2H, C*H*$_2$), 3.39 (s, 6H, 3 x C*H*$_2$), 2.80 (m, 6H, 3 x C*H*$_2$), 2.36 (m, 2H, C*H*$_2$). δF (376 MHz, DMSO-d6): -115.43, -115.60. δC (100 MHz, DMSO-d6): 174.66, 174.63, 173.07, 170.88, 163.52, 161.23, 144.37, 144.02, 143.38, 143.19, 141.24, 141.16, 135.44, 134.93, 131.42, 130.84, 130.76, 130.36, 130.20, 130.07, 129.94, 129.67, 129.65, 129.28, 126.93, 126.89, 126.82, 126.63, 116.59, 116.38, 116.28, 116.07, 65.98, 57.24, 56.27, 56.19, 50.23, 50.10, 48.62, 47.81, 34.83, 33.84, 33.52, 32.84, 22.12, 16.23. ESI-HRMS (m/z) [M+H]$^+$: calculated for $C_{28}H_{33}FN_3O_5S$ 542.2125; found 542.2131.

3-((2-((Naphthalen-2-ylmethyl)(4-sulfamoylphenethyl)amino)-2-oxoethyl)(phenethyl)amino)propanoic acid (A48).

Compound **A48** was obtained according the general procedure earlier reported using 2-((2-cyanoethyl)(phenethyl)amino)-N-(naphthalen-2-ylmethyl)-N-(4-sulfamoylphenethyl)acetamide **A37**. The obtained solid was purified by flash chromatography to give **A48** as a powder. Yield 37 %; mp 96-98°C; silica gel TLC R_f 0.43 (TFA/MeOH/DCM 3/5/92% v/v). δH (400 MHz, DMSO-d6): 12.34 (brs, 1H, exchange with D_2O, COO*H*), 7.88 (m, 3H, Ar-*H*), 7.72 (m, 3H, Ar-*H*), 7.32 (m, 10H, Ar-*H*), 7.22 (s, 2H, exchange with D_2O, SO_2NH_2, overlap with signal at 7.32), 3.48 (m, 3.1H, 2 x C*H*$_2$), 3.17 (s, 0.9H, C*H*$_2$), 2.75 (m, 8H, 4 x C*H*$_2$), 2.32 (m, 2H, C*H*$_2$). δC (100 MHz, DMSO-d6): 175.33, 175.19, 171.15, 171.11, 144.40, 144.12, 143.40, 143.18, 141.34, 141.22, 136.77, 136.44, 134.12, 133.95, 133.32, 133.25, 130.38, 130.10, 129.65, 129.41, 129.28, 129.25, 129.15, 128.71, 128.64, 128.61, 127.42, 127.29, 127.14, 127.10, 126.96, 126.83, 126.28, 125.95, 57.54, 57.38, 56.29, 56.26, 51.41, 50.52, 50.34, 49.67, 48.66, 48.64, 48.13, 48.12, 34.93, 33.97, 33.48, 33.35, 33.31. ESI-HRMS (m/z) [M+H]$^+$: calculated for $C_{32}H_{36}N_3O_5S$ 574.2376; found 574.2371.

3-(2-(Dihexylamino)-N-(4-sulfamoylphenethyl)acetamido)propanoic acid (A49). Compound **A49** was obtained according the general procedure earlier reported using N-(2-cyanoethyl)-2-(dihexylamino)-N-(4-sulfamoylphenethyl)acetamide **A33**. The obtained solid was purified by flash chromatography to give **A49** as a powder. Yield 33 %; mp >300 °C; silica gel TLC R_f 0.36 (TFA/MeOH/DCM 3/5/92% v/v). δH (400 MHz, DMSO-d6): 12.14 (brs, 1H, exchange with D_2O, COO*H*), 7.73 (d, J = 8.0 Hz, 2H, Ar-*H*), 7.40 (d, J = 8.0 Hz, 2H, Ar-*H*), 7.31 (s, 2H, exchange with D_2O, SO$_2$N*H$_2$*), 3.66 (m, 2H, C*H$_2$*), 3.48 (m, 2H, C*H$_2$*), 3.25 (s, 1.1H, C*H$_2$*), 2.99 (s, 0.9H, C*H$_2$*), 2.91 (m, 1H, C*H$_2$*), 2.79 (m, 1H, C*H$_2$*), 2.42 (m, 2H, C*H$_2$*), 2.32 (m, 2H, C*H$_2$*), 2.10 (m, 2H, C*H$_2$*), 1.30 (m, 16H, 8 x C*H$_2$*), 0.84 (m, 6H, 2 x C*H$_3$*). δC (100 MHz, DMSO-d6): 175.95, 175.28, 170.94, 170.61, 144.84, 144.49, 143.37, 143.20, 130.27, 130.11, 126.80, 126.76, 59.22, 57.99, 54.91, 54.80, 48.91, 47.61, 38.89, 35.54, 34.23, 32.27, 32.20, 27.67, 27.64, 27.52, 27.35, 25.62, 23.19, 23.14, 14.99, 14.95. ESI-HRMS (m/z) [M+H]$^+$: calculated for $C_{25}H_{44}N_3O_5S$ 498.3001; found 498.2997.

Synthesis of (Z)-3-((2-((furan-2-ylmethyl)(4-sulfamoylphenethyl)amino)-2-oxoethyl)(phenethyl)amino) -N-(octadec-9-en-1-yl)propanamide (A50). To a solution of **A46** (0.5 mmol, 1.0 eq) in DMF dry (1 mL), oleylamine (1.1 eq), EDC·HCl (1.2 eq) and DMAP (catalytic) were added and reaction mixture was stirred at r.t for 6h. The reaction was quenched with water and extracted with EtOAc (15 mL x 3). The organic layers were washed with brine (20 mL x 4), dried over Na_2SO_4, filtered-off and evaporated under *vacuum*. The obtained residue was purified by flash chromatography (3% MeOH in DCM) to give the compound **A50** as an oil. Yield 73%; silica gel TLC R_f 0.29 (TFA/MeOH/DCM 3/5/92% v/v). δH (400 MHz, DMSO-d6): 7.93 (s, 1H, exchange with D_2O, CON*H*), 7.73 (t, J = 7.2 Hz, 2H, Ar-*H*), 7.63 (s, 0.5H, Ar-*H*), 7.57 (s, 0.5H, Ar-*H*), 7.27 (m, 7H, Ar-*H*), 7.21 (s, 2H, exchange with D_2O, SO$_2$N*H$_2$*, overlap with signal at 7.27), 6.39 (m, 2H, Ar-*H*), 5.31 (m, 2H, 2 x =C*H*), 4.55 (s, 2H, C*H$_2$*) 3.48 (m, 3.1 H, 2 x C*H$_2$*), 3.21 (s, 0.9H, C*H$_2$*), 2.99 (m, 2H, C*H$_2$*), 2.73 (m, 10H, 5 x C*H$_2$*), 2.21 (m, 2H, C*H$_2$*), 1.97 (m, 4H, 2 x C*H$_2$*), 1.29 (m, 22H, 11 x C*H$_2$*), 0.83 (m, 3H, C*H$_3$*). δC (100 MHz, DMSO-d6): 171.94, 171.93, 171.89, 171.88, 170.88, 170.76, 170.75, 170.69, 152.29, 152.07, 144.44, 144.16, 143.40, 143.12, 141.47, 141.33, 131.14, 130.69, 130.34, 130.04, 129.68, 129.63, 129.23, 126.84, 126.81, 111.61,

111.57, 109.42, 109.39, 65.97, 57.81, 57.55, 56.03, 55.96, 55.41, 50.91, 50.82, 48.61, 47.91, 44.54, 39.49, 34.27, 34.20, 34.18, 33.81, 33.55, 33.52, 33.49, 32.94, 32.32, 30.17, 30.14, 30.13, 30.08, 30.05, 29.94, 29.88, 29.82, 29.73, 29.63, 29.51, 27.67, 27.61, 27.50, 23.13, 16.23, 15.00. ESI-HRMS (m/z) $[M+H]^+$: calculated for $C_{44}H_{67}N_4O_5S$ 763.4832; found 763.4826.

7.2.2 Carbonic Anhydrase Inhibition.

The CA inhibitory profiles of compounds belonging to series **A** were obtained according to the general procedures described at the beginning of the experimental section.

7.2.3 X-Ray Crystallography studies.

The experimental procedure of these studies, performed by research group of Prof. Robert McKenna from the University of Florida, is reported in Bonardi, A., et al. *J. Med. Chem.* **2020**, *63*, 7422-7444.[283]

7.2.4 Computational studies.

Computational studies, for compounds belonging to series **A**, were performed according to the general procedures described at the beginning of the experimental section (procedure **a-e**), using hCA I (PDB: 2NMX),[492] hCA II (PDB:5LJT),[276] hCA IV (PDB: 1ZNC),[62] and hCA XII (PDB: 1JD0) [30] crystal structures.

7.2.5 Hypertensive Rabbit IOP Lowering Studies.

These studies were performed by research group of Prof. Carla Ghelardini from the University of Florence.

Male New Zealand albino rabbits weighing 1500−2000 g were used in these studies. Animals were anesthetized using Zoletil (tiletamine chloride plus zolazepam chloride, 3 mg/kg body weight, im) and elevated IOP was induced by the injection of 0.05 mL of hypertonic saline solution (5% in distilled water) into the vitreous of both eyes. IOP was determined using a

pneumo-tonometer Reichert, model 30 (Reichert Inc. Depew, NY, USA) prior to hypertonic saline injection (basal), and at 1, 2, 3, and 4 hours after administration of the different drugs. Vehicle (hydroxypropylcellulose at 0.05%) or drugs were instilled immediately after the injection of hypertonic saline. Eyes were randomly assigned to different groups. Vehicle or drug (0.05 mL) was directly instilled into the conjunctive pocket at the desired doses (1−2%).[493] Four different animals were used for each tested compound. All animal manipulations were carried out according to the European Community guidelines for animal care [DL 116/92, application of the European Communities Council Directive of 24 November 1986 (86/609/EEC)]. The ethical policy of the University of Florence complies with the Guide for the Care and Use of Laboratory Animals of the US National Institutes of Health (NIH Publication no. 85-23, revised 1996; University of Florence assurance number A5278-01). Formal approval to conduct the experiments described was obtained from the Animal Subjects Review Board of the University of Florence and upon authorization of the National Ethics Committee of the Italian Ministry of Health (number 1179/2015-PR). Experiments involving animals have been reported according to ARRIVE, Animal Research: Reporting of *in Vivo* Experiments, guidelines.[494] All efforts were made to minimize animal suffering and to reduce the number of animals used.

7.3 Development of H$_2$S donors-carbonic anhydrase inhibitor hybrids for the treatment of inflammatory diseases and tumors (Series B)

7.3.1 Chemistry.

The general chemistry protocols are reported at the beginning of the experimental section.

Synthesis of Ethyl 4-isopropylbenzoate (B1). To a solution of 4-isopropylbenzoic acid (12,7 mmol, 1.0 equiv) in EtOH dry (30 mL) cooled at 0°C, SOCl$_2$ (1.8 equiv) was added dropwise and the reaction mixture was stirred to 60°C for 6h. The solvent was evaporated under vacuum and the crude was dissolved in EtOAc (40 mL) and washed with water and NaHCO$_3$ sol. (30 mL x 2). The organic layer was dried over Na$_2$SO$_4$, filtered and evaporated under vacuum. The obtained colorless oil was purified with flash

chromatography (EtOAc 20%/Hex) to give the compounds (**B1**). Yield 92 %; δH (400 MHz, DMSO-d6): 7.78 (d, J = 8.1 Hz, 2H, Ar-*H*), 7.29 (d, J = 8.2 Hz, 2H, Ar-*H*), 4.19 (q, J = 7.1 Hz, 2H, C*H*$_2$), 2.86 (hept, J = 6.9 Hz, 1H, C*H*), 1.21 (t, J = 7.1 Hz, 3H, CH$_2$C*H*$_3$), 1.11 (d, J = 6.9 Hz, 6H, CH(C*H*$_3$)$_2$). ESI-MS (m/z) [M+H]$^+$: calculated for C$_{12}$H$_{16}$O$_2$ 193.1; found 193.1.[495]

Synthesis of Ethyl 4-(3-thioxo-3H-1,2-dithiol-4-yl)benzoate (B2). Compound **B1** (10.4 mmol, 1.0 equiv) was added dropwise to stirred melted sulfur (10 equiv) at 135 °C and the reaction mixture was stirred at 220°C for 6-8h. The temperature is lowered to 135°C and, after the addiction of 20 mL of a toluene/acetone mixture (3:7), the suspension was triturated at r.t.. The solvent was evaporated under vacuum and the residue was purified with flash chromatography (EtOAc 20%/Hex) to give (**B2**) as a brown powder. Yield 75 %; δH (400 MHz, DMSO-d6): 9.26 (s, 1H, =C*H*), 8.02 (d, *J* = 8.5 Hz, 2H, Ar-*H*), 7.73 (d, *J* = 8.5 Hz, 2H, Ar-*H*), 4.34 (q, *J* = 7.1 Hz, 2H, C*H*$_2$), 1.33 (t, *J* = 7.1 Hz, 3H, C*H*$_3$). ESI-MS (m/z) [M+H]$^+$: calculated for C$_{12}$H$_{10}$O$_2$S$_3$ 282.9; found 283.0.[495]

Synthesis of 4-(3-Thioxo-3H-1,2-dithiol-4-yl)benzoic acid (B3). To a solution of **B2** (7.09 mmol, 1.0 equiv) in acetic acid (50 mL), was added H$_2$SO$_4$ 9M (16 mL) and the reaction mixture was stirred at 100°C for 4h. After cooling at r.t. and adding slush, the mixture was extracted with MeOH 10%/DCM (40 ml x 3) and washed with HCl 0,1M (1 x 30 mL). The organic layer was dried over Na$_2$SO$_4$, filtered and evaporated under vacuum. The obtained residue was triturated with Et$_2$O, collected by filtration and purified with flash chromatography (EtOAc 50%/Hex) to give the compounds (**B3**) as a brown-orange powder. Yield 81 %; m.p. 235-236 °C; δH (400 MHz, DMSO-d6): 12.94 (bs, 1H, exchange with D$_2$O, COO*H*), 9.25 (s, 1H, =C*H*), 8.00 (d, *J* = 8.3 Hz, 2H, Ar-*H*), 7.71 (d, *J* = 8.2 Hz, 2H, Ar-*H*). ESI-MS (m/z) [M+H]$^+$: calculated for C$_{10}$H$_6$O$_2$S3 254.9; found 255.0.[495]

General Synthetic Procedures for preparation of 4-(2-(arylalkyl)amino)ethyl)benzenesulfonamides (A1-3, A6, A7, B4-13). *Procedure 1.* To a solution of 4-(2-aminoethyl)benzenesulfonamide (9.99 mmol, 1.0 equiv) in dry MeOH (40

mL), the appropriate aldehyde (1.1 equiv) was added and the mixture was heated at reflux temperature under stirring for 0.5-4h. Sodium borohydride (1.6 equiv) was added portion-wise at 0°C and the reaction mixture was stirred at reflux temperature for 0.5-3 h. The solvent was evaporated under *vacuum*, and water was added (25 mL). pH was taken to 7 with HCl 1M. The suspension was filtered, and the collected powder was purified with flash silica chromatography (5% MeOH in DCM) to give compounds **A1-3**, and **B4-13**.

Procedure 2. To a solution of 4-(2-aminoethyl)benzenesulfonamide (9.99 mmol, 1.0 equiv) in dry DMF (5 mL), triethylamine (1.2 equiv) and the appropriate halide (1.1 equiv) were added at room temperature and the mixture was stirred at room temperature for 0.5 h (**A6**) or 60°C for 8 h (**A7**). The reaction mixture was quenched by the addition of water (20 mL) and extracted with DCM (30 mL x 3). The organic layer was collected, washed with brine (40 mL x 3), dried over Na_2SO_4, filtered and evaporated under *vacuum* to give compounds **A6-7** as powders.

4-(2-((4-Chlorobenzyl)amino)ethyl)benzenesulfonamide (B4). Compound **B4** was obtained as a white powder according the general procedure 1 earlier reported using 4-chlorobenzaldehyde (1.1 equiv). Yield 91%; mp 152-154 °C. δH (400 MHz, DMSO-d6): 7.73 (d, J = 7.7 Hz, 2H, Ar-*H*), 7.39 (d, J = 7.9 Hz, 2H, Ar-*H*), 7.36 (s, 4H, Ar-*H*), 7.28 (s, 2H, exchange with D_2O, SO_2NH_2), 3.76 (s, 2H, C*H*$_2$), 2.80 (m, 4H, 2 x C*H*$_2$). δC (100 MHz, DMSO-d6): 145.30, 142.84, 139.65, 132.31, 130.96, 129.99, 129.03, 126.60, 52.47, 50.38, 35.87. ESI-MS (m/z) $[M+H]^+$: calculated for $C_{15}H_{17}ClN_2O_2S$ 325.0; found 325.0.

4-(2-((4-Bromobenzyl)amino)ethyl)benzenesulfonamide (B5). Compound **B5** was obtained as a white powder according the general procedure 1 earlier reported using 4-bromobenzaldehyde (1.1 equiv). Yield 87%; mp 163-165 °C. δH (400 MHz, DMSO-d6): 7.80 (d, J = 8.1 Hz, 2H, Ar-*H*), 7.62 (d, J = 8.2 Hz, 2H, Ar-*H*), 7.47 (m, 4H, Ar-*H*), 7.37 (s, 2H, exchange with D_2O, SO_2NH_2), 4.02 (s, 2H, C*H*$_2$), 3.03 (s, 4H, 2 x C*H*$_2$). δC (100 MHz, DMSO-d6): 143.70, 143.38, 135.48, 132.73, 132.50, 130.30, 127.00, 122.54, 51.41, 49.24, 33.77. ESI-MS (m/z) $[M+H]^+$: calculated for $C_{15}H_{17}BrN_2O_2S$ 369.0; found 369.0.

4-(2-((4-Cyanobenzyl)amino)ethyl)benzenesulfonamide (B6). Compound **B6** was obtained as a white powder according the general procedure 1 earlier reported using 4-cyanobenzaldehyde (1.1 equiv). Yield 94%; mp 149-151 °C. δH (400 MHz, DMSO-d6): 7.75 (d, J = 8.1 Hz, 2H, Ar-*H*), 7.71 (d, J = 8.1 Hz, 2H, Ar-*H*), 7.49 (d, J = 8.0 Hz, 2H, Ar-*H*), 7.37 (d, J = 8.2 Hz, 2H, Ar-*H*), 7.29 (s, 2H, exchange with D_2O, SO_2NH_2), 3.79 (s, 2H, C*H*$_2$), 2.76 (m, 4H, 2 x C*H*$_2$), 2.32 (bs, 1H, exchange with D_2O, N*H*). δC (100 MHz, DMSO-d6): 148.09, 145.61, 143.17, 133.06, 130.03, 129.75, 126.60, 120.08, 110.25, 53.24, 50.93, 36.54. ESI-MS (m/z) [M+H]$^+$: calculated for $C_{16}H_{17}N_3O_2S$ 316.1; found 316.1.

4-(2-((4-(Dimethylamino)benzyl)amino)ethyl)benzenesulfonamide (B7). Compound **B7** was obtained as a white powder according the general procedure 1 earlier reported using 4-(dimethylamino)benzaldehyde (1.1 equiv). Yield 92%; mp 146-148 °C.δH (400 MHz, DMSO-d6): 7.76 (d, J = 8.2 Hz, 2H, Ar-*H*), 7.42 (d, J = 8.2 Hz, 2H, Ar-*H*), 7.35 (s, 2H, exchange with D_2O, SO_2NH_2), 7.28 (d, J = 8.5 Hz, 2H, Ar-*H*), 6.70 (d, J = 8.6 Hz, 2H, Ar-*H*), 3.91 (s, 2H, C*H*$_2$), 2.99 (s, 4H, 2 x C*H*$_2$), 2.88 (s, 6H, 2 x C*H*$_3$). δC (100 MHz, DMSO-d6): 151.33, 143.40, 143.26, 131.57, 130.04, 126.86, 121.66, 112.98, 51.26, 48.22, 40.99, 33.06. ESI-MS (m/z) [M+H]$^+$: calculated for $C_{17}H_{23}N_3O_2S$ 334.1; found 334.2.

4-(2-((2-Methoxy-4-nitrobenzyl)amino)ethyl)benzenesulfonamide (B8). Compound **B8** was obtained as a white powder according the general procedure 1 earlier reported using 2-methoxy-4-nitrobenzaldehyde (1.1 equiv). Yield 79%; mp 141-143 °C. δH (400 MHz, DMSO-d6): 7.83 (dd, *J* = 8.3, 2.1 Hz, 1H, Ar-*H*), 7.73 (m, 3H, Ar-*H*), 7.59 (d, *J* = 8.3 Hz, 1H, Ar-*H*), 7.41 (d, *J* = 8.3 Hz, 2H, Ar-*H*), 7.30 (s, 2H, exchange with D_2O, SO_2NH_2), 3.90 (s, 3H, C*H*$_3$), 3.86 (s, 2H, C*H*$_2$), 2.85 (s, 4H, 2 x C*H*$_2$). δC (100 MHz, DMSO-d6): 158.31, 148.56, 145.02, 142.96, 136.08, 130.50, 130.06, 126.66, 116.32, 106.04, 57.04, 50.48, 47.42, 35.60. ESI-MS (m/z) [M+H]$^+$: calculated for $C_{16}H_{19}N_3O_5S$ 366.1; found 366.1.

4-(2-((4-Methoxybenzyl)amino)ethyl)benzenesulfonamide (B9). Compound **B9** was obtained as a white powder according the general procedure 1 earlier reported using 4-methoxybenzaldehyde (1.1 equiv). Yield 81%; mp 136-138 °C. δH (400 MHz, DMSO-d6):

7.72 (d, J = 8.1 Hz, 2H, Ar-*H*), 7.38 (d, J = 8.1 Hz, 2H, Ar-*H*), 7.26 (s, 2H, exchange with D$_2$O, SO$_2$N*H*$_2$), 7.21 (d, J = 7.6 Hz, 2H, Ar-*H*), 6.85 (d, J = 7.6 Hz, 2H, Ar-*H*), 3.72 (s, 3H, OC*H*$_3$), 3.64 (s, 2H, C*H*$_2$), 2.76 (m, 4H, 2 x C*H*$_2$). δC (100 MHz, DMSO-d6): 159.02, 145.79, 142.73, 133.41, 130.11, 129.99, 126.57, 114.46, 55.94, 53.08, 50.69, 36.35. ESI-MS (m/z) [M+H]$^+$: calculated for C$_{16}$H$_{20}$N$_3$O$_3$S 321.1; found 321.1.

4-(2-((3,4-Dimethoxybenzyl)amino)ethyl)benzenesulfonamide (B10). Compound **B10** was obtained as a white powder according the general procedure 1 earlier reported using 3,4-dimethoxybenzaldehyde (1.1 equiv). Yield 86%; mp 129-131 °C. δH (400 MHz, DMSO-d6): 7.74 (d, J = 8.1 Hz, 2H, Ar-*H*), 7.41 (d, J = 8.1 Hz, 2H, Ar-*H*), 7.29 (s, 2H, exchange with D$_2$O, SO$_2$N*H*$_2$), 7.04 s, 1H, Ar-*H*), 6,89 (s, 2H, Ar-*H*), 3.81 (s, 2H, C*H*$_2$), 3.73 (s, 6H, 2 x OC*H*$_3$), 2.89 (s, 4H, 2 x C*H*$_2$). δC (100 MHz, DMSO-d6): 149.65, 149.24, 144.62, 143.08, 130.58, 130.17, 126.80, 122.09, 113.54, 112.57, 56.57, 56.51, 52.52, 49.63, 34.78. ESI-MS (m/z) [M+H]$^+$: calculated for C$_{17}$H$_{22}$N$_2$O$_4$S 351.1; found 351.1.

4-(2-((4-(Methylthio)benzyl)amino)ethyl)benzenesulfonamide (B11). Compound **B11** was obtained as a white powder according the general procedure 1 earlier reported using 4-(methylthio)benzaldehyde (1.1 equiv). Yield 87%; mp 154-156 °C. δH (400 MHz, DMSO-d6): 7.77 (d, J = 8.2 Hz, 2H, Ar-*H*), 7.44 (m, 4H, Ar-*H*), 7.33 (s, 2H, exchange with D$_2$O, SO$_2$N*H*$_2$), 7.29 (d, J = 8.3 Hz, 2H, Ar-*H*), 4.05 (s, 2H, C*H*$_2$), 3.06 (m, 4H, 2 x C*H*$_2$), 2.48 (s, 3H, SC*H*$_3$). δC (100 MHz, DMSO-d6): 143.55, 143.03, 139.97, 131.54, 130.65, 130.27, 127.04, 126.87, 51.09, 48.54, 32.89, 15.64. ESI-MS (m/z) [M+H]$^+$: calculated for C$_{16}$H$_{20}$N$_2$O$_2$S$_2$ 337.0; found 327.1.

4-(2-((Naphthalen-1-ylmethyl)amino)ethyl)benzenesulfonamide (B12). Compound **B12** was obtained as a white powder according the general procedure 1 earlier reported using 4-bromobenzaldehyde (1.1 equiv). Yield 86%; mp 180-182 °C C. δH (400 MHz, DMSO-d6): 8.18 (m, 1H, Ar-*H*), 7.94 (m, 1H, Ar-*H*), 7.84 (d, J = 8.0 Hz, 1H, Ar-*H*), 7.77 (d, J = 8.1 Hz, 2H, Ar-*H*), 7.52 (m, 6H, Ar-*H*), 7.31 (s, 2H, exchange with D$_2$O, SO$_2$N*H*$_2$), 4.20 (s, 2H, C*H*$_2$), 2.89 (s, 4H, 2 x C*H*$_2$), 2.13 (bs, 1H, exchange with D$_2$O, N*H*). δC (100 MHz, DMSO-d6):

145.89, 142.75, 137.29, 134.32, 132.45, 130.03, 129.28, 128.12, 126.76, 126.64, 126.58, 126.52, 126.32, 125.04, 51.56, 51.43, 36.51. ESI-MS (m/z) [M+H]$^+$: calculated for C$_{19}$H$_{20}$N$_2$O$_2$S 341.1; found 341.1.

4-(2-((Benzo[b]thiophen-3-ylmethyl)amino)ethyl)benzenesulfonamide (B13). Compound **B13** was obtained as a white powder according the general procedure 1 earlier reported using 4-bromobenzaldehyde (1.1 equiv). Yield 90%; mp 177-179 °C. δH (400 MHz, DMSO-d6): 7.98 (d, J = 7.4 Hz, 2H, Ar-*H*), 7.92 (d, J = 7.2 Hz, 2H, Ar-*H*), 7.74 (d, J = 7.9 Hz, 2H, Ar-*H*), 7.68 (s, 1H, Ar-*H*), 7.40 (m, 4H, Ar-*H*), 7.31 (s, 2H, exchange with D$_2$O, SO$_2$N*H*$_2$), 4.11 (s, 2H, C*H*$_2$), 2.94 (m, 4H, 2 x C*H*$_2$). δC (100 MHz, DMSO-d6): 144.77, 143.00, 140.73, 139.09, 134.05, 130.05, 126.69, 126.03, 125.43, 125.02, 123.79, 123.18, 50.30, 46.48, 35.10. ESI-MS (m/z) [M+H]$^+$: calculated for C$_{17}$H$_{18}$N$_2$O$_2$S$_2$ 347.0; found 347.1.

General synthetic procedure for preparation of H$_2$S releaser-CAI hybrids B14-B28. To a solution of **B3** (0.98 mmol, 1.0 equiv) in DMF dry (1 mL), was added the appropriate secondary amine (0.98 equiv), DIPEA (2.2 equiv) and PyBOP (1.1 equiv), and the reaction mixture was stirred o.n. at room temperature. The reaction was quenched with water and the formed precipitate was collected by filtration, washed with NaHCO$_3$ sol. and water. The obtained residue was purified with flash chromatography (MeOH 1%/DCM) to give the compounds **x, y, z**.

N-Benzyl-N-(4-sulfamoylphenethyl)-4-(3-thioxo-3H-1,2-dithiol-4-yl)benzamide (B14). Compound **B14** was obtained as orange powder according the general procedure earlier reported using **A1** (1.1 equiv). Yield 56 %; m.p. 139-140 °C. (400 MHz, DMSO-d6): 9.20 (s, 1H, =C*H*), 7.43 (m, 13H, Ar-*H*), 7.30 (s, 2H, exchange with D$_2$O, SO$_2$N*H*$_2$, overlap with signal at 7.43), 4.80 (s, 1.1H, C*H*$_2$), 4.43 (s, 0.9H, C*H*$_2$), 3.59 (m, 1H, C*H*$_2$), 3.34 (m, 1H, C*H*$_2$), 2.98 (m, 1H, C*H*$_2$), 2.85 (m, 1H, C*H*$_2$). δC (100 MHz, DMSO-d6): 214.15, 214.00, 171.07, 170.97, 160.26, 160.10, 147.79, 147.58, 143.78, 142.85, 142.78, 138.18, 137.30, 136.85, 134.85, 134.67, 129.70, 129.41, 129.25, 129.11, 128.10, 127.67, 127.45, 126.73,

126.58, 126.27, 52.56, 50.19, 47.35, 45.88, 34.18, 32.92. ESI-MS (m/z) [M+H]$^+$: calculated for $C_{25}H_{22}N_2O_3S_4$ 527.0; found 527.0.

N-(4-Nitrobenzyl)-N-(4-sulfamoylphenethyl)-4-(3-thioxo-3H-1,2-dithiol-4-yl)benzamide (B15). Compound **B15** was obtained as yellow powder according the general procedure earlier reported using **A2** (1.1 equiv). Yield 57 %; m.p. 223-224 °C. δH (400 MHz, DMSO-d6): 9.22 (s, 1H, =C*H*), 8.25 (d, *J* = 7.7 Hz, 2H, Ar-*H*), 7.56 (m, 7H, Ar-*H*), 7.30 (s, 2H, exchange with D$_2$O, SO$_2$N*H$_2$*, overlap with signal at 7.56), 7.12 (d, *J* = 7.3 Hz, 2H, Ar-*H*), 4.91 (s, 1.3H, C*H$_2$*), 4.60 (s, 0.7H, C*H$_2$*), 3.62 (m, 1H, C*H$_2$*), 3.13 (m, 1H, C*H$_2$*), 3.02 (m, 1H, C*H$_2$*), 2.88 (m, 1H, C*H$_2$*). δC (100 MHz, DMSO-d6): 214.15, 213.93, 171.29, 160.13, 147.76, 147.30, 147.15, 146.52, 143.26, 142.81, 142.44, 136.53, 136.43, 134.96, 134.87, 129.73, 129.42, 129.01, 128.66, 127.08, 126.65, 126.27, 124.18, 123.79, 52.16, 50.91, 47.52, 46.49, 34.30, 32.93. ESI-MS (m/z) [M+H]$^+$: calculated for $C_{25}H_{21}N_3O_5S_4$ 572.0; found 572.0.

N-(4-Fluorobenzyl)-N-(4-sulfamoylphenethyl)-4-(3-thioxo-3H-1,2-dithiol-4-yl)benzamide (B16). Compound **B16** was obtained as orange powder according the general procedure earlier reported using **A3** (1.1 equiv). Yield 59 %; m.p. 158-159 °C. δH (400 MHz, DMSO-d6): 9.21 (s, 1H, =C*H*), 7.44 (m, 12H, Ar-*H*), 7.29 (s, 2H, exchange with D$_2$O, SO$_2$N*H$_2$*, overlap with signal at 7.47), 4.77 (s, 1.1H, C*H$_2$*), 4.41 (s, 0.9H, C*H$_2$*), 3.58 (m, 1H, C*H$_2$*), 3.34 (m, 1H, C*H$_2$*), 2.98 (m, 1H, C*H$_2$*), 2.85 (m, 1H, C*H$_2$*). δF (376 MHz, DMSO-d6): -115.56 (s, 1F). δC (100 MHz, DMSO-d6): 214.16, 214.12, 171.11, 170.94, 160.21, 160.11, 148.62, 147.73, 147.57, 146.90, 144.76, 143.76, 142.79, 141.22, 139.78, 138.15, 136.76, 134.71, 134.43, 130.17, 130.04, 129.70, 129.41, 126.69, 126.60, 126.26, 51.85, 50.14, 46.69, 45.87, 34.19, 32.96.. ESI-MS (m/z) [M+H]$^+$: calculated for $C_{25}H_{21}FN_2O_3S_4$ 545.0; found 545.0.

N-(4-Chlorobenzyl)-N-(4-sulfamoylphenethyl)-4-(3-thioxo-3H-1,2-dithiol-4-yl)benzamide (B17). Compound **B17** was obtained as orange powder according the general procedure earlier reported using **B4** (1.1 equiv). Yield 61 %; m.p. 104-105 °C. δH (400 MHz, DMSO-d6): 9.21 (s, 1H, =C*H*), 7.42 (m, 12H, Ar-*H*), 7.30 (s, 2H, exchange with D$_2$O,

SO$_2$N*H$_2$*, overlap with signal at 7.42), 4.74 (s, 1.1H, C*H$_2$*), 4.41 (s, 0.9H, C*H$_2$*), 3.57 (m, 1H, C*H$_2$*), 3.34 (m, 1H, C*H$_2$*), 2.98 (m, 1.1H, C*H$_2$*), 2.85 (m, 0.9H, C*H$_2$*). δC (100 MHz, DMSO-d6): 214.04, 213.96, 171.18, 160.02, 147.81, 147.55, 143.73, 142.80, 137.29, 136.67, 136.39, 134.99, 134.75, 132.59, 132.31, 130.02, 129.74, 129.43, 129.19, 129.05, 126.63, 126.31, 51.89, 50.34, 46.93, 46.01, 34.18, 32.97. ESI-MS (m/z) [M+H]$^+$: calculated for C$_{25}$H$_{21}$ClN$_2$O$_3$S$_4$ 561.0; found 561.0.

N-(4-Bromobenzyl)-N-(4-sulfamoylphenethyl)-4-(3-thioxo-3H-1,2-dithiol-4-yl)benzamide (B18). Compound **B18** was obtained as orange powder according the general procedure earlier reported using **B5** (1.1 equiv). Yield 58 %; m.p. 65-66 °C. δH (400 MHz, DMSO-d6): 9.21 (s, 1H, =C*H*), 7.40 (m, 12H, Ar-*H*), 7.30 (s, 2H, exchange with D$_2$O, SO$_2$N*H$_2$*, overlap with signal at 7.40), 4.75 (s, 1.2H, C*H$_2$*), 4.41 (s, 0.8H, C*H$_2$*), 3.57 (m, 1H, C*H$_2$*), 3.34 (m, 1H, C*H$_2$*), 2.99 (m, 1H, C*H$_2$*), 2.85 (m, 1H, C*H$_2$*). δC (100 MHz, DMSO-d6): 214.13, 213.98, 171.14, 160.07, 147.77, 147.55, 143.69, 143.65, 142.80, 137.76, 137.59, 136.78, 136.67, 134.94, 134.75, 132.10, 131.95, 130.39, 129.72, 129.42, 126.62, 126.29, 121.07, 120.74, 51.97, 50.38, 49.38, 46.96, 46.01, 34.26, 34.03, 32.93. ESI-MS (m/z) [M+H]$^+$: calculated for C$_{25}$H$_{21}$BrN$_2$O$_3$S$_4$ 603.9; found 604.0.

N-(4-Cyanobenzyl)-N-(4-sulfamoylphenethyl)-4-(3-thioxo-3H-1,2-dithiol-4-yl)benzamide (B19). Compound **B19** was obtained as orange powder according the general procedure earlier reported using **B6** (1.1 equiv). Yield 55 %; m.p. 251-252 °C. δH (400 MHz, DMSO-d6): 9.22 (s, 1H, =C*H*), 7.50 (m, 12H, Ar-*H*), 7.30 (s, 2H, exchange with D$_2$O, SO$_2$N*H$_2$*, overlap with signal at 7.50), 4.87 (s, 1.3H, C*H$_2$*), 4.54 (s, 0.7H, C*H$_2$*), 3.60 (m, 1H, C*H$_2$*), 3.40 (m, 1H, C*H$_2$*), 3.01 (m, 1H, C*H$_2$*), 2.87 (m, 1H, C*H$_2$*). δC (100 MHz, DMSO-d6): 214.73, 214.51, 171.89, 171.77, 160.85, 160.67, 148.34, 148.13, 144.90, 143.39, 143.34, 137.05, 135.41, 133.75, 133.58, 130.33, 130.02, 129.38, 129.02, 128.89, 127.26, 126.88, 119.96, 119.76, 111.31, 110.95, 52.94, 51.47, 48.30, 46.90, 34.88, 33.54. ESI-MS (m/z) [M+H]$^+$: calculated for C$_{26}$H$_{21}$N$_3$O$_3$S$_4$ 552.0; found 552.0.

N-(4-(dimethylamino)benzyl)-N-(4-sulfamoylphenethyl)-4-(3-thioxo-3H-1,2-dithiol-4-yl)benzamide (B20). Compound **B20** was obtained as orange powder according the general procedure earlier reported using **B7** (1.1 equiv). Yield 57 %; m.p. 185-186 °C. δH (400 MHz, DMSO-d6): 9.20 (s, 1H, =CH), 7.38 (m, 10H, Ar-H), 7.30 (s, 2H, exchange with D_2O, SO$_2$NH_2, overlap with signal at 7.38), 6.56 (m, 2H, Ar-H), 4.66 (s, 1H, CH_2), 4.28 (s, 1H, CH_2), 3.61 (s, 1H, CH_2), 3.53 (s, 1H, CH_2), 3.29 (m, 1H, CH_2), 3.14 (m, 1H, CH_2), 2.88 (m, 6H, 2 x CH_3). δC (100 MHz, DMSO-d6): 214.12, 214.03, 170.89, 170.69, 160.21, 160.04, 150.32, 150.25, 147.80, 147.61, 143.86, 142.98, 142.70, 137.09, 134.74, 134.53, 129.82, 129.41, 128.51, 126.86, 126.47, 126.27, 125.27, 123.99, 113.00, 52.07, 49.48, 46.55, 45.31, 40.67, 34.10, 32.95. ESI-MS (m/z) [M+H]$^+$: calculated for $C_{27}H_{27}N_3O_3S_4$ 570.0; found 570.0.

N-(2-methoxy-4-nitrobenzyl)-N-(4-sulfamoylphenethyl)-4-(3-thioxo-3H-1,2-dithiol-4-yl)benzamide (B21). Compound **B21** was obtained as orange powder according the general procedure earlier reported using **B8** (1.1 equiv). Yield 58 %; m.p. 190-191 °C. δH (400 MHz, DMSO-d6): 9.22 (s, 1H, =CH), 8.25 (d, J = 7.7 Hz, 2H, Ar-H), 7.56 (m, 11H, Ar-H), 7.29 (s, 2H, exchange with D_2O, SO$_2$NH_2, overlap with signal at 7.56), 4.78 (s, 1.2H, CH_2), 4.46 (s, 0.8H, CH_2), 4.04 (s, 1.7H, OCH_3), 3.82 (s, 1.3H, OCH_3), 3.61 (m, 1H, CH_2), 3.46 (m, 1H, CH_2), 2.99 (m, 1H, CH_2), 2.88 (m, 1H, CH_2). δC (100 MHz, DMSO-d6): 214.23, 214.04, 171.18, 160.24, 160.08, 157.66, 148.46, 148.09, 142.76, 136.78, 136.55, 134.86, 133.99, 133.18, 129.71, 129.36, 128.51, 126.67, 126.24, 116.15, 105.83, 56.70, 56.58, 51.11, 48.50, 46.59, 43.56, 34.49, 33.01. ESI-MS (m/z) [M+H]$^+$: calculated for $C_{26}H_{23}N_3O_6S_4$ 602.0; found 602.0.

N-(4-Methoxybenzyl)-N-(4-sulfamoylphenethyl)-4-(3-thioxo-3H-1,2-dithiol-4-yl)benzamide (B22). Compound **B22** was obtained as orange powder according the general procedure earlier reported using **B9** (1.1 equiv). Yield 64 %; m.p. 151-152 °C. δH (400 MHz, DMSO-d6): 9.20 (s, 1H, =CH), 7.33 (m, 12H, Ar-H), 7.31 (s, 2H, exchange with D_2O, SO$_2$NH_2, overlap with signal at 7.33), 4.71 (s, 1.1H, CH_2), 4.34 (s, 0.9H, CH_2), 3.74 (s, 3H, CH_3), 3.53 (s, 1H, CH_2), 3.34 (s, 1H, CH_2), 2.95 (s, 1H, CH_2), 2.83 (s, 1H, CH_2). δC (100 MHz, DMSO-d6): 214.14, 213.99, 170.97, 170.81, 160.20, 160.07, 159.13, 158.99, 147.84,

147.61, 143.83, 142.92, 142.77, 136.94, 134.84, 134.61, 129.71, 129.42, 128.87, 126.76, 126.53, 126.27, 114.63, 114.51, 55.56, 51.98, 49.81, 46.64, 45.55, 34.13, 32.94. ESI-MS (m/z) [M+H]$^+$: calculated for $C_{26}H_{24}N_2O_4S_4$ 557.0; found 557.0.

N-(3,4-Dimethoxybenzyl)-N-(4-sulfamoylphenethyl)-4-(3-thioxo-3H-1,2-dithiol-4-yl)benzamide (B23). Compound **B23** was obtained as orange powder according the general procedure earlier reported using **B10** (1.1 equiv). Yield 60 %; m.p. 183-184 °C. δH (400 MHz, DMSO-d6): 9.20 (s, 1H, =C*H*), 7.69 (m, 4H, Ar-*H*), 7.33 (m, 3H, Ar-*H*), 7.30 (s, 2H, exchange with D$_2$O, SO$_2$N*H$_2$*, overlap with signal at 7.33), 7.03 (m, 3H, Ar-*H*), 6.71 (m, 1H, Ar-*H*), 4.71 (s, 1.1H, C*H$_2$*), 4.35 (s, 0.9H, C*H$_2$*), 3.58 (m, 1H, C*H$_2$*), 3.35 (m, 1H, C*H$_2$*), 3.32 (s, 3H, C*H$_3$*), 3.30 (s, 3H, C*H$_3$*), 2.97 (m, 1H, C*H$_2$*), 2.83 (m, 1H, C*H$_2$*). δC (100 MHz, DMSO-d6): 214.14, 213.93, 170.99, 170.79, 160.24, 160.06, 149.33, 148.54, 147.79, 147.58, 146.10, 145.42, 143.84, 142.93, 142.73, 138.11, 136.94, 134.79, 134.59, 131.10, 130.45, 129.68, 129.59, 129.52, 129.40, 126.80, 126.50, 126.24, 112.32, 112.15, 55.96, 55.91, 52.22, 49.80, 46.91, 45.68, 39.95, 34.09, 32.98. ESI-MS (m/z) [M+H]$^+$: calculated for $C_{27}H_{26}N_2O_5S_4$ 587.0; found 587.0.

N-(4-(Methylthio)benzyl)-N-(4-sulfamoylphenethyl)-4-(3-thioxo-3H-1,2-dithiol-4-yl)benzamide (B24). Compound **B24** was obtained as orange powder according the general procedure earlier reported using **B11** (1.1 equiv). Yield 58 %; m.p. 161-162 °C. δH (400 MHz, DMSO-d6): 9.21 (s, 1H, =C*H*), 7.68 (m, 4H, Ar-*H*), 7.31 (m, 8H, Ar-*H*), 7.30 (s, 2H, exchange with D$_2$O, SO$_2$N*H$_2$*, overlap with signal at 7.31), 4.74 (s, 1.2H, C*H$_2$*), 4.38 (s, 0.8H, C*H$_2$*), 3.56 (m, 1H, C*H$_2$*), 3.38 (m, 1H, C*H$_2$*), 2.98 (m, 1H, C*H$_2$*), 2.85 (m, 1H, C*H$_2$*), 2.48 (s, 3H, C*H$_3$*). δC (100 MHz, DMSO-d6): 214.13, 214.00, 171.03, 170.94, 160.26, 160.10, 147.78, 147.57, 143.75, 143.69, 142.86, 142.79, 137.85, 137.37, 136.82, 134.86, 134.66, 133.78, 129.71, 129.42, 128.93, 128.11, 126.70, 126.56, 126.27, 52.11, 50.09, 46.88, 45.76, 34.14, 32.96, 15.25, 15.16. ESI-MS (m/z) [M+H]$^+$: calculated for $C_{26}H_{24}N_2O_3S_5$ 573.0; found 573.0.

N-(Naphthalen-1-ylmethyl)-N-(4-sulfamoylphenethyl)-4-(3-thioxo-3H-1,2-dithiol-4-yl)benzamide (B25). Compound **B25** was obtained as orange powder according the general procedure earlier reported using **B12** (1.1 equiv). Yield 56 %; m.p. 116-117 °C. δH (400 MHz, DMSO-d6): 9.21 (s, 1H, =CH), 9.14 (s, 1H, =CH), 8.17 (d, J = 7.9 Hz, 1H, Ar-H), 7.96 (m, 2H, Ar-H), 7.53 (m, 11H, Ar-H), 7.30 (s, 2H, exchange with D$_2$O, SO$_2$NH_2, overlap with signal at 7.53), 7.07 (d, J = 7.8 Hz, 1H, Ar-H), 5.28 (s, 1.3H, CH_2), 4.96 (s, 0.7H, CH_2), 3.65 (m, 1H, CH_2), 3.35 (m, 1H, CH_2), 3.02 (m, 1H, CH_2), 2.83 (m, 2H, CH_2). δC (100 MHz, DMSO-d6): 214.15, 213.92, 171.08, 170.91, 160.20, 159.98, 147.83, 147.43, 143.83, 142.81, 136.83, 136.70, 135.08, 134.70, 133.97, 133.82, 133.01, 132.79, 131.96, 131.62, 130.87, 129.72, 129.43, 129.20, 128.51, 128.39, 126.97, 126.54, 126.41, 126.28, 126.06, 124.46, 123.84, 123.18, 50.68, 49.67, 46.87, 45.23, 34.00, 33.18. ESI-MS (m/z) [M+H]$^+$: calculated for C$_{29}$H$_{24}$N$_2$O$_3$S$_4$ 577.0; found 577.0.

N-(benzo[b]thiophen-3-ylmethyl)-N-(4-sulfamoylphenethyl)-4-(3-thioxo-3H-1,2-dithiol-4-yl)benzamide (B26). Compound **B26** was obtained as orange powder according the general procedure earlier reported using **B13** (1.1 equiv). Yield 51 %; m.p. 113-114 °C. δH (400 MHz, DMSO-d6): 9.20 (s, 1H, =CH), 8.00 (m, 2H, Ar-H), 7.52 (m, 10H, Ar-H), 7.30 (s, 2H, exchange with D$_2$O, SO$_2$NH_2, overlap with signal at 7.52), 7.08 (d, J = 7.8 Hz, 1H, Ar-H), 5.07 (s, 1.3H, CH_2), 4.69 (s, 0.7H, CH_2), 3.67 (m, 1H, CH_2), 3.34 (m, 1H, CH_2), 3.00 (m, 1H, CH_2), 2.84 (m, 1H, CH_2). δC (100 MHz, DMSO-d6): 214.15, 213.98, 170.88, 170.27, 160.03, 142.80, 142.07, 140.47, 138.33, 136.78, 136.42, 134.68, 133.20, 132.41, 132.22, 129.67, 129.58, 129.50, 129.38, 126.78, 126.50, 126.26, 125.16, 124.87, 123.59, 123.43, 123.12, 122.30, 49.60, 47.92, 43.74, 41.60, 34.45, 33.10. ESI-MS (m/z) [M+H]$^+$: calculated for C$_{27}$H$_{22}$N$_2$O$_3$S$_5$ 583.0; found 583.0.

N-(2-cyanoethyl)-N-(4-sulfamoylphenethyl)-4-(3-thioxo-3H-1,2-dithiol-4-yl)benzamide (B27). Compound **B27** was obtained as orange powder according the general procedure earlier reported using **A6** (1.1 equiv). Yield 54 %; m.p. 154-155 °C. δH (400 MHz, DMSO-d6): 9.25 (s, 1H, =CH), 7.50 (m, 8H, Ar-H), 7.26 (s, 2H, exchange with D$_2$O, SO$_2$NH_2, overlap with signal at 7.50), 3.79 (m, 4H, 2 x CH_2), 2.96 (m, 4H, 2 x CH_2). δC (100 MHz,

DMSO-d6): 214.12, 213.99, 171.19, 170.88, 160.36, 160.09, 147.78, 147.51, 142.98, 142.79, 142.18, 141.73, 136.66, 136.52, 134.95, 134.84, 133.00, 129.77, 129.41, 128.96, 128.38, 127.66, 126.96, 126.57, 126.25, 119.55, 119.39, 50.59, 49.71, 45.17, 42.27, 34.41, 33.35, 16.11, 16.02. ESI-MS (m/z) [M+H]$^+$: calculated for $C_{21}H_{19}N_3O_3S_4$ 490.0; found 490.0.

N-phenethyl-N-(4-sulfamoylphenethyl)-4-(3-thioxo-3H-1,2-dithiol-4-yl)benzamide (B28). Compound **B28** was obtained as orange powder according the general procedure earlier reported using **A7** (1.1 equiv). Yield 59 %; m.p. 228-229 °C. δH (400 MHz, DMSO-d6): 9.20 (s, 1H, =CH), 7.42 (m, 13H, Ar-H), 7.31 (s, 2H, exchange with D_2O, SO_2NH_2, overlap with signal at 7.42), 3.73 (m, 2H, CH_2), 3.48 (m, 2H, CH_2), 2.86 (m, 4H, 2 x CH_2). δC (100 MHz, DMSO-d6): 214.16, 170.73, 160.09, 147.88, 147.27, 146.74, 146.26, 143.92, 143.00, 142.73, 139.74, 138.74, 137.54, 137.32, 136.14, 134.47, 129.82, 129.71, 129.29, 129.16, 128.87, 127.34, 126.77, 126.43, 126.21, 52.35, 50.61, 46.36, 46.32, 34.54, 33.36, 26.43, 26.35. ESI-MS (m/z) [M+H]$^+$: calculated for $C_{26}H_{24}N_2O_3S_4$ 541.0; found 541.0.

7.3.2 Carbonic Anhydrase Inhibition.

The CA inhibitory profiles of compounds belonging to series **B** were obtained according to the general procedures described at the beginning of the experimental section.

7.3.3 Pain Relief Efficacy Tests

These studies were performed by research group of Prof. Carla Ghelardini from the University of Florence.

Animals. Sprague Dawley rats (Harlan, Varese, Italy) weighing 200-250 g at the beginning of the experimental procedure were used. Animals were housed in the Centro Stabulazione Animali da Laboratorio (University of Florence) and used at least 1 week after their arrival. Four rats were housed per cage (size 26 cm × 41 cm); animals were fed a standard laboratory diet and tap water ad libitum and kept at 23 ± 1 °C with a 12 h light/dark cycle (light at 7 a.m.). All animal manipulations were carried out according to the European Community

guidelines for animal care [DL 116/92, application of the European Communities Council Directive of November 24th 1986 (86/609/EEC)]. The ethical policy of the University of Florence complies with the Guide for the Care and Use of Laboratory Animals of the US National Institutes of Health (NIH Publication No. 85-23, revised 1996; University of Florence assurance number A5278-01). Formal approval to conduct the experiments described was obtained from the Animal Subjects Review Board of the University of Florence. Experiments involving animals have been reported according to ARRIVE - Animal Research: Reporting of *in Vivo* Experiments – guidelines.[496] All efforts were made to minimize animal suffering and to reduce the number of animals used.

Complete Freund's adjuvant-induced arthritis. Articular damage was induced by injection of complete Freund's adjuvant (CFA; Sigma-Aldrich St Louis, MO, USA), containing 1 mg/ml of heat-killed and dried Mycobacterium tuberculosis in paraffin oil and mannide monooleate, into the tibiotarsal joint.[497-499] Briefly, the rats were lightly anesthetized by 2% isoflurane, the left leg skin was sterilized with 75% ethyl alcohol and the lateral malleolus located by palpation. A 28-gauge needle was then inserted vertically to penetrate the skin and turned distally for insertion into the articular cavity at the gap between the tibiofibular and tarsal bone until a distinct loss of resistance was felt. A volume of 50 μl of CFA was then injected (day 0). Control rats received 50 μl of saline solution (day 0) in the tibiotarsal joint. Behavioral experiments were performed 14 days after.

Administration of compounds. Compounds **B3**, **B12**, **B21**, **B24**, **B25** and **B26** were suspended in a 1% solution of carboxymethylcellulose sodium salt (CMC) and administered per os (p.o.) once on day 14 at the dose of 1, 10, and 30 mg kg^{-1}.[497]

Paw-pressure test. The nociceptive threshold of rats was determined with an analgesimeter (Ugo Basile, Varese, Italy), according to the method described by Leighton et al.[500] Briefly, a constantly increasing pressure was applied to a small area of the dorsal surface of the hind paw using a blunt conical probe by a mechanical device. Mechanical pressure was increased until vocalization or a withdrawal reflex occurred while rats were lightly restrained. Vocalization or withdrawal reflex thresholds were expressed in grams. Rats scoring below 40 g or over 75 g during the test before drug administration were rejected (25%). For analgesia measures, mechanical pressure application was stopped at 120 g.

Incapacitance test. Weight-bearing changes were measured using an incapacitance apparatus (Linton Instrumentation, Norfolk, UK) to detect changes in postural equilibrium after a hind limb injury.[501] Rats were trained to stand on their hind paws in a box with an inclined plane (65° from horizontal). This box was placed above the incapacitance apparatus. This allowed us to independently measure the weight that the animal applied on each hind limb. The value reported for each animal is the mean of five consecutive measurements. In the absence of hind limb injury, rats applied an equal weight on both hind limbs, indicating postural equilibrium, whereas an unequal distribution of weight on the hind limbs indicated a monolateral decreased pain threshold. Data are expressed as the difference between the weight applied to the limb contralateral to the injury and the weight applied to the ipsilateral limb (Δ Weight).

Statistical analysis. Behavioural measurements were performed on eight rats for each treatment carried out in two different experimental sets. Results were expressed as mean (S.E.M.) with one-way analysis of variance. A Bonferroni's significant difference procedure was used as a post hoc comparison. P-values <0.05 or <0.01 were considered significant. Data were analysed using the Origin 9 software (OriginLab, Northampton, MA, USA).

7.4 From random to rational: a discovery approach to selective subnanomolar inhibitors of human carbonic anhydrase IV based on the Castagnoli-Cushman multicomponent reaction (Series C)

7.4.1 Carbonic anhydrase inhibition.

The CA inhibitory profiles of compounds belonging to series **C** were obtained according to the general procedures described at the beginning of the experimental section.

7.4.2 Computational studies.

Computational studies, for compounds belonging to series **C**, were performed according to the general procedures described at the beginning of the experimental section (procedure **a-e**), using hCA IV (pdb 5JN8)[502] crystal structure.

7.5 The antibiotic furagin and its derivatives are isoform-selective human carbonic anhydrase inhibitors (Series D)

7.5.1 Carbonic anhydrase inhibition.

The CA inhibitory profiles of compounds belonging to series **D** were obtained according to the general procedures described at the beginning of the experimental section.

7.5.2 Computational studies.

Computational studies, for compounds belonging to series **D**, were performed according to the general procedures described at the beginning of the experimental section (procedure **a-f**), using hCA II (pdb 5LJT)[359], hCA IX (pdb 5FL4)[276] and hCA XII (pdb JLD0)[30] crystal structures. The imidic nitrogen of the hydantoin nucleus was negatively charged in simulations (Epik)[487c].

7.6 Novel insights on saccharin- and acesulfame-based carbonic anhydrase inhibitors: design, synthesis and biological activity (Series E)

7.6.1 Carbonic anhydrase inhibition.

The CA inhibitory profiles of compounds belonging to series **E** were obtained according to the general procedures described at the beginning of the experimental section.

7.6.2 Computational studies.

Computational studies, for compounds belonging to series **E**, were performed according to the general procedures described at the beginning of the experimental section (procedure **a-f**), using hCA IX (pdb 5DVX)[503] and hCA XII (pdb 1JCZ)[30] crystal structures.

7.7 Synthesis, biological and molecular dynamics investigations with a series of triazolopyrimidine/triazole-based benzenesulfonamides as novel carbonic anhydrase inhibitors (Series F)

7.7.1 Carbonic anhydrase inhibition.

The CA inhibitory profiles of compounds belonging to series **F** were obtained according to the general procedures described at the beginning of the experimental section.

7.7.2 Computational studies.

Computational studies, for compounds belonging to series **F**, were performed according to the general procedures described at the beginning of the experimental section (procedure **a-f**), using hCA II (pdb 5LJT)[359], hCA IX (pdb 5FL4)[276] and hCA XII (pdb 1JCZ)[30] crystal structures.

7.8 N-Nitrosulfonamides as carbonic anhydrase inhibitors: a promising chemotype for targeting Chagas disease and Leishmaniasis (Series G)

7.8.1 Chemistry.

The general chemistry protocols are reported at the beginning of the experimental section.

General synthetic procedure of N-nitrobenzenesulfonamides G9-16. *Procedure 1.* NH_4NO_3 (1.1 equiv) was added portion wise to a solution of aromatic sulfonamides **G1-7**

(0.25g, 1.0 equiv) in 95% H_2SO_4 (1 mL) at 0°C. The suspension was stirred at the same temperature for 15 min, then quenched with slush (8 mL) and the formed precipitate was filtered-off and washed with cold water. The collected powder was recrystallized with water to afford the title compound **G9-15**. The characterization of derivatives **G9-11**, **G14**, **G15** was previously reported.[20]

Procedure 2. NH_4NO_3 (1.1 equiv) was added portionwise to a solution of aromatic sulfonamides **G8**, **G17**, **G19** (0.25 g, 1.0 equiv) in 95% H_2SO_4 (1 mL) at 0°C. The suspension was stirred at the same temperature for 15 min, then slowly quenched with $NH_4OH_{(aq.)}$ until pH=8 was obtained. The yellow solution was concentrated under *vacuum*. MeOH (15 mL) was added and the formed suspension was filtered-off. The organic solvent was concentrated under *vacuum* and the obtained residue was triturated with Et_2O to afford the title compound **G16**, **G18**, **G20**.

2-(Dimethylamino)-N-nitrobenzenesulfonamide (G12). Compound **12** was obtained according the general procedure 1 earlier reported. White solid. 71 % yield; δ_H (400 MHz, DMSO-d_6): 8.14 (d, $J = 8.3$ Hz, 1H), 7.90 (m, 2H, Ar), 7.72 (t, $J = 7.6$ Hz, 1H, Ar), 3.36 (s, 6H, 2 x CH_3). δ_C (100 MHz, DMSO-d_6): 143.11, 135.98, 133.65, 131.61, 131.56, 122.91, 48.43; ESI-MS (m/z) [M-H]$^-$: calculated for $C_8H_{10}N_3O_4S$ 244.0, found 244.0

3-(Dimethylamino)-N-nitrobenzenesulfonamide (G13). Compound **G13** was obtained according the general procedure 1 earlier reported. White solid. 75 % yield; δ_H (400 MHz, DMSO-d_6): 8.17 (d, $J = 8.1$ Hz, 1H, Ar), 7.91 (m, 2H, Ar), 7.73 (t, $J = 7.4$ Hz, 1H, Ar), 3.37 (s, 6H, 2 x CH_3). δ_C (100 MHz, DMSO-d_6): 143.02, 136.00, 133.65, 131.70, 131.56, 122.95, 48.46; ESI-MS (m/z) [M-H]$^-$: calculated for $C_8H_{10}N_3O_4S$ 244.0; found 244.0

3-Amino-4-hydroxy-N,5-dinitrobenzenesulfonamide ammonium salt (G16). Compound **G16** was obtained according the general procedure 2 earlier reported. Brownish solid. 67 % yield; δ_H (400 MHz, DMSO-d_6): 7.71 (d, $J = 2.4$, 1H), 7.53 (d, $J = 2.4$, 1H), 7.25 (s, 4H, exchange with D_2O, NH_4^+); δ_C (100 MHz, DMSO-d_6): 145.81, 135.92, 135.54, 134.12, 121.67, 116.29; ESI-MS (m/z) [M-H]$^-$: calculated for $C_6H_5N_4O_7S$ 277.0, found 276.9.

5-Amino-N-nitro-1,3,4-thiadiazole-2-sulfonamide ammonium salt (G18). Compound **G18** was obtained according the general procedure 2 earlier reported. Yellow solid. 77 % yield; δ_H (400 MHz, DMSO-d_6): 7.63 (s, 2H, exchange with D_2O, NH_2), 7.22 (s, 4H, exchange with D_2O, NH_4^+); δ_C (100 MHz, DMSO-d_6): 172.66, 158.98; ESI-MS (m/z) [M-H]$^-$: calculated for $C_2H_2N_5O_4S_2$ 224.0, found 223.9.

5-Imino-4-methyl-N-nitro-4,5-dihydro-1,3,4-thiadiazole-2-sulfonamide ammonium salt (G20). Compound **G20** was obtained according the general procedure 2 earlier reported. Yellow solid. 77 % yield; δ_H (400 MHz, DMSO-d_6): 10.05 (s, 1H, exchange with D_2O, NH), 7.18 (s, 4H, exchange with D_2O, NH_4^+), 3.94 (s, 3H, CH_3); δ_C (100 MHz, DMSO-d_6): 168.22, 154.70, 38.72; ESI-MS (m/z) [M-H]$^-$: calculated for $C_3H_4N_5O_4S_2$ 238.0; found 237.9.

General synthetic procedure of Ag salts of N-nitrobenzenesulfonamides G21-30.
Procedure 3. Ag_2CO_3 (0.5 equiv) was added to a suspension of N-nitrobenzenesulfonamides **G9-14** (0.2 g, 1.0 equiv) in H_2O (5 mL), and the mixture was stirred o.n. at rt protected from light. The reaction was heated to boiling point, filtered quickly and the recrystallized powder was collected by filtration to afford the title compound **G21-26**.
Procedure 4. $AgNO_3$ (1.1 equiv) was added to a solution of N-nitrobenzenesulfonamides **G15**, **G16**, **G18**, **G20** (0.2 g, 1.0 equiv) and NaOH (0.9 equiv) in H_2O (5 mL) and the formed precipitate was filtered-off and recrystallized from water to afford the title compound **G27-30.**

2-Amino-N-nitrobenzenesulfonamide silver salt (G21). Compound **G21** was obtained according the general procedure 3 earlier reported. Grey solid. 72 % yield; δ_H (400 MHz, DMSO-d_6): 7.51 (d, J = 7.9 Hz, 1H, Ar), 7.17 (t, J = 7.5 Hz, 1H, Ar), 6.70 (d, J = 8.2 Hz, 1H, Ar), 6.55 (t, J = 7.5 Hz, 1H, Ar), 5.81 (bs, 2H, exchange with D_2O, NH_2); δ_C (100 MHz, DMSO-d_6): 146.80, 132.66, 130.66, 121.40, 116.28, 114.45; ESI-MS (m/z) [M-H]$^-$: calculated for $C_2H_2N_5O_4S_2$ 224.0, found 223.9; [M$^+$]: calculated for Ag 106.9, found 106.9.

3-Amino-N-nitrobenzenesulfonamide silver salt (G22). Compound **G22** was obtained according the general procedure 3 earlier reported. Grey solid. 74 % yield; δ_H (400 MHz, DMSO-d_6): 7.45 (d, J = 8.8 Hz, 2H, Ar), 6.55 (d, J = 8.8 Hz, 2H, Ar), 5.84 (bs, 2H, exchange with D_2O, NH_2); δ_C (100 MHz, DMSO-d_6): 148.52, 142.77, 128.46, 116.49, 114.76, 112.86; ESI-MS (m/z) [M-H]$^-$: calculated for $C_2H_2N_5O_4S_2$ 224.0, found 223.9; [M$^+$]: calculated for Ag 106.9, found 106.9.

4-Amino-N-nitrobenzenesulfonamide silver salt (G23). Compound **G23** was obtained according the general procedure 3 earlier reported. Grey solid. 79 % yield; δ_H (400 MHz, DMSO-d_6): 7.45 (d, J = 8.8 Hz, 2H, Ar), 6.55 (d, J = 8.8 Hz, 2H, Ar), 5.84 (bs, 2H, exchange with D_2O, NH_2); δ_C (100 MHz, DMSO-d_6): 153.35, 131.26, 126.94, 113.10; ESI-MS (m/z) [M-H]$^-$: calculated for $C_2H_2N_5O_4S_2$ 224.0, found 223.9; [M$^+$]: calculated for Ag 106.9, found 106.9.

2-(Dimethylamino)-N-nitrobenzenesulfonamide silver salt (G24). Compound **G24** was obtained according the general procedure 3 earlier reported. Grey solid. 71 % yield; δ_H (400 MHz, DMSO-d_6): 7.91 (d, J = 7.9 1H, Ar), 7.56 (t, J = 7.1 Hz, 1H, Ar), 7.45 (d, J = 7.8 Hz, 1H, Ar), 7.25 (t, J = 7.5 Hz, 1H, Ar), 2.71 (s, 6H, 2 x CH_3); δ_C (100 MHz, DMSO-d_6): 154.19, 136.75, 134.54, 132.29, 124.97, 124.17, 47.16; ESI-MS (m/z) [M-H]$^-$: calculated for $C_2H_2N_5O_4S_2$ 224.0, found 223.9; [M$^+$]: calculated for Ag 106.9, found 106.9.

3-(Dimethylamino)-N-nitrobenzenesulfonamide silver salt (G25). Compound **G25** was obtained according the general procedure 3 earlier reported. Grey solid. 70 % yield; δ_H (400 MHz, DMSO-d_6): 7.90 (d, J = 7.8 Hz, 2H, Ar), 7.68 (m, 2H, Ar), 7.41 (m, 2H, Ar), 3.00 (s, 6H, 2 x CH_3); δ_C (100 MHz, DMSO-d_6): 151.32, 134.79, 134.65, 131.85, 124.72, 123.06, 47.58; ESI-MS (m/z) [M-H]$^-$: calculated for $C_2H_2N_5O_4S_2$ 224.0, found 223.9; [M$^+$]: calculated for Ag 106.9, found 106.9.

4-(Dimethylamino)-N-nitrobenzenesulfonamide silver salt (G26). Compound **G26** was obtained according the general procedure 3 earlier reported. Grey solid. 73 % yield; δ_H (400

MHz, DMSO-d$_6$): 7.61 (d, J = 8.9 Hz, 2H, Ar), 6.71 (d, J = 8.9 Hz, 2H, Ar), 2.97 (s, 6H, 2 x CH$_3$); δ$_C$ (100 MHz, DMSO-d$_6$): 159.24, 153.48, 131.03, 126.82, 111.39, 40.75; ESI-MS (m/z) [M-H]⁻: calculated for C$_2$H$_2$N$_5$O$_4$S$_2$ 224.0, found 223.9; [M⁺]: calculated for Ag 106.9, found 106.9.

4-(Aminomethyl)-N-nitrobenzenesulfonamide silver salt (G27). Compound **G27** was obtained according the general procedure 4 earlier reported. Grey solid. 62 % yield; δ$_H$ (400 MHz, DMSO-d$_6$): 7.75 (d, J = 8.3 Hz, 2H, Ar), 7.50 (d, J = 8.3 Hz, 2H, Ar), 4.10 (bs, 2H, exchange with D$_2$O, NH$_2$), 3.83 (s, 2H, CH$_2$); δ$_C$ (100 MHz, DMSO-d$_6$): 145.40, 141.09, 128.57, 128.11, 47.27; ESI-MS (m/z) [M-H]⁻: calculated for C$_2$H$_2$N$_5$O$_4$S$_2$ 224.0, found 223.9; [M⁺]: calculated for Ag 106.9, found 106.9.

3-Amino-4-hydroxy-N,5-dinitrobenzenesulfonamide silver salt (G28). Compound **G28** was obtained according the general procedure 4 earlier reported. Brownish solid. 42 % yield; δ$_H$ (400 MHz, DMSO-d$_6$): 7.59 (d, J = 2.4, 1H, Ar), 7.38 (d, J = 2.4, 1H, Ar); δ$_C$ (100 MHz, DMSO-d$_6$): 143.76, 141.18, 135.82, 133.48, 117.54, 112.47; ESI-MS (m/z) [M-H]⁻: calculated for C$_2$H$_2$N$_5$O$_4$S$_2$ 224.0, found 223.9; [M⁺]: calculated for Ag 106.9, found 106.9.

5-Amino-N-nitro-1,3,4-thiadiazole-2-sulfonamide silver salt (G29). Compound **G29** was obtained according the general procedure 3 earlier reported. Grey solid. 58 % yield; δ$_H$ (400 MHz, DMSO-d$_6$): 8.04 (bs, 2H, exchange with D$_2$O, NH$_2$); δ$_C$ (100 MHz, DMSO-d$_6$): 173.60, 160.94; ESI-MS (m/z) [M-H]⁻: calculated for C$_2$H$_2$N$_5$O$_4$S$_2$ 224.0, found 223.9; [M⁺]: calculated for Ag 106.9, found 106.9.

5-Imino-4-methyl-N-nitro-4,5-dihydro-1,3,4-thiadiazole-2-sulfonamide silver salt (G30). Compound **G30** was obtained according the general procedure 4 earlier reported. Grey solid. 51 % yield; δ$_H$ (400 MHz, DMSO-d$_6$): 9.79 (bs, 1H, exchange with D$_2$O, NH$_2$), 3.75 (s, 3H, CH3); δ$_C$ (100 MHz, DMSO-d$_6$): 169.43, 157.49, 38.80; ESI-MS (m/z) [M-H]⁻: calculated for C$_3$H$_4$N$_5$O$_4$S$_2$ 238.0; found 237.9; [M⁺]: calculated for Ag 106.9, found 106.9.

7.8.2 Carbonic anhydrase inhibition.

The CA inhibitory profiles of compounds belonging to series **G** were obtained according to the general procedures described at the beginning of the experimental section.

7.8.3 Anti-parasitic and cytotoxicity assays

Trypansoma cruzi and Leishmania parasites cultures. Epimastigote forms of the *T. cruzi* clone Dm28c,[504] *T. cruzi* Y[505] strains obtained from the Laboratory of Cellular Ultrastructure), *Leishmania (L.) infantum* MHOM/BR/1974/PP75 and *L. amazonensis* IFLA/BR/1967/PH8 were donate by the Leishmania Type Culture Collection (LTCC) all parasites of Oswaldo Cruz Institute/Fiocruz (Rio de Janeiro, RJ, Brazil) were used. The parasites were maintained in PBHIL medium supplemented with 10% bovine serum (FBS) at 28 °C.[506]

RAW 264.7 Macrophage cell line cultures. RAW 264.7 murine macrophages were obtained from the National Institute of Metrology, Quality and Technology (Instituto Nacional de Metrologia, Qualidade e Tecnologia, INMETRO) and maintained in DMEM medium supplemented with 10% FBS at 37ºC in a 5% controlled CO_2 atmosphere. Cell maintenance was performed every 48-72 h, time necessary for cells to achieve confluent monolayers.

Inhibitory activity of inhibitor on epimastigotes of *Trypanosoma cruzi* and promastigotes of *Leishmania Trypanosoma cruzi* Dm28c e Y and promastigotes of *Leishmania amazonensis* and *L.infantum*. The evaluation of anti-parasites activity was performed by successive microdilutions in 96 well plates (1.8x 106 parasites/well) incubated for 48 hours with the synthetic compounds in the PHBIL medium supplemented with 10% FBS in the following concentrations: 256, 128, 64, 32, 16, 8, 4, and 2 μM. The experiment controls were: negative control (culture medium without parasite) and positive culture (culture medium with parasite). Benznidazole and Amphotericin B were used as reference drugs of *T. cruzi* and *Leishmania* respectively and were progressively diluted with the parasite. The Minimum inhibitory concentration (MIC) for epimastigotes (*T. cruzi* DM28c

and Y) and promastigotes (*L. amazonensis* and *L. infantum*) was performed using resazurin (125 µM) as an indicator of cellular metabolic function. MIC was determined as the lowest concentration of the inhibitor capable of inhibiting in vitro growth of the parasites by spectrophotometricanalysis at 490 and 595[507] The determination of IC_{50} (concentration of drug which reducesepimastigotes number cells by 50%).

Cytotoxicity assay in macrophages. Cytotoxicity was performed using tetrazolium dye (MTT) colorimetric assay. RAW 264.7 macrophages cells were harvest after confluent monolayer achievement.[508] The cells were washed twice with PBS and a cellular suspension of 106 cells/ml was prepared in fresh DMEM culture medium. Aliquots of 100 ml of the cellular suspension were placed into polystyrene 96-well plates, and then incubated at 37 0C in a 5% CO2 atmosphere for 6 h (in order to obtain an adherence of macrophages. After this period, the adherent cells were subjected to treatment with several concentrations of the drugs (2–256 µM), and then incubated for additional 48 h. Finally, 20 ml of a MTT solution (5 mg/ml) were added to each well and the plates incubated for 4 h. Macrophage viability was determined after formazan crystals solubilization with DMSO followed by the absorbance measurement at 570 nm using a SpectraMax M5 spectrophotometer (Molecular Devices, Sunnyvale, CA).

Determination of selectivity index. A selectivity index (SI) was calculated and is defined as the RAW IC_{50} value divided by the *T. cruzi* IC_{50} value ($SI = CC_{50}/CI_{50}$), which expresses the safety index of the tested substance Benznidazole (Sigma-Aldrich, Milan, Italy) was kept as a positive control drug for the cytotoxicity assay on RAW 264.7.

Cytotoxicity assay with tripomastigotes forms of *Trypanosma cruzi.* Vero cells were subculture weakly by enzyme dissociation. Briefly, confluent cultures were dissociated with trypsin and EDTA solution (0,02%) and isolated cells seeded at a density of 8 x 105 cells/ 150 cm2 culture flask in RPMI 1640 medium supplemented with 10% fetal bovine serum (FBS). Cultures were maintained at 37 °C in 5% of CO2 atmosphere. Vero cells (1.5 x 104) were seeded on 96-well white culture plates (Greiner Bio-One North America, Inc.) and, after 24 h of culture in RPMI 1640 medium supplemented with 10% fetal bovine serum, the monolayers were treated for 72 h at 37 °C with a serial two-fold dilution of benznidazole (Bz) and silver N-nitrosulfonamides (1.95 – 500 µM). Cell viability, determined by

quantitation of ATP in metabolic active cells, was measured with CellTiter-Glo kit (Promega Corporation, Madison, WI, USA). The luminescent signal was read on FlexStation 3 reader (Molecular Devices, Sunnyvale, CA, USA). CC_{50} value, the concentration of compound that reduced 50% of Vero cells viability, was determined by linear regression. Controls were performed in dimethyl sulfoxide (DMSO; $\leq$1%). Three independent assays were performed in duplicate.

In vitro trypanocidal activity assay: trypomastigote and amastigote forms. Tissue culture-derived trypomastigotes were harvested from *T. cruzi*-infected Vero cells cultures at 4 days post infection (4 dpi). Briefly, Vero cells monolayers were infected with *T. cruzi*, Dm28c clone genetically modified to express luciferase (Dm28c-Luc), at a ratio of 10:1 parasites/host cell and, after 24h of infection, free trypomastigotes were washed out and replaced by RPMI 1640 medium supplemented with 10% FBS. At 4 dpi, trypomastigotes released by infected cells were harvested and used in experimental assays.[509]

The effect of silver N-nitrosulfonamides was evaluated against trypomastigote and intracellular amastigote forms of *T. cruzi*. Tissue culture-derived trypomastigotes (1 x 106 parasites/well), Dm28c clone genetically modified to express luciferase (Dm28c-Luc), were exposed for 24 h at 37 °C to a range concentration of Bnz and N-nitrosulfonamides derivatives (0.41 - 100 μM). For intracellular amastigotes, Vero cells cultures infected with *T. cruzi* (Dm28c-Luc clone) for 24 h were treated for 72 h at 37 °C with different concentrations of the inhibitors and Bz (0.41 - 100 μM). The viability of parasites, both trypomastigotes and intracellular amastigotes, was evaluated after addition of the enzyme substrate, luciferin (300 μg/mL), followed by luminescence measurement using FlexStation 3 reader. The concentration of compound capable of reducing the number of viable parasites by 50% (IC50 value) was calculated by linear regression. The final concentration of DMSO did not exceed 1%. Three independent assays were performed in duplicate.

7.9 Benzoxaboroles: new potent inhibitors of the carbonic anhydrases of the pathogenic bacterium Vibrio cholerae (Series H)

7.9.1 Carbonic anhydrase inhibition.

The CA inhibitory profiles of compounds belonging to series **H** were obtained according to the general procedures described at the beginning of the experimental section.

7.9.2 Computational studies.

The primary sequences of VchCA, VchCAβ, and VchCAγ were retrieved from the UniProt Consortium. The crystal structure of α-CA from *Photobacterium profundum* (PDB 5HPJ)[510], β-CA from *Pseudomonas aeruginosa* (PDB 6D2N),[511] and γ-CA homologous protein from *Escherichia coli* (PDB 3TIO)[512] were used as templates in the homology modeling procedure. Multiple models were generated using the Prime module of Schrödinger (Prime, v.5.5)[487d] and the SwissModel platform[513] and submitted to loop refinements and quality evaluation procedures. The best-scored structures of VchCAα, VchCAβ and the VchCAγ crystal structures were used for computational studies of compounds belonging to series **H** according to the general procedures described at the beginning of the experimental section (procedure **a-f**).

Sequence alignment of VchCA (α-CA) with the template α-CA from *Photobacterium profundum* (pdb 5HPJ):

```
                 10         20         30         40         50         60
        ....|....| ....|....| ....|....| ....|....| ....|....| ....|....|
VchCAα 1   MKKTTWVLAM AASMSFGVQA SEWGYEGEHA PEHWGKVAPL CAEGKNQSPI DVSQSVEADL
5HPJ   22  ---------- ---------- -EWSYTGEHG TEHWGDSFAT CAEGVNQTPI DINQTTQAEL

                 70         80         90        100        110        120
        ....|....| ....|....| ....|....| ....|....| ....|....| ....|....|
VchCAα 61  QPFTLNYQGQ VVGLLNNGHT LQAIVSGNNP LQIDGKTFQL PEHWGKVAPL CAEGKNQSPI
5HPJ   61  APLHLDYEGQ VTELVNNGHT IQANLTGKNT LTVDGKTFEL KQFHFHTPSE NYLKGKQYPL

                130        140        150        160        170        180
        ....|....| ....|....| ....|....| ....|....| ....|....| ....|....|
VchCAα 121 DVSQSVEADL QPFTLNYQGQ VVGLLNNGHT LQAIVSGNNP LQIDGKTFQL KQFHFHTPSE
5HPJ   121 EAHFVHATDK GELAVVAVMF DFGPRSNNEL TTLLASIPSK GQTVELKEAL NPADLLPRDR

                190        200        210        220        230        240
        ....|....| ....|....| ....|....| ....|....| ....|....| ....|....|
VchCAα 181 NLLKGKQFPL EAHFVHADEQ GNLAVVAVMY QVGS-ENPLL KALTADMPTK GNSTQLTQGI
5HPJ   181 EYYRFNGSLT TPPCSEGVRW FVMQEPQTSS KAQTEKLQAV MGNNARPLQP LNARLILE--

                250        260        270        280        290        300
        ....|....| ....|....| ....|....| ....|....| ....|....| ....|....|
VchCAα 241 PLADWIPESK HYYRFNGSLT TPPCSEGVRW IVLKEPAHVS NQQEQQLSAV MGHNNRPVQP
5HPJ       ---------- ---------- ---------- ---------- ---------- ----------

                310
        ....|....|
VchCAα 301 HNARLVLQAD
5HPJ       ----------
```

Sequence alignment of type-I VchCAβ with the template type-I β-CA from *Pseudomonas aeruginosa* (pdb 6D2N):

```
                  10         20         30         40         50         60
         ....|....| ....|....| ....|....| ....|....| ....|....| ....|....|
VchCAβ_A 1   MPEIKQLFEN NSKWSESIKA ETPEYFAKLA KGQNPDFLWI GCADSRVPAE RLTGLYSGEL
VchCAβ_B 1   MPEIKQLFEN NSKWSESIKA ETPEYFAKLA KGQNPDFLWI GCADSRVPAE RLTGLYSGEL
6D2N     3   --ALQQLFEN NVRWAEAIKQ EDPDFFAKLA RQQTPEYLWI GCSDARVPAN EIVGMLPGDL

                  70         80         90        100        110        120
         ....|....| ....|....| ....|....| ....|....| ....|....| ....|....|
VchCAβ_A 61  FVHRNVANQV IHTDLNCLSV VQYAVDVLQV KHIIVCGHYG CGGVTAAIDN PQLGLINNWL
VchCAβ_B 61  FVHRNVANQV IHTDLNCLSV VQYAVDVLQV KHIIVCGHYG CGGVTAAIDN PQLGLINNWL
6D2N     61  FVHRNVANVV LHTDLNCLSV IQFAVDVLKV KHILVTGHYG CGGVRASLHN DQLGLIDGWL

                 130        140        150        160        170        180
         ....|....| ....|....| ....|....| ....|....| ....|....| ....|....|
VchCAβ_A 121 LHIRDYYLKH REYLDQMPAE D-RSDKLAEI NVAEQVYNLA NSTVLQNAWE RGQAVEVHGF
VchCAβ_B 121 LHIRDYYLKH REYLDQMPAE D-RSDKLAEI NVAEQVYNLA NSTVLQNAWE RGQAVEVHGF
6D2N     121 RSIRDLAYEY REHLEQLPTE EERVDRLCEL NVIQQVANVS HTSIVQNAWH RGQSLSVHGC

                 190        200        210        220
         ....|....| ....|....| ....|....| ....|....| ...
VchCAβ_A 180 VYGIEDGRLE YLGVRCASRS AVEDNYHKAL EKILNPNHRL LCR
VchCAβ_B 180 VYGIEDGRLE YLGVRCASRS AVEDNYHKAL EKILNPNHRL LCR
6D2N     181 IYGIKDGLWK NLNVTVSG--- ---------L DQLP-PQYRL SPL
```

Sequence alignment of VchCAγ with the template γ-CA from *Escherichia coli* (pdb 3TIO):

```
                        10         20         30         40         50         60
               ....|....| ....|....| ....|....| ....|....| ....|....| ....|....|
VchCAγ_A   1   SSIRSYKGIV PKLGEGVYVD SSAVLVGDIE LGDDASIWPL VAARGDVNHI RIGKRTNIQD
VchCAγ_B   1   SSIRSYKGIV PKLGEGVYVD SSAVLVGDIE LGDDASIWPL VAARGDVNHI RIGKRTNIQD
VchCAγ_C   1   SSIRSYKGIV PKLGEGVYVD SSAVLVGDIE LGDDASIWPL VAARGDVNHI RIGKRTNIQD
3TIO       1   DVLHPYRDLF PQIGQRVMID DSSVVIGDVR LADDVGIWPL VVIRGDVHYV QIGARTNIQD

                        70         80         90        100        110        120
               ....|....| ....|....| ....|....| ....|....| ....|....| ....|....|
VchCAγ_A  61   GSVLHVTHKN AENPNGYPLC IGDDVTIGHK VMLHGCTIHD RVLVGMGSIV LDGAVIENDV
VchCAγ_B  61   GSVLHVTHKN AENPNGYPLC IGDDVTIGHK VMLHGCTIHD RVLVGMGSIV LDGAVIENDV
VchCAγ_C  61   GSVLHVTHKN AENPNGYPLC IGDDVTIGHK VMLHGCTIHD RVLVGMGSIV LDGAVIENDV
3TIO      61   GSMLHVTHKS SYNPDGNPLT IGEDVTVGHK VMLHGCTIGN RVLVGMGSIL LDGAIVEDDV

                       130        140        150        160        170        180
               ....|....| ....|....| ....|....| ....|....| ....|....| ....|....|
VchCAγ_A 121   MIGAGSLVPP GKRLESGFLY MGSPVKQARP LSDKERAFLV KSSSNYVQSK NDYLNDVKTV
VchCAγ_B 121   MIGAGSLVPP GKRLESGFLY MGSPVKQARP LSDKERAFLV KSSSNYVQSK NDYLNDVKTV
VchCAγ_C 121   MIGAGSLVPP GKRLESGFLY MGSPVKQARP LSDKERAFLV KSSSNYVQSK NDYLNDVKTV
3TIO     121   MIGAGSLVPQ NKRLESGYLY LGSPVKQIRP LSDEEKAGLR YSANNYVKWK DEYL------


                ..
VchCAγ_A 181   RE
VchCAγ_B 181   RE
VchCAγ_C 181   RE
3TIO           --
```

7.10 (+)-Catharanthine potentiates GABA$_A$ receptors by interacting with a site shared with loreclezole and (+)-etomidate: an electrophysiological and molecular modeling study

7.10.1 Computational studies.

The primary sequences of the hα$_1$, hα$_2$, hβ$_1$, hβ$_2$, hβ$_3$, and hγ$_2$ GABA$_A$R subunits were retrieved from the UniProt Consortium.[514] Subunit sequence alignment, model building, loop refinements, and quality evaluation procedures were performed by using the Prime module (v.5.5)[487d] of the Schrödinger Suite Release 2019-1 (Schrödinger, LLC, NY, USA). The structure of the hα$_1$β$_2$γ$_2$ GABA$_A$R obtained by cryo-electron microscopy (PDB: 6HUJ)[481] was used as a template in the homology modeling procedure. The GABA$_A$R models, including the hα$_1$β$_2$(M286C)γ$_2$, hα$_1$β$_2$(N265S)γ$_2$, hα$_1$β$_2$(D282A)γ$_2$, and hα$_1$β$_2$(R269A)γ$_2$ mutants, were were used for computational studies of (+)-catharanthine, loreclezole and (+)-

etomidate according to the general procedures described at the beginning of the experimental section (procedure **a-f**).

References

[1] Supuran, C.T. Carbonic anhydrases: novel therapeutic applications for inhibitors and activators. *Nat. Rev. Drug Discovery* **2008**, *7*, 168-181.

[2] Alterio, V.; Di Fiore, A.; D'Ambrosio, K.; Supuran, C.T.; De Simone, G. Multiple binding modes of inhibitors to carbonic anhydrases: how to design specific drugs targeting 15 different isoforms? *Chem. Rev.* **2012**, *112*, 4421-4468.

[3] Nocentini, A.; Supuran, C.T. Advances in the structural annotation of human carbonic anhydrases and impact on future drug discovery. *Expert Opin. Drug Discov.* **2019**, *14*, 1175-1197.

[4] Xu, Y.; Feng, L.; Jeffrey, P. D.; Shi, Y.; Morel, F. M. Structure and metal exchange in the cadmium carbonic anhydrase of marine diatoms. *Nature* **2008**, *452*, 56-61.

[5] Jensen, E.L.; Clement, R.; Kosta, A.; Maberly, S.C.; Gontero, B. A new widespread subclass of carbonic anhydrase in marine phytoplankton. *ISME J.* **2019**, *13*, 2094-2106.

[6] Maren, T. H. Carbonic anhydrase: chemistry, physiology, and inhibition. *Physiol. Rev.* **1967**, *47*, 595-781.

[7] Del Prete, S.; Vullo, D.; Fisher, G.M.; Andrews, K.T.; Poulsen, S.A.; Capasso, C.; Supuran, C.T. Discovery of a new family of carbonic anhydrases in the malaria pathogen Plasmodium falciparum-the η-carbonic anhydrases. *Bioorg. Med. Chem. Lett.* **2014**, *24*, 4389-4396.

[8] Tripp, B. C.; Smith, K.; Ferry, J. G. Carbonic anhydrase: new insights for an ancient enzyme. *J. Biol. Chem.* **2001**, *276*, 48615-48618.

[9] Ferry, J. F. The gamma class of carbonic anhydrases. *Biochim. Biophys. Acta* **2010**, 1804, 374-381.

[10] Smith, K.S.; Jakubzick, C.; Whittam, T. S.; Ferry, J.G. Carbonic anhydrase is an ancient enzyme widespread in prokaryotes. *Proc. Natl. Acad. Sci. U.S.A.* **1999**, *96*, 15184–15189.

[11] Kikutani, S.; Nakajima, K.; Nagasato, C.; Tsuji, Y.; Miyatake, A.; Matsuda, Y. Thylakoid luminal θ-carbonic anhydrase critical for growth and photosynthesis in the marine diatom Phaeodactylum tricornutum. *Proc. Natl. Acad. Sci. U.S.A.* **2016**, *113*, 9828–9833.

[12] Capasso, C.; Supuran, C.T. An overview of the alpha-, beta- and gamma-carbonic anhydrases from Bacteria: can bacterial carbonic anhydrases shed new light on evolution of bacteria? *J. Enzyme Inhib. Med. Chem.* **2015**, *30*, 325–332.

[13] Supuran, C.T. Structure and function of carbonic anhydrases. *Biochem. J.* **2016**, *473*, 2023-2032.

[14] Supuran, C.T.; Scozzafava, A.; Casini, A. Carbonic anhydrase inhibitors. *Med. Res. Rev.* **2003**, *23*, 146-189.

[15] Supuran, C.T.; Scozzafava, A. Carbonic anhydrases as targets for medicinal chemistry. *Bioorg. Med. Chem.* **2007**, *15*, 4336-4350.

[16] Temperini, C.; Scozzafava, A.; Supuran, C.T. In Drug Design of Zinc-Enzyme Inhibitors: Functional, Structural, and Disease Applications; Supuran, C.T., Winum, J.-Y., Eds.; Wiley: Hoboken, NJ, **2009**; p 473.

[17] Gao, B. B.; Clermont, A.; Rook, S.; Fonda, S. J.; Srinivasan, V. J.; Wojtkowski, M.; Fujimoto, J. G.; Avery, R. L.; Arrigg, P. G.; Bursell, S. E.; Aiello, L. P.; Feener, E. P. Extracellular carbonic anhydrase mediates hemorrhagic retinal and cerebral vascular permeability through prekallikrein activation. *Nat. Med.* **2007**, *13*, 181-188.

[18] Mincione, F.; Scozzafava, A.; Supuran, C.T. The development of topically acting carbonic anhydrase inhibitors as antiglaucoma agents. *Curr. Pharm. Des.* **2008**, *14*, 649-654.

[19] Supuran, C.T. Diuretics: from classical carbonic anhydrase inhibitors to novel applications of the sulfonamides. *Curr. Pharm. Des.* **2008**, *14*, 641-648.

[20] De Simone, G.; Scozzafava, A.; Supuran, C.T. Which carbonic anhydrases are targeted by the antiepileptic sulfonamides and sulfamates? *Chem. Biol. Drug Des.* **2009**, *74*, 317-321.

[21] Basnyat, B.; Gertsch, J. H.; Johnson, E. W.; Castro-Marin, F.; Inoue, Y.; Yeh, C. Efficacy of low-dose acetazolamide (125 mg BID) for the prophylaxis of acute mountain sickness: a prospective, double-blind, randomized, placebo-controlled trial. *High Alt. Med. Biol.* **2003**, *4*, 45-52.

[22] Nocentini, A.; Supuran, C.T. Carbonic anhydrase inhibitors as antitumor/antimetastatic agents: a patent review (2008-2018). *Expert Opin. Ther. Pat.* **2018,** *28*, 729-740

[23] Barreiro, E.; Hussain, S. N. A. Protein carbonylation in skeletal muscles: impact on function. *Antioxid. Redox Signal.* **2010**, *12*, 417-429.

[24] Nishimori, I.; Minakuchi, T.; Kohsaki, T.; Onishi, S.; Takeuchi, H.; Vullo, D.; Scozzafava, A.; Supuran, C.T. Carbonic anhydrase inhibitors: the beta-carbonic anhydrase from Helicobacter pylori is a new target for sulfonamide and sulfamate inhibitors. *Bioorg. Med. Chem. Lett.* **2007**, *17*, 3585-3594.

[25] Capasso, C.; Supuran, C.T. Bacterial, fungal and protozoan carbonic anhydrases as drug targets. *Expert Opin. Ther. Targets.* **2015**, *19*, 1689-1704.

[26] Del Prete, S.; Nocentini, A.; Supuran, C.T.; Capasso, C. Bacterial ι-carbonic anhydrase: a new active class of carbonic anhydrase identified in the genome of the Gram-negative bacterium Burkholderia territorii. *J. Enzyme Inhib. Med. Chem.* **2020**, 35, 1060-1068.

[27] Supuran, C.T.; De Simone, G. In Carbonic Anhydrases as Biocatalysts; Supuran C.T., De Simone G., Eds.; *Elsevier: Walthman*, MA, **2015**, p. 3.

[28] Berman, H.M.; Westbrook, J.; Feng, Z.; Gilliland, G.; Bhat, T.N.; Weissig, H.; Shindyalov, I.N.; Bourne, P.E.The Protein Data Bank. *Nucleic Acids Research*, **2000**, *28*, 235-242. www.rcsb.org

[29] De Simone, G.; Supuran, C.T. Carbonic anhydrase IX: Biochemical and crystallographic characterization of a novel antitumor target. *Biochim. Biophys. Acta* **2010**, *1804*, 404-409.

[30] Whittington, D. A.; Waheed, A.; Ulmasov, B.; Shah, G. N.; Grubb, J. H.; Sly, W. S.; Christianson, D. W. Crystal structure of the dimeric extracellular domain of human carbonic anhydrase XII, a bitopic membrane protein overexpressed in certain cancer tumor cells. *Proc. Natl. Acad. Sci. U.S.A.* **2001**, *98*, 9545-9550.

[31] Schlicker, C.; Hall, R. A.; Vullo, D.; Middelhaufe, S.; Gertz, M.; Supuran, C.T.; Muehlschlegel, F. A.; Steegborn, C. Structure and Inhibition of the CO2-Sensing Carbonic Anhydrase Can2 from the Pathogenic Fungus Cryptococcus neoformans. *J. Mol. Biol.* **2009**, *385*, 1207-1220.

[32] Alber, B.E.; Ferry, J.G. A carbonic anhydrase from the archaeon Methanosarcina thermophila. *Proc Natl Acad Sci U S A.* **1994**, *91*, 6909-6913.

[33] Supuran C.T. Carbonic anhydrase activators. *Future Med Chem.* **2018**, *10*, 561-573.

[34] Masini, E.; Carta, F.; Scozzafava, A.; Supuran, C.T. Antiglaucoma carbonic anhydrase inhibitors: a patent review. *Expert Opin Ther Pat* **2013**, *23*, 705–716.

[35] Matsui, H.; Murakami, M.; Wynns, G. C.; Conroy, C. W.; Mead, A.; Maren, T. H.; Sears, M. L. Membrane carbonic anhydrase (IV) and ciliary epithelium. Carbonic anhydrase activity is present in the basolateral membranes of the non-pigmented ciliary epithelium of rabbit eyes. *Exp. Eye Res.* **1996**, *62*, 409-417.

[36] Tang, Y.; Xu, H.; Du, X.; Lit, L.; Walker, W.; Lu, A.; Ran, R.; Gregg, J. P.; Reilly, M.; Pancioli, A.; Khoury, J. C.; Sauerbeck, L. R.; Carrozzella, J. A.; Spilker, J.; Clark, J.; Wagner, K. R.; Jauch, E. C.; Chang, D. J.; Verro, P.; Broderick, J. P.; Sharp, F. R. Gene expression in blood changes rapidly in neutrophils and monocytes after ischemic stroke in humans: a microarray study. *J. Cereb. Blood Flow Metab.* **2006**, *26*, 1089-1102.

[37] De Simone, G.; Supuran, C.T. In Drug Design of Zinc-Enzyme Inhibitors: Functional, Structural, and Disease Applications; Supuran, C.T., Winum, J.-Y., Eds.; Wiley: Hoboken, NJ, **2009**; p 241.

[38] Liu, C.; Wei, Y.; Wang, J.; Pi, L.; Huang, J.; Wang, P.; Carbonic anhydrases III and IV autoantibodies in rheumatoid arthritis, systemic lupus erythematosus, diabetes, hypertensive renal disease, and heart failure. *Clin. Dev. Immunol.* **2012**, 354594.

[39] Margheri, F.; Ceruso, M.; Carta, F.; Laurenzana, A.; Maggi, L.; Lazzeri, S.; Simonini, G.; Annunziato F.; Del Rosso M.; Supuran C.T.; Cimaz, R. Overexpression of the transmembrane carbonic anhydrase isoforms IX and XII in the inflamed synovium. *J. Enzyme Inhib. Med. Chem.* **2016**, *31*, 60-63.

[40] De Simone, G.; Di Fiore, A.; Supuran, C.T. Are carbonic anhydrase inhibitors suitable for obtaining antiobesity drugs? *Curr. Pharm. Des.* **2008**, *14*, 655-660.

[41] De Simone, G.; Supuran, C.T. Antiobesity carbonic anhydrase inhibitors. *Curr. Top. Med. Chem.* **2007**, *7*, 879-884.

[42] Supuran, C.T.; Di Fiore, A.; De Simone, G. Carbonic anhydrase inhibitors as emerging drugs for the treatment of obesity. *Expert Opin. Emerg. Drugs.* **2008**, *13*, 383-392.

[43] Nishimori, I.; Minakuchi, T.; Onishi, S.; Vullo, D.; Scozzafava, A.; Supuran, C.T. Carbonic anhydrase inhibitors. DNA cloning, characterization, and inhibition studies of the human secretory isoform VI, a new target for sulfonamide and sulfamate inhibitors. *J. Med. Chem.* **2007**, *50*, 381-388.

[44] Kivelä, J.; Parkkila, S.; Parkkila, A.K.; Rajaniemi, H. A low concentration of carbonic anhydrase isoenzyme VI in whole saliva is associated with caries prevalence. *Caries Res.* **1999**, *33*, 178-184.

[45] Ruusuvuori, E.; Li, H.; Huttu, K.; Palva, J.M.; Smirnov, S.; Rivera, C.; Kaila, K.; Voipio, J. Carbonic anhydrase isoform VII acts as a molecular switch in the development of synchronous gamma-frequency firing of hippocampal CA1 pyramidal cells. *J. Neurosci.* **2004**, *24*, 2699-2707.

[46] Aspatwar, A.; Tolvanen, M.E.; Ortutay, C.; Parkkila, S. Carbonic anhydrase related protein VIII and its role in neurodegeneration and cancer. *Curr. Pharm. Des.* **2010**, *16*, 3264-3276.

[47] Nishimori, I. In Carbonic Anhydrase: Its Inhibitors and Activators; Supuran, C.T., Scozzafava, A., Conway, J., Eds.; *CRC Press: Boca Raton*, FL, **2004**; p 25.

[48] Neri, D.; Supuran, C.T. Interfering with pH regulation in tumours as a therapeutic strategy. *Nat. Rev. Drug Discov.* **2011**, *10*, 767-777.

[49] Pastorekova, S.; Parkkila, S.; Zavada, J. Tumor-associated carbonic anhydrases and their clinical significance. *Adv. Clin. Chem.* **2006**, *42*, 167-216.

[50] Dai, H.T.; Hong, C.C.; Liang, S.C; Yan, M.D.; Lai, G.M., Cheng, A.L.; Chuang S.E. Carbonic anhydrase III promotes transformation and invasion capability in hepatoma cells through FAK signaling pathway. *Mol Carcinog* **2008**, *47*, 956–963.

[51] Battke, C.; Kremmer, E.; Mysliwietz, J.; Gondi, G.; Dumitru, C.; Brandau, S.; Lang, S.; Vullo, D.; Supuran, C.T.; Zeidler, R. Generation and characterization of the first inhibitory antibody targeting tumour-associated carbonic anhydrase XII. *Cancer Immunol. Immunother.* **2011**, *60*, 649-658.

[52] Liao, S.Y.; Ivanov, S.; Ivanova, A.; Ghosh, S.; Cote, M.A.; Keefe, K.; Coca-Prados, M.; Stanbridge, E. J.; Lerman, M. I. Expression of cell surface transmembrane carbonic anhydrase genes CA9 and CA12 in the human eye: overexpression of CA12 (CAXII) in glaucoma. *J. Med. Genet.* **2003**, *40*, 257-261.

[53] Pastorek, J.; Pastorekova, S. Hypoxia-induced carbonic anhydrase IX as a target for cancer therapy: From biology to clinical use. *Semin. Cancer Biol.* **2015**, *31*, 52−64.

[54] Monti, S. M.; Supuran, C.T.; De Simone, G. Anticancer carbonic anhydrase inhibitors: a patent review (2008 -2013). *Expert Opin. Ther. Pat.* **2013**, *23*, 737−749.

[55] Lehtonen, J.; Shen, B.; Vihinen, M.; Casini, A.; Scozzafava, A.; Supuran, C.T.; Parkkila, A. K.; Saarnio, J.; Kivelä, A. J.; Waheed, A.; Sly, W. S.; Parkkila, S. Characterization of CA XIII, a novel member of the carbonic anhydrase isozyme family. *J. Biol. Chem.* **2004**, *279*, 2719-2727.

[56] Shah, G. N.; Ulmasov, B.; Waheed, A.; Becker, T.; Makani, S.; Svichar, N.; Chesler, M.; Sly, W. S. Carbonic anhydrase IV and XIV knockout mice: roles of the respective carbonic anhydrases in buffering the extracellular space in brain. *Proc. Natl. Acad. Sci .U.S.A.* **2005**, *102*, 16771-16776.

[57] Ogilvie, J.M.; Ohlemiller, K.K.; Shah, G. N.; Ulmasov, B.; Becker, T.A.; Waheed, A.; Hennig, A.K.; Lukasiewicz, P. D.; Sly, W. S. Carbonic anhydrase XIV deficiency produces a functional defect in the retinal light response. *Proc. Natl. Acad. Sci. U.S.A.* **2007**, *104*, 8514-8519.

[58] Alterio, V.; Di Fiore, A.; D'Ambrosio, K.; Supuran, C.T.; De Simone, G. In Drug Design of Zinc-Enzyme Inhibitors: Functional, Structural, and Disease Applications; Supuran, C.T., Winum, J.-Y., Eds.; Wiley: Hoboken, NJ, **2009**; p 73.

[59] Eriksson, A. E.; Kylsten, P. M.; Jones, T. A.; Liljas, A. Crystallographic studies of inhibitor binding sites in human carbonic anhydrase II: a pentacoordinated binding of the SCN- ion to the zinc at high pH. *Proteins* **1988**, *4*, 283-293.

[60] Boriack-Sjodin, P.A.; Heck, R.W.; Laipis, P.J.; Silverman, D.N.; Christianson, D.W. Structure determination of murine mitochondrial carbonic anhydrase V at 2.45-A resolution: implications for catalytic proton transfer and inhibitor design. *Proc. Natl. Acad. Sci. U.S.A.* **1995**, *92*, 10949-10953.

[61] Eriksson, A. E.; Liljas, A. Refined structure of bovine carbonic anhydrase III at 2.0 A resolution. *Proteins* **1993**, *16*, 29-42.

[62] Stams, T.; Nair, S.K.; Okuyama, T.; Waheed, A.; Sly, W.S.; Christianson, D.W. Crystal structure of the secretory form of membrane-associated human carbonic anhydrase IV at 2.8-A resolution. *Proc. Natl. Acad. Sci. U.S.A.* **1996**, *93*, 13589-13594.

[63] Angeli, A.; Vaiano, F.; Mari, F.; Bertol E.; Supuran, C.T. Psychoactive substances belonging to the amphetamine class potently activate brain carbonic anhydrase isoforms VA, VB, VII, and XII. *J Enzyme Inhib Med Chem.* **2017**, *32*, 1253-1259.

[64] Whittington, D.A.; Grubb, J.H.; Waheed, A.; Shah, G.N.; Sly, W.S.; Christianson, D.W. Expression, assay, and structure of the extracellular domain of murine carbonic anhydrase XIV: implications for selective inhibition of membrane-associated isozymes. *J. Biol. Chem.* **2004**, *279*, 7223-7228.

[65] Duda, D.M.; Tu, C.; Fisher, S.Z.; An, H.; Yoshioka, C.; Govindasamy, L.; Laipis, P.J.; Agbandje-McKenna, M.; Silverman, D. N.; McKenna, R. Human carbonic anhydrase III: structural and kinetic study of catalysis and proton transfer. *Biochemistry* **2005**, *44*, 10046-10053.

[66] Di Fiore, A.; Monti, S. M.; Hilvo, M.; Parkkila, S.; Romano, V.; Scaloni, A.; Pedone, C.; Scozzafava, A.; Supuran, C.T.; De Simone, G. Crystal structure of human carbonic anhydrase XIII and its complex with the inhibitor acetazolamide. *Proteins* **2008**, *74*, 164-175.

[67] Alterio, V.; Hilvo, M.; Di Fiore, A.; Supuran, C.T.; Pan, P.; Parkkila, S.; Scaloni, A.; Pastorek, J.; Pastorekova, S.; Pedone, C.; Scozzafava, A.; Monti, S.M.; De Simone, G. Crystal structure of the catalytic domain of the tumor-associated human carbonic anhydrase IX *Proc. Natl. Acad. Sci. U.S.A.* **2009**, *106*, 16233-16238.

[68] Di Fiore, A.; Truppo, E.; Supuran, C.T.; Alterio, V.; Dathan, N.; Bootorabi, F.; Parkkila, S.; Monti, S. M.; De Simone, G. Crystal structure of the C183S/C217S mutant of human CA VII in complex with acetazolamide. *Bioorg. Med. Chem. Lett.* **2010**, *20*, 5023-5026.

[69] Capasso, C.; Supuran C.T. Anti-infective carbonic anhydrase inhibitors: a patent and literature review. *Expert Opin. Ther. Pat.* **2013**, *23*, 693-704.

[70] Chirica, L.C.; Petersson, C.; Hurtig, M.; Jonsson, B.H.; Borén, T.; Lindskog, S. Expression and localization of alpha- and beta-carbonic anhydrase in Helicobacter pylori. *Biochim. Biophys. Acta.* **2002**, *1601*, 192-199.

[71] Nishimori, I.; Minakuchi, T.; Morimoto, K.; Sano, S.; Onishi, S.; Takeuchi, H.; Vullo, D.; Scozzafava, A.; Supuran, C.T. Carbonic anhydrase inhibitors: DNA cloning and inhibition studies of the alpha-carbonic

anhydrase from Helicobacter pylori, a new target for developing sulfonamide and sulfamate gastric drugs. *J. Med. Chem*. **2006**, *49*, 2117-2126.

[72] Shahi, D.R.; Zdeh, R.; Opekun, A.; Shiotani, A; Graham D.Y. Effect of the carbonic anhydrase inhibitor, acetazolamide, on Helicobacter pylori infection in vivo: a pilot study. *Helicobacter* **2005**, *10*, 136-138.

[73] Del Prete, S.; Isik, S.; Vullo, D.; De Luca, V.; Carginale, V.; Scozzafava, A.; Supuran C.T.; Capasso, C. DNA cloning, characterization, and inhibition studies of an alpha-carbonic anhydrase from the pathogenic bacterium Vibrio cholerae. *J. Med. Chem.* **2012**, *55*, 10742-10748.

[74] Vullo, D.; Isik, S.; Del Prete, S.; De Luca, V.; Carginale, V.; Scozzafava, A.; Supuran, C.T.; Capasso, C. Anion inhibition studies of the alpha-carbonic anhydrase from the pathogenic bacterium Vibrio cholerae. *Bioorg. Med. Chem. Lett.* **2013**, *23*, 1636-1638.

[75] Innocenti, A.; Hall, R.A.; Schlicker, C.; Scozzafava, A.; Steegborn, C.; Mühlschlegel, F.A.; Supuran, C.T. Carbonic anhydrase inhibitors. Inhibition and homology modeling studies of the fungal beta-carbonic anhydrase from Candida albicans with sulfonamides. *Bioorg. Med. Chem.* **2009**, *17*, 4503-4509.

[76] Monti, S.M.; Maresca, A.; Viparelli, F.; Carta, F.; De Simone, G.; Mühlschlegel, F.A.; Scozzafava, A.; Supuran, C.T. Dithiocarbamates are strong inhibitors of the beta-class fungal carbonic anhydrases from Cryptococcus neoformans, Candida albicans and Candida glabrata. *Bioorg. Med. Chem. Lett.* **2012**, *22*, 859-862.

[77] Cottier, F.; Leewattanapasuk, W.; Kemp, L.R.; Murphy, M.; Supuran, C.T.; Kurzai, O.; Mühlschlegel, F. A. Carbonic anhydrase regulation and CO(2) sensing in the fungal pathogen Candida glabrata involves a novel Rca1p ortholog. *Bioorg. Med. Chem.* **2013**, *21*, 1549-1554.

[78] Davis. R.A.; Hofmann, A.; Osman, A.; Hall, R.A.; Mühlschlegel, F.A.; Vullo, D.; Innocenti, A.; Supuran, C.T.; Poulsen, S.A. Natural product-based phenols as novel probes for mycobacterial and fungal carbonic anhydrases. *J. Med. Chem.* **2011**, *54*, 1682-1692.

[79] Isik, S.; Kockar, F.; Arslan, O.; Guler, O.O.; Innocenti, A.; Supuran, C.T. Carbonic anhydrase inhibitors. Inhibition of the beta-class enzyme from the yeast Saccharomyces cerevisiae with anions. *Bioorg. Med. Chem. Lett*. **2008**, *18*, 6327-6331.

[80] Hewitson, K.S.; Vullo, D.; Scozzafava. A.; Mastrolorenzo, A.; Supuran, C.T. Molecular cloning, characterization, and inhibition studies of a beta-carbonic anhydrase from Malassezia globosa, a potential antidandruff target. *J. Med. Chem.* **2012**, *55*, 3513-3520.

[81] Krungkrai, J.; Scozzafava, A.; Reungprapavut, S.; Krungkrai, S. R.; Rattanajak, R.; Kamchonwongpaisan, S.; Supuran C.T. Carbonic anhydrase inhibitors. Inhibition of Plasmodium falciparum carbonic anhydrase with aromatic sulfonamides: towards antimalarials with a novel mechanism of action? *Bioorg. Med. Chem.* **2005**, *13*, 483-489.

[82] Krungkrai, S. R; Suraveratum, N.; Rochanakij, S.; Krungkrai, J. Characterisation of carbonic anhydrase in Plasmodium falciparum. *Int. J. Parasitol* **2001**, *31*, 661-668.

[83] Supuran C.T.; Capasso C. The eta-class carbonic anhydrases as drug targets for antimalarial agents. *Expert Opin. Ther. Targets* **2015**, *19*, 551-563.

[84] Pan, P.; Vermelho, A.B.; Capaci Rodrigues, G.; Scozzafava, A.; Tolvanen, M.E.; Parkkila, S.; Capasso, C.; Supuran, C.T. Cloning, characterization, and sulfonamide and thiol inhibition studies of an alphacarbonic anhydrase from Trypanosoma cruzi, the causative agent of Chagas disease. *J. Med. Chem.* **2013**, *56*, 1761-1771.

[85] Guzel-Akdemir, O.; Akdemir, A.; Pan, P.; Vermelho, A.B.; Parkkila, S.; Scozzafava, A.; Capasso, C.; Supuran, C.T. A class of sulfonamides with strong inhibitory action against the alpha-carbonic anhydrase from Trypanosoma cruzi. *J. Med. Chem.* **2013**, *56*, 5773-5781.

[86] Syrjanen, L.; Vermelho, A.B.; Rodrigues Ide, A.; Corte-Real, S.; Salonen, T.; Pan, P.; Vullo, D.; Parkkila, S.; Capasso, C.; Supuran, C.T. Cloning, characterization, and inhibition studies of a beta-carbonic anhydrase from *Leishmania donovani chagasi*, the protozoan parasite responsible for leishmaniasis. *J. Med. Chem* **2013**, *56*, 7372-7381.

[87] Supuran, C.T. Structure-based drug discovery of carbonic anhydrase inhibitors. *J. Enzyme Inhib. Med. Chem.* **2012**, *27*, 759–772.

[88] Supuran, C.T. Carbonic anhydrase inhibitors. *Bioorg. Med. Chem. Lett*. **2010**, *20*, 3467–3474.

[89] Carta, F.; Supuran, C.T.; Scozzafava, A. Sulfonamides and their isosters as carbonic anhydrase inhibitors. *Future Med. Chem.* **2014**, *6*, 1149-1165.

[90] Winum, J.-Y.; Supuran, C.T. Recent advances in the discovery of zinc-binding motifs for the development of carbonic anhydrase inhibitors. *J. Enzyme Inhib. Med. Chem*. **2015**, *30*, 321-324.

[91] Supuran, C.T. How many carbonic anhydrase inhibition mechanisms exist? *J. Enzyme Inhib. Med. Chem.* **2016**, *31*, 345-360.

[92] Keilin, D.; Mann, T. Carbonic anhydrase. Purification and nature of the enzyme. *Biochem. J.* **1940**, *34*, 1163-1176.

[93] Winum, J.-Y.; Monter, J,-L.; Scozzafava, A.; Supuran, C.T. In Drug Design of Zinc-Enzyme Inhibitors: Functional, Structural, and Disease Applications; Supuran, C.T., Winum, J.-Y., Eds.; *Wiley: Hoboken*, NJ, **2009**; p 39.

[94] Supuran, C.T.; De Simone, G. Carbonic Anhydrases as Biocatalysts: From Theory to Medical and Industrial Applications; Supuran, C.T., De Simone, G. Eds.; *Elsevier.* **2015**.

[95] Bozdag, M.; Ferraroni, M.; Nuti, E.; Vullo, D.; Rossello, A.; Carta, F.; Scozzafava, A.; Supuran, C.T. Combining the tail and the ring approaches for obtaining potent and isoform-selective carbonic anhydrase inhibitors: solution and X-ray crystallographic studies. *Bioorg. Med. Chem.* **2014**, *22*, 334−340.

[96] Scozzafava, A.; Menabuoni, L.; Mincione, F.; Briganti, F.; Mincione, G.; Supuran, C.T. Carbonic anhydrase inhibitors. Synthesis of water-soluble, topically effective, intraocular pressure-lowering aromatic/heterocyclic sulfonamides containing cationic or anionic moieties: Is the tail more important than the ring? *J. Med. Chem.* **1999**, *42*, 2641−2650.

[97] Menchise, V.; De Simone, G.; Alterio, V.; Di Fiore, A.; Pedone, C.; Scozzafava, A.; Supuran, C.T. Carbonic anhydrase inhibitors: stacking with Phe131 determines active site binding region of inhibitors as exemplified by the X-ray crystal structure of a membrane-impermeant antitumor sulfonamide complexed with isozyme II. *J. Med. Chem.* **2005**, *48*, 5721-5727.

[98] Scozzafava, A.; Briganti, F.; Ilies, M.A.; Supuran, C.T. Carbonic anhydrase inhibitors: synthesis of membrane-impermeant low molecular weight sulfonamides possessing in vivo selectivity for the membrane-bound versus cytosolic isozymes. *J. Med. Chem.* **2000**, *43*, 292-300.

[99] Pacchiano, F.; Carta, F.; McDonald, P.C.; Lou, Y.; Vullo, D.; Scozzafava, A.; Dedhar, S.; Supuran, C.T. Ureido-substituted benzenesulfonamides potently inhibit carbonic anhydrase IX and show antimetastatic activity in a model of breast cancer metastasis. *J. Med. Chem.* **2011**, *54*, 1896−1902.

[100] ClinicalTrials.gov, https://clinicaltrials.gov/ct2/results?term=slc-0111Search=Search (Accessed on October 10th 2019); https://clinicaltrials.gov/ct2/show/NCT03450018 (last updated on March 1, 2018); last accessed on October 10th, 2019.

[101] Carta, F.; Aggarwal, M.; Maresca, A.; Scozzafava, A.; McKenna, R.; Supuran, C.T. Dithiocarbamates: a new class of carbonic anhydrase inhibitors. Crystallographic and kinetic investigations. *Chem. Commun. (Camb).* **2012**, *48*, 1868-1870.

[102] Carta, F.; Aggarwal, M.; Maresca, A; Scozzafava, A.; McKenna, R.; Masini, E.; Supuran, C.T. Dithiocarbamates strongly inhibit carbonic anhydrases and show antiglaucoma action in vivo. *J. Med. Chem.* **2012**, *55*,1721-1730.

[103] Carta, F.; Akdemir, A.; Scozzafava, A.; Masini, E; Supuran, C.T. Xanthates and trithiocarbonates strongly inhibit carbonic anhydrases and show antiglaucoma effects in vivo. *J. Med. Chem.* **2013**, *56*, 4691-4700.

[104] Vullo, D.; Durante, M.; Di Leva, F. S.; Cosconati, S.; Masini, E.; Scozzafava, A.; Novellino, E.; Supuran, C.T.; Carta, F. Monothiocarbamates Strongly Inhibit Carbonic Anhydrases in Vitro and Possess Intraocular Pressure Lowering Activity in an Animal Model of Glaucoma. *J. Med. Chem.* **2016**, *59*, 5857-5867.

[105] Mori, M.; Cau, Y.; Vignaroli, G.; Laurenzana, I.; Caivano, A.; Vullo, D.; Supuran, C.T.; Botta, M. Hit recycling: discovery of a potent carbonic anhydrase inhibitor by in silico target fishing. *ACS Chem. Biol.* **2015**, *10*, 1964–1969.

[106] Innocenti, A.; Vullo, D.; Scozzafava, A.; Casey, J.R.; Supuran, C.T. Carbonic anhydrase inhibitors. Interaction of isozymes I, II, IV, V and IX with carboxylates. *Bioorg. Med. Chem. Lett.* **2005**, *15*, 573–578.

[107] Scozzafava, A.; Supuran, C.T. Hydroxyurea is a carbonic anhydrase inhibitor. *Bioorg. Med. Chem.* **2003**, *11*, 2241–2246.

[108] Di Fiore, A.; Maresca, A.; Supuran, C.T.; De Simone, G. Hydroxamate represents a versatile zinc binding group for the development of new carbonic anhydrase inhibitors. *Chem. Commun. (Camb.)* **2012**, *48*, 8838–8840.

[109] Nocentini, A.; Gratteri, P.; Supuran, C.T. Phosphorus versus Sulfur: Discovery of Benzenephosphonamidates as Versatile Sulfonamide-Mimic Chemotypes Acting as Carbonic Anhydrase Inhibitors. *Chemistry.* **2019**, *5*, 1188-1192.

[110] Alterio, V.; Cadoni, R.; Esposito, D., Vullo, D.; Fiore, A.D.; Monti, S.M.; Caporale, A.; Ruvo, M.; Sechi, M.; Dumy, P.; Supuran, C.T.; De Simone, G.; Winum J.Y. Benzoxaborole as a new chemotype for carbonic anhydrase inhibition. *Chem Commun (Camb).* **2016**, *52*, 11983-11986.

[111] Angeli, A.; Tanini, D.; Nocentini, A., Capperucci, A.; Ferraroni, M.; Gratteri, P.; Supuran, C.T. Selenols: a new class of carbonic anhydrase inhibitors. *Chem Commun (Camb).* **2019**, *55*, 648-651.

[112] Nair, S. K.; Ludwig, P. A.; Christianson, D. W. Two-site binding of phenol in the active site of human carbonic anhydrase II: structural implications for substrate association. *J. Am. Chem. Soc.* **1994**, *116*, 3659–3660.

[113] Innocenti, A.; Vullo, D.; Scozzafava, A.; Supuran, C.T. Carbonic anhydrase inhibitors. Interactions of phenols with the 12 catalytically active mammalian isoforms (CA I–XIV). *Bioorg. Med. Chem. Lett*. **2008**, *18*, 1583–1587.

[114] Carta, F.; Temperini, C.; Innocenti, A.; Scozzafava, A.; Kaila, K.; Supuran, C.T. Polyamines inhibit carbonic anhydrases by anchoring to the zinc-coordinated water molecule. *J. Med. Chem.* **2010,** *53*, 5511–5522.

[115] Innocenti, A.; Ozturk Sarkaya, S.B.; Gulcin, I.; Supuran, C.T. Carbonic anhydrase inhibitors. Inhibition of mammalian isoforms I-XIV with a seriess of natural product polyphenols and phenolic acids. *Bioorg. Med. Chem.* **2010**, *18*, 2159–2164.

[116] Davis, R.A.; Hofmann, A.; Osman, A.; Hall, R. A.; Mühlschlegel, F.A.; Vullo, D.; Innocenti, A.; Supuran, C.T.; Poulsen, S. A. Natural product-based phenols as novel probes for mycobacterial and fungal carbonic anhydrases. *J. Med. Chem.* **2011**, *54*, 1682–1692.

[117] Martin, D.P.; Cohen, S.M. Nucleophile recognition as an alternative inhibition mode for benzoic acid based carbonic anhydrase inhibitors. *Chem. Commun. (Camb.)* **2012**, *48*, 5259–5261.

[118] Tars, K.; Vullo, D.; Kazaks, A.; Leitans, J.; Lends, A.; Grandane, A.; Zalubovskis, R.; Scozzafava, A.; Supuran, C.T. Sulfocoumarins (1,2- benzoxathiine-2,2-dioxides): a class of potent and isoform-selective inhibitors of tumor-associated carbonic anhydrases. *J. Med. Chem.* **2013**, *56*, 293–300.

[119] Buchieri, M.V.; Riafrecha, L.E.; Rodrıguez, O. M.; Vullo, D.; Morbidoni, H. R.; Supuran, C.T.; Colinas, P. A. Inhibition of the b-carbonic anhydrases from Mycobacterium tuberculosis with C-cinnamoyl glycosides: identification of the first inhibitor with anti-mycobacterial activity. *Bioorg. Med. Chem. Lett*. **2013**, *23*, 740–743.

[120] Maresca, A.; Temperini, C.; Vu, H.; Pham, N.B.; Poulsen, S.A.; Scozzafava, A.; Quinn, R.J. Supuran, C.T. Non-zinc mediated inhibition of carbonic anhydrases: coumarins are a new class of suicide inhibitors. *J. Am. Chem. Soc.* **2009**, *131*, 3057–3062.

[121] Maresca, A.; Temperini, C.; Pochet, L.; Masereel, B.; Scozzafava, A.; Supuran, C.T. Deciphering the mechanism of carbonic anhydrase inhibition with coumarins and thiocoumarins. *J. Med. Chem.* **2010**, *53*, 335–344.

[122] Temperini, C.; Innocenti, A.; Scozzafava, A.; Parkkila, S.; Supuran, C.T. The coumarin binding site in carbonic anhydrase accommodates structurallydiverse inhibitors: the antiepileptic lacosamide as an example and lead molecule for novel classes of carbonic anhydrase inhibitors. *J. Med. Chem*. **2010**, *53*, 850–854.

[123] Touisni, N.; Maresca, A.; McDonald, P.C.; Lou, Y.; Scozzafava, A.; Dedhar, S.; Winum, J.Y.; Supuran, C.T. Glycosyl coumarin carbonic anhydrase IX and XII inhibitors strongly attenuate the growth of primary breast tumors. *J. Med. Chem.* **2011***, 54*, 8271–8277.

[124] Bonneau, A; Maresca, A.; Winum, J.-Y.; Supuran, C.T. Metronidazolecoumarin conjugates and 3-cyano-7-hydroxy-coumarin act as isoform-selective carbonic anhydrase inhibitors. *J. Enzyme Inhib. Med. Chem.* **2013**, *28*, 397–401.

[125] Sharma, A.; Tiwari, M.; Supuran, C.T. Novel coumarins and benzocoumarins acting as isoform-selective inhibitors against the tumor-associated carbonic anhydrase IX. *J. Enzyme Inhib. Med. Chem.* **2014**, *29*, 292–296.

[126] Maresca, A.; Supuran, C.T. Coumarins incorporating hydroxy- and chloro- moieties selectively inhibit the transmembrane, tumor-associated carbonic anhydrase isoforms IX and XII over the cytosolic ones I and II. *Bioorg. Med. Chem. Lett.* **2010**, *20*, 4511–4514.

[127] Maresca, A.; Scozzafava, A.; Supuran, C.T. 7,8-Disubstituted- but not 6,7-disubstituted coumarins selectively inhibit the transmembrane, tumor-associated carbonic anhydrase isoforms IX and XII over the cytosolic ones I and II in the low nanomolar/subnanomolar range. *Bioorg. Med. Chem. Lett.* **2010**, *20*, 7255–7258.

[128] D'Ambrosio, K.; Carradori, S.; Monti, S.M.; Buonanno, M.; Secci, D.; Vullo, D.; Supuran, C.T.; De Simone, G. Out of the active site binding pocket for carbonic anhydrase inhibitors. *Chem Commun* **2015**, *51*, 302–305.

[129] D'Ascenzio, M.; Carradori, S.; De Monte, C.; Secci, D.; Ceruso, M.; Supuran, C.T. Design, synthesis and evaluation of N-substituted saccharin derivatives as selective inhibitors of tumor-associated carbonic anhydrase XII. *Bioorg Med Chem* **2014**, *22*, 1821–1831.

[130] De Monte, C.; Carradori, S.; Secci, D.; D'Ascenzio, M.; Vullo, D.; Ceruso, M.; Supuran, C.T. Cyclic tertiary sulfamates: selective inhibition of the tumor-associated carbonic anhydrases IX and XII by N- and O-substituted acesulfame derivatives. *Eur J Med Chem* **2014**, *84*, 240–246.

[131] Parkkila, S.; Innocenti, A.; Kallio, H.; Hilvo, M.; Scozzafava, A.; Supuran, C.T. The protein tyrosine kinase inhibitors imatinib and nilotinib strongly inhibit several mammalian a-carbonic anhydrase isoforms. *Bioorg Med Chem Lett* **2009**, *19*, 4102–4106.

[132] Briganti, F.; Mangani, S.; Orioli, P.; Scozzafava, A.; Vernaglione, G.; Supuran, C.T. Carbonic anhydrase activators: x-ray crystallographic and spectroscopic investigations for the interaction of isozymes I and II with histamine. *Biochemistry* **1997**, *36*, 10384–10392.

[133] Supuran, C.T. Carbonic anhydrases: from biomedical applications of the inhibitors and activators to biotechnologic use for CO2 capture. *J. Enzyme Inhib Med Chem* **2013**, *28*, 229–230.

[134] Temperini, C.; Scozzafava, A.; Supuran, C.T. Carbonic anhydrase activation and the drug design. *Curr Pharm Des*. **2008**, *14*, 708-715.

[135] Temperini, C.; Scozzafava, A.; Vullo, D.; Supuran, C.T. Carbonic anhydrase activators. Activation of isozymes I, II, IV, VA, VII, and XIV with l- and d-histidine and crystallographic analysis of their adducts with isoform II: engineering proton-transfer processes within the active site of an enzyme. *Chemistry.* **2006**, *12*, 7057-7066.

[136] Temperini, C.; Scozzafava, A.; Puccetti, L.; Supuran, C.T. Carbonic anhydrase activators: X-ray crystal structure of the adduct of human isozyme II with L-histidine as a platform for the design of stronger activators. *Bioorg Med Chem Lett.* **2005**, *15*, 5136-5141.

[137] Temperini, C.; Scozzafava, A.; Supuran, C.T. Carbonic anhydrase activators: the first X-ray crystallographic study of an adduct of isoform I. *Bioorg Med Chem Lett.* **2006**, *16*, 5152-5156.

[138] Somogyi, P.; Klausberger, T.; Defined types of cortical interneurone structure space and spike timing in the hippocampus. *J Physiol.* **2005**, *562*, 9-26.

[139] Buzsáki, G.; Kaila, K.; Raichle, M. Inhibition and brain work. *Neuron.* **2007**, *56*, 771–83.

[140] Ferando, I.; Mody, I. Interneuronal GABAA receptors inside and outside of synapses. *Curr. Opin. Neurobiol.* **2014**, *26*, 57-63.

[141] Rudolph, U.; Knoflach, F. Beyond classical benzodiazepines: novel therapeutic potential of GABAA receptor subtypes. *Nat. Rev. Drug. Discov.* **2011**, *10*, 685-97.

[142] Sigel E.; Steinmann M.E. Structure, function, and modulation of GABA(A) receptors. *J. Biol. Chem.* **2012**, *287*, 40224-31.

[143] Korpi, E.R.; Grunder, G.; Lüddens, H. Drug interactions at GABA(A) receptors. *Prog. Neurobiol.* **2002**, *67*, 113-59.

[144] Tsang, S.Y.; Xue, H. Development of effective therapeutics targeting the GABAA receptor: naturally occurring alternatives. *Curr. Pharm. Des.* **2004**, *10*, 1035-44.

[145] Licata, S.C.; Rowlett, J.K. Abuse and dependence liability of benzodiazepine-type drugs: GABA(A) receptor modulation and beyond. *Pharmacol. Biochem. Behav.* **2008**, *90*, 74-89.

[146] Vlainić, J.; Peričić D. Effects of acute and repeated zolpidem treatment on pentylenetetrazole-induced seizure threshold and on locomotor activity: comparison with diazepam. Neuropharmacol. **2009**, 56, 1124-30.

[147] Vinkers, C.H.; Olivier, B. Mechanisms underlying tolerance after long-term benzodiazepine use: a future for subtype-selective GABAA receptor modulators? *Adv. Pharmacol. Sci.* **2012**: 416864.

[148] Jazvinšćak, J.M.; Vlainić, J.; Šuran, J. Zolpidem withdrawal induced uncoupling of GABAA receptors in vitro associated with altered GABAA receptor subunit mRNA expression. *Acta Neurobiol. Exp.* **2015**, *75*, 160-71.

[149] Bowery, N.G.; Bettler, B.; Froestl, W.; Gallagher, J.P.; Marshall, F.; Raiteri, M.; Bonner, T.I.; Enna, S.J. International Union of Pharmacology. XXXIII. Mammalian γ-aminobutyric acid (B) receptors: structure and function. *Pharmacol. Rev.* **2002**, *54*, 247-64.

[150] Miller, P.S.; Smart, T.G. Binding, activation and modulation of Cys-loop receptors. *Trends Pharmacol. Sci.* **2010**, *31*, 161-74.

[151] Olsen, R.W.; Sieghart, W. International Union of Pharmacology. LXX. Subtypes of gamma-aminobutyric acid (A) receptors: classification on the basis of subunit composition, pharmacology, and function. *Update Pharmacol. Rev.* **2008**, *60*, 243-60.

[152] Barnard, E.A.; Skolnick, P.; Olsen, R.W, Mohler, H.; Sieghart, W.; Biggio, G.; Braestrup, C.; Bateson, A.N.; Langer S.Z. International union of pharmacology: XV. Subtypes of γ-Aminobutyric acidA receptors: classification on the basis of subunit structure and receptor function. *Pharmacol. Rev.* **2008**, *50*, 291-313.

[153] Sieghart, W.; Fuchs, K.; Tretter, V.; Ebert, V.; Jechlinger M.; Höger, H.; Adamiker, D. Structure and subunit composition of GABA receptors. *Neurochem. Int.* **1999**, *34*, 379-85.

[154] Uusi-Oukari, M, Korpi, ER. Regulation of GABAA receptor subunit expression by pharmacological agents. *Pharmacol. Rev.* **2010***, 62*, 97-135.

[155] Hörtnagl, H.; Tasan, R.O.; Wieselthaler, A.; Kirchmair, E.; Sieghart, W.; Sperk, G. Patterns of mRNA and protein expression for 12 GABAA receptor subunits in the mouse brain. *Neurosci.* **2013**, *236*, 345-72.

[156] Laurie, D.J.; Seeburg, P.H.; Wisden, W. The distribution of 13 GABAA receptor subunit mRNAs in the rat brain. II. Olfactory bulb and cerebellum. *J. Neurosci.* **1992**, *12*, 1063-1076.

[157] Wisden, W.; Laurie, D.J.; Monyer, H.; Seeburg, P.H. The distribution of 13 GABAA receptor subunit mRNAs in the rat brain. I. Telencephalon, diencephalon, mesencephalon. *J. Neurosci.* **1992**, *12*, 1040-1062.

[158] Zhang, D.; Pan, Z.H.; Awobuluyi, M.; Lipton, S.A. Structure and function of GABA(C) receptors: a comparison of native versus recombinant receptors. *Trends Pharmacol. Sci.* **2001**, *22*, 121-132.

[159] Glykys, J.; Mann, E.O.; Mody, I. Which GABA(A) receptor subunits are necessary for tonic inhibition in the hippocampus? *J. Neurosci.* **2008**, *28*, 1421-1426.

[160] Fritschy, J.M.; Panzanelli, P. GABAA receptors and plasticity of inhibitory neurotransmission in the central nervous system. *Eur. J. Neurosci.* **2014**, *39*, 1845-1865.

[161] Olsen, R.W.; Sieghart, W. GABAA receptors: subtypes provide diversity of function and pharmacology. *Neuropharmacol.* **2009**, *56*, 141-148.

[162] Chen, Z.W.; Olsen, R.W. GABAA receptor associated proteins: a key factor regulating GABAA receptor function. *J. Neurochem.* **2007**; *100*, 279-294.

[163] Tretter, V.; Ehya, N.; Fuchs, K.; Sieghart, W. Stoichiometry and assembly of a recombinant GABAA receptor subtype. *J. Neurosci.* **1997**, *17*, 2728-2737.

[164] Gunn, B.G.; Cunningham, L.; Mitchell, S.G.; Swinny, J.D.; Lambert, J.J.; Belelli, D. GABAA receptor-acting neurosteroids: a role in the development and regulation of the stress response. *Front. Neuroendocrinol.* **2015**, *36*, 28-48.

[165] Baumann, S.W.; Baur, R.; Sigel, E. Forced subunit assembly in α1β2γ2 GABAA receptors. Insight into the absolute arrengement. *J. Biol. Chem.* **2002**, *277*, 46020-46025.

[166] Pöltl, A.; Hauer, B.; Fuchs, K.; Tretter, V.; Sieghart, W. Subunit composition and quantitative importance of GABA(A) receptor subtypes in the cerebellum of mouse and rat. *J. Neurochem.* **2003**, *87*, 1444-1455.

[167] Sieghart, W.; Sperk, G. Subunit composition, distribution and function of GABA(A) receptor subtypes. *Curr. Top. Med. Chem.* **2002**, *2*, 795-816.

[168] Minier, F.; Sigel, E. Positioning of the α-subunit isoforms confers a functional signature to γ-aminobutyric acid type A receptors. *Proc. Natl. Acad. Sci. USA* **2004**, *101*, 7769-7774.

[169] Zezula, J.; Slany, A.; Sieghart, W. Interaction of allosteric ligands with GABAA receptors containing one, two, or three different subunits. *Eur. J. Pharmacol.* **1996**, *301*, 207–214.

[170] Farrant, M.; Nusser, Z. Variations on an inhibitory theme: phasic and tonic activation of GABAA receptors. *Nat. Rev. Neurosci* **2005**, *6*, 215-229.

[171] Belelli, D.; Harrison, N.L.; Maguire, J.; Macdonald, R.L.; Walker, M.C.; Cope, D.W. Extrasynaptic GABAA receptors: form, pharmacology, and function. *J. Neurosci.* **2009**, *29*, 12757–12763.

[172] Brickley, S.G.; Mody, I. Extrasynaptic GABA(A) receptors: their function in the CNS and implications for disease. *Neuron.* **2012**, *73*, 23-34.

[173] Carver, C.M.; Reddy, D.S. Neurosteroid interactions with synaptic and extrasynaptic GABA(A) receptors: regulation of subunit plasticity, phasic and tonic inhibition, and neuronal network excitability. *Psychopharmacol.* (Berl) **2013**, *230*, 151-188.

[174] Whissell, P.D.; Lecker, I.; Wang, D.S.; Yu, J, Orser BA. Altered expression of δGABAA receptors in health and disease. *Neuropharmacol.* **2015**, *88*, 24-35.

[175] Chebib, M.; Johnston, G.A.R. The 'ABC' of GABA receptors: a brief review. Clin. *Exp. Pharmacol. Physiol.* **1999**, *26*, 937-940.

[176] Johnston, G.A.R. Medicinal chemistry and molecular pharmacology of GABAC receptors. *Curr. Top. Med. Chem.* **2000**, *2*, 903-913.

[177] Johnston, G.A.R. GABA(A) receptor channel pharmacology. *Curr. Pharm. Des.* **2005**; *11*: 1867-1885.

[178] Zhang, D.; Pan, Z-H.; Awobuluyi M.; Lipton S.A. Structure and function of GABAC receptors: a comparison of native versus recombinant receptors. *Trends Pharmacol. Sci.* **2001**, *22*, 121-132.

[179] Ng, C.K.L.; Kim, H.L.; Gavande, N.; Yamamoto, I..; Kumar, R.J.; Mewett, K.N.; Johnston G.A.R.; Hanrahan, J.R.; Chebib, M.; Medicinal chemistry of ρ GABAC receptors. *Future Med. Chem.* **2011**, *3*, 197-209.

[180] Cunha, C.; Monfils, M.H.; Ledoux, J.E. GABA(C) Receptors in the Lateral Amygdala: A Possible Novel Target for the Treatment of Fear and Anxiety Disorders? *Front. Behav. Neurosci.* **2010**, *4*, 6.

[181] Gavande, N.; Kim, H.L.; Doddareddy, M.R.; Johnston, G.A.; Chebib, M.; Hanrahan, J.R. Design, synthesis, and pharmacological evaluation of fluorescent and biotinylated antagonists of ρ1 GABAC receptors. *ACS Med. Chem. Lett.* **2013**, *4*, 402-407.

[182] Johnston, G.A.R. Advantages of an antagonist: bicuculline and other GABA antagonists. *Br. J. Pharmacol.* **2013**, *169*, 328-336.

[183] Morris, K.D.W.; Moorefield, C.N.; Amin J. Differential modulation of the γ-aminobutyric acid type C receptor by neuroactive steroids. *Mol. Pharmacol.* **1999**, *56*, 752-759.

[184] Johnston, G.A.R. GABAA receptor pharmacology. *Pharmacol. Ther.* **1996**, *69*, 173-198.

[185] Zhang, J.; Xue, F.; Chang, Y. Structural determinants for antagonist pharmacology that distinguish the rho1 GABAC receptor from GABAA receptors. *Mol. Pharmacol.* **2008**, *74*, 941-951.

[186] Bettler, B.; Kaupmann, K.; Mosbacher, J.; Gassmann, M. Molecular structure and physiological functions of GABA(B) receptors. *Physiol. Rev.* **2004**, *84*, 835-867.

[187] Bowery, N.G.; Hudson, A.L.; Price, G.W. GABAA and GABAB receptor site distribution in the rat central nervous system. *Neurosci.* **1987**, *20*, 365-383.

[188] Armijo, J.A.; Shushtarian, M.; Valdizan, E.M.; Cuadrado, A.; de las Cuevas, I.; Adín, J. Ion channels and epilepsy. *Curr. Pharm. Des.* **2005**, *11*, 1975-2003.

[189] Cryan, J.F.; Kaupmann, K. Don't worry 'B' happy!: a role for GABAB receptors in anxiety and depression. *Trends Pharmacol. Sci.* **2005**, *26*, 36-43.

[190] Bettler, B.; Tiao, J.Y-H. Molecular diversity, trafficking and subcelullar localization of GABAB receptors. *Pharmacol. Ther.* **2006**, *110*, 533-543.

[191] Kulik, A.; Vida, I.; Luján, R.; Haas, C.A.; López-Bendito, G.; Shigemoto, R.; Frotscher, M. Subcellular localization of metabotropic GABA(B) receptor subunits GABA(B1a/b) and GABA(B2) in the rat hippocampus. *J. Neurosci.* **2003**; *23*(35): 11026-11035.

[192] Tao, W.; Higgs, M.H.; Spain, W.J.; Ransom, C.B. Postsynaptic GABAB receptors enhance extrasynaptic GABAA receptor function in dentate gyrus granule cells. *J. Neurosci.* **2013**; *33*, 3738-3743.

[193] Shaye, H.; Ishchenko, A.; Lam, J.H.; Han, G.W.; Xue, L.; Rondard, P.; Pin, J.P.; Katritch, V.; Gati, C.; Cherezov, V. Structural basis of the activation of a metabotropic GABA receptor. *Nature* **2020**, *584*, 298-303.

[194] Kaupmann, K.; Malitschek, B.; Schuler V. GABA(B)-receptor subtypes assemble into functional heteromeric complexes. *Nature* **1998**; *396*(6712): 683-687.

[195] Malitschek, B.; Schweizer, C.; Keir, M.; Heid, J.; Froestl, W.; Mosbacher, J.; Kuhn, R.; Henley, J.; Joly, C.; Pin, J-P.; Kaupmann, K.; Bettle, B. The N-terminal domain of γ-aminobutyric Acid(B) receptors is sufficient to specify agonist and antagonist binding. *Mol. Pharmacol.* **1999**, *56*, 448-454.

196] Pin, J-P.; Kniazeff, J.; Binet, V.; Binet, V.; Liu, J.; Maurel, D.; Galvez, T.; Duthey, B.; Havlickova, M.; Blahos, J.; Prézeau, L.; Rondard, P. Activation mechanism of the heterodimeric GABAB receptor. *Biochem. Pharmacol.* **2004**, 68, 1565-1572.

[197] Steiger, J.L.; Bandyopadhyay, S.; Farb, D.H.; Russek, S.J. cAMP response element-binding protein, activating transcription factor-4, and upstream stimulatory factor differentially control hippocampal GABABR1a and GABABR1b subunit gene expression through alternative promoters. *J. Neurosci.* **2004**, *24*, 6115-6126.

[198] Galvez, T.; Duthey, B.; Kniazeff, J.; Blahos, J.; Rovelli, G.; Bettler, B.; Prézeau, L.; Pin, J-P. Allosteric interactions between GB1 and GB2 subunits are required for optimal GABA(B) receptor function. *EMBO J.* **2001**, *20*, 2152-2159.

[199] Pin, J-P.; Kniazeff, J.; Liu, J.; Binet, V.; Goudet, C.; Rondard, P.; Prézeau, L. Allosteric functioning of dimeric class C G-protein-coupled receptors. *FEBS J.* **2005**, *272*, 2947-2955.

[200] Monnier, C.; Tu, H.; Bourrier, E.; Vol, C.; Lamarque, L.; Trinquet, E.; Pin, J-P.; Rondard, P. Trans-activation between 7TM domains: implication in heterodimeric GABAB receptor activation. *EMBO J.* **2011**, *30*, 32-42.

[201] Froestl, W. Novel GABA(B) receptor positive modulators: a patent survey. *Expert Opin. Ther. Pat.* **2010**, *20*, 1007-1017

[202] Mehta, A.K.; Ticku, M.K. An update on GABAA receptors. *Brain Res. Rev.* **1999**, *29*, 196-217.

[203] Sieghart, W. Structure and pharmacology of GABAA receptor subtypes. *Pharmacol. Rev.* **1995**, *47*, 181-234.

[204] Rho, J.M.; Donevan, S.D.; Rogawski, MA. Direct activation of GABAA receptors by barbiturates in cultured rat hippocampal neurons. *J. Physiol.* **1996**, *497*, 509-522.

[205] Rosen, A.; Bali, M.; Horenstein, J.; Akabas, M.H. Channel opening by anesthetics and GABA induces similar changes in the GABAA receptor M2 segment. *Biophys. J.* **2007**, *92*, 3130-3139.

[206] Bianchi, M.T.; Botzolakis, E.J.; Lagrange, A.H.; Macdonald, R.L. Benzodiazepine modulation of GABA(A) receptor opening frequency depends on activation context: a patch clamp and simulation study. *Epilepsy Res.* **2009**, *85*, 212-220.

[207] Garcia, P.S.; Kolesky, S.E.; Jenkins A. General anesthetic actions on GABA(A) receptors. *Curr. Neuropharmacol.* **2010**, *8*, 2-9.

[208] Wagner, D.A.; Czajkowski, C. Structure and dynamics of the GABA binding pocket: a narrowing cleft that constricts during activation. *J. Neurosci.* **2001**, *21*, 67-74.

[209] Berezhnoy, D.; Baur, R.; Gonthier, A.; Foucaud, B.; Goeldner, M.; Sigel, E. Conformational changes at benzodiazepine binding sites of GABAA receptors detected with a novel technique. *J. Neurochem.* **2005**, *92*, 859-866.

[210] Sieghart, W. Allosteric modulation of GABAA receptors via multiple drug-binding sites. *Adv. Pharmacol.* **2015**, *72*, 53-96.

[211] Nikolaus, S.; Antke, C.; Beu, M.; Müller, H.W. Cortical GABA, striatal dopamine and midbrain serotonin as the key players in compulsive and anxiety disorders - results from in vivo imaging studies. *Rev. Neurosci.* **2010**, *21*, 119-139.

[212] Ravindran, L.N.; Stein, M.B. The pharmacologic treatment of anxiety disorders: a review of progress. *J. Clin. Psychiatry* **2010**, *71*, 839-854.

[213] Rudolph, U.; Möhler, H. GABAA receptor subtypes: Therapeutic potential in Down syndrome, affective disorders, schizophrenia, and autism. *Annu. Rev. Pharmacol. Toxicol.* **2014**, *54*, 483-507.

[214] Zarnowska, E.D.; Keist, R.; Rudolph, U.; Pearce, R.A. GABAA receptor α5 subunits contribute to GABAA, slow synaptic inhibition in mouse hippocampus. *J. Neurophysiol.* **2009**, *101*, 1179-1191.

[215] Babateen, O.; Jin, Z.; Bhandage, A.; Korol, S.V.; Westermark, B.; Forsberg Nilsson, K.; Uhrbom, L.; Smits, A.; Birnira, B. Etomidate, propofol and diazepam potentiate GABA-evoked GABAA currents in a cell line derived from human glioblastoma. *Eur. J. Pharmacol.* **2015**, *748*, 101-107.

[216] Lynagh, T.; Pless, S.A. Principles of agonist recognition in Cys-loop receptors. *Front. Physiol.* **2014**, *5*, 1-12.

[217] Baumann, S.W.; Baur, R.; Sigel, E. Individual properties of the two functional agonist sites in GABAA receptors. *J. Neurosci.* **2013**, *23*, 11158-11166.

[218] Macdonald, R.L.; Rogers, C.J.; Twyman, R.E. Kinetic properties of the GABAA receptor main conductance state of mouse spinal cord neurones in culture. *J. Physiol.* **1989**, *410*, 479–499.

[219] Twyman, R.E.; Rogers, C.J.; Macdonald, R.L. Intraburst kinetic properties of the GABAA receptor main conductance state of mouse spinal cord neurones in culture. *J. Physiol.* **1990**, *423*, 193-220.

[220] Zhu, S.; Noviello, C.M.; Teng, J.; Walsh, R.M.; Kim, J.J.; Hibbs, R.E. Structure of a human synaptic GABAAreceptor. *Nature* **2018**, *559*, 67-72

[221] Bianchi, M.T.; Macdonald, R.L. Neurosteroids shift partial agonist activation of GABAA receptor channels from low- to high-efficacy gating patterns. *J. Neurosci.* **2003**, *23*, 10934-10943.

[222] Brown, N.; Kerby, J.; Bonnert, T. P.; Whiting, P. J.; Wafford, K.A. Pharmacological characterization of a novel cell line expressing human α4β3δ GABAA receptors. *Br. J. Pharmacol.* **2002**, *136*, 965-974.

[223] Mortensen, M.; Ebert, B.; Wafford, K.; Smart, T.G. Distinct activities of GABA agonists at synaptic- and extrasynaptic-type GABAA receptors. *J. Physiol.* **2010**, *588*, 1251-1268.

[224] Stòrustovu, S.ı.; Ebert, B. Pharmacological characterization of agonists at δ-containing GABAA receptors: Functional selectivity for extrasynaptic receptors is dependent on the absence of γ2. *J. Pharmacol. Exp. Ther.* **2006**, *316*, 1351-1359.

[225] Lee, H.J.; Absalom, N.L.; Hanrahan, J.R.; van Nieuwenhuijzen, P.; Ahring, P.K.; Chebib, M. A pharmacological characterization of GABA, THIP and DS2 at binary α4β3 and β3δ receptors: GABA activates β3δ receptors via the β3(+)δ( ) interface. *Brain Res*. **2016**, *1644*, 222-230.

[226] Yamaura, K.; Kiyonaka, S.; Numata, T.; Inoue, R.; Hamachi, I. Discovery of allosteric modulators for GABAA receptors by ligand-directed chemistry. *Nat. Chem. Biol.* **2016**, *12*, 822-830.

[227] Bergmann, R.; Kongsbak, K.; Sorensen, P.L.; Sander, T.; Balle, T. A unified model of the GABAA receptor comprising agonist and benzodiazepine binding sites. *PLoS One* **2013**, *8*, e52323.

[228] Laha, K.T.; Tran, P.N. Multiple tyrosine residues at the GABA binding pocket influence surface expression and mediate kinetics of the GABAA receptor. *J. Neurochem.* **2013**, *124*, 200-209.

[229] Chua, H.C.; Christensen, E.T.H.; Hoestgaard-Jensen, K.; Hartiadi, L.Y.; Ramzan, I.; Jensen, A.A.; Absalom N.L.; Chebib M. Kavain, the major constituent of the anxiolytic kava extract, potentiates GABAA receptors: Functional characteristics and molecular mechanism. *PLoS One*, **2016**, *11*. e0157700.

[230] Benson, J.A.; Low, K.; Keist, R.; Mohler, H.; Rudolph, U. Pharmacology of recombinant γ-aminobutyric acidA receptors rendered diazepam-insensitive by point-mutated α-subunits. *FEBS Lett.* **1998**, *431*, 400-404.

[231] Wieland, H. A.; Luddens, H. Four amino acid exchanges convert a diazepaminsensitive, inverse agonist-preferring GABAA receptor into a diazepam-preferring GABAA receptor. *J. Med. Chem.* **1994**, *37*, 4576-4580.

[232] Wieland, H. A.; Luddens, H.; Seeburg, P.H. A single histidine in GABAA receptors is essential for benzodiazepine agonist binding. *J. Biol. Chem.* **1992**, *267*, 1426-1429.

[233] Ralvenius, W.T.; Benke, D.; Acuna, M.A.; Rudolph, U.; Zeilhofer, H.U. Analgesia and unwanted benzodiazepine effects in point-mutated mice expressing only one benzodiazepine-sensitive GABAA receptor subtype. *Nat. Comm.* **2015**, *6*, 6803.

[234] Rudolph, U.; Mohler, H. Analysis of GABAA receptor function and dissection of the pharmacology of benzodiazepines and general anesthetics through mouse genetics. *Annu. Rev. Pharmacol. Toxicol.* **2014**, *44*, 475-498.

[235] Skolnick, P. Anxioselective anxiolytics: On a quest for the holy grail. *Trends Pharmacol. Sci.* **2012**, *33*, 611-620.

[236] Walters, R.J.; Hadley, S.H.; Morris, K.D.; Amin, J. Benzodiazepines act on GABAA receptors via two distinct and separable mechanisms. *Nat. Neurosci.* **2000**, *3*, 1274-1281.

[237] Feng, H.-J.; Macdonald, R.L. Multiple actions of propofol on αβγ and αβδ GABAA receptors. *Mol. Pharmacol.* **2004**, *66*, 1517-1524.

[238] Hill-Venning, C.; Belelli, D.; Peters, J.A.; Lambert, J.J. Subunit-dependent interaction of the general anaesthetic etomidate with the γ-aminobutyric acid type a receptor. *Br. J. Pharmacol.* **1997**, *120*, 749-756.

[239] Chiara, D.C.; Dostalova, Z.; Jayakar, S.S.; Zhou, X.; Miller, K.W.; Cohen, J.B. Mapping general anesthetic binding site(s) in human α1β3 γ-aminobutyric acid type a receptors with [3H]TDBzl-etomidate, a photoreactive etomidate analogue. *Biochem.* **2012**, *51*, 836-847.

[240] Stewart, D.S.; Hotta, M.; Desai, R.; Forman, S.A. State-dependent etomidate occupancy of its allosteric agonist sites measured in a cysteine-substituted GABAA receptor. *Mol. Pharmacol.* **2013**, *83*, 1200–1208.

[241] Belelli D.; Lambert J.J.; Peters J.A.; Wafford K.; Whiting P.J. The interaction of the general anesthetic etomidate with the γ-aminobutyric acid type A receptor is influenced by a single amino acid. *Proc. Natl. Acad. Sci. USA* **1997**, *94*, 11031-11036.

[242] Chiara, D.C.; Jayakar, S.S.; Zhou, X.; Zhang, X.; Savechenkov, P.Y.; Bruzik, K.S.; Miller, K.W.; Cohen, J.B. Specificity of intersubunit general anesthetic-binding sites in the transmembrane domain of the human α1β3γ2 γ-aminobutyric acid type a (GABAA) receptor. *J. Biol. Chem.* **2013**, *288*, 19343-19357.

[243] Jayakar, S.S.; Zhou, X.; Chiara, D.C.; Dostalova, Z.; Savechenkov, P.Y.; Bruzik, K.S.; Dailey, W.P.; Miller, K.W.; Eckenhoff, R.G.; Cohen, J.B. Multiple propofol-binding sites in a γ-aminobutyric acid type a receptor (GABAAR) identified using a photoreactive propofol analog. *J. Biol. Chem.* **2014**, *289*, 27456-27468.

[244] Eaton, M.M.; Cao, L.Q.; Chen, Z.; Franks, N.P.; Evers, A.S.; Akk, G. Mutational analysis of the putative high-affinity propofol binding site in human β3 homomeric GABAA receptors. *Mol. Pharmacol.* **2015**, *88*, 736-745.

[245] Yip, G.M.S.; Chen, Z.-W.; Edge, C.J.; Smith, E.H.; Dickinson, R.; Hohenester, E.; Townsend, R.R.; Fuchs, K.; Sieghart, W.; Evers, A.S.; Franks, N.P. A propofol binding site on mammalian GABAA receptors identified by photolabeling. *Nat. Chem. Biol.* **2013**, *9*, 715-720.

[246] Bali, M.; Akabas, M H. Defining the propofol binding site location on the GABAA receptor. *Mol. Pharmacol.* **2004**, *65*, 68-76.

[247] Stewart, D.S.; Pierce, D.W.; Hotta, M.; Stern, A.T.; Forman, S.A. Mutations at beta N265 in γ-aminobutyric acid type a receptors alter both binding affinity and efficacy of potent anesthetics. *PLoS One* **2014**, *9*, e111470.

[248] Hammer, H.; Bader, B.M.; Ehnert, C.; Bundgaard, C.; Bunch, L.; Hoestgaard-Jensen, K.; Schroeder, O.H-U.; Bastlund, J.F.; Gramowski-Voß, A.; Jensen, A.A. A multifaceted GABAA receptor modulator: Functional properties and mechanism of action of the sedative-hypnotic and recreational drug methaqualone (Quaalude). *Mol. Pharmacol.* **2015**, *88*, 401-420.

[249] Chua, H.C.; Absalom, N.L.; Hanrahan, J.R.; Viswas, R.; Chebib, M. The directactions of GABA, 2'-methoxy-6-methylflavone and general anaesthetics at β3γ2L GABAA receptors: Evidence for receptors with different subunit stoichiometries. *PLoS One* **2015**, *10*, e0141359.

[250] Sanna, E.; Motzo, C.; Usala, M.; Serra, M.; Dazzi, L.; Maciocco, E.; Trapani, G.; Latrofa, A.; Liso, G.; Biggio, G. Characterization of the electrophysiological and pharmacological effects of 4-iodo-2,6-diisopropylphenol, a propofol analogue devoid of sedative-anaesthetic properties. *Br. J. Pharmacol.* **1999**, *126*, 1444-1454.

[251] Jayakar, S.S.; Zhou, X.; Savechenkov, P.Y.; Chiara, D.C.; Desai, R.; Bruzik, K.S.; Miller, K.W.; Cohen, J.B. Positive and negative allosteric modulation of an α1β3γ2 γ-aminobutyric acid type a (GABAA) receptor by binding to a site in the transmembrane domain at the γ+-β- interface. *J. Biol. Chem.* **2015**, *290*, 23432-23446.

[252] Belelli, D.; Lambert, J.J. Neurosteroids: Endogenous regulators of the GABAA receptor. *Nat. Rev. Neurosci.* **2005**, *6*, 565-575.

[253] Siegwart, R.; Krahenbuhl, K.; Lambert, S.; Rudolph, U. Mutational analysis of molecular requirements for the actions of general anaesthetics at the γ-aminobutyric acidA receptor subtype, α1β2γ2. *BMC Pharmacol.* **2003**, *3*, 1-9.

[254] Akk, G.; Bracamontes, J.R.; Covey, D.F.; Evers, A.; Dao, T.; Steinbach, J.H. Neuroactive steroids have multiple actions to potentiate GABAA receptors. *J. Physiol.* **2004**, *558*, 59-74.

[255] Li, G.-D.; Chiara, D.C.; Cohen, J.B.; Olsen, R.W. Neurosteroids allosterically modulate binding of the anesthetic etomidate to γ-aminobutyric acid type a receptors. *J. Biol. Chem.* **2009**, *284*, 11771-11775.

[256] Jurd, R.; Arras, M.; Lambert, S.; Drexler, B.; Siegwart, R.; Crestani, F.; Zaugg, M.; Vogt, K.E.; Ledermann, B.; Antkowiak, B.; Rudolph, U. General anesthetic actions in vivo strongly attenuated by a point mutation in the GABAA receptor β3 subunit. *FASEB J.* **2003**, *17*, 250-252.

[257] Rudolph, U.; Crestani, F.; Benke, D.; Brunig, I.; Benson, J.A.; Fritschy, J.-M.; Martin, J.R.; Bluethmann, H.; Möhler, H. Benzodiazepine actions mediated by specific γ-aminobutyric acidA receptor subtypes. *Nature* **1999**, *401*, 796-800.

[258] Hosie, A.M.; Wilkins, M.E.; da Silva, H.M.A.; Smart, T.G. Endogenous neurosteroids regulate GABAA receptors through two discrete transmembrane sites. *Nature*, **2006**, *444*, 486-489.

[259] Li, P.; Bandyopadhyaya, A.K.; Covey, D.F.; Steinbach, J.H.; Akk, G. Hydrogen bonding between the 17β-substituent of a neurosteroid and the GABAA receptor is not obligatory for channel potentiation. *Br. J. Pharmacol.* **2009**, *158*, 1322-1329.

[260] Akk, G.; Bracamontes, J.; Steinbach, J.H. Pregnenolone sulfate block of GABAA receptors: Mechanism and involvement of a residue in the M2 region of the α subunit. *J. Physiol.* **2001**, *532*, 673-684.

[261] Seljeset, S.; Laverty, D.; Smart, T.G. Inhibitory neurosteroids and the GABAA receptor. *Adv. Pharmacol.* **2015**, *72*, 165-187.

[262] Hanrahan, J.R.; Chebib, M.; Johnston, G.A.R. Flavonoid modulation of GABAA receptors. *Br. J. Pharmacol.* **2011**, *163*, 234-245.

[263] Johnston, G.A.; Hanrahan, J.R.; Chebib, M.; Duke, R.K.; Mewett, K.N. Modulation of ionotropic GABA receptors by natural products of plant origin. *Adv. Pharmacol.* **2006**, *54*, 285-316.

[264] Khom, S.; Strommer, B.; Ramharter, J.; Schwarz, T.; Schwarzer, C.; Erker, T.; Mulzer, J.; Hering, S. Valerenic acid derivatives as novel subunit-selective GABAA receptor ligands—In vitro and in vivo characterization. *Br. J. Pharmacol.* **2010**, *161*, 65-78.

[265] Alexeev, M.; Grosenbaugh, D.K.; Mott, D.D.; Fisher, J.L. The natural products magnolol and honokiol are positive allosteric modulators of both synaptic and extrasynaptic GABAA receptors. *Neuropharmacol.* **2012**, *62*, 2507-2514.

[266] Fuchs, A.; Baur, R.; Schoeder, C.; Sigel, E.; Muller, C.E. Structural analogues of the natural products magnolol and honokiol as potent allosteric potentiators of GABAA receptors. *Bioorg. Med. Chem.* **2014**, *22*, 6908-6917.

[267] Taferner, B.; Schuehly, W.; Huefner, A.; Baburin, I.; Wiesner, K.; Ecker, G.F.; Hering, S. Modulation of GABAA-receptors by honokiol and derivatives: Subtype selectivity and structure-activity relationship. *J. Med. Chem.* **2011**, *54*, 5349-5361.

[268] Arias, H.R.; Do Rego, J.L.; Do Rego, J.C.; Chen, Z.; Anouar, Y.; Scholze, P.; Gonzales, E.B.; Huang, R.; Chagraoui, A. Coronaridine congeners potentiate GABAA receptors and induce sedative activity in mice in a benzodiazepine-insensitive manner. *Prog. Neuropsychopharmacol. Biol. Psychiatry* **2020**, *101*, 109930.

[269] Csermely, P.; Agoston, V.; Pongor, S. The efficiency of multitarget drugs: the network approach might help drug design. *Trends Pharmacol. Sci.* **2005**, *26*, 178-182.

[270] Espinoza-Fonseca, L.M. The benefits of the multi-target approach in drug design and discovery. *Bioorg. Med. Chem.* **2006**, *14*, 896-897.

[271] Zimmermann, G.R.; Lehár, J.; Keith, C.T. Multi-target therapeutics: when the whole is greater than the sum of the parts. *Drug Discovery Today* **2007**, *12*, 34-42.

[272] Sikazwe, D.M.N. The multi-target drug design era is here, consider it. *Drug Des.: Open Access* **2012**, *1*, 1000-1101.

[273] Wilkinson, B.L.; Bornaghi, L.F.; Houston, T.A.; Innocenti, A.; Supuran, C.T.; Poulsen, S.-A. A novel class of carbonic anhydrase inhibitors: glycoconjugate benzene sulfonamides prepared by "click-tailing". *J. Med. Chem.* **2006**, 49, 6539-6548.

[274] Nocentini, A.; Carta, F.; Ceruso, M.; Bartolucci, G.; Supuran C.T. Click-tailed coumarins with potent and selective inhibitory action against the tumor-associated carbonic anhydrases IX and XII. *Bioorg. Med. Chem.* **2015**, 23, 6955-6966.

[275] De Simone, G.; Alterio, V.; Supuran, C.T. Exploiting the hydrophobic and hydrophilic binding sites for designing carbonic anhydrase inhibitors. *Expert Opin. Drug Discov.* **2013**, 8, 793-810.

[276] Nocentini, A.; Ferraroni, M.; Carta, F.; Ceruso, M.; Gratteri, P.; Lanzi, C.; Masini, E.; Supuran C.T. Benzenesulfonamides incorporating flexible triazole moieties are highly effective Carbonic anhydrase inhibitors: synthesis and kinetic, crystallographic, computational, and intraocular pressure lowering investigations. *J. Med. Chem.* **2016**, 59, 10692-10704.

[277] Tanpure R.P.; Ren B.; Peat T. S.; Bornaghi L.F.; Vullo D.; Supuran C.T.; Poulsen S. A. Carbonic anhydrase inhibitors with dual-tail moieties to match the hydrophobic and hydrophilic halves of the carbonic anhydrase active site. *J. Med. Chem.* **2015**, 58, 1494-501.

[278] Fares, M.; Eldehna, W.M.; Bua, S.; Lanzi, C.; Lucarini, L.; Masini E.; Peat, T.S.; Abdel-Aziz, H.A.; Nocentini, A.; Keller, P.A.; Supuran, C.T. Discovery of potent dual-tailed benzenesulfonamide inhibitors of human Carbonic anhydrases implicated in Glaucoma and in vivo profiling of their intraocular pressure-lowering action. *J. Med. Chem.* **2020**, 63, 3317-3326.

[279] Kalinin, S.; Nocentini, A.; Kovalenko, A.; Sharoyko, V.; Bonardi, A.; Angeli, A.; Gratteri, P.; Tennikova, T.B.; Supuran, C.T.; Krasavin, M. From random to rational: a discovery approach to selective subnanomolar inhibitors of human carbonic anhydrase IV based on the Castagnoli-Cushman multicomponent reaction. *Eur. J. Med. Chem.* **2019**, 182, 111642.

[280] Said, M.A.; Eldehna, W.M.; Nocentini, A.; Bonardi, A.; Fahim, S.H.; Bua, S.; Soliman, D. H.; Abdel-Aziz H.A.; Gratteri, P.; Abou-Seri, S.M.; Supuran, C.T. Synthesis, biological and molecular dynamics investigations with a series of triazolopyrimidine/triazole-based benzenesulfonamides as novel carbonic anhydrase inhibitors. *Eur. J. Med. Chem.* **2020**, 185, 111843.

[281] Pustenko, A.; Nocentini, A.; Gratteri, P.; Bonardi, A.; Vozny, I.; Žalubovskis, R.; Supuran, C.T. The antibiotic furagin and its derivatives are isoform-selective human carbonic anhydrase inhibitors. *J. Enzyme Inhib. Med. Chem.* **2020**, 35, 1011-1020.

[282] Khalifah, R.G. The carbon dioxide hydration activity of carbonic anhydrase I. Stop-flow kinetic studies on the native human isoenzymes B and C. *J. Biol. Chem.* **1971**, 246, 2561-2573.

[283] Bonardi, A.; Nocentini, A.; Bua, S.; Combs, J.; Lomelino, C.; Andring, J.; Lucarini, L.; Sgambellone, S.; Masini, E.; McKenna, R.; Gratteri, P.; Supuran, C.T. Sulfonamide inhibitors of human carbonic anhydrases designed through a three-tails approach: Improving ligand/isoform matching and selectivity of action. *J. Med. Chem.* **2020**, *63*, 7422-7444.

[284] Aletaha, D.; Smolen, J. S. Diagnosis and management of rheumatoid arthritis: a review. *JAMA* **2018**, *320*, 1360-1372.

[285] Smolen, J.S.; Aletaha, D.; Barton, A.; Burmester, G.R.; Emery, P.; Firestein, G.S.; Kavanaugh, A.; McInnes, I.B.; Solomon, D.H.; Strand V.; Yamamoto, K. Rheumatoid arthritis. *Nat. Rev. Dis. Primers* **2018**, *4*, 18001.

[286] Thatayatikom, A.; De Leucio, A. Juvenile Idiopathic Arthritis (JIA). *StatPearls* [Internet]. Treasure Island (FL): StatPearls Publishing; **2020** Feb 21.

[287] Wada, T.; Nakashima, T.; Hiroshi, N.; Penninger, J.M. RANKL-RANK signaling in osteoclastogenesis and bone disease. *Trends Mol Med.* **2006**, *12*, 17-25.

[288] Farr, M.; Garvey, K.; Bold, A.M.; Kendall, M.J.; Bacon, P.A. Significance of the hydrogen ion concentration in synovial fluid in rheumatoid arthritis. *Clin. Exp. Rheumatol.* **1985**, *3*, 99-104;

[289] Gobelet, C.; Gerster, J. C. Synovial fluid lactate levels in septic and nonseptic arthritides. *Ann. Rheum. Dis.* **1984**, 43, 742-745.

[290] Steen, K.H.; Steen, A.E.; Reeh, P.W. A dominant role of acid pH in inflammatory excitation and sensitization of nociceptors in rat skin, in vitro. *J. Neurosci.* **1995**, *15*, 3982-3989.

[291] Steen, K.H.; Anton, F.; Reeh, P.W.; Handwerker, H.O. Protons selectively induce lasting excitation and sensitization to mechanical stimulation of nociceptors in rat skin, in vitro. *J. Neurosci.* **1992**, *12*, 86-95.

[292] Goldie, I.; Nachemson, A. Synovial pH in rheumatoid knee-joints. I. The effect of synovectomy. *Acta Orthop. Scand.* **1969**, *40*, 634-641.

[293] Dawson-Hughes, D.; Harris, S.S.; Palermo, N.J.; Castaneda-Sceppa, C.; Rasmussen, H.M.; Dallal, G.L. Treatment with potassium bicarbonate lowers calcium excretion and bone resorption in older men and women. *J. Clin. Endocrinol Metab.* **2009**, *94*, 96-102.

[294] Revici, E.; Stoopen, E.; Frenk, E.; Ravich, R.A. The painful focus. II. The relation of pain to local physico-chemical changes. *Bull Inst. Appl. Biol.* **1949**, *1*, 21.

[295] Steen, K.H.; Reeh, P.W. Sustained graded pain and hyperalgesia from experimental tissue acidosis in human subjects. *Neurosci. Lett.* **1993**, *154*, 113-l16.

[296] Chang, X.; Han, J.; Zhao, Y.; Yan, X.; Sun S.; Cui, Y. Increased expression of carbonic anhydrase I in the synovium of patients with ankylosing spondylitis. *BMC Musculoskelet Disord.* **2010**, *11*, 279-290.

[297] Zheng, Y.; Wang, L.; Zhang, W.; Xu, H.; Chang, X. Transgenic mice over-expressing carbonic anhydrase I showed aggravated joint inflammation and tissue destruction. *BMC Musculoskelet Disord.* **2012**, *13*, 256-265.

[298] Maxwell, P.H.; Wiesener, M.S.; Chang, C.W.; Clifford, S.C.; Vaux, E.C.; Cockman, M.E.; Wykoff, C.C.; Pugh, C.W.; Maher, E.R.; Ratcliffe, P.J. The tumour suppressor protein VHL targets hypoxia-inducible factors for oxygendependent proteolysis. *Nature* **1999**, *399*, 271-275.

[299] Pastorekova, S.; Pastorek, J. in Carbonic Anhydrase — Its Inhibitors and Activators (eds Supuran, C.T.; Scozzafava, A.; Conway, J.) 255–281 (CRC, Boca Raton, **2004**).

[300] Semenza, G.L. Hypoxia and cancer. *Cancer Metastasis Rev.* **2007**, *26*, 223-224.

[301] Brahimi-Horn, M.C.; Pouyssegur, J. Oxygen, a source of life and stress. *FEBS Lett.* **2007**, *581*, 3582-3591.

[302] Jaakkola, P.; Mole, D.R.; Tian, Y.M.; Wilson, M.I.; Gielbert, J.; Gaskell, S.J.; von Kriegsheim, A.; Hebestreit, H.F.; Mukherji, M.; Schofield, C.J.; Maxwell, P.H.; Pugh, C.W.; Ratcliffe P.J. Targeting of HIF-α to the von Hippel-Lindau ubiquitylation complex by O2-regulated prolyl hydroxylation. *Science* **2001**, *292*, 468-472.

[303] Hon, W.C.; Wilson, M.I.; Harlos, K.; Claridge, T.D.W.; Schofield, C.J.; Pugh, C.W.; Maxwell, P.H.; Ratcliffe, P.J.; Stuart D.I.; Jones E.Y. Structural basis for the recognition of hydroxyproline in HIF-1α by pVHL. *Nature* **2002**, *417*, 975-978.

[304] Thiry, A.; Dogne, J.-M.; Masereel, B.; Supuran, C.T. Targeting tumor-associated carbonic anhydrase IX in cancer therapy. *Trends Pharmacol. Sci.* **2006**, *27*, 566–573.

[305] Ratcliffe, P.J.; Pugh, C.W.; Maxwell, P.H. Targeting tumors through the HIF system. *Nature Med.* **2000**, *6*, 1315-1316.

[306] Trastour, C.; Benizri, E.; Ettore, F.; Ramaioli, A.; Chamorey, E.; Pouysségur, J.; Berra E. HIF-1α and CA IX staining in invasive breast carcinomas: prognosis and treatment outcome. *Int. J. Cancer* **2007**, *120*, 1451-1458.

[307] Pouyssegur, J.; Dayan, F.; Mazure, N.M. Hypoxia signalling in cancer and approaches to enforce tumour regression. *Nature* **2006**, *441*, 437-443.

[308] Ord, J.J.; Agrawal, S.; Thamboo, T.P.; Roberts, I.; Campo, L.; Turley, H.; Han, C.; Fawcett, D.W.; Kulkarni, R.P.; Cranston, D.; Harris, A.L. An investigation into the prognostic significance of necrosis and hypoxia in high grade and invasive bladder cancer. *J. Urol.* **2007**, *178*, 677-682.

[309] Swietach, P.; Vaughan-Jones, R.D.; Harris, A.L. Regulation of tumor pH and the role of carbonic anhydrase 9. *Cancer Metastasis Rev.* **2007**, *26*, 299-310.

[310] Hutchison, G.J.; Valentine, H.R.; Loncaster, J.A.; Davidson, S.E.; Hunter, R.D.; Roberts, S.A.; Harris, A.L.; Stratford, I.J.; Price, P.M.; West, C.M.L. Hypoxia-inducible factor 1-α expression as an intrinsic marker

of hypoxia: correlation with tumor oxygen, pimonidazole measurements, and outcome in locally advanced carcinoma of the cervix. *Clin. Cancer Res.* **2004**, *10*, 8405-8412.

[311] Sung, F.L.; Hui, E.P.; Tao, Q.; Li, H.; Tsui, N.B.Y.; Lo, Y.M.D.; Ma, B.B.Y.; To, K.F.; Harris, A.L.; Chan, A.T.C. Genome-wide expression analysis using microarray identified complex signaling pathways modulated by hypoxia in nasopharyngeal carcinoma. *Cancer Lett.* **2007**, *253*, 74-88.

[312] Koukourakis, M.I.; Giatromanolaki, A.; Sivridis, E.; Pastorek, J.; Karapantzos, I.; Gatter, K.C.; Harris, A.L. Hypoxia-activated tumor pathways of angiogenesis and pH regulation independent of anemia in head-and-neck cancer. *Int. J. Radiat. Oncol. Biol. Phys.* **2004**, *59*, 67-71.

[313] Potter, C.P. Harris, A.L. Diagnostic, prognostic and therapeutic implications of carbonic anhydrases in cancer. *Br. J. Cancer* **2003**, *89*, 2-7.

[314] Hussain, S.A.; Ganesan, R.; Reynolds, G.; Gross, L.; Stevens, A.; Pastorek, J.; Murray, P.G.; Perunovic, B.; Anwar, M.S.; Billingham, L.; James, N.D.; Spooner, D.; Poole, C.J.; Rea, D.W.; Palmer, D.H. Hypoxia-regulated carbonic anhydrase IX expression is associated with poor survival in patients with invasive breast cancer. *Br. J. Cancer* **2007**, *96*, 104-109.

[315] Swinson, D. E.; Jones J.L.; Richardson, D.; Wykoff, C.; Turley, H.; Pastorek, J.; Taub, N.; Harris, H.L.; O'Byrne, K.J. Carbonic anhydrase IX expression, a novel surrogate marker of tumor hypoxia, is associated with a poor prognosis in non-small-cell lung cancer. *J. Clin. Oncol.* **2003**, *21*, 473-482.

[316] Dorai, T.; Sawczuk, I.; Pastorek, J.; Wiernik, P.H.; Dutcher, J.P. Role of carbonic anhydrases in the progression of renal cell carcinoma subtypes: proposal of a unified hypothesis. *Cancer Invest.* **2006**, *24*, 754-779.

[317] Szabo, C.; Papapetropoulos, A. International Union of Basic and Clinical Pharmacology. CII: Pharmacological Modulation of H2S Levels: H2S Donors and H2S Biosynthesis Inhibitors. *Pharmacol. Rev.* **2017**, *69*: 497-564.

[318] Zhao, Y.; Biggs, T. D.; Xian, M. Hydrogen Sulfide (H$_2$S) Releasing Agents: Chemistry and Biological Applications. *Chem. Commun. (Camb).* **2014**, *50*, 11788-11805.

[319] Powell, C. R.; Dillon, K. M.; Matson, J. B. A Review of Hydrogen Sulfide (H$_2$S) Donors: Chemistry and Potential Therapeutic Applications. *Biochem. Pharmacol*. **2018**, *149*, 110-123.

[320] Kimura, Y.; Koike, S.; Shibuya, N.; Lefer, D.; Ogasawara, Y.; Kimura, H. 3-Mercaptopyruvate sulfurtransferase produces potential redox regulators cysteine and glutathione-persulfide (Cys-SSH and GSSH) together with signaling molecules H$_2$S$_2$, H$_2$S$_3$ and H$_2$S. *Sci. Rep.* **2017**, *7*, 10459.

[321] Cuevasanta, E.; Denicola, A.; Alvarez, B.; Möller, M. N. Solubility and Permeation of Hydrogen Sulfide in Lipid Membranes. *PLoS One.* **2012**, *7*, e34562.

[322] Wallace, J. L.; Blackler, R. W.; Chan, M. V.; Da Silva, G. J.; Elsheikh, W.; Flannigan, K. L.; Gamaniek, I.; Manko, A.; Wang, L.; Motta, J. P.; Buret, A. G. Anti-inflammatory and cytoprotective actions of hydrogen sulfide: translation to therapeutics. *Antioxid. Redox Signal.* **2015**, *22*, 398-410.

[323] McCarberg, B. H.; Cryer, B. Evolving therapeutic strategies to improve nonsteroidal anti-inflammatory drug safety. *Am. J. Ther.* **2015**, *22*, e167-78.

[324] Wallace J.L. Hydrogen sulfide-releasing anti-inflammatory drugs. *Opinion.* **2007**, *28*, 501-505.

[325] Gambari, L.; Grigolo, B.; Grassi, F. Hydrogen Sulfide in Bone Tissue Regeneration and Repair: State of the Art and New Perspectives. *Int. J. Mol. Sci.* **2019**, *20*, pii: E5231.

[326] Sun, H. J.; Wu, Z. Y.; Cao, L.; Zhu, M. Y.; Liu, T. T.; Guo, L.; Lin, Y.; Nie, X. W.; Bian, J. S. Hydrogen Sulfide: Recent Progression and Perspectives for the Treatment of Diabetic Nephropathy. *Molecules.* **2019**, *24*, pii: E2857.

[327] Gopalakrishnan, P.; Shrestha, B.; Kaskas, A. M.; Green, J.; Alexander, J. S.; Pattillo, C. B. Hydrogen sulfide: Therapeutic or injurious in ischemic stroke? *Pathophysiology.* **2019**, *26*, 1-10.

[328] Zhang, L.; Wang, Y.; Li, Y.; Li, L.; Xu, S.; Feng, X.; Liu, S. Hydrogen Sulfide (H_2S)-Releasing Compounds: Therapeutic Potential in Cardiovascular Diseases. *Front. Pharmacol.* **2018**, *9*, 1066.

[329] Hsu, C. N.; Tain, Y. L. Hydrogen Sulfide in Hypertension and Kidney Disease of Developmental Origins. *Int. J. Mol. Sci.* **2018**, *19*, pii: E1438.

[330] Citi, V.; Piragine, E.; Testai, L.; Breschi, M. C.; Calderone, V.; Martelli, A. The Role of Hydrogen Sulfide and H_2S-donors in Myocardial Protection Against Ischemia/Reperfusion Injury. *Curr. Med. Chem.* **2018**, *25*, 4380-4401.

[331] Cao, X.; Cao, L.; Ding, L.; Bian, J.S. A New Hope for a Devastating Disease: Hydrogen Sulfide in Parkinson's Disease. *Mol Neurobiol.* **2018**, *55*, 3789-3799.

[332] Szczesny, B.; Marcatti, M.; Zatarain, J.R.; Druzhyna, N.; Wiktorowicz, J.E.; Nagy, P.; Hellmich, M.R.; Szabo C. Inhibition of hydrogen sulfide biosynthesis sensitizes lung adenocarcinoma to chemotherapeutic drugs by inhibiting mitochondrial DNA repair and suppressing cellular bioenergetics. *Nat. Rev.* **2016**, *15*, 185-203.

[333] Bua, S.; Lucarini, L.; Micheli, L.; Menicatti, M.; Bartolucci, G.; Selleri, S.; Di Cesare Mannelli, L.; Ghelardini, C.; Masini, E.; Carta, F.; Gratteri, P.; Nocentini, A.; Supuran, C. T. Bioisosteric Development of Multi-target Nonsteroidal Anti-inflammatory Drug – Carbonic Anhydrases Inhibitor Hybrids for the Management of Rheumatoid Arthritis. *J. Med. Chem.* **2020**, *63*: 2325-2342.

[334] Behera, J.; George, A.K.; Voor, M.J.; Tyagi, S.C.; Tyagi, N. Hydrogen sulfide epigenetically mitigates bone loss through OPG/RANKL regulation during hyperhomocysteinemia in mice. *Bone.* **2018**, *14*, 90-108.

[335] Powell, C.R.; Dillon, K.M.; Matson, J.B. A review of hydrogen sulfide (H2S) donors: Chemistry and potential therapeutic applications. *Biochem Pharmacol.* **2018**, *149*, 110-123.

[336] Giustarini D, Tazzari V, Bassanini I, Rossi R, Sparatore A. The new H_2S-releasing compound ACS94 exerts protective effects through the modulation of thiol homeostasis. *J Enzyme Inhib Med Chem.* **2018**, *33*, 1392-1404.

[337] Li, L. Rossoni, G.;Sparatore, A.; Lee, L.C.; Del Soldato, P.; Moore, P.K. Anti-inflammatory and gastrointestinal effects of a novel diclofenac derivative. Free Radic. Biol. Med. 2007, 42, 706-719.

[338] Mboge, M.Y.; Mahon, B.P.; McKenna, R.; Frost, S.C. Carbonic anhydrases: role in pH control and cancer. *Metabolites* **2028**, *8*, 19.

[339] Uhlen, M.; Zhang, C.; Lee, S.; Sjostedt, E.; Fagerberg, L.; Bidkhori, G.; Benfeitas, R.; Arif, M.; Liu, Z.; Edfors, F.; Sanli, K.; von Feilitzen, K.; Oksvold, P.; Lundberg, E.; Hober, S.; Nilsson, P.; Mattsson, J.; Schwenk, J.M.; Brunnstrom, H.; Glimelius, B.; Sjoblom, T.; Edqvist, P.H.; Djureinovic, D.; Micke, P.; Lindskog, C.; Mardinoglu, A.; Ponten, F. A pathology atlas of the human cancer transcriptome. *Science* **2017**, *357*, eaan2507.

[340] Cerami, E.; Gao, J.; Dogrusoz, U.; Gross, B.E.; Sumer, S.O.; Aksoy, B.A.; Jacobsen, A.; Byrne, C.J.; Heuer, M.L.; Larsson, E.; Antipin, Y.; Reva, B.; Goldberg, A.P.; Sander, C.; Schultz, N.; The cBio Cancer Genomics Portal: an open platform for exploring multidimensional cancer genomics data. *Cancer Discov.* **2012**, *2*, 401e404.

[341] Gao, J.; Aksoy, B.A.; Dogrusoz, U.; Dresdner, G.; Gross, B.; Sumer, S.O.; Sun, Y.; Jacobsen, A.; Sinha, R.; Larsson, E.; Cerami, E.; Sander, C.; Schultz, N. Integrative analysis of complex cancer genomics and clinical profiles using the cBioPortal. *Sci. Signal.* **2013**, *6*, pl1.

[342] Mboge, B.A.; Chen, Z.; Wolff, A.; Mathias, J.V.; Tu, C.; Brown, K.D.; Bozdag, M.; Carta, F.; Supuran, C.T.; McKenna, R.; Frost, S.C. Selective inhibition of carbonic anhydrase IX over carbonic anhydrase XII in breast cancer cells using benzene sulfonamides: disconnect between activity and growth inhibition. *PLoS One* **2018**, *13*, e0207417.

[343] Angapelly, S.; Ramya, P.V.; Angeli, A.; Monti, S.M.; Buonanno, M.; Alvala, M.; Supuran, C.T.; Arifuddin, M. Discovery of 4-sulfamoyl-phenyl-b-lactams as a new class of potent carbonic anhydrase isoforms I, II, IV and VII inhibitors: the first example of subnanomolar CA IV inhibitors, *Bioorg. Med. Chem.* **2017**, *25*, 539e544.

[344] Genhenden, S.; Ryde, U. The MM/PBSA and MM/GBSA methods to estimate ligand-binding affinities. *Expert Opin. Drug Discov.* **2015**, *10*, 449e461.

[345] Ferraroni, M.; Luccarini, L.; Masini, E.; Korsakov, M.; Scozzafava, A.; Supuran, C.T.; Krasavin, M. 1,3-Oxazole-based selective picomolar inhibitors of cytosolic human carbonic anhydrase II alleviate ocular hypertension in rabbits: potency is supported by X-ray crystallography of two leads. *Bioorg. Med. Chem.* **2017**, *25*, 4560e4565.

[346] Supuran CT. Advances in structure-based drug discovery of carbonic anhydrase inhibitors. *Expert Opin. Drug. Discov.* **2017**, *12*, 61-88.

[347] De Simone, G.; Supuran, C.T. (In)organic anions as carbonic anhydrase inhibitors. *J. Inorg. Biochem.* **2012**, *111*, 117-129.

[348] Tars, K.; Vullo, D.; Kazaks, A.; Leitans, J.; Lends, A.; Grandane, A.; Zalubovskis, R.; Scozzafava, A.; Supuran, C.T. Sulfocoumarins (1,2-benzoxathiine 2,2-dioxides): a class of potent and isoform-selective inhibitors of tumor-associated carbonic anhydrases. *J. Med. Chem.* **2013**, *56*, 293-300.

[349] Nocentini, A.; Ceruso, M.; Carta, F.; Supuran, C.T. 7-Aryl-triazolyl-substituted sulfocoumarins are potent, selective inhibitors of the tumorassociated carbonic anhydrase IX and XII. *J. Enzyme Inhib. Med. Chem.* **2016**, *31*, 1226-1233.

[350] Grandane, A.; Tanc, M.; Di Cesare Mannelli, L.; Carta, F.; Ghelardini, C.; Žalubovskis, R.; Supuran, C.T. 6-Substituted sulfocoumarins are selective carbonic anhdydrase IX and XII inhibitors with significant cytotoxicity against colorectal cancer cells. *J. Med. Chem.* **2015**, *58*, 3975-3983.

[351] Tanc, M.; Carta, F.; Bozdag, M.; Scozzafava, A.; Supuran, C.T. 7-Substituted-sulfocoumarins are isoform-selective, potent carbonic anhydrase II inhibitors. *Bioorg. Med. Chem.* **2013**, *21*, 4502-4510.

[352] Touisni, N.; Maresca, A.; McDonald, P.C.; Lou, Y.; Scozzafava, A.; Dedhar, S.; Winum, J.-Y.; Supuran, C.T. Glycosylcoumarin carbonic anhydrase IX and XII inhibitors strongly attenuate the growth of primary breast tumors. *J. Med. Chem.* **2011**, *54*, 8271-8277.

[353] Pustenko, A.; Stepanovs, D.; Zalubovskis, R.; Vullo, D.; Kazaks, A.; Leitans, J.; Tars K.; Supuran, C.T. 3H-1,2-benzoxathiepine 2,2-dioxides: a new class of isoform-selective carbonic anhydrase inhibitors. *J. Enzyme Inhib. Med. Chem.* **2017**, *32*, 767-775.

[354] Ivanova, J.; Carta, F.; Vullo, D.; Leitans, J.; Kazaks, A.; Tars, K.; Žalubovskis, R.; Supuran, C.T. 7. N-Substituted and ring opened saccharin derivatives selectively inhibit transmembrane, tumor-associated carbonic anhydrases IX and XII. *Bioorg. Med. Chem.* **2017**, *25*, 3583-3589.

[355] Alterio, V.; Tanc, M.; Ivanova, J.; Zalubovskis, R.; Vozny, I.; Monti, S.M.; Di Fiore, A.; De Simone, G.; Supuran, C.T. X-ray crystallographic and kinetic investigations of 6-sulfamoyl-saccharin as a carbonic anhydrase inhibitor. *Org. Biomol. Chem.* **2015**, *13*, 4064-4069.

[356] Ivanova, J.; Leitans, J.; Tanc, M.; Kazaks, A.; Zalubovskis, R.; Supuran, C.T.; Tars, K. X-ray crystallography-promoted drug design of carbonic anhydrase inhibitors. *Chem. Commun. (Camb.)* **2015**, *51*, 7108-7111.

[357] Chernov, N.M.; Koshevenko, A.S.; Yakovlev, I.P. Synthesis and antimicrobial activity of 4-hydroxy-2-[5-nitrofuran(thien)-2-yl]-6h-1,3-oxazin-6-ones. *Pharm. Chem. J.* **2017**, *51*, 644-647.

[358] Dybowski, B.; Jabłońska, O.; Radziszewski, P.; Gromadzka-Ostrowska, J.; Borkowski, A.; Ciprofloxacin and furagin in acute cystitis: comparison of early immune and microbiological results. *Int. J. Antimicrob. Agents* **2008**, *31*, 130-134.

[359] Leitans, J.; Kazaks, A.; Balode, A.; Ivanova, J.; Zalubovskis, R.; Supuran, C.T.; Tars, K. Efficient expression and crystallization system of cancer-associated carbonic anhydrase isoform IX. *J. Med. Chem.* **2015**, *58*, 9004-9009.

[360] Verdolino, V.; Cammi, R.; Munk, B.H.; Schlegel, H.B. Calculation of pKa values of nucleobases and the guanine oxidation products guanidinohydantoin and spiroiminodihydantoin using density functional theory and a polarizable continuum model. *J. Phys. Chem. B* **2008**, *112*, 16860-16873.

[361] Berrino E.; Supuran, C.T. Novel approaches for designing drugs that interfere with pH regulation. *Expert Opin. Drug. Discov.* **2019**, *14*, 231-248.

[362] Kohler, K.; Hillebrecht, A.; Schulze, Wischeler, J.; Innocenti, A.; Heine, A.; Supuran, C.T. Klebe, G. Saccharin inhibits carbonic anhydrases: possible explanation for its unpleasant metallic aftertaste. *Angew. Chem. Int. Ed. Engl.* **2007**, *46*, 7697-7699.

[363] Carradori, S.; Secci, D.; De Monte, C.; Mollica, A.; Ceruso, M.; Akdemir, A.; Sobolev, A.P.; Codispoti, R.; De Cosmi, F.; Guglielmi, P.; Supuran, C.T. A novel library of saccharin and acesulfame derivatives as potent and selective inhibitors of carbonic anhydrase IX and XII isoforms. *Bioorg. Med. Chem.* **2016**, *24*, 1095-1105.

[364] D'Ascenzio, M.; Guglielmi, P.; Carradori, S.; Secci, D.; Florio, R.; Mollica, A.; Ceruso, M.; Akdemir, A.; Sobolev, A.P.; Supuran, C.T. Open saccharin- based secondary sulfonamides as potent and selective inhibitors of cancer-related carbonic anhydrase IX and XII isoforms. *J. Enzyme Inhib. Med. Chem.* **2017**, *32*, 51-59.

[365] D'Ascenzio, M.; Secci, D.; Carradori, S.; Zara, S.; Guglielmi, P.; Cirilli, R.; Pierini, M.; Poli, G.; Tuccinardi, T.; Angeli, A.; Supuran C.T. 1,3-dipolar cycloaddition, HPLC enantioseparation, and docking studies of saccharin/isoxazole and saccharin/isoxazoline derivatives as selective carbonic anhydrase IX and XII inhibitors. *J. Med. Chem.* **2020**, *63*, 2470-2488.

[366] El-Gazzar, M.G.; Nafie, N.H.; Nocentini, A.; Ghorab, M.M.; Heiba, H.I.; Supuran, C.T. Carbonic anhydrase inhibition with a series of novel benzenesulfonamidetriazole conjugates. *J. Enzyme Inhib. Med. Chem.* **2018**, *33*, 1565-1574.

[367] Kumar, R.; Vats, L.; Bua, S.; Supuran, C.T.; Sharma, P.K. Design and synthesis of novel benzenesulfonamide containing 1,2,3-triazoles as potent human carbonic anhydrase isoforms I, II, IV and IX inhibitors. *Eur. J. Med. Chem.* **2018**, *155*, 545-551.

[368] Vats, L.; Sharma, V.; Angeli, A.; Kumar, R.; Supuran, C.T.; Sharma, P.K. Synthesis of novel 4-functionalized 1,5-diaryl-1,2,3-triazoles containing benzenesulfonamide moiety as carbonic anhydrase I, II, IV and IX inhibitors. *Eur. J. Med. Chem.* **2018**, *150*, 678-686.

[369] Murray, A.B.; Lomelino, C.L.; Supuran, C.T.; McKenna, R. "Seriously Sweet": acesulfame K exhibits selective inhibition using alternative binding modes in carbonic anhydrase isoforms. *J. Med. Chem.* **2018**, *61*, 1176-1181.

[370] Lomelino, C.L.; Supuran, C.T.; McKenna R. Non-Classical Inhibition of Carbonic Anhydrase. *Int. J. Mol. Sci.* **2016**, *17*, 1150

[371] Guglielmi, P.; Rotondi, G.; Secci, D.; Angeli, A.; Chimenti, P.; Nocentini, A.; Bonardi, A.; Gratteri, P.; Carradori, S.; Supuran, C.T. Novel insights on saccharin- and acesulfame-based carbonic anhydrase inhibitors: design, synthesis, modelling investigations and biological activity evaluation. *J. Enzyme Inhib. Med. Chem.* **2020**, *35*, 1891-1905.

[372] Chiaramonte, N.; Bua, S.; Ferraroni, M.; Nocentini, A.; Bonardi, A.; Bartolucci, G.; Durante, M.; Lucarini, L.; Chiapponi, D.; Dei, S.; Manetti, D.; Teodori, E.; Gratteri, P.; Masini, E.; Supuran, C.T.; Romanelli, M.N. 2-Benzylpiperazine: A new scaffold for potent human carbonic anhydrase inhibitors. Synthesis, enzyme

inhibition, enantioselectivity, computational and crystallographic studies and in vivo activity for a new class of intraocular pressure-lowering agents. *Eur. J. Med. Chem.* **2018**, *151*, 363-375.

[373] Ibrahim, H.S.; Allam, H.A.; Mahmoud, W.R.; Bonardi, A.; Nocentini, A.; Gratteri, P.; Ibrahim, E.S.; Abdel-Aziz, H.A.; Supuran, C.T. Dual-tail arylsulfone-based benzenesulfonamides differently match the hydrophobic and hydrophilic halves of human carbonic anhydrases active sites: Selective inhibitors for the tumor-associated hCA IX isoform. *Eur. J. Med. Chem.* **2018**, *152*, 1-9.

[374] Nocentini, A.; Bonardi, A.; Gratteri, P.; Cerra, B.; Gioiello, A.; Supuran, C.T. Steroids interfere with human carbonic anhydrase activity by using alternative binding mechanisms. *J. Enzyme Inhib. Med. Chem.* **2018**, *33*, 1453-1459.

[375] Angeli, A.; Clima, L.; Craciun, B.F.; Petreni, A.; Bonardi, A.; Nocentini, A.; Carta, F.; Gratteri, P.; Pinteala, M.; Supuran, C.T. Synthesis, computational studies and assessment of in vitro inhibitory activity of squalene derivatives as carbonic anhydrase inhibitors. *Chem. Med. Chem.* **2020**, doi: 10.1002/cmdc.202000500.

[376] Eldehna, W.M.; Abo-Ashour, M.F.; Nocentini, A.; El-Haggar, R.S.; Bua, S.; Bonardi, A.; Al-Rashood, S.T.; Hassan, G.S.; Gratteri, P.; Abdel-Aziz, HA.; Supuran, C.T. Enhancement of the tail hydrophobic interactions within the carbonic anhydrase IX active site via structural extension: Design and synthesis of novel N-substituted isatins-SLC-0111 hybrids as carbonic anhydrase inhibitors and antitumor agents. *Eur. J. Med. Chem.* **2019**, *162*, 147-160.

[377] Abdelrahman, M.A.; Eldehna, W.M.; Nocentini, A.; Bua, S.; Al-Rashood, S.T.; Hassan, G.S.; Bonardi, A.; Almehizia, A.A.; Alkahtani, H.M.; Alharbi, A.; Gratteri, P.; Supuran, C.T. Novel Diamide-Based Benzenesulfonamides as Selective Carbonic Anhydrase IX Inhibitors Endowed with Antitumor Activity: Synthesis, Biological Evaluation and In Silico Insights. *Int. J. Mol. Sci.* **2019**, *20*, 2484.

[378] Eldehna, W.M.; Abdelrahman, M.A.; Nocentini, A.; Bua, S.; Al-Rashood, S.T.; Hassan, G.S.; Bonardi, A.; Almehizia, A.A.; Alkahtani, H.M.; Alharbi, A.; Gratteri P.; Supuran, C.T. Synthesis, biological evaluation and in silico studies with 4-benzylidene-2-phenyl-5(4H)-imidazolone-based benzenesulfonamides as novel selective carbonic anhydrase IX inhibitors endowed with anticancer activity. *Bioorg. Chem.* **2019**, *90*, 103102.

[379] Abo-Ashour, M.F.; Eldehna, W.M.; Nocentini, A.; Bonardi, A.; Bua, S.; Ibrahim, H.S.; Elaasser, M.M.; Kryštof, V.; Jorda, R.; Gratteri, P.; Abou-Seri, S.M.; Supuran, C.T. 3-Hydrazinoisatin-based benzenesulfonamides as novel carbonic anhydrase inhibitors endowed with anticancer activity: Synthesis, in vitro biological evaluation and in silico insights. *Eur. J. Med. Chem.* **2019**, *184*, 111768.

[380] Said, M.A.; Eldehna, W.M.; Nocentini, A.; Fahim, S.H.; Bonardi, A.; Elgazar, A.A.; Kryštof, V.; Soliman, D.H.; Abdel-Aziz, H.A.; Gratteri, P.; Abou-Seri, S.M.; Supuran, C.T. Sulfonamide-based ring-fused analogues for CAN508 as novel carbonic anhydrase inhibitors endowed with antitumor activity: Design, synthesis, and in vitro biological evaluation. *Eur. J. Med. Chem.* **2020**, *189*, 112019.

[381] Alkhaldi, A.A.M.; Al-Sanea, M.M.; Nocentini, A.; Eldehna, W.M.; Elsayed, Z.M.; Bonardi, A.; Abo-Ashour, M.F.; El-Damasy, A.K.; Abdel-Maksoud, M.S.; Al-Warhi, T.; Gratteri, P.; Abdel-Aziz, H.A.; Supuran C.T.; El-Haggar, R. 3-Methylthiazolo[3,2-a]benzimidazole-benzenesulfonamide conjugates as novel carbonic

anhydrase inhibitors endowed with anticancer activity: Design, synthesis, biological and molecular modeling studies. *Eur. J. Med. Chem*. **2020**, *207*, 112745.

[382] Sharma, V.; Kumar, R.; Bua, S.; Supuran, C.T.; Sharma, P.K. Synthesis of novel benzenesulfonamide bearing 1,2,3-triazole linked hydroxytrifluoromethylpyrazolines and hydrazones as selective carbonic anhydrase isoforms IX and XII inhibitors. *Bioorg. Chem.* **2019**, *85*, 198-208.

[383] Carta, F.; Ferraroni, M.; Scozzafava, A.; Supuran, C.T. Fluorescent sulfonamide carbonic anhydrase inhibitors incorporating 1, 2, 3-triazole moieties: kinetic and X-ray crystallographic studies. *Bioorg. Med. Chem.* **2016**, *24*, 104-112.

[384] Fares, M.; Eladwy, R.A.; Nocentini, A.; El Hadi, S.R.A.; Ghabbour, H.A.; Abdel- Megeed, A.; Eldehna, W.M.; Abdel-Aziz, H.A.; Supuran, C.T. Synthesis of bulkytailed sulfonamides incorporating pyrido[2,3-d][1,2,4]triazolo[4,3-a]pyrimidin- 1(5H)-yl) moieties and evaluation of their carbonic anhydrases I, II, IV and IX inhibitory effects. *Bioorg. Med. Chem.* **2017**, *25*, 2210-2217.

[385] Brown, E.D.; Wright, G.D.; Antibacterial drug discovery in the resistance era. *Nature* **2016**, *529*, 336-343.

[386] Fairlamb, A.H.; Gow, N.A.; Matthews, K.R.; Waters, A.P. Drug resistance in eukaryotic microorganisms. *Nat. Microbiol*. **2016**, *1*, 16092.

[387] Cardoso, T.; Ribeiro, O.; Aragao, I.C.; Costa-Pereira, A.; Sarmento, A.E. Additional risk factors for infection by multidrug-resistant pathogens in healthcare-associated infection: a large cohort study. *BMC Infect. Dis.* **2012**, *12*, 375.

[388] Cox, G.M.; McDade, H.C.; Chen, S.C.; Tucker, S.C.; Gottfredsson, M.; Wright, L.C.; Sorrell, T.C.; Leidich, S.D.; Casadevall, A.; Ghannoum, M.A.; Perfect, J.R. Extracellular phospholipase activity is a virulence factor for Cryptococcus neoformans. *Mol. Microbiol*. **2001**, *39*, 166-175.

[389] Cox, G.M.; Mukherjee, J.; Cole, G.T.; Casadevall, A.; Perfect, J.R. Urease as a virulence factor in experimental cryptococcosis. *Infect. Immun.* **2000**, *68,* 443-448.

[390] Gaynor, M.; Mankin, A.S. Macrolide antibiotics: binding site, mechanism of action, resistance. *Curr. Top. Med. Chem.* **2003**, *3,* 949-961.

[391] Khelaifia, S.; Drancourt, M. Susceptibility of archaea to antimicrobial agents: applications to clinical microbiology. *Clin. Microbiol. Infect.* **2012**, *18*, 841-848.

[392] Schleifer, K.H.; Kandler, O. Peptidoglycan types of bacterial cell walls and their taxonomic implications. *Bacteriol. Rev.* **1972**, *36*, 407-477.

[393] Robbins, N.; Wright, G.D.; Cowen L.E. Antifungal drugs: the current armamentarium and development of new agents*. Microbiol. Spectr.* **2016**, *4*, FUNK-0002.

[394] De Simone, G.; Di Fiore, A.; Capasso, C.; Supuran, C.T. The zinc coordination pattern in the eta-carbonicanhydrase from Plasmodium falciparumis different from all other carbonic anhydrase genetic families. *Bioorg. Med. Chem. Lett.* **2015**, *25*, 1385-1389.

[395] Mackey, T.K.; Liang, B.A.; Cuomo, R.; Hafen, R.; Brouwer, K.C.; Lee, D.E. Emerging and reemerging neglectedtropical diseases: a review of key characteristics, risk factors, and the policy and innovation environment. *Clin. Microbiol. Rev.* **2014**, *27*, 949-979.

[396] WHO, World Health Organization. Sustaining the drive to overcome the global impact of neglectedtropical diseases. Second WHO report on neglected tropical diseases. **2013**.

[397] Turk, V.E.; Simic, I.; Likic, R.; Makar-Ausperger, K.; Radacic-Aumiler, M.; Cegec, I.; Nahal, D.J.; Kraljickovic, I. New drugs for bad bugs: what's new and what's in the pipeline? *Clin. Ther.* **2016**, *38*, e9.

[398] Decker, B.; Masur, H. Bad bugs, no drugs: are we part of the problem, or leaders in developing solutions? *Crit. Care Med.* **2015**, *43*, 1153-1155.

[399] Johnson, X.; Alric, J. Interaction between starch breakdown, acetate assimilation, and photosynthetic cyclic electron flow in Chlamydomonas reinhardtii. *J. Biol. Chem.* **2012**, *287*, 26445-26452.

[400] Tcherkez, G.; Boex-Fontvieille, E.; Mahe, A.; Hodges, M. Respiratory carbon fluxes in leaves. *Curr. Opin. Plant Biol.* **2012**, *15*, 308-314.

[401] Smith, K.S.; Ferry, J.G. Prokaryotic carbonic anhydrases. *FEMS Microbiol. Rev.* **2000**, *24*, 335-366.

[402] Maeda, S.; Price, G.D.; Badger, M.R.; Enomoto, C.; Omata, T. Bicarbonate binding activity of the CmpA protein of the cyanobacterium Synechococcus sp. strain PCC 7942 involved in active transport of bicarbonate. *J. Biol. Chem.* **2000**, *275*, 20551-20555.

[403] Joseph, P.; Ouahrani-Bettache, S.; Montero, J.L.; Nishimori, I.; Minakuchi, T.; Vullo, D.; Scozzafava, A.; Winum, J.-Y.; Köhler, S.; Supuran, C.T. A new beta-carbonic anhydrase from Brucella suis, its cloning, characterization, and inhibition with sulfonamides and sulfamates, leading to impaired pathogen growth. *Bioorg. Med. Chem.* **2011**, *19*, 1172-1178.

[404] Joseph P, Turtaut F, Ouahrani-Bettache S, Montero JL, Nishimori I, Minakuchi T, et al. Cloning, characterization, and inhibition studies of a beta-carbonic anhydrase from Brucella suis. *J. Med. Chem.* **2010**, *53*, 2277-2285.

[405] Murima, P.; McKinney, J.D.; Pethe, K. Targeting bacterial central metabolism for drug development. *Chem. Biol.* **2014**, *21*, 1423-1432.

[406] WHO. World Health Organization. Available from: http://www.who.int/chagas/en/ and http://www.who.int/leishmaniasis/en/

[407] Mackey, T.K.; Liang, B.A.; Cuomo, R.; Hafen, R.; Brouwer, K.C.; Lee, D.E. Emerging and reemerging neglected tropical diseases: a review of key characteristics, risk factors, and the policy and innovation environment. *Clin. Microbiol. Rev.* **2014**, *27*, 949-979.

[408] Barrett, M.P.; Croft, S.L. Management of trypanosomiasis and leishmaniasis. *Br. Med. Bull.* **2012**, *104*, 175-196

[409] Guedes, P.M.; Silva, G.K.; Gutierrez, F.R.; Silva, J.S. Current status of Chagas disease chemotherapy. *Expert Rev. Anti Infect Ther.* **2011**, *9,* 609-620.

[410] WHO. World Health Organization. Sustaining the drive to overcome the global impact of neglected tropical diseases. Second WHO report on neglected tropical diseases; **2013**. Available from: http://www.who.int/neglected_diseases/ 9789241564540/en/

[411] Vermelho, A.B.; Capaci, G.R.; Rodrigues, I.A.; Cardoso, V.S.; Mazotto, A.M.; Supuran, C.T. Carbonic anhydrases from Trypanosoma and Leishmania as anti-protozoan drug targets. *Bioorg. Med. Chem.* **2017**, *25*, 1543-1555.

[412] Ortiz, C.; Moraca. F.; Medeiros, A.; Botta, M.; Hamilton, N.; Comini, M.A. Binding Mode and Selectivity of Steroids towards Glucose-6-phosphate Dehydrogenase from the Pathogen Trypanosoma cruzi. *Molecules* **2016**, *21*, 368.

[413] Supuran, C.T. Inhibition of carbonic anhydrase from Trypanosoma cruzi for the management of Chagas disease: an underexplored therapeutic opportunity. *Future Med. Chem.* **2016**, *8*, 311-324.

[414] Pan, P.; Vermelho, A.B.; Capaci, G.R.; Scozzafava A.; Tolvanen, M.E.E.; Parkkila S.; Capasso C.; Supuran, C.T. Cloning, characterization, and sulfonamide and thiol inhibition studies of an a-carbonic anhydrase from Trypanosoma cruzi, the causative agent of Chagas disease. *J. Med. Chem.* **2013**, *56*, 1761-1771.

[415] de Menezes, D.R.; Calvet, C.M.; Rodrigues, G.C.; de Souza Pereira, M.C.; Almeida, I.R.; de Aguiar, A.P.; Supuran, C.T.; Vermelho, A.B. Hydroxamic acid derivatives: a promising scaffold for rational compound optimization in Chagas disease. *J. Enzyme Inhib. Med. Chem.* **2016**, *31*, 964-973.

[416] Syrjanen, L.; Vermelho, A.B.; Rodrigues, I.A.; Corte-Real, S.; Salonen, T.; Pan, P.; Vullo, D.; Parkkila, S.; Capasso, C.; Supuran, C.T. Cloning, characterization, and inhibition studies of a b-carbonic anhydrase from Leishmania donovani chagasi, the protozoan parasite responsible for leishmaniasis. *J. Med. Chem.* **2013**, *56*, 7372–7381.

[417] Guzel-Akdemir, O.; Akdemir, A.; Pan, P.; Vermelho, A.B.; Parkkila, S.; Scozzafava A.; Capasso, C.; Supuran C.T. A class of sulfonamides with strong inhibitory action against the a-carbonic anhydrase from Trypanosoma cruzi. *J. Med. Chem.* **2013**, *56*, 5773-5781.

[418] Alafeefy, A.M.; Ceruso, M.; Al-Jaber, N.A.; Parkkila, S.; Vermelho, A.B.; Supuran, C.T. A new class of quinazoline-sulfonamides acting as efficient inhibitors against the a-carbonic anhydrase from Trypanosoma cruzi. *J. Enzyme Inhib. Med. Chem*. **2015**, *30*, 581-585.

[419] Pan, P.; Vermelho, A.B.; Scozzafava, A.; Parkkila, S.; Capasso, C.; Supuran, C.T. Anion inhibition studies of the a-carbonic anhydrase from the protozoan pathogen Trypanosoma cruzi, the causative agent of Chagas disease. *Bioorg. Med. Chem.* **2013**, *21*, 4472-4476.

[420] Rodrigues, G.C.; Feijo, D.F.; Bozza, M.T.; Pan, P.; Vullo, D.; Parkkila, S.; Supuran, C.T.; Capasso, C.; Aguiar, A.P.; Vermelho, A.B. Design, synthesis,and evaluation of hydroxamic acid derivatives as promising agents for the management of Chagas disease. *J. Med. Chem*. **2014**, *57*, 298-308.

[421] Nocentini, A.; Cadoni, R.; Dumy, P.; Supuran, C.T.; Winum, J.Y. Carbonic anhydrases from Trypanosoma cruzi and Leishmania donovani chagasi are inhibited by benzoxaboroles. *J. Enzyme Inhib. Med. Chem.* **2018**, *33*, 286-289.

[422] Ceruso, M.; Carta, F.; Osman, S.M.; Alothman, Z.; Monti, S.M.; Supuran, C.T. Inhibition studies of bacterial, fungal and protozoan b-class carbonic anhydrases with Schiff bases incorporating sulfonamide moieties. *Bioorg. Med. Chem.* **2015**, *23*, 4181-4187.

[423] Crespillo-Andújar, C.; Chamorro-Tojeiro, S.; Norman, F.; Monge-Maillo, B.; López-Velez, R.; Pérez-Molina, J.A. Toxicity of nifurtimox as second-line treatment after benznidazole intolerance in patients with chronic Chagas disease: When available options fail. *Clin. Microbiol. Infect.* **2018**, *S1198-743X*, 30465-30468

[424] Nocentini, A.; Vullo, D.; Bartolucci, G.; Supuran, C.T. N-Nitrosulfonamides: A new chemotype for carbonic anhydrase inhibition. *Bioorg. Med. Chem.* **2016**, *24*, 3612-3617.

[425] Lansdown, A.B. Silver in health care: antimicrobial effects and safety in use. *Curr. Probl. Dermatol.* **2006**, *33*, 17-34.

[426] Lok, C.N.; Ho, C.M.; Chen, R.; He, Q.Y.; Yu, W.Y.; Sun, H.; Tam, P.K.; Chiu, J.F.; Che, C.M. Silver nanoparticles: partial oxidation and antibacterial activities. *JBIC, J. Biol. Inorg. Chem.* **2007**, *12*, 527-534.

[427] Rai, M.; Yadav, A.; Gade, A. Silver nanoparticles as a new generation of antimicrobials. *Biotechnol. Adv.* **2009**, *27*, 76-83.

[428] Allahverdiyev, A.M.; Abamor, E.S.; Bagirova, M.; Ustundag, C.B.; Kaya, C.; Kaya, F.; Rafailovich, M. Antileishmanial effect of silver nanoparticles and their enhanced antiparasitic activity under ultraviolet light. *Int. J. Nanomed.* **2011**, *6*, 2705-2714.

[429] Minksztym, K. Synthesis of Aromatic Aminosulfonic Acid Nitroamides Synthesis. *Synthesis* **2007**, *12*, 1819.

[430] Mathews, B. R. Benzene Sulfonnitramide, Toluene-4-sulfonnitramide, 2-nitroluene-4-sulfonnitranimide and Some of their Salts. *J. Phys. Chem.* **1920**, *24*, 108.

[431] Bonardi, A.; Vermelho, A.B.; da Silva Cardoso, V.; de Souza Pereira, M.C.; da Silva Lara, L.; Selleri, S.; Gratteri, P.; Supuran, C.T.; Nocentini, A. N-Nitrosulfonamides as Carbonic Anhydrase Inhibitors: A Promising Chemotype for Targeting Chagas Disease and Leishmaniasis. *ACS Med. Chem. Lett.* **2018**, *10*, 413-418.

[432] Baker-Austin, C.; Oliver, J.D.; Alam, M.; Ali, A.; Waldor, M.K.; Qadri, F.; Martinez-Urtaza, J. *Vibrio* spp. Infections. *Nat. Rev. Dis. Primers* **2018**, *4*, 8.

[433] Baker-Austin, C.; Trinanes, J.; Gonzalez-Escalona, N.; Martinez-Urtaza, J. Non-Cholera vibrios: the microbial barometer of climate change. *Trends. Microbiol.* **2017**, *25*, 76-84.

[434] World Health Organization. Weekly epidemiological record. **2016**, *21*, 421-428.

[435] World Health Organization. Cholera. *WHO* **2020**, https://www.who.int/en/news-room/fact-sheets/detail/cholera.

[436] Zuckerman, J.N.; Rombo, L.; Fisch, A. The true burden and risk of cholera: implications for prevention and control. *Lancet. Infect. Dis.* **2017**, *7*, 521-530.

[437] World Health Organization. Weekly epidemiological record. **2010**, *85*, 117-128.

[438] Rabbani, G.H.; Greenough, W.B. III. Food as a vehicle of transmission of cholera. *J. Diarrhoeal Dis. Res.* **1999**, *17*, 1-9.

[439] Sugimoto, J.D.; Koepke, A.A.; Kenah, E.E.; Halloran, M.E.; Chowdhury, F.; Khan, A.I.; LaRocque, R.C.; Yang, Y.; Ryan, E.T.; Qadri, F.; Calderwood, S.B.; Harris, J.B.; Longini, L.I.J.; Vinetz, J.M. Household transmission of Vibrio cholerae in Bangladesh. *PLoS Negl. Trop. Dis.* **2014**, *8*, e3314e3314.

[440] Goh, K.T.; Teo, S.H.; Lam, S.; Ling, M.K. Person-to-person transmission of cholera in a psychiatric hospital. *J. Infect.* **2017**, *20*, 193-200.

[441] Gangarosa, E.F.; Beisel, W.R.; Benyajati, C, Sprinz, H, Piyaratn, P. The nature of the gastrointestinal lesion in asiatic cholera and its relation to pathogenesis: a biopsy study. *Am. J. Trop. Med. Hyg.* **1960**, *9*, 125-135.

[442] Abuaita, B.H.; Withey, J.H. Bicarbonate induces vibrio cholerae virulence gene expression by enhancing ToxT activity. *Infect. Immun.* **2009**, *77*, 4111-4120.

[443] Weber, G.G.; Klose, K.E.K. The complexity of ToxT-dependent transcription in Vibrio cholerae. *Indian J. Med. Res.* **2011**, *133*, 201-206.

[444] Kirn TJ, Lafferty MJ, Sandoe CM, Taylor RK. Delineation of pilin domains required for bacterial association into microcolonies and intestinal colonization by Vibrio cholerae. *Mol. Microbiol.* **2000**, *35*, 896-910.

[445] Herrington, D.A.; Hall, R.H.; Losonsky, G.; Mekalanos, J.J.; Taylor, R.K.; Levine, M.M. Toxin, toxin-coregulated pili, and the toxR regulon are essential for Vibrio cholerae pathogenesis in humans. *J. Exp. Med.* **1988**, *168,* 1487-1492.

[446] Fishman, P.H.; Atikkan, E.E. Mechanism of action of cholera toxin: effect of receptor density and multivalent binding on activation of adenylate cyclase. *J. Membr. Biol.* **1980**, *54*, 51-60.

[447] De, S.N.; Chatterje, D.N. Enterotoxicity of bacteria-free culture filtrate of Vibrio cholerae. *Nature* **1959**, *183*, 1533-1534.

[448] Levine, M.M.; Kaper, J.B.; Black, R.E.; Clements, M.L. New knowledge on pathogenesis of bacterial enteric infections as applied to vaccine development. *Microbiol. Rev.* **1983**, *47*, 510-550.

[449] World Health Organization. Prevention and control of cholera. *WHO* **2020**, https://www.who.int/health-topics/cholera#tab=tab_2.

[450] World Health Organization. Treatment diarrhoea: manual - a manual for physicians other senior health workers. *WHO* **1990**.

[451] Alam, N.H.; Ashraf, H. Treatment of infectious diarrhea in children. *Paediatr. Drugs* **2003**, *5*, 151-165.

[452] Ahmed, T.; Ali, M.; Ullah, M.M.; Choudhury, I.A.; Haque, M.E.; Salam, M.A.; Rabbani, G.H.; Suskind, R.M.; Fuchs, G.J. Mortality in severely malnourished children with diarrhoea and use of a standardized management protocol. *Lancet* **1999**, *353*, 1919-1922.

[453] World Health Organization WHO/Unicef joint statement: Clin. Management Acute Diarrhoea. *WHO* **2004**.

[454] Lindenbaum J, Greenough WB, Islam MR. Antibiotic therapy of Cholera in children. *Bull World Health Organ.* **1967**, *37*, 52938.

[455] Kaushik, J.S, Gupta, P, Faridi, M.M, Das S. Single-dose azithromycin versus ciprofloxacin for cholera in children: a randomized controlled trial. *Indian Pediatr.* **2010**, *47*, 309-315.

[456] Roy, S.K.; Hossain, M.J.; Khatun, W.; Roy, S.K.; Hossain, M.J.; Khatun, W.; Chakraborty, B.; Chowdhury, B.; Begum, A.; Mah-e-Muneer, S.; Shafique, S.; Khanam, M.; Chowdhury, R. Zinc supplementation in children with cholera in Bangladesh: randomised controlled trial. *BMJ.* **2008**, *336*, 266-268.

[457] Del Prete.; S, Isik, S.; Vullo, D.; De Luca, V.; Carginale, V.; Scozzafava, A.; Supuran, C.T.; Capasso, C. DNA cloning, characterization, and inhibition studies of an α-carbonic anhydrase from the pathogenic bacterium vibrio cholerae. *J. Med. Chem.* **2012**, *55*, 10742-10748.

[458] Del Prete, S.; De Luca, V.; Scozzafava, A.; Carginale, V.; Supuran, C.T.; Capasso, C. Biochemical properties of a new α-carbonic anhydrase from the human pathogenic bacterium, vibrio cholerae. *J. Enzyme Inhib. Med. Chem.* **2014**, *29*, 23-27.

[459] Vullo, D.; Isik, S.; Del Prete, S.; De Luca, V.; Carginale, V.; Scozzafava, A.; Supuran, C.T.; Capasso, C. Anion inhibition studies of the α-carbonic anhydrase from the pathogenic bacterium vibrio cholerae. *Bioorg. Med. Chem. Lett.* **2013**, *23*, 1636-1638.

[460] Cummins, E.P.; Selfridge, A.C.; Sporn, P.H.; Sznajder, J.I.; Taylor, C.T. Carbon dioxide-sensing in organisms and its implications for human disease. *Cell. Mol. Life Sci.* **2014**, *71*, 831-845.

[461] Del Prete, S.; Vullo, D.; De Luca, V.; Carginale, V.; Osman, S.M.; AlOthman, Z.; Supuran, C.T.; Capasso, C. Comparison of the sulfonamide inhibition profiles of the α-, β- and γ-carbonic anhydrases from the pathogenic bacterium Vibrio cholerae. *Bioorg. Med. Chem. Lett.* **2016**, *26*, 1941-1946.

[462] Del Prete, S.; Vullo, D.; Di Fonzo, P.; Osman, S.M.; AlOthman, Z.; Donald, W.A.; Supuran, C.T.; Capasso, C. Sulfonamide inhibition profile of the γ-carbonic anhydrase identified in the genome of the pathogenic bacterium Burkholderia pseudomallei the etiological agent responsible of melioidosis. *Bioorg. Med. Chem. Lett.* **2017**, *27*, 490-495.

[463] Del Prete, S.; Vullo, D.; Osman, S.M.; Scozzafava, A.; AlOthman, Z.; Capasso, C.; Supuran, C.T. Sulfonamide inhibition study of the carbonic anhydrases from the bacterial pathogen Porphyromonas gingivalis: the β-class (PgiCAb) versus the γ-class (PgiCA) enzymes. *Bioorg. Med. Chem.* **2014**, *22*, 4537-43.

[464] De Luca, V.; Vullo, D.; Del Prete, S.; Carginale, V.; Osman , S.M.; AlOthman, Z.; Supuran, C.T.; Capasso, C. Cloning, characterization and anion inhibition studies of a γ-carbonic anhydrase from the Antarctic bacterium Colwellia psychrerythraea. *Bioorg. Med. Chem.* **2016**, *24*, 835-840.

[465] De Luca, V.; Vullo, D.; Del Prete, S.; Carginale, V.; Scozzafava, A.; Osman, S.M.; AlOthman, Z.; Supuran, C.T.; Capasso, C. Cloning, characterization and anion inhibition studies of a new γ-carbonic anhydrase from the Antarctic bacterium Pseudoalteromonas haloplanktis. *Bioorg. Med. Chem.* **2015**, *23*, 4405-4409.

[466] Nocentini, A.; Cadoni, R.; Del Prete, S.; Capasso, C.; Dumy, P.; Gratteri, P.; Supuran, C.T.; Winum, J.-Y. Benzoxaboroles as Efficient Inhibitors of the β-Carbonic Anhydrases from Pathogenic Fungi: Activity and Modeling Study. *ACS Med. Chem. Lett.* **2017**, *8*, 1194-1198.

[467] Nocentini, A.; Supuran, C.T.; Winum, J.-Y. Benzoxaborole compounds for therapeutic uses: a patent review (2010- 2018). *Expert Opin. Ther. Pat.* **2018**, *28*, 493-504.

[468] Larcher, A.; Nocentini, A.; Supuran, C.T.; Winum, J.-Y.; van der Lee, A.; Vasseur, J.J.; Laurencin, D.; Smietana, M. Bis-benzoxaboroles: Design, Synthesis, and Biological Evaluation as Carbonic Anhydrase Inhibitors. *ACS Med. Chem. Lett.* **2019**, *10*, 1205-1210.

[469] Langella, E.; Alterio, V.; D'Ambrosio, K.; Cadoni, R.; Winum, J.-Y.; Supuran, C.T.; Monti, S.M.; De Simone, G.; Di Fiore, A. Exploring benzoxaborole derivatives as carbonic anhydrase inhibitors: a structural and computational analysis reveals their conformational variability as a tool to increase enzyme selectivity. *J. Enzyme Inhib. Med. Chem.* **2019**, *34*, 1498-1505.

[470] Ferraroni, M.; Del Prete, S.; Vullo, D.; Capasso, C.; Supuran, C.T. Crystal structure and kinetic studies of a tetrameric type II β-carbonic anhydrase from the pathogenic bacterium Vibrio cholerae. *Acta Crystallogr. D. Biol. Crystallogr.* **2015**, *71*, 2449-2456.

[471] Bonardi, A.; Nocentini, A.; Cadoni, R.; del Prete, S.; Dumy, P.; Capasso, C.; Gratteri, P.; Supuran, C.T, Winum, J.-Y. Benzoxaboroles: New Potent Inhibitors of the Carbonic Anhydrases of the Pathogenic Bacterium Vibrio cholerae. *ACS Med. Chem. Lett.* **2020**, doi.org/10.1021/acsmedchemlett.0c00403

[472] Maisonneuve, I.M.; Glick, S.D. Anti-addictive actions of an iboga alkaloid congener: a novel mechanism for a novel treatment. *Pharmacol. Biochem. Behav.* **2003**, *75*, 607-618.

[473] Glick, S.D.; Sell, E.M.; McCallum, S.E.; Maisonneuve, I.M. Brain regions mediating alpha3beta4 nicotinic antagonist effects of 18-MC on nicotine self-administration. *Eur. J. Pharmacol.* **2011**, *669*, 71-75.

[474] Arias, H.R.; Targowska-Duda, K.M.; Feuerbach, D.; Jozwiak, K. Coronaridine congeners inhibit human α3β4 nicotinic acetylcholine receptors by interacting with luminal and non-luminal sites. *Int. J. Biochem. Cell Biol.* **2015**, *65*, 81-90.

[475] Arias, H.R.; Jin, X.; Feuerbach, D.; Drenan, R.M. Selectivity of coronaridine congeners at nicotinic acetylcholine receptors and inhibitory activity on mouse medial habenula. *Int. J. Biochem. Cell. Biol.* **2017**, 92, 202-209.

[476] Kalueff, A.V.; Kaluyeva, A.; Maillet, E.L. Anxiolytic-like effects of noribogaine in zebrafish. *Behav. Brain Res.* **2017**, *330,* 63-67.

[477] Miller, P. S.; Scott, S.; Masiulis, S.; De Colibus, L.; Pardon, E.; Steyaert, J.; Aricescu, A.R. Structural basis for GABA$_A$ receptor potentiation by neurosteroids. *Nat. Struct. Mol. Biol.* **2017** *24*, 986-992.

[478] Sieghart, W.; Savic, M.M. "International Union of Basic and Clinical Pharmacology. CVI: GABAA Receptor Subtype- and Function-selective Ligands: Key Issues in Translation to Humans." *Pharmacol. Rev.* **2018**, *70*, 836-878.

[479] Weir, C.J.; Mitchell, S.J.; Lambert, J.J. Role of GABA$_A$ receptor subtypes in the behavioural effects of intravenous general anaesthetics. *Br. J. Anaesth.* **2017**, *119*, i167-i175.

[480] Forman S.A.Clinical and molecular pharmacology of etomidate. *Anesthesiology* **2011**, *114*, 695-707.

[481] Masiulis, S.; Desai, R.; Uchanski, T.; Serna Martin, I.; Laverty, D.; Karia, D.; Malinauskas, T.; Zivanov, J.; Pardon, E.; Kotecha, A.; Steyaert, J.; Miller, K.W.; Aricescu, A.R. GABA$_A$ receptor signalling mechanisms revealed by structural pharmacology. *Nature* **2019**, *565*, 454-459.

[482] Wafford, K.A.; Bain, C.J.; Quirk, K.; McKernan, R.M.; Wingrove, P.B.; Whiting, P.J.; Kemp, J.A. A novel allosteric modulatory site on the GABAA receptor beta subunit. *Neuron.* **1994**, *12*, 775-782.

[483] Keramidas, A.; Kash, T.; Harrison, N.L. The pre-M1 segment of the α1 subunit is a transduction element in the activation of the GABAA receptor. *J. Physiol.* **2006**, *575*, 11-22.

[484] Sigel, E.; Buhr, A; Baur, R. Role of the conserved lysine residue in the middle of the predicted extracellular loop between M2 and M3 in the GABAA receptor. *J. Neurochem.* **2002**, *73*, 1758-1763.

[485] Chiara, D. C., Z. Dostalova, S. S. Jayakar, X. Zhou, K. W. Miller, J. B. Cohen. Mapping general anesthetic binding site(s) in human alpha1beta3 gamma-aminobutyric acid type A receptors with [^{3}H]TDBzl-etomidate, a photoreactive etomidate analogue. *Biochem.* **2012**, *51*, 836-847.

[486] Ziemba, A. M.; Szabo, A.; Pierce, D.W.; Haburcak, M.; Stern, A.T.; Nourmahnad, A.; Halpin, E.S.; Forman, S.A. Alphaxalone Binds in Inner Transmembrane beta+-alpha- Interfaces of alpha1beta3gamma2 gamma-Aminobutyric Acid Type A Receptors. *Anesthesiol.* **2018**, *128*, 338-351.

[487] Schrödinger Suite Release 2019-1, Schr€odinger, LLC, New York, NY, **2019** (a) Maestro v.11.9; (b) Epik, v.4.7; (c) Impact, v.8.2; (d) Prime, v.5.5; (e) Macromodel v.12.3; (f) Glide, v.8.2; (g) Jaguar, v.10.3; (h) Desmond, 5.7.

[488] Kaminski, G.A.; Friesner, R.A.; Tirado-Rives, J.; Jorgensen, W.L. Evaluation and Reparametrization of the OPLS-AA Force Field for Proteins via Comparison with Accurate Quantum Chemical Calculations on Peptides. *J. Phys. Chem. B.* **2001**, *105*, 6474-6487;

[489] Hornak, V.; Abel, R.; Okur, A.; Strockbine, B.; Roitberg, A.; Simmerling, C. Comparison of multiple Amber force fields and development of improved protein backbone parameters. *Proteins* **2006**, *65*, 712-725.

[490] Roos, K.; Wu, C.; Damm, W.; Reboul, M.; Stevenson, J.M.; Lu, C.; Dahlgren, M.K.; Mondal, S.; Chen, W.; Wang, L.; Abel, R.; Friesner, A.R.; Harder, E.D. OPLS3e: Extending Force Field Coverage for Drug-Like Small Molecules. *J. Chem. Theory Comput.* **2019**, *15,* 1863-1874.

[491] Durgun, M.; Turkmen, H; Ceruso, M.; Supuran, C.T. Synthesis of Schiff base derivatives of 4-(2-aminoethyl)-benzenesulfonamide with inhibitory activity against carbonic anhydrase isoforms I, II, IX and XII. Bioorg. *Med. Chem. Lett.* **2015**, *25*, 2377-2381.

[492] Srivastava, D.K.; Jude, K.M.; Banerjee, A.L.; Haldar, M.; Manokaran, S.; Kooren, J.; Mallik, S.; Christianson, D.W. Structural analysis of charge discrimination in the binding of inhibitors to human carbonic anhydrases I and II. *J. Am. Chem. Soc.* **2007**, *129*, 5528-5537.

[493] Lanzi, C.; Lucarini, L.; Durante, M.; Sgambellone, S.; Pini, A.; Catarinicchia, S.; Lazewska, D.; Kieć-Kononowicz, K.; Stark, H.; Masini, E. Role of histamine H3 receptor antagonists on intraocular pressure reduction in rabbit models of transient ocular hypertension and glaucoma. *Int. J. Mol. Sci.* **2019**, *20*, 981.

[494] Kilkenny, C.; Browne, W.; Cuthill, I.C.; Emerson, M.; Altman, D.G. Animal research: reporting in vivo experiments: the ARRIVE guidelines. NC3Rs reporting guidelines working group. *Br. J. Pharmacol.* **2010**, *160*, 1577-1579.

[495] Adelaere, B. Preparation of new 4-aryl-3H-1,2-dithiole-3-thiones from functionalized cumenes and liquid sulfur. Dithiolylium salts. *Sulfur letters.* **1989**, *10*, p.31.

[496] Kilkenny, C.; Browne, W. J.; Cuthill, I. C.; Emerson, M.; Altman, D. G. Improving bioscience research reporting: the ARRIVE guidelines for reporting animal research. *J. Pharmacol. Pharmacother.* **2010**, *1*, 94-99.

[497] Di Cesare Mannelli, L.; Bani, D.; Bencini, A.; Brandi, M. L.; Calosi, L.; Cantore, M.; Carossino, A. M.; Ghelardini, C.; Valtancoli, B.; Failli, P. Therapeutic effects of the superoxide dismutase mimetic compound MnIIMe2DO2A on experimental articular pain in rats. *Mediators Inflamm.* **2013**, 905360.

[498] Butler, S. H.; Godefroy, F.; Besson, J. M.; Weil-Fugazza, J. A limited arthritic model for chronic pain studies in the rat. *Pain* **1992**, *48*, 73-81.

[499] Di Cesare Mannelli, L.; Micheli, L.; Cinci, L.; Maresca, M.; Vergelli, C.; Pacini, A.; Quinn, M. T.; Giovannoni, M. P.; Ghelardini, C. Effects of the neutrophil elastase inhibitor EL-17 in rat adjuvant- induced arthritis. *Rheumatology* **2016**, *55*, 1285-1294.

[500] Leighton, G. E.; Rodriguez, R. E.; Hill, R. G.; Hughes, J. κ-Opioid agonist produce antinociception after i.v. and i.c.v. but not intrathecal administration in the rat. *Br. J. Pharmacol.* **1988**, *93*, 553-560.

[501] Bove, S.E.; Calcaterra, S.L.; Brooker, R.M.; Huber, C.M.; Guzman, R E.; Juneau, P.L.; Schrier, D.J.; Kilgore, K.S. Weight bearing as a measure of disease progression and efficacy of anti- inflammatory compounds in a model of monosodium iodoacetate- induced osteoarthritis. *Osteoarthr. Cartil.* **2003**, *11*, 821-830.

[502] Mickeviciute, A.; Timm, D.D.; Gedgaudas, M.; Linkuviene, V.; Chen, Z.; Waheed, A.; Michailoviene, V.; Zubriene, A.; Smirnov, A.; Capkauskaite, E.; Baranauskiene, L.; Jachno, J.; Revuckiene, J.; Manakova, E.; Grazulis, S.; Matuliene, J.; Di Cera, E.; Sly, W.S.; Matulis, D. Intrinsic thermodynamics of high affinity inhibitor binding to recombinant human carbonic anhydrase IV. *Eur. Biophys. J.* **2018**, *47*, 271-290.

[503] Mahon, B.P.; Bhatt, A.; Socorro, L.; Driscolla, J.M.; Okoh, C.; Lomelino, C.L.; Mboge, M.Y.; Kurian, J.J.; Tu, C., Agbandje-McKenna, M.; Frosta, S.C.; Robert McKenna. The structure of carbonic anhydrase IX is adapted for low-pH catalysis. *Biochem.* **2016**, *55*, 4642-4653.

[504] Aymerich, S.; Goldenberg, S. The karyotype of Trypanosoma cruzi Dm 28c: Comparison with other T. cruzi strains and trypanosomatids. *Experiment. Parasitol.* **1989**, *69*, 107-115.

[505] Alvarenga, N. J.; Bronfen, E. *Rev. Soc. Bras. Med. Trop.* **1997**, *30*, 247-250.

[506] Rodrigues, G.C.; Feijó, D.F.; Bozza, M.T.; Pan, P.; Vullo, D.; Parkkila, S.; Supuran, C.T.; Capasso, C.; Aguiar, A.P.; Vermelho, A.B. Design, synthesis, and evaluation of hydroxamic acid derivatives as promising agents for the management of Chagas disease. *J. Med. Chem.* **2014**, *57*, 298-308.

[507] Rólon, M.; Vega, C.; Escario, J.A.; Gémez-Barrio, A. Development of resazurin microtiter assay for drug sensibility testing of Trypanosoma cruzi epimastigotes. *J. Parasitol. Res.* **2006**, *99*, 103-107.

[508] Mosmann T. Rapid colorimetric assay for cellular growth and survival: application to proliferation and cytotoxicity assays. *J. Immunol. Methods* **1983**, *983*, 55-63.

[509] Lara, L.S.; Moreira, C.S.; Calvet, C.M.; Lechuga, G.C.; Souza, R.S.; Bourguignon, S.C.; Ferreira, V.F.; Rocha, D.; Pereira, M.C.S. Efficacy of 2-hydroxy-3-phenylsulfanylmethyl-[1,4]-naphthoquinone derivatives against different Trypanosoma cruzi discrete type units: Identification of a promising hit compound. *Eur. J. Med. Chem.* **2018**, *144*, 572-581

[510] Somalinga, V.; Buhrman, G.; Arun, A.; Rose, R.B.; Grunden, A.M. A High-Resolution Crystal Structure of a Psychrohalophilic α-Carbonic Anhydrase From Photobacterium Profundum Reveals a Unique Dimer Interface. *PLoS One* **2016**, *11*, e0168022.

[511] Murray, A.B.; Aggarwal, M.; Pinard, M.; Vullo, D.; Patrauchan, M.; Supuran, C.T.; McKenna, R. Structural mapping of anion inhibitors to β-carbonic anhydrase psCA3 from Pseudomonas aeruginosa. *Chem. Med. Chem.* **2018**, *13*, 2024-9.

[512] Park, H.M.; Park, J.H.; Choi, J.W.; Lee, J.; Kim, B.Y.; Jung, C.H.; Kim, J.S. Structures of the γ-Class Carbonic Anhydrase Homologue YrdA Suggest a Possible Allosteric Switch. *Acta Crystallogr. D. Biol. Crystallogr.* **2012**, *68*, 920-926.

[513] Waterhouse, A.; Bertoni, M.; Bienert, S.; Studer, G.; Tauriello, G.; Gumienny, R.; Heer, F.T.; de Beer, T.A.P.; Rempfer, C.; Bordoli, L.; Lepore, R.; Schwede, T. SWISS-MODEL: homology modelling of protein structures and complexes. *Nucleic Acids Re*s. **2018**, *46*, W296-W303.

[514] The UniProt Consortium. UniProt: a worldwide hub of protein knowledge. *Nucleic Acids Research* **2019**, *47*, D506–D515.